Photoinduced Electron Transfer Based Fluorescent Sensors For Metal Ion Detection

Jason Paul Geue, B. Sc. (Hons)

A thesis submitted for the degree of
Doctor of Philosophy
in
The University of Adelaide
Department of Chemistry

October 2002

THE UNIVERSITY
OF ADELAIDE
AUSTRALIA

Contents

Abstract i
Declaration ii
Acknowledgments iii
Abbreviations iv

Chapter 1 Introduction 1

1.1 Metal Ion Detection 1

1.2 Design Principles of a Fluorescent Sensor 2

1.3 Photoinduced Electron Transfer (PET) Based Fluorescent Sensors 3

1.3.1 Principles 3

1.3.2 Crown Containing PET Sensors 5

1.3.3 Cryptand Based PET Sensors 7

1.3.4 Simple Podand Based PET Sensors 8

1.3.5 PET Sensors with Rigid Spacers 9

1.3.6 Other Sensor Designs that Harness PET 9

1.3.7 Dual PET input sensors 11

1.3.8 PET Sensors for Anions or Molecular Analytes 12

1.3.9 Ternary PET Sensors 14

1.4 Photoinduced Charge Transfer (PCT) Based Fluorescent Sensors 14

1.4.1 Principles 14

1.4.2 Examples of PCT Based Fluorescent Sensors 16

1.5 Other Fluorescent Sensor Design Strategies 19

1.5.1 Excimer Based Fluorescent Sensors 19

1.5.2 Fluorescence Sensors Based on Geometrical Conformation 21

1.5.3 Peptide Based Fluorescent Sensors 23

1.5.4 Fluorescent Sensors Based on π,π-Stacking Interactions 23

1.5.5 Isomerisable Fluorescent Sensors 24

1.5.6 Fluorescent Sensor Ensembles for Indirect Signalling 24

1.6 Work Described in this Thesis 25

Chapter 2 Synthesis and Physical Properties of Functionalised Anthracene Ligands 27

2.1 Introduction 27

2.2 Synthesis 28

2.2.1 Synthesis of 9,10-Bis(morpholinoethyl)anthracene (**36**) 28

2.2.2 Synthesis of 9,10-Bis(morpholinomethyl)anthracene (**38**) 29

2.2.3 Synthesis of 9,10-Bis(morpholinopropyl)anthracene (**42**) 30

2.2.4 Synthesis of 9,10-Bis[(1,4,7,10-tetraoxa-13-azacyclopentadecyl)-ethyl]anthracene (**45**) 32

2.2.5 Synthesis of 9-Ethyl-10-[(1,4,7,10-tetraoxa-13-azacyclopentadecyl)-ethyl]anthracene (**51**) 33

2.2.6 Synthesis of 9,10-Bis(thiomorpholinoethyl)anthracene (**52**) and 9,10-Bis(piperazinoethyl)anthracene (**53**) 35

2.3 Acid Dissociation Constants 36

2.4 Metal Complex Formation 40

2.5 Summary 41

Chapter 3 Photophysical Properties of Anthracene Ligands in Partially Aqueous Solution 43

3.1 Introduction 43

3.2 Photophysical Properties in 1,4-Dioxane-Water Solution 48

3.2.1 UV-Visible Absorbance Properties 48

3.2.2 Fluorescence Properties 52

3.3 Metal Hydroxide Formation 55

3.4 Photophysical Properties in Buffered 1,4-Dioxane-Water Solution 56

3.4.1 UV-Visible Absorbance Properties 57

3.4.2 Fluorescence Properties 57

3.5 Summary and Conclusions 63

Chapter 4 Fluorescence Sensing of Metal Ions by Anthracene Ligands in Acetonitrile Solution 65

4.1 Introduction 65

4.2 UV-Visible Absorbance Properties in the Presence of Metal Ions 66

4.3 Determination of Stability Constants from Fluorescence 68

4.4 Fluorescence Properties in the Presence of Metal Ions 70

4.4.1 Metal Ion Complexation by Bis(morpholinomethyl) **38** 71

4.4.2 Metal Ion Complexation by Bis(morpholinoethyl) **36** 73

4.4.3 Metal Ion Complexation by Bis(morpholinopropyl) **42** 79

4.4.4 Metal Ion Complexation by Bis(thiomorpholine) **52** 84

4.4.5 Metal Ion Complexation by Bis(piperazine) **53** 88

4.4.6 Metal Ion Complexation by Mono(azacrown) **51** 95

4.4.7 Metal Ion Complexation by Bis(azacrown) **45** 100

4.4.8 Emission Spectra of Bis(hydroxyethyl) **34** and Bis(propylamide) **41** .. 108

4.5 Fluorescence Quantum Yields for the Calculated Spectra Obtained from Data Fitting 109

4.6 Discussion 111

Chapter 5 Conclusions and Future Directions 122

Chapter 6 Experimental 126

6.1 General Physical Methods 126

6.2 Standardisation of Metal Ion Solutions 127

6.3 Potentiometric Titrations in 1,4-Dioxane-Water Solution 127

6.4 Ultraviolet-Visible Spectroscopy 130

6.5 Fluorescence Spectroscopy 130

6.6 Stability Constants from Fluorescence 131

6.7 Relative Quantum Yields 131

6.8 General Synthetic Methods 132

6.9 Syntheses 133

Appendix A Fluorescence Spectra and Derived Binding Curves for Ligands in Acetonitrile Solution 141

A.1 Bis(morpholinomethyl) **38** 141

A.2 Bis(morpholinoethyl) **36** 143

A.3 Bis(morpholinopropyl) **42** 147

A.4 Bis(thiomorpholine) **52** 151

A.5 Bis(piperazine) **53** 155

A.6 Mono(azacrown) **51** 163

A.7 Bis(azacrown) **45** 172

Bibliography 180

Abstract

This thesis describes the synthesis and complexation characteristics of a series of fluorescent sensors of the photoinduced electron transfer (PET) based Fluorophore-Spacer-Receptor design. The ligands synthesised consist of a 9,10-disubstituted anthracene, an alkyl spacer (methyl, ethyl or propyl) and a receptor (morpholine and analogues or monoaza-15-crown-5). Upon metal ion complexation (or protonation) the fluorescence emission of the synthesised ligands is significantly increased (up to 30-fold) due to the suppression of the fluorescence quenching PET process.

The acid dissociation constants were determined in 1,4-dioxane-water (40:60; v/v) solution (I = 0.05 mol dm^{-3}) for the soluble ligands, although no metal ion complexation was observed. The protonation of only one (of the two) nitrogen amines in close proximity to the anthracene was found not to restore the fluorescence emission in 1,4-dioxane-water. In addition, it was necessary to use buffered solutions to prevent protons liberated from metal ion hydrolysis causing increased fluorescence.

The alkali and alkaline earth metal ion complexation characteristics of the ligands were studied in anhydrous acetonitrile and a series of spectrofluorimetric titrations were performed to determine the stability constants (K_1 and K_2) of the complexes that formed. Minimal changes in the absorption spectra were observed. Increasing the spacer length (methyl to propyl) increased the quantum yield of the unbound ligand and the stability of the complexes formed (350-fold increase for Mg^{2+}). Little cooperative binding between the two receptors was observed and K_1 was always larger than K_2. The general stability series observed for the six-membered ring receptors was $Mg^{2+} > Ca^{2+} > Sr^{2+} \leq Ba^{2+}$.

Utilising the larger azacrown receptor, the stability constants in acetonitrile could not accurately be determined for the alkaline earths as K_1 and $K_2 \geq 10^7$ dm^3 mol^{-1}. Biphasic binding curves were observed due to the low fluorescence of the (metal)•(ligand) complex and high fluorescence of the $(metal)_2$•(ligand) complex. This receptor also displayed increased fluorescence emission with alkali metal ions, although of lower stability. The magnitude of the stability constants and quantum yield changes was chiefly controlled by the charge density of the bound metal ion.

This work furthers understanding of the requirements for PET based fluorescent sensors to detect metal ions.

Declaration

This work contains no material which has been accepted for the award of any other degree or diploma in any university or other tertiary institution and, to the best of my knowledge and belief, contains no material previously published or written by another person, except where due reference has been made in the text.

I give consent to this copy of my thesis, when deposited in the University Library, being available for loan and photocopying.

Jason Geue

October, 2002

Acknowledgments

The Ph.D. road is long, dangerous and fraught with peril. Consequently, many people are owed thanks now that my journey is near completion.

I would like to unreservedly thank Assoc. Prof. David Ward and Prof. Stephen Lincoln for their guidance throughout my studies. Their enthusiasm and knowledge of all aspects of chemistry is overwhelming and it was a pleasure to share in it awhile.

Special thanks must go to Dr. Nicholas Head as working with you allowed me to achieve far more than would have been possible alone. Our Friday afternoon brainstorming sessions were always informative and enlightening, if not fruitful.

To all those within the Department of Chemistry that have furthered my chemical endeavours, your contributions were appreciated.

Those who know me well are aware that my stomach drives much that I do. Thus, I (and my belly) sincerely thank the multitude of people that have kept me fed and watered over the course of my postgraduate study. Special mention must go to Rebecca, Amy, the Simpson family and the van der Wyst family in this regard for all those fabulous meals.

A sincere thankyou to all those friends and colleagues (coming, going and gone), who have kept me going by various means, and/or helped to drown our collective sorrows. You are too numerous to name, although none of you are forgotten.

Mum (Gemma), thanks for always supporting my academic endeavours and enabling their wholehearted pursuit. I am most appreciative for all that you have given.

To Rebecca I am most indebted for your complete love and devotion. You are my island within the maelstrom of chemistry. Words are inadequate. Thankyou.

Done.

Abbreviations

Å	Ångström (10^{-10} m)
β	overall stability constant
Calcd	calculated
[ ]	concentration
dec.	decomposes
δ	chemical shift
DMF	*N,N*-dimethylformamide
DMSO	dimethyl sulphoxide
ε	molar extinction coefficient
HEPES	*N*-2-hydroxyethylpiperazine-*N'*-2-ethanesulphonic acid
HSAB	Hard and Soft Acids and Bases
I	ionic strength
J	coupling constant
K	apparent stability constant
L	unspecified ligand
lit.	literature
λ_{ex}	fluorescence excitation wavelength
λ_{max}	maximum wavelength
M^+	univalent metal ion
M^{2+}	divalent metal ion
M^{n+}	unspecified metal ion
m/z	mass to charge ratio

NMR	nuclear magnetic resonance
PCT	photoinduced charge transfer
PET	photoinduced electron transfer
ppm	parts per million
Φ_F	relative quantum yield
SSD	sum of the squared deviation
T	temperature
THF	tetrahydrofuran
TLC	thin layer chromatography
Tosyl	*p*-toluene sulfonyl
UV	ultraviolet

Chapter 1 Introduction

Numerous metal ions are ubiquitous in living organisms and the environment at large. A multitude of basic functions could not be achieved without them. The transmission of nerve impulses, muscle contractions and the regulation of cell activity are dependent upon the action of Na^+, K^+, Mg^{2+} and, amongst others.[1] In addition, many proteins (the so-called metalloenzymes) are regulated by metal ions such as carbonic anhydrase which contains Zn^{2+} at the active site. Metal ions such as Mg^{2+} and Mn^{2+} have a central role in photosynthesis, from light harvesting by chlorophylls containing a magnesium porphyrin-based system to oxidation of water for oxygen production.[2] From the environmental viewpoint, Hg^+, Cd^{2+} and Pb^{2+} are all major pollutants. For instance, Pb^{2+} toxicity has been implicated in anaemia and the impairment of childhood development, particularly intellectual performance.[3]

Due to the widespread importance of metal ions there is a general need to detect and monitor the presence, absence or levels of metal ions in a variety of areas, whether it be measuring environmental pollution or determining the role of metal ions in individual cells or tissues in biomedical research.[4]

1.1 Metal Ion Detection

Numerous analytical methods are currently available for the detection of metal ions. Techniques such as atomic absorption spectrometry, ion selective electrodes, electron microprobe analysis, etc., are all extremely useful.[5] However, they are often expensive, may require sample pre-treatment, separation or concentration, and they do not allow for real-time monitoring. Fluorescence usually occurs in the visible spectral region and can be determined in real time, in solution or at interfaces, without excessively sophisticated and expensive instrumentation.[6] The sensitivity of fluorescence can even enter the single molecule domain, under appropriate conditions.[7,8]

Accordingly, fluorescence based sensors can have distinct advantages. There are many ways in which a fluorescent signal can be modulated, including an increase or decrease at a single wavelength, simultaneous intensity increase at one wavelength and a decrease at another (ratiometry) or even fluorescent lifetime changes.[9] Moreover, for biochemical

applications local observation is possible with the use of fluorescent imaging spectroscopy.[10]

A fluorescent sensor can generally also be used under UV-visible absorbance conditions since fluorescence is intimately related to the process of absorption (see Section 3.1). However, UV-visible absorbance sensors can be less desirable for a range of reasons. For biological applications, exposure to significant levels of UV radiation can cause cell and tissue damage. Fluorescence sensors are more sensitive than those based on absorption due to the lower sensor concentrations involved and the easy detection of fluorescence against a dark background (as emission occurs at a different wavelength to excitation).

1.2 Design Principles of a Fluorescent Sensor

Sensors in general are devices that signal the presence of an analyte reversibly and in real-time. Like catalysts, sensors are not consumed by the act of sensing. In supramolecular chemistry, defined as "chemistry beyond the molecule",[11] a sensor is a two component system in which an intended substrate receptor is connected to a subunit capable of signalling the occurrence of the receptor-substrate interaction.[12]

Arising from the two different processes occurring during analyte detection, molecular recognition and signal transduction, a modular approach to rational sensor design is generally employed.[13] Therefore, a fluorescent sensor for metal ion recognition may consist of three different components.

The first requirement is a recognition element (receptor) capable of the complexation of a single species from amongst a mixture of other possible analytes. Secondly, a responsive signalling unit (fluorophore) is required that produces a distinct signal alteration immediately upon a complexation event occurs. The final requirement is a spacer (real or virtual) that covalently links the fluorophore and receptor moieties so as to allow their interaction. In principle, a fluorescent sensor for any kind of analyte can be built following the Fluorophore-Spacer-Receptor approach.[14]

Most crucially, an intramolecular mechanism must exist that associates substrate binding and emission activity of the fluorophore. The recognition event can be signalled through a range of fluorescence properties (*vide supra*). Fortunately, many opportunities exist for modulating the photophysical properties of a fluorophore, such as the introduction of proton-, energy- and electron-transfer processes, the presence of heavy-atom effects,

changes of electronic density, and the destabilisation of a non-emissive nπ* excited state.[13] As a result, there are a wide range of possibilities for the design of efficient fluorescence sensors.

Many fluorescent sensors that selectively respond to biologically important ions, including H^+, Na^+, K^+, Mg^{2+}, Ca^{2+} and Zn^{2+} already exist, some of which are commercially available.[15,16] Despite this, the list of fluorescent sensors remains short and requires increased diversification.[4,6,17] Furthermore, targeting metal ions also gives insights into some of the desired characteristics that would allow the sensing of molecular analytes (glutamate, acetylcholine, carbohydrates, etc.), a topic of great interest in biological studies.[18]

1.3 Photoinduced Electron Transfer (PET) Based Fluorescent Sensors

1.3.1 Principles

Fluorescent sensors can incorporate photoinduced electron transfer (PET) as the mechanism of relating the complexation event at the receptor to the signalling fluorophore group. In these Fluorophore-Spacer-Receptor modular designs, the spacer moiety holds the fluorophore and receptor close to, but separate from, each other.[19] A scheme describing the utilisation of a PET process for fluorescent signalling is shown in Figure 1.1.

Upon excitation of the fluorophore, an electron of the highest occupied molecular orbital (HOMO) is promoted to the lowest unoccupied molecular orbital (LUMO). This enables PET from the HOMO of the donor (belonging to the metal ion free receptor) to that of the fluorophore. The resultant charge separated state has no fluorescent decay pathway available and the excited state energy is eventually lost in a non-radiative manner through back electron transfer that destroys the biradical state.[20] The net result is the fluorescence of the fluorophore is quenched when the receptor is unbound via a PET process.

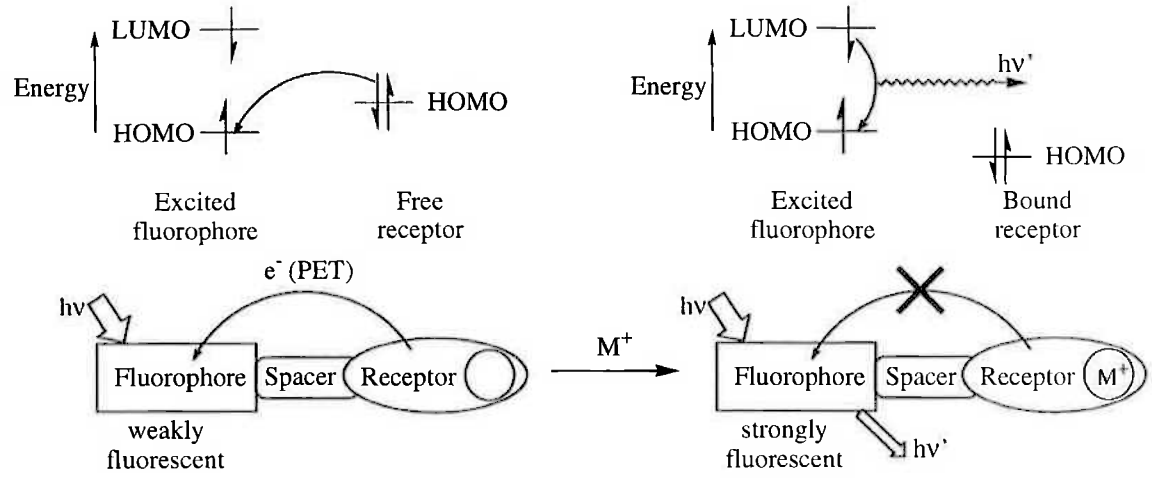

Figure 1.1. *Schematic representation of a photoinduced electron transfer (PET) processes in a Fluorophore-Spacer-Receptor signalling system.*

Metal ion complexation induces an increase in the ionisation/oxidation potential of the donor (receptor) such that the relevant HOMO becomes lower in energy than that of the fluorophore. Consequently, PET slows down (or no longer occurs) and fluorescence quenching is suppressed which thereby restores fluorescence as the dominant decay pathway of the photo-excited fluorophore. In other words, the fluorescence intensity is enhanced upon metal ion binding.[21] Alternative directions for PET are also exploitable and other ways of inhibiting electron transfer are available (e.g. conformational changes or hydrogen bonding), as will be shown below.

Direct experimental evidence for the mechanism of PET mediated fluorescence quenching was recently acquired by time-resolved fluorescence spectra with a femtosecond laser using phenylimidazoanthraquinone (fluorophore) appended, via a methylene spacer, with monoaza-15-crown-5 (receptor) (**4**, see Section 1.3.2).[22]

In the absence of metal ions, the excited singlet of **4** decayed with a lifetime of 5.8 ps, whereas in the presence of a metal ion the excited singlet fluorophore decayed with a lifetime of 200 ps. This increase in lifetime is due to the considerable retardation of the electron transfer process upon metal ion complexation and effectively describes the fluorescence switching mechanism. That is, upon metal ion complexation the PET reactions were considerably inhibited. It was found that when the receptor was metal ion bound, the PET process remained operative though only to a limited extent.[22] Furthermore, the phenylimidazoanthraquinone anion radical was observed which is direct evidence of PET mechanism.

A distinct advantage of PET based fluorescent sensors is the very large change in fluorescence intensity usually observed upon metal ion binding, such that the expression OFF/ON fluorescent sensors is often employed.[6] Large complexation-induced fluorescence enhancement is a highly desirable characteristic for a fluorescent sensor as it allows for the appearance of a signal from a dark background (low detection limits) and high signal-to-noise ratios.[23] One drawback of fluorescence OFF/ON switching of this type is the absence of any shift in the fluorescence emission (or absorption) spectra which precludes the possibility of intensity-ratio (ratiometric) measurements at two wavelengths.

The following examples of PET sensors illustrate some of the multitudinous combinations of both receptor and fluorophore that have been used in the development of fluorescent sensors. Most are directed towards metal ion sensing although some examples of other analytes are included to show the versatility of PET fluorescent sensors.

1.3.2 Crown Containing PET Sensors

The most commonly utilised design to date for PET fluorescent sensors combines an amine containing receptor with a simple aryl fluorophore with a methylene spacer which allows for the mutual interaction between the nitrogen lone pairs and the aromatic π cloud.

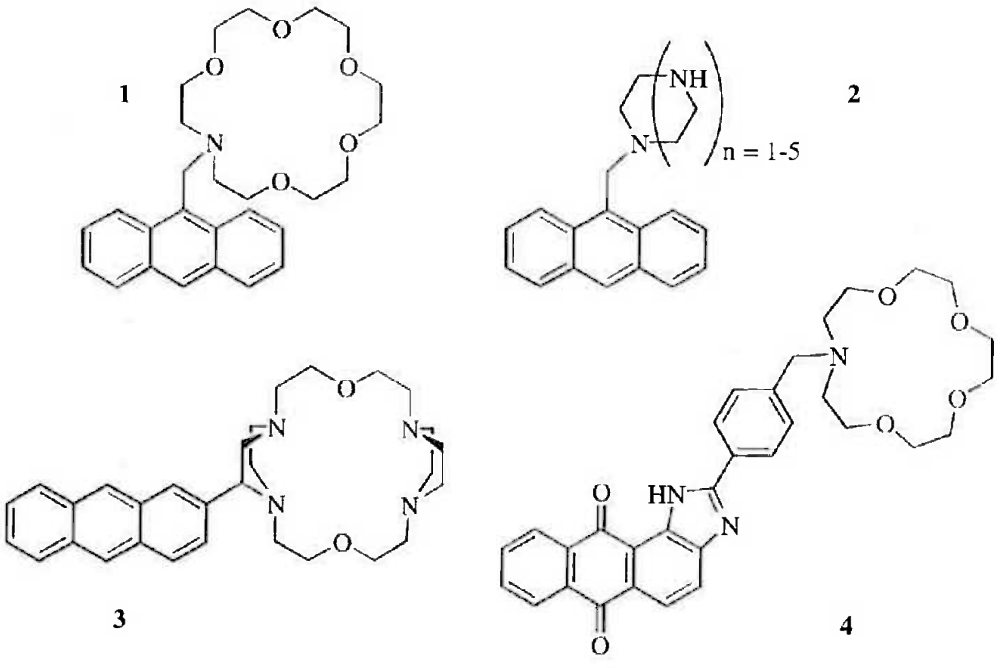

An early example of the modular Fluorophore-Spacer-Receptor PET based design system is **1** utilising monoaza-18-crown-6 as the receptor and anthracene as the fluorophore.[24] Sensor **1** was found to complex Na^+ and K^+ (K = 2.5 x 10^4 dm^3 mol^{-1}) although not Li^+ in

methanol. The increase in quantum yield (Φ_F) from 0.003 to 0.14 upon binding K^+ exemplifies the OFF/ON switching of this sensor design.

Czarnik and co-workers[25] have studied a series of polyazamacrocyles appended to an anthracene fluorophore in the 9-position (**2**). The 1,4,7,10-tetraazacyclododecane (cyclen) macrocycle containing sensor displayed a 14-fold fluorescence enhancement in the presence of Zn^{2+} in pH 10.0 buffered aqueous solution and a smaller 9-fold enhancement was observed for Cd^{2+}. Unfortunately, the series of compounds (**2**) were not stable in acidic solutions when exposed to UV light. No binding with Zn^{2+} and Cd^{2+} (or Al^{3+}, Pb^{2+} and Cu^{2+}) was observed when cyclen was replaced with piperazine.[25] A further aspect of compound **2** are the basic nitrogen sites, a common feature in PET based sensors. Protonation of the benzylic amine nitrogen was found to give the largest increase in fluorescence (20-fold for the cyclen receptor) as a proton interacts most efficiently the amine nitrogen lone pair, suppressing PET.[25,26]

Using the same anthracene fluorophore with different substitution shows a marked influence. Compound **3** was designed to be soluble in water yet no metal ion complexation could be observed in an aqueous environment.[27] However, it was found that quenching by a benzylic amine in the 2-position of anthracene was not as efficient as in the 9-position as only a 3.6-fold increase in fluorescence was observed upon protonation of **3**.[27] This compound is also an example of the modular design concept, as the receptor was used since it had a known propensity for a particular metal ion (Pb^{2+}) in an attempt to achieve selectivity.[28]

Other fluorophores have also been exploited for PET based sensors, such as the phenylimidazoanthraquinone compound **4** (Φ_F 0.00021).[29] Utilising monoaza-15-crown-5 as the receptor, a maximum stability constant of 3.24×10^6 dm^3 mol^{-1} is obtained with Ca^{2+} in acetonitrile (Li^+, Na^+, Mg^{2+}, Ca^{2+} and Ba^{2+} were also studied).[29] Only a 7.7-fold increase in fluorescence when complexed with Ca^{2+} was observed and the low quantum yield values probably preclude the use of **4** as a fluorescent sensor.

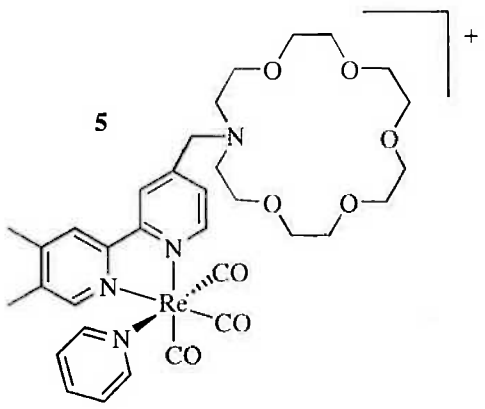

The fluorophore used can even be transition metal based as shown by **5**.[30] Complexation of Pb^{2+} (K = 2.5 x 10^4 dm^3 mol^{-1} for deprotonated **5**) in aqueous solution restores the metal-to-ligand charge transfer (MLCT) based fluorescence emission although the fluorescence increase is small.

1.3.3 Cryptand Based PET Sensors

Cryptands have been used in an attempt to increase the selectivity of a sensor for a particular metal ion as they show strong complexation due to the cryptate effect.[31] Also, the cavity is somewhat shielded from outside interference. A simple anthraceno-cryptand **6** could complex K^+ with a 7.5-fold increase in the quantum yield with little change in the UV-visible absorbance spectrum.[32] The lack of any significant changes in absorption is expected for a PET based fluorescent sensor since the quenching mechanism only affects the excited state.[6]

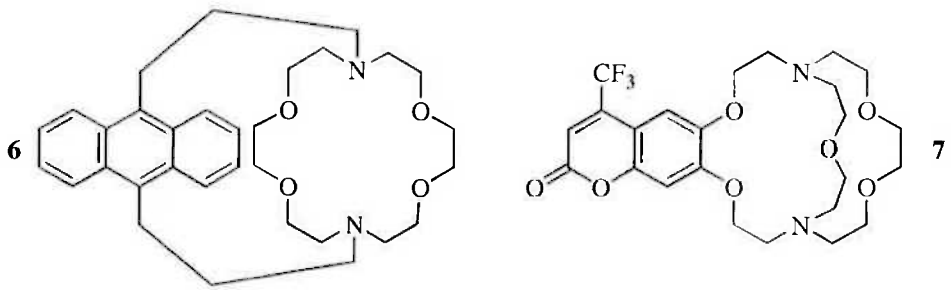

A similar design is shown by the trifluoromethylcoumarino cryptand **7** which can selectively bind Na^+ over K^+, as expected due to the known selectivity of the cryptand receptor.[33] This ligand has been further studied and it was found that protonation of both nitrogens was necessary to restore the maximum fluorescence emission (Φ_F 0.60) as singly protonated **7** (Φ_F 0.07) was only slightly more fluorescent than the fully deprotonated

ligand (Φ_F 0.04).[34] As will be discussed later, this result shows that the participation of a single amine nitrogen in the PET mechanism is sufficient to quench the fluorescence of **7**.

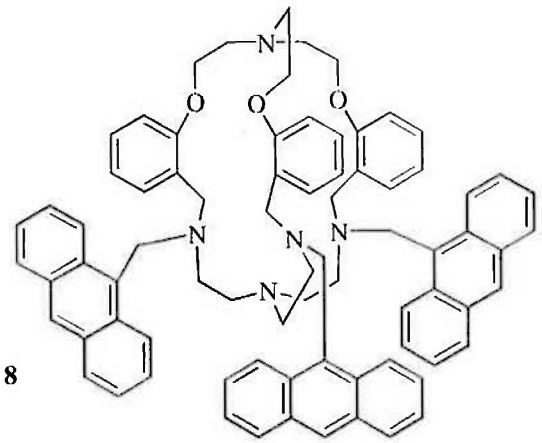

8

Compound **8** utilises a cryptand as an effective means of insulating the fluorophore (anthracene in this case) from direct interaction with the metal ion.[35] This design was chosen to afford fluorescence enhancement in the presence of metal ions know to exert a 'heavy atom' effect.[36,37] For example, Pb^{2+} (180-fold) and Fe^{3+} (226-fold) displayed significant fluorescence enhancement in tetrahydrofuran.[35]

1.3.4 Simple Podand Based PET Sensors

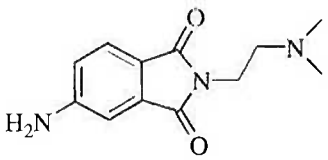

9

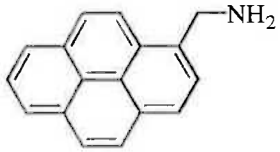

10

In contrast to the elaborately designed cryptands, a structurally very simple sensor for transition metal ions is exemplified by **9**.[38] For efficient fluorescent sensing, the metal ion-fluorophore communication should be much less than the metal ion-receptor interaction and so using an electron deficient fluorophore minimises the redox interaction between the fluorophore and the metal ion.[38] This enhances PET quenching in the unbound state and can negate the inherent quenching ability of some metal ions. The concept was successful as **9** showed fluorescence enhancement with transition metal ions such as Cu^{2+} (41-fold) and Ni^{2+} (37-fold) in acetonitrile.[38]

The substituted pyrene **10** is among the simplest PET fluorescent sensors yet designed.[39] It utilises reversible covalent binding of carbon dioxide in *N,N*-dimethylformamide solution to retard the nitrogen-to-pyrene PET quenching mechanism by carbamate formation.

Subsequent bubbling of nitrogen through the CO_2 rich solution containing **10** caused the fluorescence emission to return to basal levels. Again, as is usual for the PET mechanism, no change in the UV-visible absorbance spectrum was observed.[39]

1.3.5 PET Sensors with Rigid Spacers

Utilising a short, rigid spacer can allow the conformational separation of the receptor and fluorophore that can be advantageous for the detection of inherently quenching metal ions. Substituted 1,3,5-triaryl-Δ^2–pyrazoline **11** affords isolation of the *N*-phenylazacrown receptor from the 1,3-diarylpyrazoline fluorophore in terms of their π-electron systems via the pseudo-spiro conformation of the *N*-phenylazacrown receptor.[40]

11

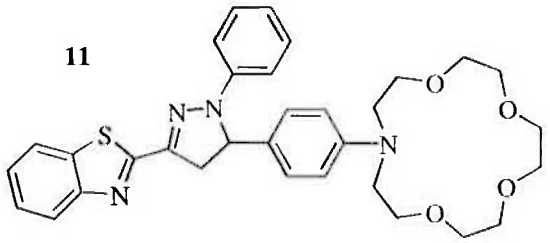

The best fluorescent response for **11** in the presence of metal ions was a 44-fold increase in the quantum yield upon the complexation of Ca^{2+} (K = 7.76 x 10^4 dm^3 mol^{-1}) in acetonitrile, with a concomitant increase in the fluorescence lifetime (0.03 to 3.99 ns).[41] When complexed, **11** displayed a large decrease in the rate of non-radiative decay of the excited state with little change in the rate of fluorescence decay, compared with the unbound state. That is, the fluorescence decay rate remains almost constant but the rate of non-radiative decay is altered upon complexation. Consequently, upon metal ion complexation, fluorescence can compete more effectively to become the preferred excited state decay pathway and so the fluorescence emission increases. This result is a further elucidation of the PET quenching mechanism.

1.3.6 Other Sensor Designs that Harness PET

The compounds described thus far all utilise an amine nitrogen-to-fluorophore PET pathway. However, a PET based fluorescent sensor can exploit other pathways for photoinduced electron transfer, as illustrated by **12**. Employing the open-chain counterpart of dioxocyclam as the receptor, **12** displays fluorescence emission quenching when complexing Cu^{2+} or Ni^{2+} in acetonitrile-water (4:1) solution. The quenching is derived from a photoinduced electron transfer mechanism. Quenching was shown not to be a

Dexter type energy-transfer mechanism (simultaneous double electron exchange)[42] by studies in frozen glass solution as the fluorescence emission was restored upon cooling a solution of **12** and Cu^{2+} to 77 K.[43] This is because the PET pathway mechanism generates charge separation that requires a drastic rearrangement of the solvation sphere, a process prevented by immobilising the solvent in a frozen glass. Consequently, upon cooling, PET becomes inoperative and fluorescence emission is restored.[43] In a related compound containing only amine groups, quenching solely by an energy transfer mechanism was observed.[43] Without the amide groups the oxidation potentials had changed such that the Cu^{3+} state could not be attained, precluding the occurrence of PET from metal-to-fluorophore.[43]

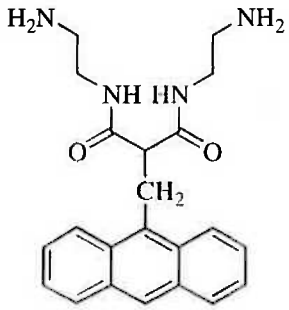

12

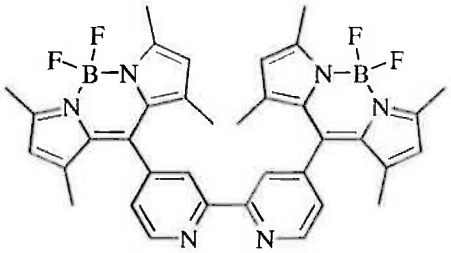

13

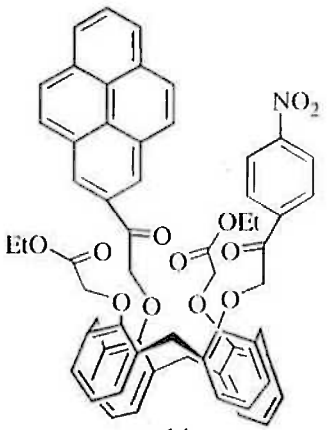

14

An example of excited state fluorophore-to-receptor quenching (oxidative PET) is the boradiazaindacene (BODIPY, BDP) fluorophore appended bipyridyl receptor compound **13**.[44] When **13** is complexed by Zn^{2+} (K = 1.1 x 10^7 dm^3 mol^{-1}) in acetonitrile the fluorescence emission is significantly quenched, with a decrease in the quantum yield from 0.39 to 0.002 in the complex.[44] Similar quenching was also observed for Cd^{2+}, Cu^{2+}, Hg^{+} and K^{+}, although to a lesser extent as these metal ions were complexed less strongly.

Another method of controlling a PET process for fluorescent sensing is through manipulating the proximity of a donor and acceptor. Shinkai and co-workers have achieved this by employing nitrobenzene as the electron acceptor and pyrene as the electron donor on a calixarene scaffold.[45] Addition of Na^{+} (K = 2.0 x 10^4 dm^3 mol^{-1}) to diethyl ether-acetonitrile (97:3) solutions of **14** caused the intensity of fluorescence emission to increase 6-fold although the quantum yield remained low (Φ_F 0.016). The emission of pyrene is quenched in the free ligand as a consequence of PET from excited state pyrene to the nitrobenzene acceptor. Complexation of Na^{+} causes the arms of the

calixarene to be conformationally restricted such that the nitrobenzene acceptor group is far removed from the electronically excited pyrene. Accordingly, PET is diminished and fluorescence is revived.[45]

1.3.7 Dual PET input sensors

Compounds with two distinct PET pathways have been used for the study of logic operations at the molecular scale.[46] Selectivity of two different metal ions depending on the acidity of the medium has been achieved.[47-49] A molecule with a third PET pathway has also been studied.[50]

15

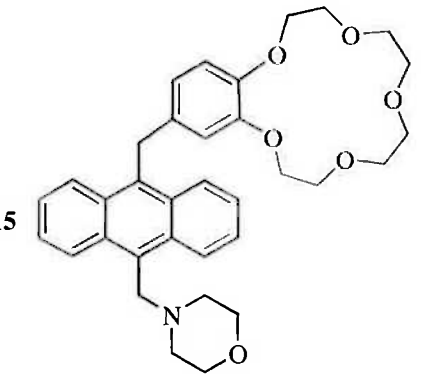

An example of the general concept is **15**, a 9,10-disubstitued anthracene that contains a benzo-15-crown-5 ring and morpholine ring.[51] As expected, the fluorescence emission of **15** is quenched by the tertiary amine at high pH. Upon protonation, the fluorescence is not restored since the protonated amine moiety acts as an electron withdrawing group on the anthracene leading to a second PET pathway from the benzo-crown to the excited fluorophore. Accordingly, only when this second PET pathway is disrupted by the addition of Na^+ is a 92-fold fluorescence enhancement observed (compared with non-protonated **15**).[51]

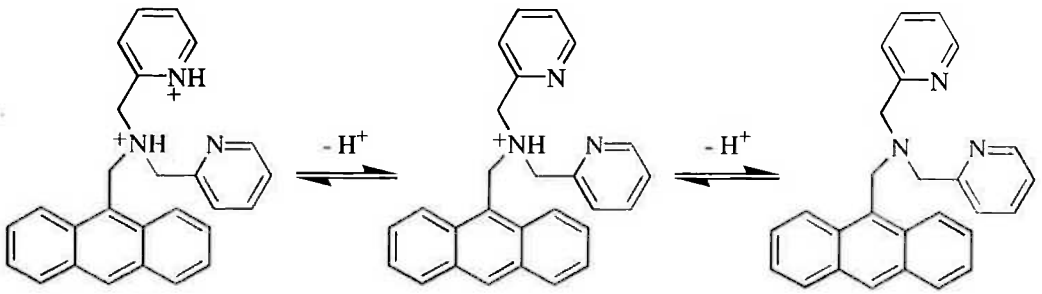

16.2H+ non-fluorescent

16.H+ fluorescent

16 non-fluorescent

In a similar manner, dual fluorescence switching has also been utilised in **16** which incorporates two independent PET switches (the tertiary amine and the pyridyl group).[52] The fluorescence of **16** is quenched by the non-protonated aliphatic tertiary amine at high pH and at low pH by the protonated pyridinium group (PET process from excited fluorophore to pyridinium group). Consequently, fluorescence is only observed within a narrow pH window (pH 4-8) in which the aliphatic tertiary amine is protonated and the pyridyl moiety is non-protonated.[52] This idea as been further extended to allow for modulation of the pH-window response by a metal ion.[53]

1.3.8 PET Sensors for Anions or Molecular Analytes

17

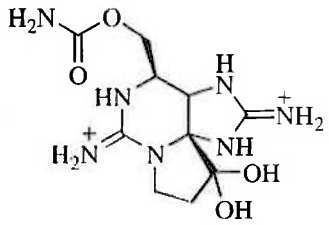

The PET based fluorescent sensor design is not limited to detecting metal ions as exemplified by **1** (Section 1.3.2) which, in addition to metal ions, binds the molecular target saxitoxin **17**.[54] Saxitoxin is a marine toxin produced by dinoflagellates and several blue-green algae species that can contaminate shellfish. As human death (from respiratory paralysis), arising from the consumption of contaminated shellfish, is caused by the ingestion of less than 0.5 mg of saxitoxin, its sensitive detection is of some importance.

Upon binding of saxitoxin by **1** in ethanol (K = 3.8 x 10^3 dm^3 mol^{-1}), hydrogen-bond formation to the benzylic nitrogen retards the normal PET process and so fluorescence enhancement (up to 20-fold) is attained.[54] It was established that it was not simple protonation of **1** causing the fluorescence enhancement.[54] Attempts have also been made to utilise **1** as a fibre optical fluorescence sensor via the use of a thin film such as a self-assembled-monolayer, although self-quenching and other issues remain to be resolved.[55]

18

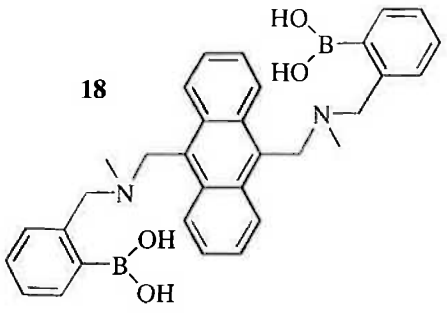

A fluorescent sensor (**18**) for glucose consisting of two boronic acids with adjacent tertiary nitrogens arranged to form a cleft like structure has been studied.[56] The Lewis acidity of boronic acids is enhanced when they interact with a saccharide (via the diol moiety).[57] As a result, the boron-nitrogen interaction in **18** is strengthened upon the saccharide binding event, suppressing the usual PET process, thereby restoring fluorescence.[58] The dual receptor design of **18** was chosen to give two binding sites directed to the 1,2- and 4,6-hydroxy groups of D-glucose so that selectivity over other monosaccharides might be achieved. A stability constant of 4.0 x 10^3 dm^3 mol^{-1} with D-glucose is obtained at pH 7.77 in methanol-water (1:2) solution.[56]

This sensor also further illustrates the necessity that both nitrogens be involved in complexation for the PET quenching mechanism to be arrested as the non-cyclic (glucose)•(**18**) complex is not fluorescent (sugar occupies only one receptor). Conversely, the cyclic (glucose)•(**18**) complex (structure confirmed by ^{1}H NMR) and the $(glucose)_2$•(**18**) complex restored the fluorescence signal. Additional evidence for the cooperative binding with **18** is that the stability of the (glucose)•(**18**) complex is much higher than a related sensor containing only one boronic acid receptor.[59]

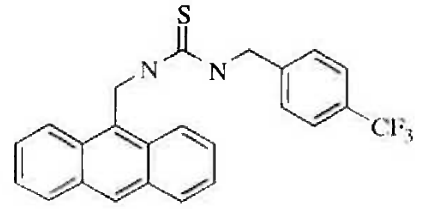

19

Finally, PET based anion fluorescence detection has also been achieved. Compound **19** binds acetate (K = 2.24 x 10^3 dm^3 mol^{-1}) in dimethyl sulphoxide solution with a resultant quenching of fluorescence.[60] Binding acetate allows PET to occur from the thiourea-acetate complex to the excited state, causing the quenching. The work was extended by the formation of a 9,10-disubstituted anthracene using the same receptor that displayed quenching with bis-anions (such as malonate).[61]

1.3.9 Ternary PET Sensors

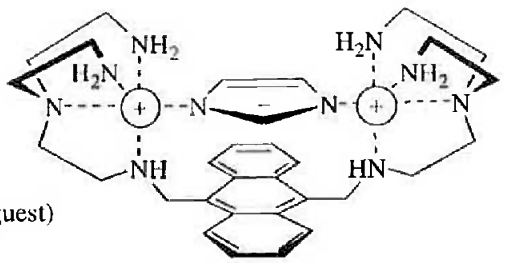

20.$(Zn^{2+})_2$.(guest)

Broadening the design of fluorescent PET sensors may be achieved through the control and modulation of PET processes through the complexation of guest molecules, which intercalate between the donor and acceptor groups. Complexation of Zn^{2+} with **20** displays the usual fluorescence enhancement due to suppression of PET. However, adding imidazole to a solution containing $(Zn^{2+})_2$•(**20**) results in the deprotonated imidazole binding between the two metal ions. This causes fluorescence quenching as PET occurs from the anion to the excited state anthracene.[62]

A similar design strategy has also been used to bind aromatic carboxylates[63]and to detect a phosphorylated peptide.[64]

1.4 Photoinduced Charge Transfer (PCT) Based Fluorescent Sensors

1.4.1 Principles

If the spacer between the fluorophore and receptor is removed completely, a fluorescent sensor is obtained where the fluorophore and receptor share the same π–system and are in direct electronic conjugation. These intrinsic sensors are usually designed as substituted π–systems with electron-donating (D) and electron-accepting (A) fragments, and their excited state behaviour is governed by a photoinduced intramolecular charge transfer (PCT) process. Upon excitation by light, PCT from donor to acceptor occurs that results in a change in the dipole moment. Thus, a metal ion that interacts closely with the donor or acceptor will induce changes in the photophysical properties of the fluorophore since the metal ion influences the efficiency of the PCT process (Figure 1.2).

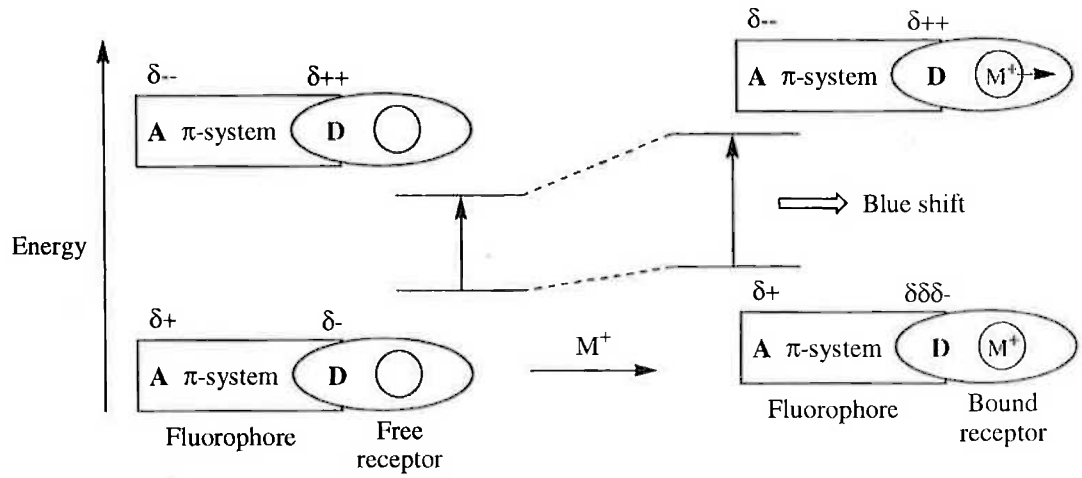

Figure 1.2. *Schematic representation for the photophysical processes occurring in an intrinsic Donor(D)-Acceptor(A) fluorescent sensor upon metal ion complexation. In the absence of M^+, electronic excitation reverses the dipole and increases its magnitude. In the ground state complexation of M^+ by D decreases the dipole in A, electronic excitation reverses and strengthens the dipole in A. δ- and δ+ represent dipole moment (δ+ < δ++, δδδ- < δ- < δ--).*

In most PCT fluorescent sensors the metal ion receptor (containing an amino group) is located in the donor part of the π–system and so metal ion complexation reduces the electron-donating character of the donor.[21,65] The resulting reduction of π–conjugation causes a blue shift of the absorption spectrum and a decrease in the molar extinction coefficient (a metal ion interacting with the acceptor group enhances the electron-withdrawing character of the acceptor, the absorption spectrum is red-shifted and the molar absorption coefficient is increased). Accordingly, the fluorescence emission spectra are in principle shifted in the same direction as that of the absorption spectra.[6,21,65]

The photophysical changes upon metal ion complexation can also be described in terms of charge dipole interaction. When a metal ion interacts with the donor group, the excited state is more strongly destabilised by the metal ion than the ground state, and a blue shift of the absorption and emission spectra is observed. Conversely, when the metal ion interacts with the acceptor group, the excited state is more stabilised by the metal ion than the ground state, and this leads to a red shift of the absorption and emission spectra.[21]

The shift in the fluorescence emission spectrum is generally less than that observed in the absorption spectrum. The PCT process reduces the electron density on the nitrogen atom of the donor, and so this nitrogen atom becomes a non-coordinating atom due to it is positive polarisation. Therefore, excitation destabilises the interaction between the

positively charged metal ion and the nitrogen atom of the donor so the metal ion moves away from the nitrogen in the excited state.[66] The result is that fluorescence emission is only slightly affected because the majority of the emission observed is emitted from species in which the interaction between the metal ion and the fluorophore is significantly weaker (or non-existent) than observed for the absorption spectrum.[21] Photo-ejection of the metal ion does not necessarily occur as a solvent-separated metal ion-sensor pair may form.[67] Furthermore, twisted intramolecular charge transfer (TICT) processes could also be involved.[68,69]

PCT based fluorescent sensors often lead to pronounced spectral shifts in both absorption and emission but only small changes in fluorescence intensity and lifetime are normally found. Consequently, they are generally used as wavelength-ratiometric sensors (contrast PET based sensors which are more focussed on ON-OFF switching).

1.4.2 Examples of PCT Based Fluorescent Sensors

Many fluorescent sensors have been designed utilising the PCT principle whereby a metal ion receptor containing a nitrogen is an integral part of a fluorescent group that contains an appropriate electron withdrawing group. A typical example is **21** where an azacrown has been appended to a merocyanine fluorophore.[70]

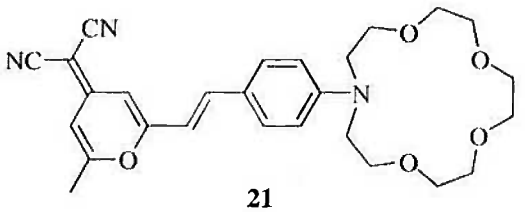

21

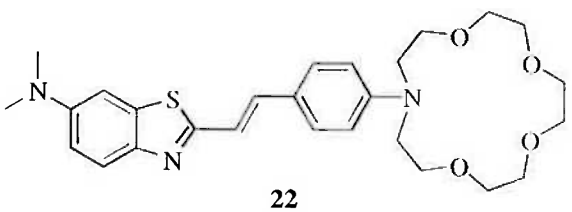

22

Complexation of **21** (Φ_F 0.73) with alkali and alkaline earth metal ions in acetonitrile results in fluorescence quenching and a slight hypsochromic shift of the emission spectra, the extent of which was strongly dependent on the nature of the metal ion.[70] For example, the presence of Li^+ (K = 3.16 x 10^2 dm^3 mol^{-1}) gave slight quenching with a quantum yield of 0.57 and further quenching for Ca^{2+} (K = 5.25 x 10^3 dm^3 mol^{-1}) was observed (Φ_F 0.27).[70] This is due to the ability of the metal ion to hinder the charge transfer, destroying the usual fluorescence decay pathway, and so the quantum yield decreases. As expected for a PCT fluorescent sensor (*vide supra*), the absorbance spectra in the presence of metal ions showed a large hypsochromic shift (from 464 to 398 nm with Ca^{2+}) with a decrease in

molar absorbance. This effect is indicative of removal of the lone electron pair of the nitrogen atom of the receptor from the conjugated π-system.

A slightly different design incorporates a second donor group into the simple donor-acceptor model. Thus, **22** contains a dimethylamino moiety in addition to the nitrogen donor that is part of the receptor and so is referred to as a $donor_1$-acceptor-$donor_2$(receptor) type sensor. This design allows a switch between the moderately fluorescent D_1-A-D_2 constitution of the free ligand to the D_1-A-A_2 constitution of the complex, provided that the subunits are well matched.[71,72]

The fluorescence emission of **22** undergoes a bathochromic shift in acetonitrile upon metal ion complexation with an increase in emission intensity (32-fold for Ca^{2+}, K = 3.31 x 10^4 dm^3 mol^{-1}).[71] This supports the idea that complexation converts D_2 into an acceptor (A_2) so PCT occurs only from the dimethylamino moiety resulting in an extension of the emissive π-system. Such a large fluorescence enhancement is rare for a PCT based fluorescent sensor and reflects the careful design.[23] Only a small 12 nm hypsochromic shift in the UV-visible absorbance with Ca^{2+} was observed.

Many of the fluorescent sensors in current medical and biological usage are based on the PCT design such as **23** (SBFI) and **24** (Indo-1) which are commercially available.[15]

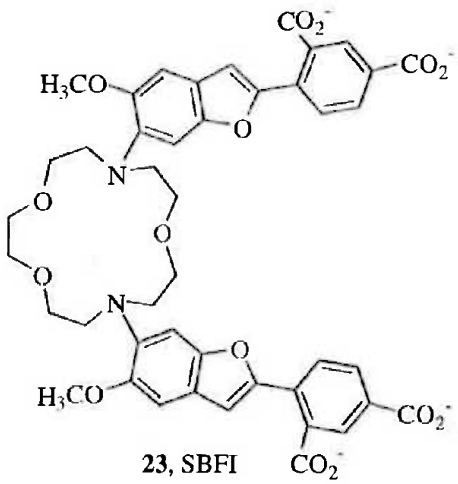

23, SBFI

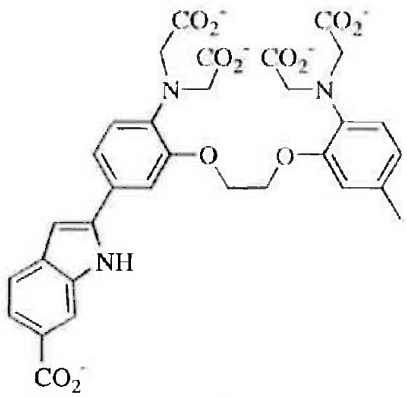

24, Indo-1

An improvement in metal ion selectivity can be achieved through the use of lariat binding. In **23**, comprised of benzofuranyl fluorophores linked to a crown ether, the oxygen atom of the methoxy substituent on the fluorophore is involved in complexation such that the stability and selectivity of **23** is greater than observed for the diazacrown alone.[73] The cavity size of the crown ether confers selectivity for Na^+ over K^+. When Na^+ binds to **23**

(K = 1.4 x 10^2 dm^3 mol^{-1}) its fluorescence quantum yield increases two-fold and the emission maximum shifts to shorter wavelengths. A shift of absorbance to shorter wavelengths also occurs and this is consistent with a mechanism in which metal ion binding causes a major loss of conjugation between the amino groups and the rest of the chromophore, at least partly by twisting the nitrogen-aryl bond.[73]

A sensor that employs a chelator as the receptor group is **24** (Indo-1).[74] The emission maximum of **24** shifts from 485 nm (Φ_F 0.38) when unbound, to 410 nm (Φ_F 0.56) when in the presence of Ca^{2+}, whereas the absorption spectrum only undergoes an 18 nm hypsochromic shift.[74] The absorption shift is expected as the Ca^{2+} monopolises the lone pair of electrons on the amine nitrogen, possibly by twisting the bond between the nitrogen and the ring, thereby disrupting the conjugation between the lone pair and the rest of the chromophore.[74] The large shift in emission wavelength is surprising as generally little change is expected (Section 1.4.1). It has been suggested that the PCT process in **24** produces a less polar charge-transfer state than is generally associated with PCT sensors and so it is insufficient to break the nitrogen-Ca^{2+} bond in the excited state. This results in a large hypsochromic shift in the emission spectrum.[21]

The above examples of PCT based fluorescent sensors involved the receptor group as an integral part of the receptor. Alternatively, the complexed metal ion can interact with the acceptor of the fluorophore. Sensor **25** appears to be a spaced PET based sensor, yet it is metal ion-acceptor type interactions that dominate and cause the photophysical changes. Complexation of Ca^{2+} with **25** (K = 6.3 x 10^7 dm^3 mol^{-1}) in acetonitrile induces a bathochromic shift (30 nm) in the absorbance spectrum due to the interaction of the complexed metal ion with the carbonyl group increasing its electron withdrawing character.[75] The dipole moment of the aminocoumarin in the excited state is larger than in the ground state due to the PCT process occurring from the nitrogen atom of the julolidyl ring to the carbonyl group. Thus, the metal ion acts to stabilise the excited state more than the ground state and so a red-shift of the fluorescence emission also results (contrast the blue shift for the sensors described above).[1]

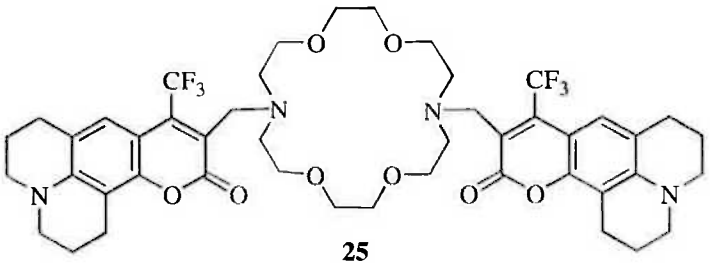

25

The bathochromic shift of the fluorescence emission of **25** correlates directly with the increased charge density of the metal ion for alkali and alkaline earth metal ions.[75] The free ligand has a low quantum yield due to self-quenching since the flexibility of the diazacrown allows the two coumarin moieties into close contact. In complexes with K^+ and Ba^{2+} (6-fold increase in quantum yield), the carbonyl groups of the coumarins are preferentially on the opposite sides with respect to the metal ion and hence quenching is largely suppressed. However, with metal ions that are a poor match for the size of the macrocycle the preferred conformation contains two carbonyls on the same side of the metal ion and so the close proximity of the coumarin moieties causes quenching.[1,75]

1.5 Other Fluorescent Sensor Design Strategies

PET and PCT based fluorescent sensors are by no means the only strategies employed for fluorescent sensors. The modular design and utility for metal ions ensures that these sensors have been well studied. The design strategies shown below may be for a particular analyte (cationic, anionic or molecular) or are more universal in utilising generic aspects of the analyte concerned. A small sample is described below.

1.5.1 Excimer Based Fluorescent Sensors

Excimer fluorescence (*exci*ted di*mer*) results from an interaction of an excited molecule with a ground state molecule of the same chemical identity. Likewise, an exciplex (*exci*ted com*plex*) arises from an interaction with a ground state molecule of different chemical identity. Excimer formation is characterised by decreased normal fluorescence emission with the concomitant appearance of a new broad, structureless emission at longer wavelengths.[69] The excimer is stabilised with respect to a single excited state molecule and so the emission occurs at longer wavelengths. The structureless nature of the emission is proof the ground state is dissociative (i.e. it does not exist) resulting from repulsion of

the ground state molecules.[42] An example of a simulated emission spectrum depicting excimer formation is shown in Figure 1.3.[65]

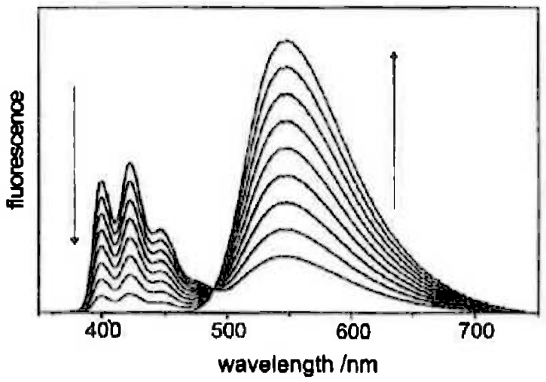

Figure 1.3. *Simulation of analyte induced changes upon complexation to an 'ideal' excimer based sensor displaying a structured monomer emission and a broad excimer emission at longer wavelength.*[65]

A distinct advantage of excimer based fluorescent sensors is that it allows ratiometric detection which is of particular benefit for *in vivo* imaging. Ratiometry is a technique to reduce artifacts in measurement by minimising the influence of extraneous factors on the fluorescence of a sensor, such as variability due to differences in instrument efficiency and content of effective sensor. Ratiometric measurement can provide precise data, and some sensors allow quantitative detection, for example **24**.

26

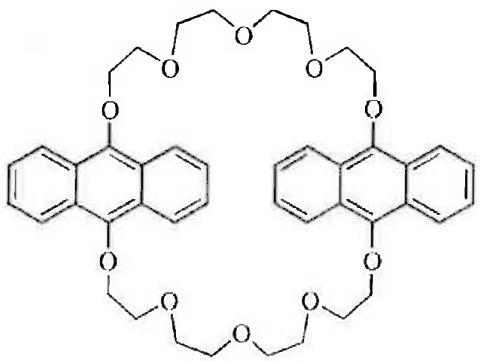

The bisanthraceno-crown ether **26** exhibits a fluorescence spectrum composed of characteristic monomer and excimer bands.[76] Complexation of Na^+ in a cooperative manner to form a $(Na^+)_2$•(**26**) complex (Na^+ in each ether pocket) brings the two anthracene units into close proximity which favours excimer formation and an increase in excimer emission is observed. The complexation of the first Na^+ probably induces the preorganisation of the second binding site favourable to the binding of an additional Na^+.[76]

Contrastingly, the larger K^+ only formed a (K^+)•(**26**) complex as a second K^+ was unable to fit within the cavity formed. Only low overall stability for the complexes in methanol was observed (Na^+, $\beta_2 = 1.18 \times 10^2$ dm^6 mol^{-2}).

1.5.2 Fluorescence Sensors Based on Geometrical Conformation

Another design strategy for fluorescent sensing involves the geometric reorientation of various groups within the molecule to signal complexation.

27

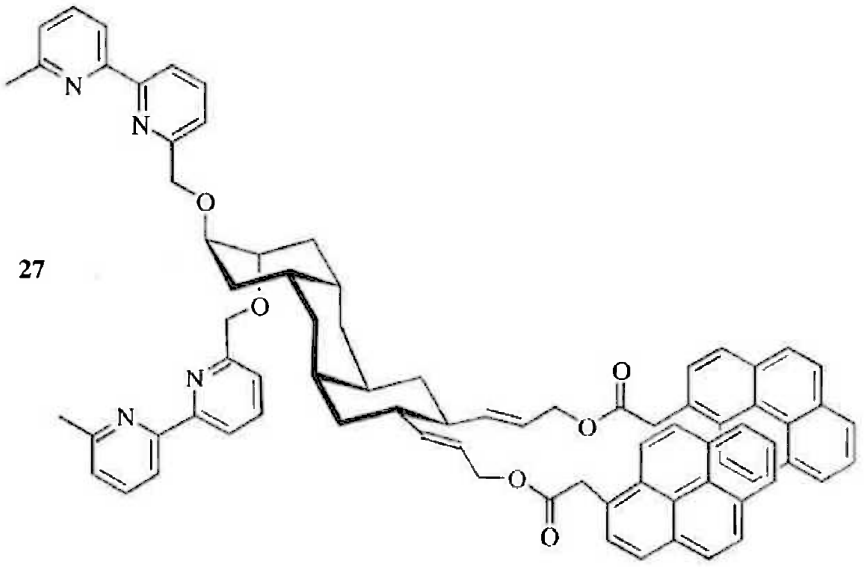

Incorporating excimer formation with a physical reorganisation is **27** which involves a triple ring flip of the perhydroanthracene spacer upon Zn^{2+} complexation by the two 2,2'-bipyridine groups.[77] The conformational rearrangement causes the pyrene groups to assume axial positions and this large movement precludes excimer formation (λ_{max} 480 nm) and so only monomer emission (λ_{max} 380 nm) is observed for the Zn^{2+} bound compound in acetonitrile-chloroform (1:1) solution.[77]

28

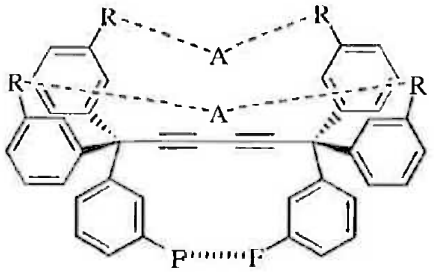

R = Receptor
A = Analyte
F = Fluorophore

Glass and co-workers have recently investigated the conformational rotation of a 'pinwheel' design for fluorescent sensing.[78-80] Compound **28** consists of a bis-trityl butadiyne core that allows free rotation of the trityl groups with respect to each other.

Each trityl group is appended with two receptor groups (1,2-diaminoethane) and one fluorophore (napthyl sulfonanilide).[79] The receptor elements are spatially convergent such that a pair can bind an analyte across the butadiyne axis. Upon coordination of an analyte, the trityl groups are conformationally locked which allows the fluorophores to interact. Thus, the fluorescence spectra in acetonitrile show a substantial increase in the excimer emission (λ_{max} 450 nm) with a smaller monomer increase (λ_{max} 335 nm) upon cooperative complexation of Ag^+ ($\beta_2 = 1.3 \times 10^{11}$ dm^6 mol^{-2}). The increased excimer emission upon complexation is due to the close proximity of the two fluorophores when Ag^+ is bound. The slight increase in monomer emission arises from suppression of PET processes between the nitrogen receptors and the fluorophore.

A related design strategy involves the conformational restriction of biaryl fluorophores by metal ion complexation to induce fluorescence.[81,82]

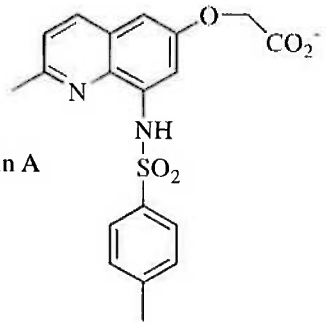

29, Zinquin A

Finally, conformational reorganisation may simply involve restriction of rotation within the extended π–system of a fluorophore to allow fluorescence emission. A sensor developed within our group is **29** (Zinquin-A) which displays a large increase in fluorescence upon Zn^{2+} coordination.[83] Coordination of Zn^{2+} to **29** increases the rigidity of the ligand due to restriction of both vibration in the quinoline ring and cessation of rotation about the sulphonamide to ring bond. This enhances the π-orbital overlap and so a bathochromic shift in the absorption spectrum results. The fluorescence emission increases upon complexation as a more rigid molecule results in fewer non-radiative decay pathways for the excited singlet exist and so fluorescence becomes the preferred relaxation pathway.

1.5.3 Peptide Based Fluorescent Sensors

30

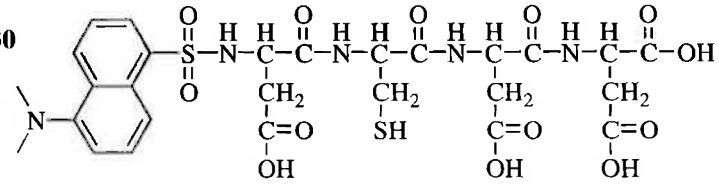

High selectivity for a metal ion can be achieved when a peptide is used as the receptor. A water soluble, peptide based, ratiometric fluorescent sensor **30** for Pb^{2+} was developed utilising the dansyl fluorophore which is extremely sensitive to the local environment.[84] Coordination of Pb^{2+} to the tetrapeptide fragment results in a shift of the fluorescence emission from 557 nm to 510 nm with a concomitant increase in emission intensity. The blue shift in the emission spectrum most likely results from the dansyl fluorophore moving to a less polar environment upon metal binding. The sensor showed good specificity for Pb^{2+} (over Ca^{2+} and Zn^{2+}) although an effective concentration of 120 μM (for Pb^{2+}) to give 50% of the maximal response is orders of magnitude greater than that biologically significant.[84]

1.5.4 Fluorescent Sensors Based on π,π-Stacking Interactions

31

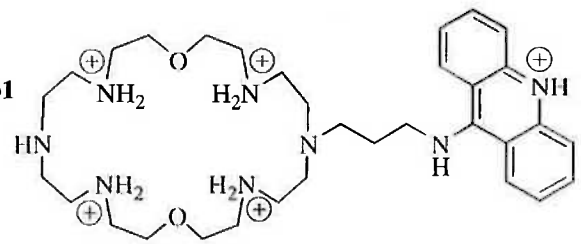

Fluorescent sensor **31** consists of a large azacrown appended with an acridine group. At pH 4, four of the six amine groups of the macrocycle are protonated and so the cyclic receptor offers two distinct, doubly positively charged, compartments.[85] This geometric array is suitable for establishing electrostatic interactions with the triphosphate fragment of adenosine triphosphate (ATP^{4-}). Furthermore, a π,π-stacking interaction between the acridine subunit and the adenine fragment is established which is responsible for the large increase of the acridine blue emission (at 452 nm).[85] No change in fluorescence emission was observed with triphosphate alone which supports the π,π-stacking interaction as necessary for fluorescence. A similar π,π-stacking interaction with ATP^{4-} was utilised in a napthalene walled molecular cavity suitable for inclusion of planar organic species.[86]

1.5.5 Isomerisable Fluorescent Sensors

Photoisomerisable fluorescent sensors, such as sensor **32**, utilising quinolinospiropyran-indoline have been designed.[87] These systems operate by either photochemically- or chemically-induced reversible formation of merocyanine-oxyquinoline metal ion (Mg^{2+}, Ca^{2+} and Zn^{2+}) complexes.

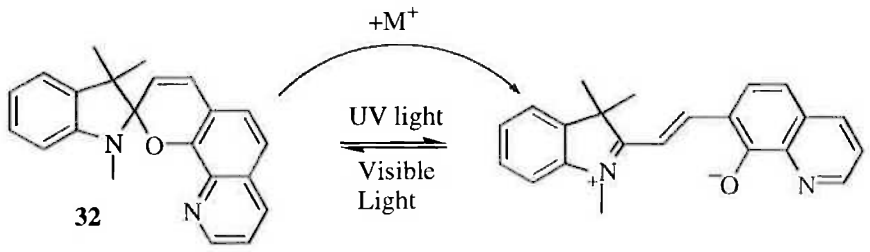

Photoisomerisation has also been utilised for molecular logic devices with multiple inputs[88,89] and for the photoswitching of metal ion complexation with dithienylethene derivatives.[90]

1.5.6 Fluorescent Sensor Ensembles for Indirect Signalling

The fluorophore group of a fluorescent sensor does not necessarily need to be covalently linked to the receptor. Inspired by antibody based biosensors in immunoassays, the basic concept involves displacement of a fluorescent reporter group from a receptor by an analyte which alters the photophysical properties of the fluorophore. The result is fluorescent recognition of a binding event. Several examples exist in the literature[91] including a carbonate sensor utilising an association between coumarin-343 and a Cu^{2+} containing cryptand receptor in water.[92]

For such analyte sensing to be achieved, various requirements must be fulfilled. For instance, the receptor/fluorophore interaction must be of sufficient strength to allow displacement and the fluorophore must show significantly different photophysical properties when bound to the receptor and when dispersed in solution. An example is shown in Figure 1.4 of an ensemble for the detection of citrate in beverages.[93]

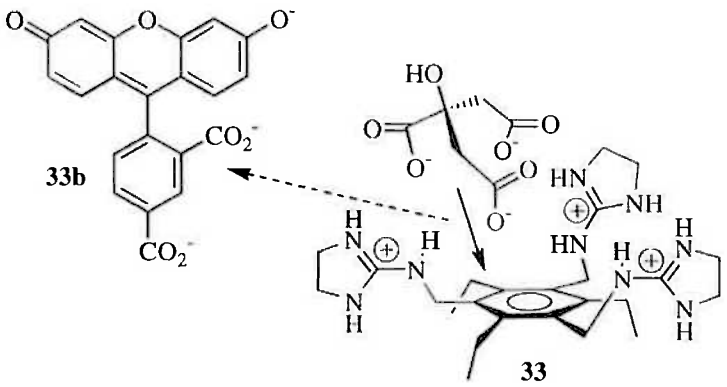

Figure 1.4. *Binding ensemble displaying the displacement of 5-carboxyfluorescein (**33b**) from **33** upon complexation of citrate.*

Receptor **33** consists of three guanidinium groups for hydrogen bonding and charge pairing with citrate. The alternating ethyl groups on **33** ensures that the guanidinium moieties are preorganised on the same face of the benzene ring which yields several hydrogen bonds and three sets of ionic interactions in the (citrate)•(**33**) complex. The stability constant of this complex is 2.9 x 10^5 dm^3 mol^{-1} in 25% aqueous methanol at pH 7.4. The fluorophore group utilised was 5-carboxyfluorescein (**33b**) which contains only two carboxylate groups for binding to the receptor (K = 4.7 x 10^3 dm^3 mol^{-1}). Consequently, the greater stability of the citrate complex allows it to displace **33b**. Displacement of **33b** raises the acidity of the phenol moiety due to the lack of the positively charged microenvironment presented by **33**. Therefore, fluorophore **33b** is less protonated when free of the receptor which decreases its fluorescence emission, signalling the complexation of citrate by **33**. The receptor displayed high selectivity for the 3- charge of citrate at neutral pH and so common contaminants present in beverages (e.g. malate, ascorbate, lactate, benzoate, phosphate and sugars) did not effect the sensing assay.

1.6 Work Described in this Thesis

Few studies exist that allow direct comparisons between a wide range of fluorescent sensors with various structural modifications. A series of coronand appended 9,10-disubstitued anthracene compounds were chosen for this study, and details of their syntheses are presented in Chapter 2. The photophysical properties of these fluorescent sensors were characterised with UV-visible spectrometry and spectrofluorimetry to establish the photophysical behaviour of the compounds upon protonation, and in the presence and absence of metal ions.

The prevailing interest in this thesis is to further develop the current understanding of the influence spacer length, receptor number and donor atom constitution of the receptor, have on PET based fluorescent sensors. Therefore, a systematic study of the metal ion complexation of alkali and alkaline earth metal ions with a synthesised range of sensors is discussed in Chapter 4.

A key issue in the development of fluorescent sensors is a thorough understanding of the relevant sensing mechanisms. That is, the chemical and physical reasons for change in quantum yield or emission wavelength is necessary in order to design a good sensor. Thus, a study of these proposed systems should result in increased understanding of PET based fluorescent sensors and possibly further the development of a sensor that displays high stability, specificity and fluorescence enhancement within an aqueous environment.

Chapter 2 Synthesis and Physical Properties of Functionalised Anthracene Ligands

2.1 Introduction

A diverse range of fluorescent sensors that utilise the mechanism of photoinduced electron transfer (PET) as the means of ON/OFF signalling have been reported.[1,6,19,21,65,94-96] However, many of the factors controlling the PET process are inadequately understood. The preparation of a series of disubstituted anthracene derivatives presents a unique opportunity to examine, in a systematic way, the factors affecting the signalling process as it pertains to the recognition and reporting of the presence (or absence) of metal ions in solution. The desired outcome is the fluorescent response of a ligand to a specific metal ion.

A disubstituted anthracene is an appropriate choice as the fluorophore of a fluorescent sensor as it has good photochemical stability[97] and a very high fluorescence quantum yield (Φ_F). For example, 9,10-dimethylanthracene has a quantum yield of 0.93 in heptane.[98] In addition, the chemistry of anthracene has been well studied and it is a useful chemical scaffold that can allow structural variation of the fluorescent sensor.[99] A further advantage of anthracene based fluorescent sensors is that they are not susceptible to microbial attack as they are not based on biochemical systems. As a result, they are potentially useful in biological environments as sensors since they are unlikely to be biochemically degraded.

To carry out such a systematic survey a variety of substituted anthracene ligands were prepared. The influence of spacer length between the fluorophore and receptor units has been insufficiently investigated for PET fluorescent sensors. To determine the effect of different spacers on various photophysical properties, a series of different length alkyl chains were synthesised with the same receptor, hence direct comparisons are possible. In regards to metal binding specificity, different donor atoms were used in a simple model ligand to explore metal complexation as it relates to the Hard and Soft Acids and Bases (HSAB) principle.[100,101] Metal complexation was further examined by altering the number of receptors present or changing the chelate ring size. The consequence of these alterations

on the fluorescent signalling ability should increase the basic understanding of anthracene based fluorescent sensors utilising PET.

The desired ligands were characterised using potentiometric titrations.[102,103] Such titrations allow the protonation constants to be determined which are important in view of the fact the protons are an efficient switch for this type of fluorescent sensor. A further advantage of this technique is that following the protonation constant determination, metal complexation of the ligands, where applicable, can also be determined.[104]

2.2 Synthesis

2.2.1 Synthesis of 9,10-Bis(morpholinoethyl)anthracene (36)

The synthesis of 9,10-disubstituted anthracene began with the addition of the alkyl arms to the aromatic core. Therefore, the initial synthetic target was the disubstituted anthracene **34** (Scheme 2.1) which was formed, using a slightly modified literature[105] procedure, through nucleophilic attack of the anthracene carbanion on ethylene oxide.

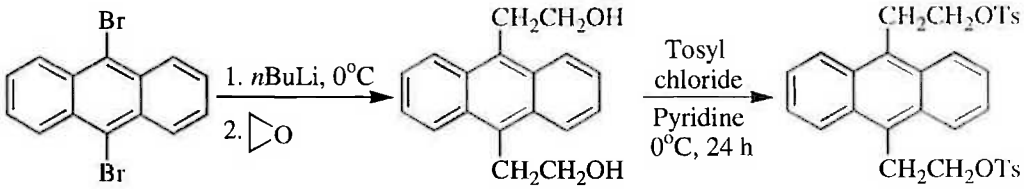

34, 38% **35**, 95%

Scheme 2.1

The ethylene oxide was added by direct condensation of the gas (using a dry-ice/acetone condenser) into the solution containing the lithiated anthracene until the yellow colour of the solution was permanent. This technique obviated the need for the difficult handling of the toxic alkylating reagent in chilled glassware due to its extreme volatility (bp 10°C). The spectral data for diol **34** was identical to that reported in the literature.[105] Tosylation of diol **34** in pyridine to give compound **35** with a far more desirable leaving group was subsequently achieved in good yield. The structure of the ditosylate **35** was confirmed by the mass spectrum with a molecular ion at *m/z* 574 and another at *m/z* 402 due to the loss of a tosylate group from the molecular ion, as well as by ^{1}H NMR data.

With ditosylate **35** in hand, nucleophilic substitution reactions with the amine of choice were used to provide the required ligands. Morpholine was selected as the initial amine to

employ, due to both its low cost and role as a useful model system for the synthesis of future ligands with more complex metal receptor units. Ligand **36** was synthesised from morpholine and ditosylate **35** in *N,N*-dimethylformamide at 80°C with sodium hydrogen-carbonate as the inorganic base. Following recrystallisation of the precipitate that formed after cooling the reaction, compound **36** was obtained in a yield of 67% as pale yellow crystals (Scheme 2.2). The structure of **36** was confirmed by ^{1}H and ^{13}C NMR spectroscopy, mass spectrometry and microanalytical data.

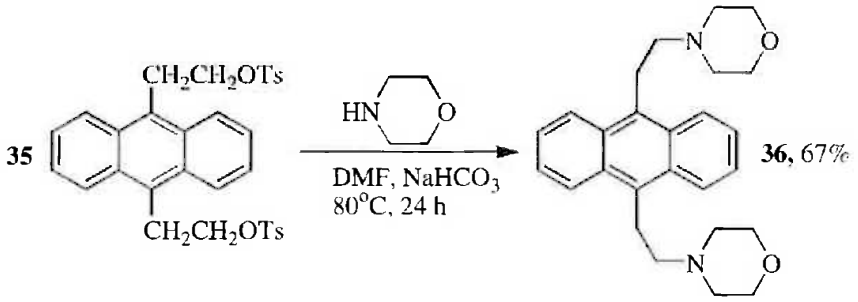

Scheme 2.2

2.2.2 Synthesis of 9,10-Bis(morpholinomethyl)anthracene (38)

To test role that carbon spacer length plays in PET based fluorescent signalling, a series of ligands must first be synthesised. The synthesis of a sensor with a one carbon spacer began with the formation of bis(chloromethyl)anthracene **37** from anthracene using a literature procedure (Scheme 2.3).[106] The method involved refluxing a hydrogen chloride saturated water/dioxane solution containing anthracene and paraformaldehyde to afford **37** as a bright yellow powder. The next step involved refluxing bis(chloromethyl)anthracene **37** and morpholine in benzene, to give the desired bis(morpholinomethyl) ligand **38** in poor yield with physical data identical to that reported previously.[107]

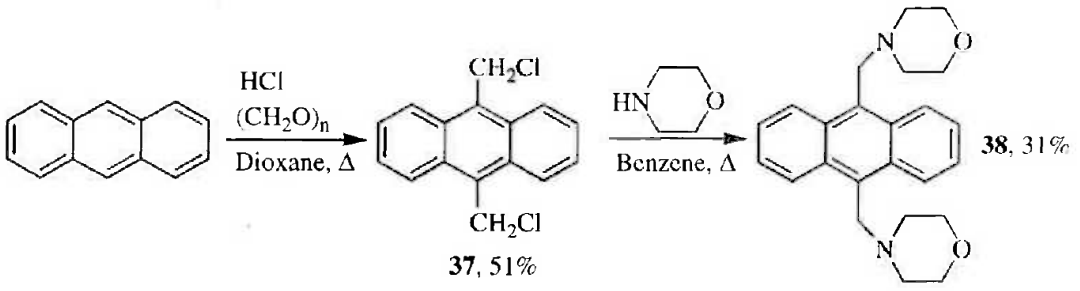

Scheme 2.3

2.2.3 Synthesis of 9,10-Bis(morpholinopropyl)anthracene (42)

The next synthetic target was a fluorescent sensor with a three carbon spacer. It was envisaged that the synthetic route employed would generate both the desired propyl amine ligand **42** and also a precursor amide compound **41** with the nitrogen present as part of an amide. Precursor **41** could possibly have interesting photophysical properties itself and could be a simple way of contrasting the difference between an amide and amine moiety at the spacer-receptor junction.

The initial synthetic route is shown in Scheme 2.4. This synthesis was desirable in that it would give the required three carbon skeleton before introduction of the receptor unit. This would allow greater future synthetic flexibility if required.

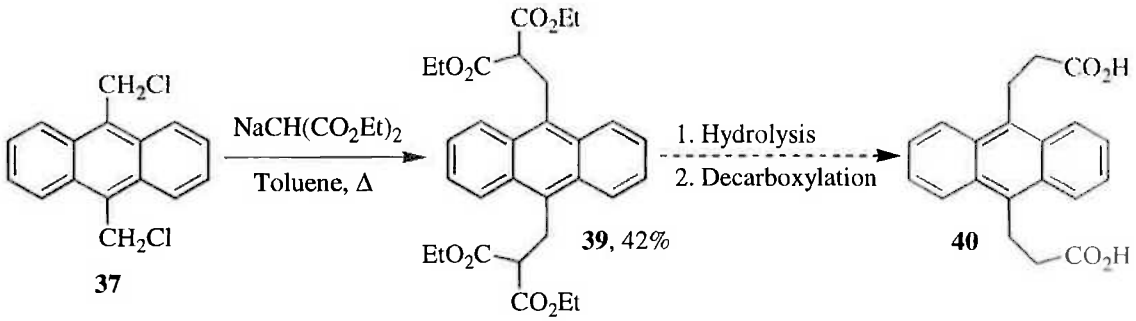

Scheme 2.4

This synthetic route involved the nucleophilic attack of sodium diethyl malonate on halide **37** in a modified literature procedure.[108] Recrystallisation of the crude product afforded **39** as yellow crystals in moderate yield. A molecular ion at *m/z* 522 in the mass spectrum confirmed the identity of the product. The next step involved ester hydrolysis in basic ethanol which gave the desired tetra-acid as a very insoluble pale yellow powder which was not purified.[109] Decarboxylation of the tetra-acid in 1,4-dioxane with sulphuric acid (6 mol dm^{-3}) as a catalyst at 100°C for 4 hours seemed to give some of the more soluble bis-acid **40** as an extremely fine precipitate. However, there were also some decomposition products as determined by TLC analysis. At this point it appeared that this synthetic route was not as attractive as originally thought and so an alternative, more concise route was investigated. The key step for this route was based upon the reaction of the carbanion of a propyl amide with benzyl iodide to obtain a carbon-alkylated product in good yield (Scheme 2.5).[110]

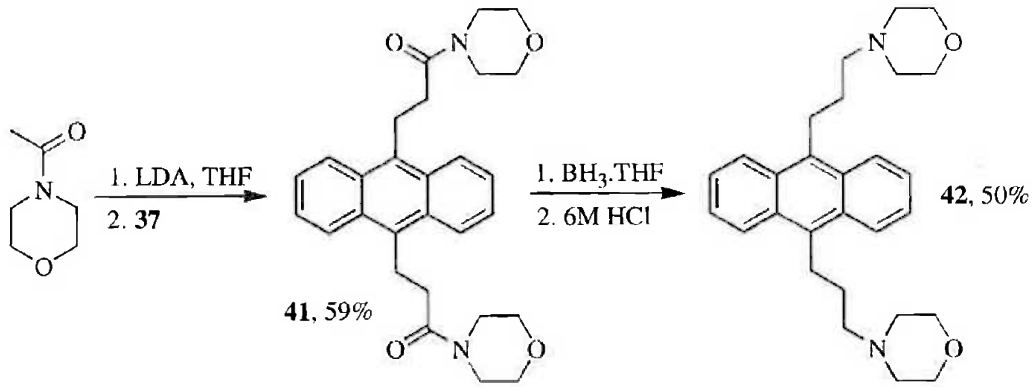

Scheme 2.5

Thus, 4-acetyl morpholine was added to a solution of lithium diisopropylamide in tetrahydrofuran to form the enolate anion to which bis(chloromethyl)anthracene **37** was added at 0°C. After quenching the reaction with water and recrystallising the crude product thus obtained from ethanol, the diamide **41** was obtained in reasonable yield. Formation of the product was indicated by the spectra obtained from NMR spectroscopy.

The ^{13}C NMR spectrum of **41** contained two peaks arising from carbons adjacent to oxygen at δ 66.19 and 66.69 ppm and also two resonances for carbons adjacent to nitrogen at δ 42.00 and 45.82 ppm. The ^{1}H NMR spectrum exhibited a similar lack of symmetry for the morpholine ring. These spectral features arise from the amide carbon-nitrogen bond having a high proportion of double bond character, which results in slow rotation about the amide bond.[111] Therefore, the two methylene chains of morpholine are in different magnetic environments and so have different resonance values, as observed. Mass spectrometry and microanalytical data were also consistent with the formation of diamide **41**.

Formation of the propyl morpholine ligand **42** was achieved by reduction of the amide moieties of compound **41** (Scheme 2.5). Borane-tetrahydrofuran complex was used to reduce the amides as a mild method suitable for compounds containing anthracene, as has been used previously for similar sensitive systems.[112,113] Thus, diamide **41** was reduced by diborane in tetrahydrofuran under reflux for two hours. Treatment of the crude borane-amine adduct thus obtained with hydrochloric acid gave the diamine **42** in good yield after recrystallisation. The formation of the diamine was confirmed by ^{13}C NMR spectroscopy with the disappearance of the amide carbonyl signal at δ 170.96 ppm and the presence of three peaks for carbons adjacent to a heteroatom at δ 53.84, 58.68 and 67.09 ppm. Mass spectrometry and microanalytical data also supported the formation of amine **42**.

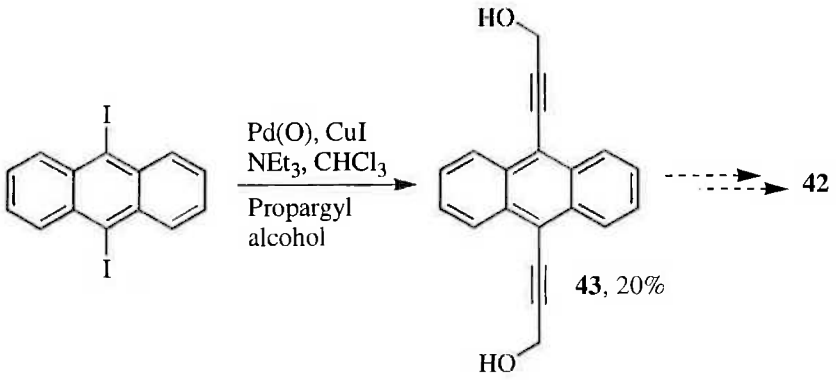

Scheme 2.6

A further synthetic alternative which was considered involved formation of the three carbon spacer by a palladium and copper catalysed cross coupling[114] with 9,10-diiodoanthracene[115] and propargyl alcohol (Scheme 2.6).[116] Due to the low yield of bis(hydroxypropyne) **43** obtained and the need to determine appropriate conditions for the subsequent triple-bond reduction, this route was not pursued further.

2.2.4 Synthesis of 9,10-Bis[(1,4,7,10-tetraoxa-13-azacyclopentadecyl)-ethyl]anthracene (45)

In order to study the influence of the receptor ring size on metal ion complexation a larger azacrown ring was appended to the ethyl anthracene core. Monoaza-15-crown-5 was selected as it is the least expensive of the monoazacrown systems commercially available. As it is known to complex a large range of metal ions this crown was ideal for use as part of a prototypical sensor system.[29,41,117] Furthermore, since only one nitrogen is present in the receptor, there is no need for nitrogen protection in the synthesis.

The synthesis of ligand **45** was modelled on that of the corresponding bis(morpholinoethyl) system **36**, as shown in Scheme 2.7. Thus, a mixture of ditosylate **35** and monoaza-15-crown-5 were heated under reflux for two days. After standard acid-base separation techniques the product was isolated as the yellow hydrochloride salt since the free amine was an unworkable gum. The hydrochloride salt had a base peak in the electrospray mass spectrum at *m/z* 335 for the doubly protonated ligand and also a peak at *m/z* 669 for the singly protonated ligand. ^{1}H and ^{13}C NMR, and microanalytical data further supported the identity of ligand **45**.

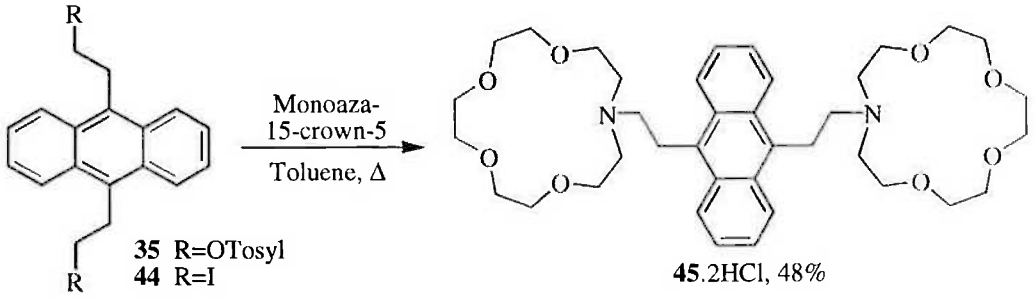

Scheme 2.7

In an attempt to improve the yield the known diiodide **44** was synthesised as described in the literature.[105] However, changing iodine for tosylate as the leaving group in the reaction generally gave the same yield (Scheme 2.7), as has been similarly observed,[118] although purification was simplified.

2.2.5 Synthesis of 9-Ethyl-10-[(1,4,7,10-tetraoxa-13-azacyclopentadecyl)ethyl]anthracene (51)

To investigate the influence that the number of receptor units has on the fluorescent sensing ability, a ligand with only one appended crown was synthesised. For direct comparison to the other ligands synthesised it was necessary to keep the central carbon skeleton identical so that the fluorescent properties of anthracene itself were not altered. To this end the mono crown ligand **51** was the desired target.

The synthesis began with the formation of 9-ethylanthracene **47** to satisfy the requirement that the mono-substituted system remained a 9,10-dialkylsubstituted anthracene (Scheme 2.8). Anthrone was added to a solution of ethyl magnesium bromide in diethyl ether and after acidic workup, 9-ethyl-9-hydroxy-9,10-dihydroanthracene **46** was obtained. The crude product **46** was then dehydrated in toluene with a catalytic amount of *p*-toluenesulphonic acid using a Dean-Stark apparatus to afford the desired 9-ethyl-anthracene **47**.[119]

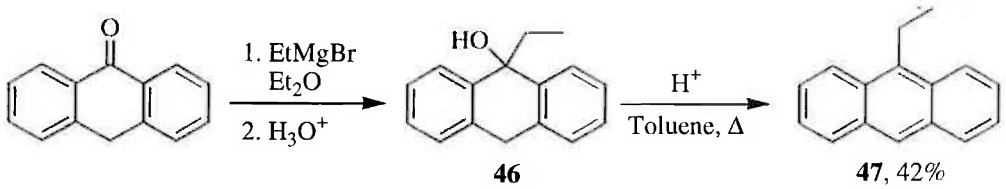

Scheme 2.8

The bromine derivative **48** was then formed by refluxing compound **47** with copper(II) bromide in benzene until the evolution of hydrogen bromide ceased (Scheme 2.9), as described in the literature.[120] The melting point of 103-105°C (lit.[121] 105°C) and the mass spectrum which contained a molecular ion at *m/z* 285 with a characteristic bromine distribution pattern confirmed the identity of the product **48**.

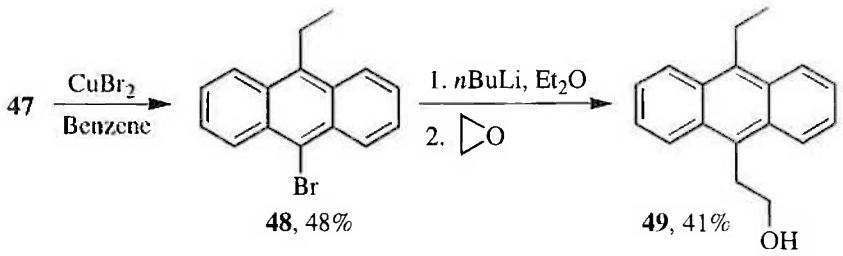

Scheme 2.9

The formation of compound **49** (Scheme 2.9) was performed in the same manner as for the analogous disubstituted diol **34** using an excess of ethylene oxide and the mono-lithiated anthracene. After recrystallisation from ethanol, 9-ethyl-10-hydroxyethylanthracene **49** was obtained in moderate yield as fluorescent yellow needles. Mass spectrometry, ^{1}H and ^{13}C NMR spectra, and microanalytical data were consistent with the formation of **49**.

Conversion of the primary alcohol in compound **49** to an iodide was achieved using the iodinating reagent methyltriphenoxyphosphonium iodide (Scheme 2.10). The product **50** formed as a precipitate in *N,N*-dimethylformamide that was recrystallised from benzene as yellow needles in good yield. It was differentiated from the precursor by the microanalytical data and the ^{13}C NMR resonance at δ 3.19 ppm arising from the carbon adjacent to iodine.

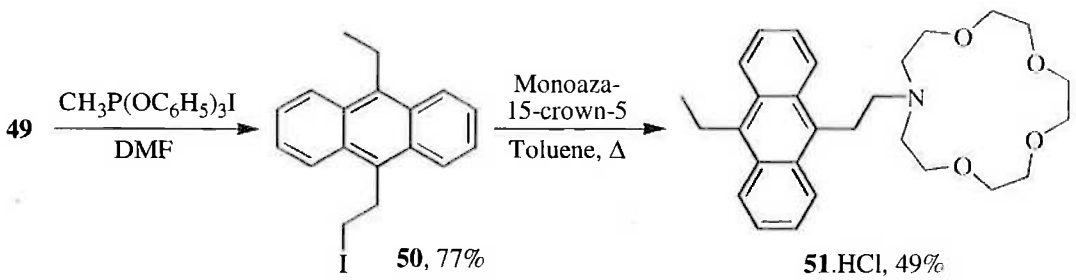

Scheme 2.10

The final step in the sequence was the formation of mono(azacrown) ligand **51**, as shown in Scheme 2.10. The initial synthetic attempt involved refluxing iodide **50** and monoaza-15-crown-5 in acetonitrile with potassium carbonate as the inorganic base. This was

unsuccessful as it resulted in significant amounts of an elimination product arising from the removal of an acidic benzylic hydrogen and the facile leaving group. Therefore, 2.2 equivalents of monoaza-15-crown-5 and iodide **50** were refluxed in toluene for two days. After filtration and acidification compound **51** was obtained, although as expected, a significant amount of unreacted monoaza-15-crown-5 was also observed in the ^{13}C NMR spectrum. Repeated aqueous base washing of a dichloromethane solution of the crude product and subsequent reacidification with hydrogen chloride in methanol yielded mono(azacrown) ligand **51** as a yellow powder. Mass spectrometry showed a molecular ion at *m/z* 453 for the singly protonated ligand and a base peak at *m/z* 233 corresponding to loss of the azacrown moiety from the molecular ion. ^{1}H and ^{13}C NMR spectra, and microanalytical data supported the structure of ligand **51**.

2.2.6 Synthesis of 9,10-Bis(thiomorpholinoethyl)anthracene (52) and 9,10-Bis(piperazinoethyl)anthracene (53)

Finally, to investigate the effect of different donor atoms on metal complexation and consequently fluorescent sensing ability, two ligands directly related to the bis(morpholinoethyl) ligand **36** were synthesised. Therefore, it was necessary to change the ether oxygen in morpholine for either a sulphur atom (using thiomorpholine) or a nitrogen atom (using piperazine).

As shown in Scheme 2.11, bis(thiomorpholine) **52** and bis(piperazine) **53** ligands were prepared by Dr. N. J. Head[122] in an analogous manner to that used for the bis(azacrown) ligand **45**. Thiomorpholine could be added directly to the iodide **44** in order to synthesise ligand **52**.

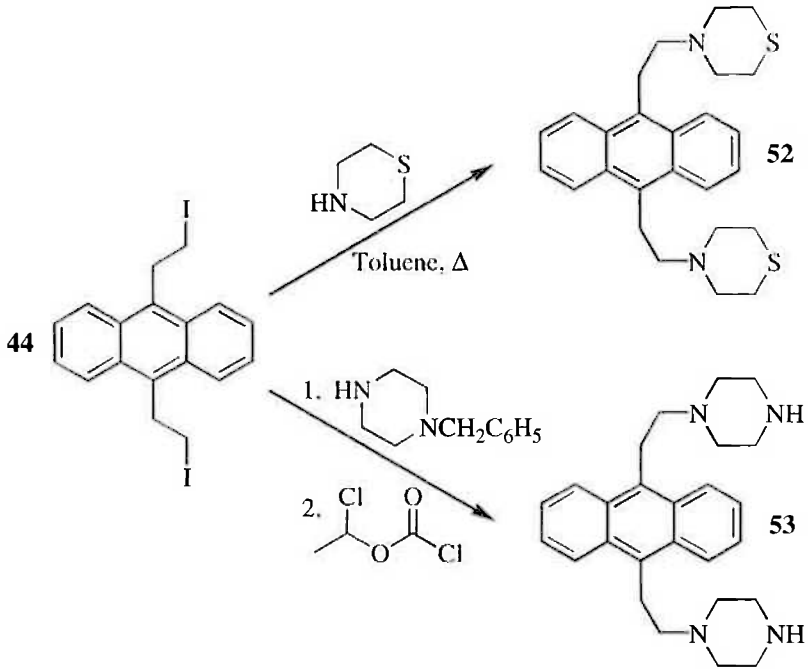

Scheme 2.11

Piperazine contains two reactive centres which necessitated its mono-protection as the *N*-benzylpiperazine before its addition to iodide **44**. Subsequent deprotection afforded the bis(piperazine) ligand **53** as required (Scheme 2.11).

2.3 Acid Dissociation Constants

Acid dissociation constants were determined in a 1,4-dioxane-water solvent mixture (40:60, v/v) and I = 0.05 mol dm^{-3} (NEt_4ClO_4) by potentiometric titration, as described in Section 6.3. A partially aqueous solvent system was used to attain a balance between sufficient water to ensure that the pH electrode could function correctly and sufficient 1,4-dioxane to dissolve the ligands. However, the bis(thiomorpholine) ligand **52** and the bis(morpholinomethyl) ligand **38** were still insufficiently soluble in this solvent system to allow their pK_a values to be determined.

In the initial acidic solution, the basic nitrogen donor groups of each ligand are fully protonated and are gradually deprotonated during titration with tetraethylammonium hydroxide. The equilibria amongst the deprotonated species may be represented as follows;

$$[LH]^+ \overset{K_{a1}}{\rightleftharpoons} H^+ + L \qquad (2.1)$$

$$[LH_2]^{2+} \rightleftharpoons^{K_{a2}} H^+ + [LH]^+ \quad (2.2)$$

$$[LH_3]^{3+} \rightleftharpoons^{K_{a3}} H^+ + [LH_2]^{2+} \quad (2.3)$$

$$[LH_4]^{4+} \rightleftharpoons^{K_{a4}} H^+ + [LH_3]^{3+} \quad (2.4)$$

$$K_{a1} = \frac{[H^+][L]}{[LH^+]} \quad (2.5)$$

$$K_{a2} = \frac{[H^+][LH^+]}{[LH_2{}^{2+}]} \quad (2.6)$$

$$K_{a3} = \frac{[H^+][LH_2{}^{2+}]}{[LH_3{}^{3+}]} \quad (2.7)$$

$$K_{a4} = \frac{[H^+][LH_3{}^{3+}]}{[LH_4{}^{4+}]} \quad (2.8)$$

Where K_{a1}, K_{a2}, K_{a3} and K_{a4} are the step-wise equilibrium constants (or acid dissociation constants) and L is the ligand under study. The pK_a of each nitrogen donor was determined from the negative logarithm of the equilibrium constant, K_a, as defined in equations 2.9- 2.12.

$$pK_{a1} = -\log K_{a1} \quad (2.9)$$

$$pK_{a2} = -\log K_{a2} \quad (2.10)$$

$$pK_{a3} = -\log K_{a3} \quad (2.11)$$

$$pK_{a4} = -\log K_{a4} \quad (2.12)$$

The protonation constants (pK_as) for the bis(piperazine) **53**, bis(morpholinoethyl) **36**, bis(morpholinopropyl) **42**, bis(azacrown) **45** and mono(azacrown) **51** ligands are shown in Table 2.1.

Table 2.1. pK_a values for the ligands at 298.2 K in 0.05 mol dm^{-3} NEt_4ClO_4 1,4-dioxane-water (40:60, v/v) solution.

Ligand	pK_{a1}	pK_{a2}	pK_{a3}	pK_{a4}
Bis(piperazine) **53**	9.02 ± 0.01	8.06 ± 0.03	4.32 ± 0.02	2.96 ± 0.06
Bis(morpholinoethyl) **36**	6.38 ± 0.04	5.62 ± 0.04		
Bis(morpholinopropyl) **42**	7.00 ± 0.04	6.25 ± 0.03		
Bis(azacrown) **45**	8.08 ± 0.04	7.12 ± 0.02		
Mono(azacrown) **51**	7.73 ± 0.02			

The pK_a values obtained for bis(piperazine) **53** (Table 2.1) decrease from pK_{a1} to pK_{a4}. The reasons for this are two-fold. The first is a statistical effect, as before any nitrogen on the ligand has been protonated, there are four sites for a H^+ from solution to bind. Once a proton has bound to a nitrogen donor of the ligand, there are now only three sites available for a H^+ from solution to bind and so there exists a lower probability that this will occur, causing a decrease in pK_a. Likewise, for any further pK_a value.

The second, and more significant, reason for decreasing pK_as is a result of the increasing net charge. Protonation of one nitrogen gives the ligand an overall single positive charge. Protonation of a second nitrogen then gives the ligand an overall 2+ charge and concomitant electrostatic repulsion between the two H^+s results in a lower pK_{a2}. This effect is most apparent for pK_{a3} and pK_{a4} since the third (and fourth) protonation must occur on an already protonated piperazine ring where the electrostatic repulsion is greater due to the proximity of charges. Also, any intramolecular hydrogen bonding is destroyed. Thus, pK_{a3} and pK_{a4} are significantly lower than pK_{a1} and pK_{a2}.

The titration profile of bis(morpholinoethyl) **36** and bis(morpholinopropyl) **42** ligands is shown in Figure 2.1. The effect of an increase in the length of the aliphatic arm on the protonation constant can be seen between the ethyl and propyl linked morpholine systems, **36** and **42**, respectively. Both pK_{a1} and pK_{a2} increase on going from the ethyl to propyl system which is a direct result of the inductive effect of the methylene groups.[123] The pK_a for morpholine is 8.55 (I = 0.5 mol dm^{-3}, 298.2 K) in water[124] which is significantly higher than that for either morpholine containing ligand. This is due to the increased steric hindrance resulting from the anthracene core which consequently hinders solvation of the ammonium ion formed (through hydrogen bonding to the solvent).[125]

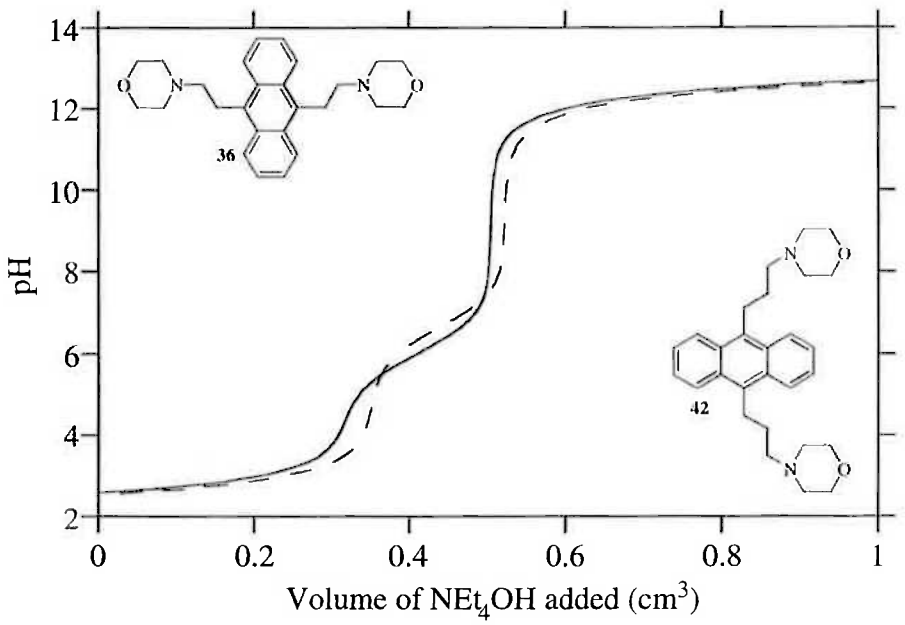

Figure 2.1. *Typical titration curves of bis(morpholinoethyl)* ***36*** *(——) and bis(morpholinopropyl)* ***42*** *(– – –) against NEt_4OH at 298.2 K. [Ligand] = 9.0 x 10^{-4} mol dm^{-3}, [$HClO_4$] = 5.0 x 10^{-3} mol dm^{-3}, [NEt_4OH] = 0.093 mol dm^{-3}, I = 0.05 mol dm^{-3} (NEt_4ClO_4).*

Of course, a decrease in pK_a value might be expected in a partially aqueous solution when compared to an aqueous solution since the protonated ligand may be more poorly solvated than in water, shifting the equilibria in equations 2.1-2.4 to the right. This would result in an increased K_{an} and thus a decrease in pK_{an}.

The effect of oxygen substitution for nitrogen can be observed in the difference in pK_{a1} of bis(morpholinoethyl) **36** and bis(piperazine) **53**. Oxygen is less solvated in aqueous solution and has a lower tendency to form hydrogen bonds than nitrogen which leads to a weakening of the cooperative binding of the bound proton by the exchanged donor atom.[126] Furthermore, oxygen has a higher electron-withdrawing effect compared to nitrogen. These combined properties cause a lower pK_{a1} to be observed for bis(morpholinoethyl) ligand **36**.

The bis(azacrown) **45** system has a significantly higher pK_a than the electronically similar bis(morpholinoethyl) ligand **36**. This difference is the result of increased stabilisation of the hydronium ion by hydrogen bonding with some of the crown ether oxygen atoms.

Essentially, the ammonium ion is solvated intramolecularly which gives a more stable complex, resulting in a higher pK_a.[127]

The pK_a difference between mono(azacrown) **51** and bis(azacrown) **45** of 0.35 log units arises simply from the statistical effect of the availability of one or two protonatable nitrogens, as previously described. The pK_a for a related C_{12} alkyl substituted monoaza-15-crown-5 is 8.7 in methanol-water (9:1; v/v).[128] This comparative value again shows that the steric hindrance resulting from the anthracene core causes decreased pK_a values,[125] solvent contributions aside.

2.4 Metal Complex Formation

The complexation of a metal ion by a ligand may be expressed as;

$$M^{n+} + L \underset{}{\overset{K}{\rightleftharpoons}} [ML]^{n+} \qquad (2.13)$$

where the stability constant, K, is given by

$$K = \frac{[ML^{n+}]}{[M^{n+}][L]} \qquad (2.14)$$

Potentiometric (pH-metric) titrations can be used to determine metal-ligand complexation constants provided that the protonation constants have been determined.[104] The technique relies on the metal ion competing with acid to bind to the ligand of interest and consequently altering the solution pH. Thus, differences in the pH titration profile in the presence of a metal ion can indicate the existence of a metal-ligand complex. The technique is best suited to higher stability constants ($K \geq 100$ dm^3 mol^{-1}).[104]

To determine the stability constants of Na^+, Ca^{2+} and Pb^{2+} with the ligands described in Table 2.1, two equivalents of the metal ion were added to the acidic titration solution before the titration was commenced (see Section 6.3). The basicity or pH of a solution of these ligands will be altered by complexation of a metal ion. Thus, by comparison and analysis of the potentiometric titration curves of a ligand in the presence and absence of an ion, the apparent stability constant (K) for the complex can be determined. Typical titration curves of bis(azacrown) **45** alone and in the presence Na^+ and Ca^{2+} are shown in Figure 2.2.

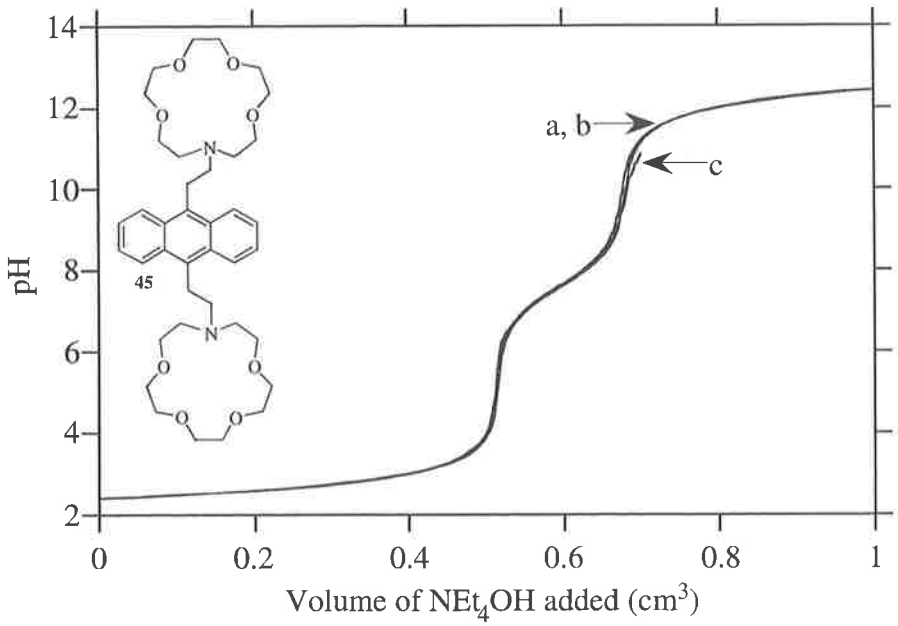

Figure 2.2. *Typical titration curves of bis(azacrown)* ***45*** *(a) alone, (b) in the presence of* Na^+ *and (c) in the presence of* Ca^{2+} *against* NEt_4OH *at 298.2 K.* ***[45]*** *= 8.0 x* 10^{-4} *mol* dm^{-3}, $[NaClO_4]$ *= 0.0016 mol* dm^{-3}, $[Ca(ClO_4)_2]$ *= 0.0016 mol* dm^{-3}, $[HClO_4]$ *= 0.0068 mol* dm^{-3}, $[NEt_4OH]$ *= 0.098 mol* dm^{-3}, *I = 0.05 mol* dm^{-3} (NEt_4ClO_4).

As can be observed in Figure 2.2, there is no discernible affect of the metal ion on the basicity of the solution of ligand **45**. Titrations in the presence of Ca^{2+} were stopped around pH 11 due to the precipitation of metal hydroxide species (eg. $Ca(OH)_2$).[129] Similarly, titrations with Pb^{2+} were halted at pH 7 as hydrolysis of Pb^{2+} at that pH has been previously observed for a 50% water-dioxane solvent mixture.[130]

Consequently, since the basicity of the solutions was unaltered by the addition of metal salts, metal hydrolysis aside, it can be concluded that under the conditions used the ligands studied do not complex Na^+, Ca^{2+} and Pb^{2+} (or $K \leq 100$ dm^3 mol^{-1}).[104] However, as will be seen in Chapter 4, metal ion complexation does occur in acetonitrile.

2.5 Summary

A series of 9,10-disubstituted anthracene ligands were synthesised in moderate yields. The general synthetic route was addition of the amine receptor to the relevant anthracene core containing the appropriate leaving groups. This route allowed an array of sensors to be formed relatively easily. It also afforded the opportunity to change various aspects such as

the receptor unit, as required when pursuing a systematic study, at will. Thus, anthracene acted as an effective scaffold for construction of the sensors. However, a degree of simplicity arose from the fact that only the bis(piperazine) ligand **53** required any protection/deprotection steps.

The pK_a values were determined by potentiometric titration for the ligands that are sufficiently soluble in 1,4-dioxane-water to be studied. The values obtained are consistent with those determined for similar receptor units in other studies. Furthermore, no metal ion (Na^+, Ca^{2+} and Pb^{2+}) complexation was observed for any ligand studied in 1,4-dioxane-water solution using this titration technique.

As these ligands are designed to be fluorescent sensors it is obviously necessary to ascertain their photophysical properties, which is the subject of the next chapter.

Chapter 3 Photophysical Properties of Anthracene Ligands in Partially Aqueous Solution

3.1 Introduction

Electromagnetic radiation consists of an enormous range of wavelengths from radio to radioactivity waves. A photon is a quantum of electromagnetic radiation and photons of different energies are classified into different spectral regions. The photons in all of these regions have the same electromagnetic nature, but because of their very different energies, they interact with matter very differently. The energy of one photon depends on its frequency or wavelength as defined in Equation 3.1;

$$E = h\upsilon = hc/\lambda \qquad (3.1)$$

Where h is Planck's constant (6.626×10^{-34} J s)

υ is the frequency of the radiation (s^{-1})

c is the velocity of light in a vacuum (3×10^{-8} m s^{-1})

λ is the wavelength of the radiation (m)

If an electron belonging to a molecule in its ground electronic state absorbs electromagnetic radiation, it is promoted to an unoccupied orbital of higher energy (an excited state) and its energy increases by an amount equal to the energy of the absorbed photon. However, since the energy levels of matter are quantised, only light of an energy that can cause an electronic transition from the ground state to a particular excited state will be absorbed. This process is called electronic excitation and the region of interest for this discussion is light of wavelengths within the range 200-800 nm, the ultraviolet-visible region.

Ultraviolet-visible spectroscopy is a sensitive technique that produces electronic absorption spectra for most organic compounds and many inorganic ions and complexes. The electronic absorption spectra of a molecule is the graphical representation of the intensity

of light absorbed in producing electronic transitions in a molecule, as a function of the wavelength of the light.

The relationship of the absorption spectra of organic compounds to their structure has been extensively studied.[37,131] Quantitative experimental measurements of UV-visible absorption are based on the Beer-Lambert laws which concern the relationship between the intensities of the radiation incident on, and transmitted by, a layer of an absorbing substance.

Lambert's law states that the proportion of light absorbed by a transparent medium is independent of the intensity of the incident light and that each successive layer of the medium absorbs an equal fraction of the incident light. Beer's law states that the amount of light absorbed is proportional to the number of absorbing molecules through which the light passes. Therefore, if the absorbing substance is dissolved in a non-absorbing medium, the absorbance of the solution will be proportional to its concentration.[131] Consequently, combination of the two laws gives the Beer-Lambert law, as shown in Equation 3.2;

$$A = \log(I_0/I) = \varepsilon Cl \qquad (3.2)$$

Where A is the absorbance of the sample

I_0 is the light intensity incident on the sample

I is the light intensity transmitted by the sample

ε is the molar extinction coefficient of the molecule ($dm^3\ mol^{-1}\ cm^{-1}$)

C is the concentration of absorbing molecules in solution ($mol\ dm^{-3}$)

l is the path length of light through the solution (cm)

Absorbance is the quantity measured with a standard spectrophotometer. The Beer-Lambert law only rigorously applies for monochromatic (homogeneous) light. Other factors that may make the law inapplicable, such as chemical changes or dichroism, can be mitigated with careful experimental design.

Thus, UV-visible absorption spectroscopy is concerned with the process by which light is absorbed by a molecule. Contrastingly, fluorescence (or phosphorescence) spectroscopy is concerned with the processes by which light is re-emitted by molecules after they have been excited by the absorption of light. For this reason, fluorescence is observed in a

direction perpendicular to the incident light, in order to avoid interference from it. A schematic energy level diagram depicting the various electronic transitions that can occur following the absorption of radiation is shown in Figure 3.1.

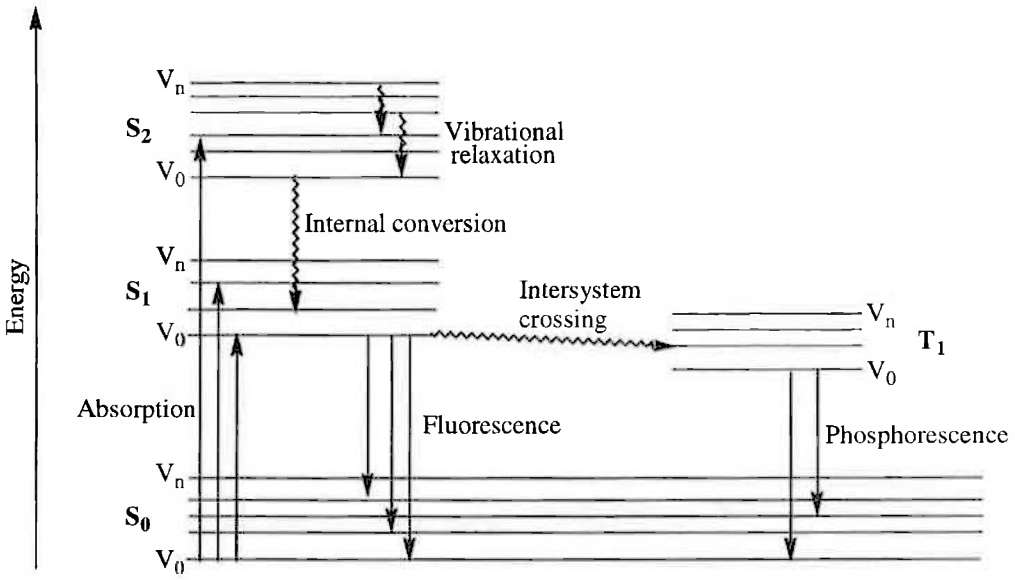

Figure 3.1. *Schematic energy level diagram of the electronic states of a model chromophore illustrating the numerous electronic transitions that can occur: S represents a singlet state, T represents a triplet state, and V represents the various vibrational sublevels. Wavy lines correspond to non-radiative energy transitions.*

Although the absorption of light is an extremely rapid process (10^{-15} s) the sequence of events depicted in Figure 3.1 that return the excited molecule to its ground state are considerably slower (10^{-14} to several seconds). The primary route of relaxation depends on the relative rates of all the processes involved, which are dependent on the particular molecule, the solvent and also the temperature.

Electronic states of organic molecules can be grouped into two broad categories called singlet states (S) and triplet states (T). A singlet state is one in which all of the electrons in the molecule have their spins paired. Triplet states are those in which one set of electron spins have become unpaired, or all electrons in the molecule except two have paired spins. Triplet states are lower in energy than their corresponding singlet states as a consequence of Hund's rule. In most organic molecules the ground state (S_0), the electronic state of lowest energy, has an even number of electrons which are paired.

Electronic state multiplicities are important since the nature of the emission process depends on them. Fluorescence is a radiative transition between states of the same

multiplicity (i.e. $S_1 \rightarrow S_0$). Phosphorescence is a radiative transition between states of different multiplicities (i.e. $T_1 \rightarrow S_0$).

Electronic states (ground or excited) have associated vibrational energy, stretching them upward into bands overlapping those of higher electronic states. The vibrational levels (numbered 1, 2, ..., n) arise since a molecule in a given electronic state may absorb small increments in energy corresponding to changes in vibrational modes, although retain the same electronic configuration. Superimposed on the vibrational levels of each electronic state are further rotational sublevels. The energy differences between rotational transitions are too closely spaced to be resolved in liquids at room temperature. However, they contribute to the broad nature of the vibrational-electronic bands in absorbance and fluorescence spectra.

Upon absorption of light, the electronically excited molecule may also be in a vibrationally excited state (with V >0). In solution, transfer of excess vibrational energy through collisions with neighbouring molecules occurs rapidly (10^{-14}-10^{-12} s), a process called vibrational relaxation. Once a molecule has relaxed to the lowest vibrational level of an excited state, it can only lose energy by moving to a lower electronic energy level. This can be accomplished by internal conversion, fluorescence or intersystem crossing to a triplet state.

Internal conversion involves crossover from a higher to a lower excited state, of the same multiplicity, by a vibrational coupling mechanism. Essentially, if the higher vibrational levels of a lower excited state overlap the lower vibrational levels of a higher excited state, the two states will be in transient thermal equilibrium which will permit population of the lower electronic state. Vibrational relaxation of the lower electronic state then follows as before. This process is fast (10^{-12} s) for higher electronic states due to greater overlap of vibrational levels. Internal conversion can occur from $S_1 \rightarrow S_0$. However, it is less likely than among the higher electronic states as they are much closer together in energy than S_1 and S_0 for aromatic molecules, such as the substituted anthracene ligands considered here. Accordingly, the radiatively emitting electronic level of a given multiplicity is the lowest excited level of that multiplicity regardless of the level to which it was initially excited. One of the few exceptions to this are seven-membered ring containing aromatic compounds such as azulene ($S_2 \rightarrow S_0$ fluorescence).[132]

As an alternative to internal conversion, the excited molecule may fluoresce in order to return to the ground state. The decay time of fluorescence is of the order of 10^{-8} s, corresponding to the lifetime of the thermally equilibrated S_1 state. Thus, if fluorescence is unperturbed by competing processes, the lifetime of fluorescence is the intrinsic lifetime of the excited singlet state. After emission, the fluorescing molecule can return to any vibrationally excited level of the ground state. Subsequent vibrational relaxation returns the molecule to its original state, before absorption.

It should be noted that energy of the photon emitted in fluorescence is generally lower than the energy of the photon absorbed, due to vibrational relaxation after both absorption and emission. This change in photon energy causes a shift of the fluorescence spectrum to longer wavelengths, relative to the absorption spectrum, and is referred to as a Stokes shift.

The transition $S_1 \rightarrow T_1$ is the final pathway of molecular deactivation and is referred to as intersystem crossing. It is an internal conversion process involving states of different multiplicity. Since the process involves a change of spin state it is classically forbidden yet, quantum mechanically it can occur although with a much lower (10^6-fold) probability than the spin-allowed process. Therefore, the average lifetime of the spin-forbidden vibrational transition is about 10^{-8} s as opposed to 10^{-14} s for spin-allowed vibrational transitions (internal conversion and vibrational relaxation). Consequently, intersystem crossing can compete with fluorescence for deactivation of the S_1 state.

Phosphorescence occurs from the lowest excited triplet state. The long radiative lifetime of phosphorescent transitions (10^{-4}-10 s) reflects the spin-forbidden nature of the triplet state, as described above. Accordingly, collisional deactivation by solvent molecules and energy transfer processes typically preclude the observation of phosphorescence in fluid media. Therefore, phosphorescence is generally studied in the glassy state at liquid nitrogen temperature to minimise collisional processes. Phosphorescence also occurs at longer wavelengths relative to fluorescence since T_1 is lower in energy than S_1.

Finally, absorption spectra reflect the vibrational states of the excited state and fluorescence (or phosphorescence) spectra reflect the vibrational states present in the ground state. Thus, if the S_0 and S_1 states have the same vibrational structures, the fluorescence and absorbance spectra will appear as mirror images. However, owing to differences in the charge distributions in the ground and excited states, the vibrational

structures are often different, so that at best an imperfect mirror image relationship frequently results.[133]

When measuring luminescence phenomena there are two different types of spectrum that can be discussed; the *emission* spectrum and the *excitation* spectrum. Fluorescence emission spectra are obtained by measuring the emission intensity as a function of wavelength for excitation at a fixed wavelength. Conversely, excitation spectra are obtained by measuring the intensity of the emission at a fixed wavelength as the excitation wavelength is altered. When the intensity of exciting light is kept constant, the excitation spectrum generally coincides with the absorption spectrum of a compound. Only fluorescence emission spectra will be discussed beyond this point.

The preceding discussion provides a brief summary of the absorptive and radiative processes that can occur for some molecules. The inter-relationship of these different pathways produces the various outcomes that occur. The way these processes can be harnessed to signal chemical events will be discussed in this chapter in regard to photoinduced electron transfer (PET) mediated fluorescent signalling.

3.2 Photophysical Properties in 1,4-Dioxane-Water Solution

As described in Sections 6.4 and 6.5, photophysical measurements were determined in a 1,4-dioxane-water solvent mixture (40:60, v/v) in the presence of 0.050 mol dm^{-3} tetraethylammonium perchlorate (NEt_4ClO_4) to maintain constant ionic strength. Dioxane is a polar, water miscible organic solvent in which the studied ligands were soluble. It also has good UV transparency (>216 nm for 1 cm path length).[134] The water-dioxane ratio remained the same as that used for the potentiometric titration study so that all results obtained were directly comparable. However, unlike the potentiometric titration study, all the ligands are soluble up to the concentrations required for photophysical studies. This is simply a result of UV-visible and fluorescence measurements requiring significantly lower concentrations (*ca.* 10^{-5} and 10^{-6} mol dm^{-3}, respectively) than potentiometric titrations (*ca.* 10^{-3} mol dm^{-3}).

3.2.1 UV-Visible Absorbance Properties

UV-visible absorbance spectra were measured over the 300-450 nm range for all ligands studied. The spectra were recorded for each ligand with a variety of metal ions (Na^+, K^+,

Mg^{2+}, Ca^{2+}, Al^{3+}, Zn^{2+}, Cd^{2+}, Pb^{2+} and H^{+}) to determine their effect on the substituted anthracene ligand absorption. The UV-visible spectra for bis(morpholinoethyl) ligand **36** alone and in the presence of perchloric acid are shown in Figure 3.2 as a typical example.

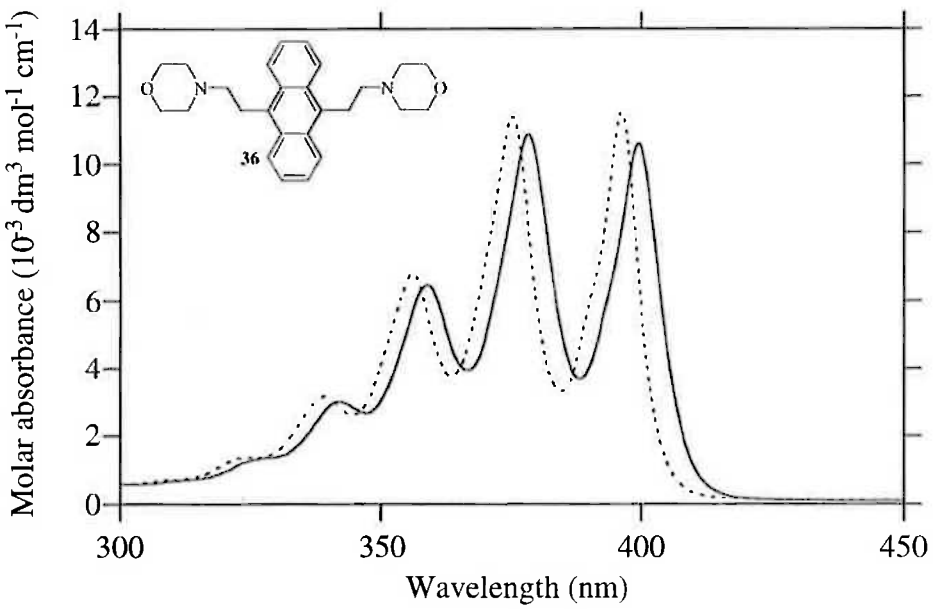

Figure 3.2. *UV-visible absorbance spectra of bis(morpholinoethyl) ligand* ***36*** *alone (——) and in the presence of* H^{+} *(-----) measured in 1,4-dioxane-water (40:60; v/v). [**36**] =* 6.6×10^{-5} *mol dm*$^{-3}$*,* $[HClO_4] = 5.0 \times 10^{-3}$ *mol dm*$^{-3}$*,* $I = 0.050$ *mol dm*$^{-3}$ (NEt_4ClO_4)*,* $T =$ *298.2 K.*

The UV-visible absorbance spectra of the ligands are characteristic of 9,10-disubstituted alkyl anthracenes.[135] The absorption spectrum of the bis(morpholinoethyl) ligand **36** displays four absorption bands at 399.5, 378.0, 359.0, and 342.0 nm and a shoulder at *ca.* 328 nm. Upon the addition of metal ions to the ligand, little or no spectral changes are observed (Table 3.1). The greatest spectral shift is observed in the presence of acid where a small hypsochromic shift of 3.5 nm and a slight increase in molar absorptivity are observed (Table 3.1). Only Al^{3+} and Pb^{2+} show similar, albeit slightly reduced, hypsochromic shifts. This shift suggests that interaction with the lone pair of the amine nitrogen slightly diminishes its electron donating character resulting in a small hypsochromic shift as there is slightly less delocalisation of the π orbitals. As will be seen later, the spectral change induced by Al^{3+} and Pb^{2+} is largely due to protonation of **36** occurring as a consequence of the hydrolysis of these metal ions.

Table 3.1. Longest wavelength absorption bands and molar absorbances (ε) observed for bis(morpholinoethyl) **36** alone and in the presence of various metal ions in 1,4-dioxane-water (40:60; v/v). **[36]** = 6.6 x 10^{-5} mol dm^{-3}, $[M^{n+}(ClO_4)_n]$ = 5.0 x 10^{-3} mol dm^{-3}, $[HClO_4]$ = 5.0 x 10^{-3} mol dm^{-3}, I = 0.050 mol dm^{-3} (NEt_4ClO_4), T = 298.2 K.

Complex	λ_{max} (nm)	ε x 10^{-3} (dm^3 mol^{-1} cm^{-1})
Free ligand, **36**	399.5	10.6
Na^+	399.5	10.8
K^+	399.5	10.8
Mg^{2+}	399.5	10.6
Ca^{2+}	399.0	10.6
Al^{3+}	396.0	11.8
Zn^{2+}	399.0	10.8
Cd^{2+}	399.0	11.1
Pb^{2+}	397.0	10.9
H^+	396.0	11.5

The influence of chain length on the absorbance properties of the disubstituted alkyl anthracenes was investigated with the bis(morpholinomethyl) **38** and bis(morpholino-propyl) **42** ligands. They were studied under the same conditions as for bis(morpholinoethyl) **36** and with the same metal ions. Similarly, the addition of metal ions shows little to no effect on the absorption spectra. As before, the largest spectral shift observed is for H^+, with Al^{3+} and Pb^{2+} the next largest. The effect observed upon the addition of acid to the morpholine containing ligands is shown in Table 3.2 since this analyte caused the greatest spectral change. Also included in Table 3.2 are the corresponding absorbance values for bis(hydroxyethyl) **34** and bis(propylamide) **41** for comparison.

Table 3.2. Effect of acid on bis(hydroxyethyl) **34**, bis(propylamide) **41**, and morpholine containing ligands with methyl **38**, ethyl **36** and propyl **42** spacers in 1,4-dioxane-water (40:60; v/v). [Ligand] = 6.6×10^{-5} mol dm^{-3}, [$HClO_4$] = 5.0×10^{-3} mol dm^{-3}, I = 0.050 mol dm^{-3} (NEt_4ClO_4), T = 298.2 K.

	Maximum wavelength (nm) ($\varepsilon \times 10^{-3}$ (dm^3 mol^{-1} cm^{-1}))	
Ligand	Free ligand	Ligand + Acid
Bis(morpholinomethyl) **38**	396.5 (8.3)	399.0 (9.3)
Bis(morpholinoethyl) **36**	399.5 (10.6)	396.0 (11.5)
Bis(morpholinopropyl) **42**	400.0 (11.1)	398.5 (11.5)
Bis(propylamide) **41**	400.0 (10.7)	[a]
Bis(hydroxyethyl) **34**	398.5 (9.2)	[a]

[a] Unchanged by the addition of acid.

All three morpholine ligands, **38**, **36** and **42**, show a spectral response to the addition of acid. Bis(morpholinopropyl) ligand **42** displays a 1.5 nm hypsochromic shift with acid, slightly smaller than for the ethyl system. Bis(morpholinomethyl) **38** is distinct in showing a bathochromic shift with acid. Both systems show a slight increase in molar absorptivity in the presence of acid. Bis(hydroxyethyl) **34** and bis(propylamide) **41** ligands, without a free amine, show no response to acid or any other metal ions. This suggests that binding of an amine nitrogen is necessary in order to observe any absorbance response. The ethyl spacer also appeared to afford the largest response. The UV-visible responses observed for the morpholine series are typical of the other ligands studied containing an ethyl spacer with different receptors (Table 3.3). UV-visible absorbance spectra (for **52**, **53** and **45**) again display little response to the addition of the analytes studied. Yet again, the largest hypsochromic spectral shift observed is for H^+, with Al^{3+} and Pb^{2+} the next largest.

Thus, UV-visible absorption spectra generally display little or no spectral change upon the addition of the various analytes tested. However, the ligands were designed as PET based fluorescent sensors so these results are not unexpected or necessarily undesirable.

Table 3.3. Effect of acid on ligands with an ethyl spacer in 1,4-dioxane-water (40:60; v/v). [Ligand] = 6.6 x 10^{-5} mol dm^{-3}, [$HClO_4$] = 5.0 x 10^{-3} mol dm^{-3}, I = 0.050 mol dm^{-3} (NEt_4ClO_4), T = 298.2 K.

	Maximum wavelength (nm) (ε x 10^{-3} (dm^3 mol^{-1} cm^{-1}))	
Ligand	Free ligand	Ligand + Acid
Bis(thiomorpholine) **52**[a]	400.0 (8.9)	396.0 (11.2)
Bis(piperazine) **53**	400.0 (10.6)	396.5 (11.8)
Bis(azacrown) **45**	399.5 (9.1)	396.5 (10.0)

[a] At 3.3 x 10^{-5} mol dm^{-3}.

3.2.2 Fluorescence Properties

Two options exist when selecting an excitation wavelength. The wavelength at which the species of interest has maximum molar absorbance or, a wavelength where the species present have the same (an isosbestic point) or comparable molar absorbances is used. The latter option has the advantage in that any difference in fluorescence observed for species sharing similar molar absorbances is real, and not due to different numbers of photons being absorbed. For these studies, the excitation wavelength was chosen at a point with comparable molar absorbances for the various species present in the UV-visible absorbance spectra. Generally the excitation wavelength was selected from within the second longest wavelength band in the UV-visible absorption spectra (centred around 378 nm), in part to assist in obtaining the full fluorescence spectrum of the substituted anthracene ligands.

Typical emission spectra for bis(morpholinoethyl) ligand **36** alone and in the presence of various metal ions (Na^+, K^+, Mg^{2+}, Ca^{2+}, Al^{3+}, Zn^{2+}, Cd^{2+}, Pb^{2+} and H^+) are shown in Figure 3.3. The emission spectra of the ligands are characteristic of 9,10-disubstituted alkyl anthracenes.[98] The fluorescence emission spectrum for bis(morpholinoethyl) ligand **36** alone shows two bands at 405.0 and 428.5 nm and a small shoulder at *ca.* 453 nm. However, in the presence of acid the emission spectrum consists of three intense bands at 401.0, 424.0 and 449.5 nm, and a small shoulder at *ca.* 475 nm. Apart from a small shift to lower wavelength, the appearance of the emission curves remains the same. Noticeably, the ligand shows a far greater spectral response under fluorescence conditions rather than for UV-visible absorption conditions.

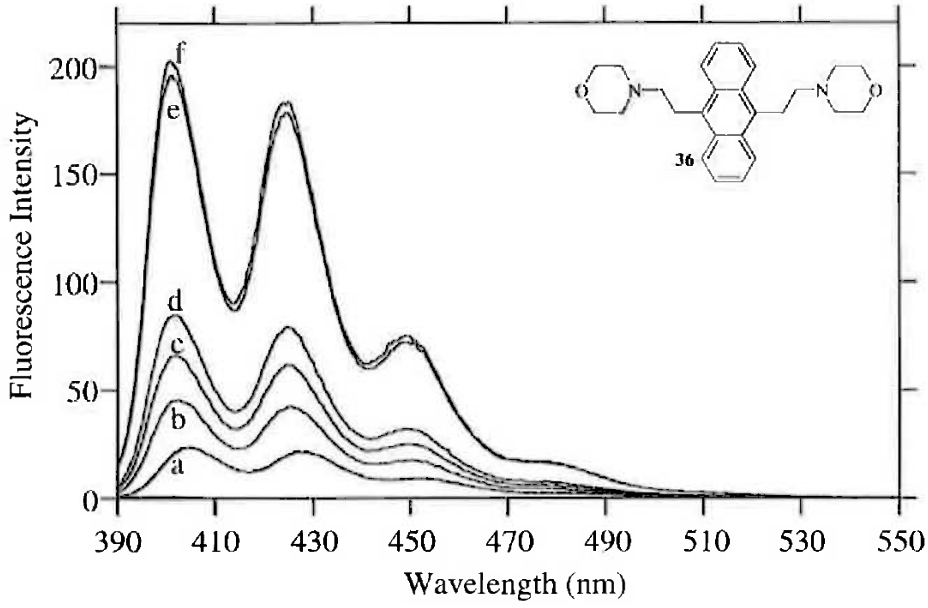

Figure 3.3. *Fluorescence emission spectra of bis(morpholinoethyl)* ***36*** *alone (a) and in the presence of (a)* Na^+, K^+ *and* Mg^{2+} *;(b)* Cd^{2+} *;(c)* Zn^{2+} *;(d)* Ca^{2+} *;(e)* Pb^{2+} *;(f)* Al^{3+} *and* H^+ *measured in 1,4-dioxane-water (40:60; v/v).* ***[36]*** $= 3.0 \times 10^{-6}$ *mol* dm^{-3}, $[M^{n+}(ClO_4)_n] = 5.0 \times 10^{-3}$ *mol* dm^{-3}, $[HClO_4] = 5.0 \times 10^{-3}$ *mol* dm^{-3}, $I = 0.050$ *mol* dm^{-3} (NEt_4ClO_4), $T = 298.2$ *K,* $\lambda_{ex} = 377.0$ *nm.*

Fluorescent responses are observed for Zn^{2+}, Ca^{2+}, Cd^{2+}, Pb^{2+}, Al^{3+} and H^+ as shown in Figure 3.3. Reflecting the UV-visible results, Pb^{2+}, Al^{3+} and H^+ ions all display the largest fluorescence enhancement. Furthermore, Zn^{2+}, Ca^{2+} and Cd^{2+} show moderate fluorescence enhancement when compared to the free ligand. The maximum intensity values for bis(morpholinoethyl) **36** in the presence of metal ions are shown in the Table 3.4. The emission curves display virtually unchanged spectral band characteristics. Apart from the intensity changes, a hypsochromic shift (4 nm) with acid is the only discernible feature. This indicates that there is little alteration in the nature of the fluorophore, simply an ON/OFF fluorescence switch is occurring. The fluorescence enhancement observed for the addition of acid equates to an approximate 8.5-fold increase by comparison with the free ligand **36**.

Table 3.4. Maximum intensity emission bands observed for bis(morpholinoethyl) **36** alone and in the presence of various metal ions in 1,4-dioxane-water (40:60; v/v). [**36**] = 3.0×10^{-6} mol dm^{-3}, [$M^{n+}(ClO_4)_n$] = 5.0×10^{-3} mol dm^{-3}, [$HClO_4$] = 5.0×10^{-3} mol dm^{-3}, I = 0.050 (NEt_4ClO_4), T = 298.2 K, λ_{ex} = 377.0 nm.

Complex	λ_{max} (nm)	Fluorescence intensity
Free ligand, **36**[a]	405.0	24
Ca^{2+}	401.5	85
Al^{3+}	401.0	200
Zn^{2+}	402.0	66
Cd^{2+}	402.5	45
Pb^{2+}	401.0	196
H^+	401.0	202

[a] Unchanged by the addition of Na^+, K^+ or Mg^{2+}.

The influence of spacer chain length on the fluorescence properties of the disubstituted alkyl anthracenes was investigated, as for the UV-visible study, with bis(morpholino-methyl) **38** and bis(morpholinopropyl) **42** ligands. The results obtained for bis(morpholinomethyl) **38** are shown in Table 3.5. With only a one carbon linker the fluorescence of the free ligand **38** is negligible under the measurement conditions. This result directly reflects the efficiency of the PET process such that, with a methyl rather than ethyl spacer, PET quenching is more efficient. The increased proximity of the amine nitrogen to the anthracene core causes the quenching process to be far more effective. A similar trend has been previously observed with phenylalkylamines and acid.[136] Only Ca^{2+}, Pb^{2+}, Al^{3+} and H^+ show any increase in fluorescence (Table 3.5) with the relative order identical to that observed for the bis(morpholinoethyl) **36** system.

A similar trend was observed for the propyl spacer, bis(morpholinopropyl) ligand **42**, where the largest fluorescence increase was in the presence of H^+. Again, Al^{3+}, Pb^{2+} and Ca^{2+} followed and there was also a fluorescent response to Zn^{2+} and Cd^{2+}. This fluorescent trend was further mirrored in the other ligands studied, bis(thiomorpholine) **52**, bis(piperazine) **53**, bis(azacrown) **45**, and mono(azacrown) **51**. Bis(hydroxyethyl) **34** and bis(propylamide) **41** however, show no alteration in fluorescence intensity regardless of analyte added. The significance of this is that a PET sensor requires a lone pair of electrons of the appropriate oxidation potential (as from an amine) for fluorescence

switching to occur. This result is a good proof of principle of the PET quenching mechanism.

Table 3.5. Maximum intensity emission bands observed for bis(morpholinomethyl) **38** alone and in the presence of various metal ions in 1,4-dioxane-water (40:60; v/v). [**38**] = 3.0 x 10^{-6} mol dm^{-3}, $[M^{n+}(ClO_4)_n]$ = 5.0 x 10^{-3} mol dm^{-3}, $[HClO_4]$ = 5.0 x 10^{-3} mol dm^{-3}, I = 0.050 mol dm^{-3} (NEt_4ClO_4), T = 298.2 K, λ_{ex} = 373.0 nm.

Complex	λ_{max} (nm)	Fluorescence intensity
Free ligand **38**[a]	403.0	1
Ca^{2+}	405.5	28
Al^{3+}	405.5	119
Pb^{2+}	405.0	51
H^+	405.0	157

[a] Unchanged by the addition of Na^+, K^+, Mg^{2+}, Zn^{2+} and Cd^{2+}.

Considering the range of different receptors used, the common fluorescence response to the same metal ions (Al^{3+}, Pb^{2+} and Ca^{2+}) appears somewhat coincidental, particularly since Pb^{2+} is generally viewed as a fluorescence quenching metal ion due to the "heavy atom" effect.[36,37] All the ligands studied show the maximum spectral response to acid, which supports the PET mechanism of action, as protonation should be the best analyte at involving the lone pair of nitrogen, thereby arresting PET quenching. In view of the sensitivity of the ligands to acid, the fluorescence response could well be due to protons liberated as a direct result of metal ion hydrolysis in aqueous solution.

3.3 Metal Hydroxide Formation

Aquo-cations, especially those of 4+, 3+, and small 2+ ions tend to act as acids in solution (Equation 3.3).[129] This behaviour can be ascribed to the influence of the positive charge on the metal ion facilitating the loss of a coordinated water proton. These metal ions can produce highly acidic hydrated species in aqueous media.

$$[M(H_2O)_x]^{n+} \rightleftharpoons [M(H_2O)_{x-1}OH]^{(n-1)+} + H^+ \qquad (3.3)$$

Frieser and co-workers[130] studied the hydrolysis of various metal ions via potentiometric titration in 50% aqueous dioxane at 298.2 K. The order of metal ion acidity they found

was $Al^{3+} > Pb^{2+} > Zn^{2+} > Cd^{2+}$ (Ca^{2+} not studied). This order appears to correlate with the order of the fluorescent responses found above for the ligands studied.

Potentiometric titrations undertaken with these ligands (Section 2.4) suggested that no metal complexation occurred (or $K \leq 100$ dm^3 mol^{-1}). Therefore, the fluorescence observed in the presence of metal ions is most probably a consequence of metal ion hydrolysis. A means to determine the plausibility, or otherwise, of this scenario is to redetermine the photophysical studies described above in the presence of a buffer, so as to exclude the possibility of H^+ mediated fluorescence.

3.4 Photophysical Properties in Buffered 1,4-Dioxane-Water Solution

It was decided to study the affect of pH on the UV-visible absorbance and fluorescence properties of the ligands at two different pH values. This was undertaken in accordance with the pK_a values previously determined (Section 2.3). It was thought that pH values could be chosen at which the metal ions were still soluble and the result of mono-protonation and complete deprotonation on the fluorescence of the free ligands could also be studied.

Thus, HEPES (*N*-2-hydroxyethylpiperazine-*N'*-2-ethanesulphonic acid) buffer system (see Section 6.1) was used to maintain a pH of 7.36 in 1,4-dioxane-water (40:60, v/v). Likewise, a boric acid/borate buffer system was used to maintain a pH of 10.00. HEPES has been previously shown to bind negligibly to the metal ions under consideration in this study.[137,138] Therefore, any affect of the buffer on the fluorescence of the solution is not a consequence of sequestration of the added metal ion.

Another possible problem with metal ions and buffers is that as the buffer removes acid from solution, the equilibrium shown in Equation 3.3 is shifted to the right, resulting in further production of metal hydroxide species. These metal hydroxides are often insoluble and so may precipitate from solution, an undesirable situation for photophysical measurements. Consequently, lower concentrations of metal ions were used than the non-buffered studies above to avoid the formation of any metal hydroxide precipitates. The alternative is to filter any prepared solution containing precipitate before measurement,

however this is undesirable since the concentrations of the species in solution become unknown.

3.4.1 UV-Visible Absorbance Properties

Several ligands were studied in both pH 7.36 and 10.00 buffered solutions under the same general conditions as used above. No alteration in the UV-visible absorbance spectra is observed for any ligand upon addition of any of the metal ions (Na^+, K^+, Mg^{2+}, Ca^{2+}, Al^{3+}, Zn^{2+}, Cd^{2+} and Pb^{2+} at 5.0×10^{-4} mol dm^{-3}) studied. In Table 3.6 are collated some UV-visible absorbance spectral data showing the values obtained in buffered solution.

Table 3.6. UV-visible molar absorbance (ε) values at pH 7.36 and 10.00 in 1,4-dioxane-water (40:60; v/v). [Ligand] = 6.6×10^{-5} mol dm^{-3}, [Buffer] = 0.050 mol dm^{-3}, I = 0.050 mol dm^{-3} (NEt_4ClO_4), T = 298.2 K.

	Maximum wavelength (nm) ($\varepsilon \times 10^{-3}$ (dm^3 mol^{-1} cm^{-1}))	
Ligand	pH 7.4 (HEPES)	pH 10.0 (borate)
Bis(morpholinoethyl) **36**	399.0 (10.7)	399.0 (10.7)
Bis(piperazine) **53**	399.0 (10.5)	399.5 (10.6)
Bis(azacrown) **45**	397.0 (9.1)	400.5 (8.3)
Mono(azacrown) **51**	399.0 (9.5)	400.5 (8.3)
Bis(hydroxyethyl) **34**	398.5 (9.2)	398.5 (9.2)

As can be seen in Table 3.6, a small bathochromic shift occurs upon measurement in higher pH solution. These changes were only observed when the ligand was capable of further deprotonation, that is, the fully non-protonated ligand is not completely present at pH 7.36 for bis(piperazine) **53** and the two azacrown containing systems, **45** and **51**. Similarly, when no further deprotonation can occur (eg. bis(morpholinoethyl) **36** and bis(hydroxyethyl) **34**), there is no spectral change in higher pH buffer (*vide infra*). Since no UV-visible spectral changes are observed for any ligand with any added analyte this suggests that the ligands are not complexing the metal ions.

3.4.2 Fluorescence Properties

The fluorescence properties of the ligands previously studied were subsequently redetermined in both pH 7.36 and 10.00 buffered solutions under the same general

conditions previously used, to ascertain whether fluorescence was due to metal ion hydrolysis induced protonation. Table 3.7 contains the fluorescence emission values for all of the ligands studied in the two buffers.

Table 3.7. Fluorescence values of ligands at pH 7.36 and 10.00 in 1,4-dioxane-water (40:60; v/v). [Ligand] = 3.0 x 10^{-6} mol dm^{-3}, [Buffer] = 0.050 mol dm^{-3}, I = 0.050 mol dm^{-3} (NEt_4ClO_4), T = 298.2 K.

	Fluorescence intensity (λ_{max} (nm))	
Ligand	pH 7.4 (HEPES)	pH 10.0 (borate)
Bis(morpholinomethyl) **38**[a]	1 (403.0)	1 (403.0)
Bis(morpholinoethyl) **36**[b]	25 (405.0)	25 (405.0)
Bis(morpholinpropyl) **42**[b]	129 (406.5)	129 (406.5)
Bis(thiomorpholine) **52**[c]	21 (406.5)	21 (406.5)
Bis(piperazine) **53**[c]	160 (405.5)	27 (406.0)
Bis(azacrown) **45**[c]	89 (401.5)	3 (406.0)
Mono(azacrown) **51**[c]	146 (404.5)	11 (406.0)
Bis(propylamide) **41**[c]	220 (405.5)	220 (405.5)
Bis(hydroxyethyl) **34**[b]	183 (405.0)	183 (405.0)

[a] λ_{ex} = 373.0 nm. [b] λ_{ex} = 377.0 nm. [c] λ_{ex} = 378.0 nm.

The emission intensity values for the ligands above are shown in the absence of any analyte as no alteration in fluorescence is observed upon the addition of any metal ion (Na^+, K^+, Mg^{2+}, Ca^{2+}, Al^{3+}, Zn^{2+}, Cd^{2+} and Pb^{2+} at 5.0 x 10^{-4} mol dm^{-3}). As there is no metal ion induced fluorescent response when the solutions were measured under constant, buffered pH conditions, this suggests that, as indicated with the UV-visible absorbance spectra, the fluorescence observed in the unbuffered solutions is a result of metal ion hydrolysis. Evidently, the relevant metal ions (Ca^{2+}, Al^{3+}, Zn^{2+}, Cd^{2+} and Pb^{2+}) undergo varying degrees of hydrolysis,[130] thus liberating acid that protonates the ligands, thereby causing a fluorescence response. This would also explain why the maximum fluorescence intensity of the metal ions often mirrored that observed for the addition of acid in the non-buffered study.

The problem of fluorescence arising from protonation being erroneously attributed to analyte complexation has also been discussed by James and co-workers.[139] The compound, *N*-(9-anthrylmethyl)diethanolamine, was designed to be utilised as a sensor for boronic and boric acids. When James *et al.* repeated some work of Wang *et al.*[140] they

discovered a discrepancy in the fluorescence results. That is, when phenylboronic acid was added to the sensor in non-buffered methanol that had not been rigorously dried, a fluorescence response was observed. However, minimal fluorescence response was noted in buffered methanolic aqueous solution. It was suggested that water molecules present in the methanol coordinated with the boron Lewis acid thereby becoming more acidic, consequently protonating the sensor.[139] The lack of significant binding of phenylboronic acid to the sensor was further confirmed by NMR studies.[139] Hence, the previously reported boronic acid sensor[140] was in fact only a proton sensor.[139] Clearly it is prudent (and necessary) to perform photophysical measurements involving PET fluorescent sensors under buffered conditions for accurate and meaningful results. Another alternative is to use a rigorously anhydrous organic solvent (see Chapter 4).

The role protonation plays in fluorescence can be seen in Figure 3.4, where representative emission spectra for bis(azacrown) **45**, mono(azacrown) **51** and bis(piperazine) **53** in the two different buffered systems are shown. The pH of the solution can significantly influence the magnitude of fluorescence emission for these ligands in the absence of any metal ions.

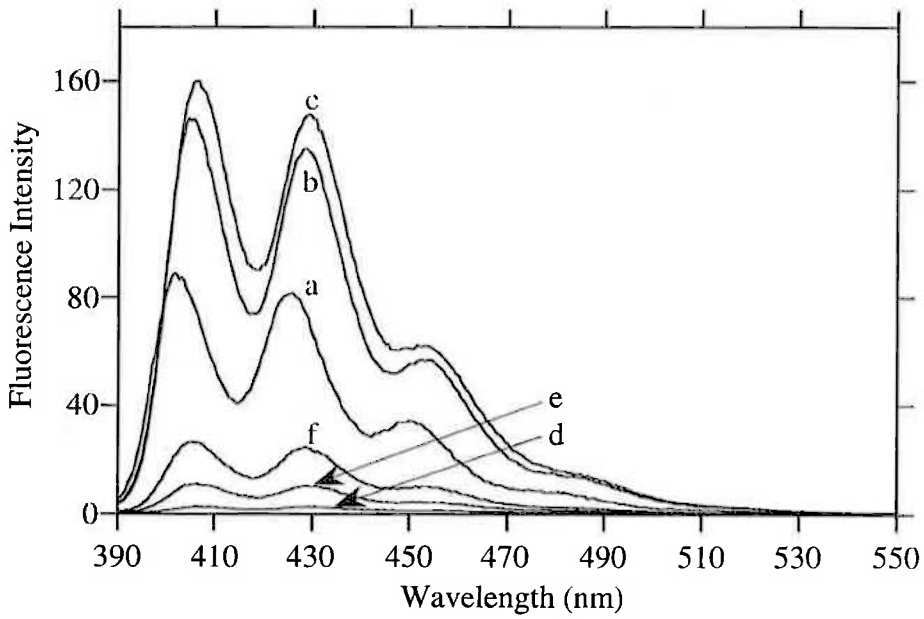

Figure 3.4. *Fluorescence emission spectra of ligands in pH 7.36 buffered solution, (a) bis(azacrown)* ***45****; (b) mono(azacrown)* ***51****; (c) bis(piperazine)* ***53*** *and in pH 10.00 buffered solution, (d) bis(azacrown)* ***45****; (e) mono(azacrown)* ***51****; (f) bis(piperazine)* ***53*** *measured in 1,4-dioxane-water (40:60; v/v). [Ligand] = 3.0 x 10^{-6} mol dm^{-3}, [Buffer] = 0.050 mol dm^{-3}, I = 0.050 mol dm^{-3} (NEt_4ClO_4), T = 298.2 K, λ_{ex} = 378.0 nm.*

Only bis(azacrown) **45**, mono(azacrown) **51**, and bis(piperazine) **53** ligands are shown above as they alone (of the ligands studied) show this effect at the two pH values studied. Clearly, these ligands are undergoing changes in protonation, at these pH values, that directly impinge upon their fluorescence, unlike the other ligands in Table 3.7.

Protonation induced fluorescence has been observed before[24,52,53,112,141-143] and is a direct consequence of the mechanism for this type of PET mediated fluorescent signalling. The cause is that the lone pair of an amine nitrogen transfers an electron to the photo-produced vacancy in the HOMO of the fluorophore, which quenches the fluorescence. When this nitrogen is protonated these electron transfer paths to the photo-excited state of anthracene are no longer operative and so fluorescence is restored.[65] Further support for this mechanism is the insensitivity of bis(propylamide) **41** to acid which has no free amine since the nitrogen is part of an amide moiety.

The different levels of fluorescence observed for bis(azacrown) **45**, mono(azacrown) **51**, and bis(piperazine) **53** ligands at pH 7.36 are the outcome of their differing degrees of protonation. The speciation diagrams for bis(azacrown) **45** and bis(piperazine) **53** ligands are shown in Figures 3.5 and 3.6, respectively.

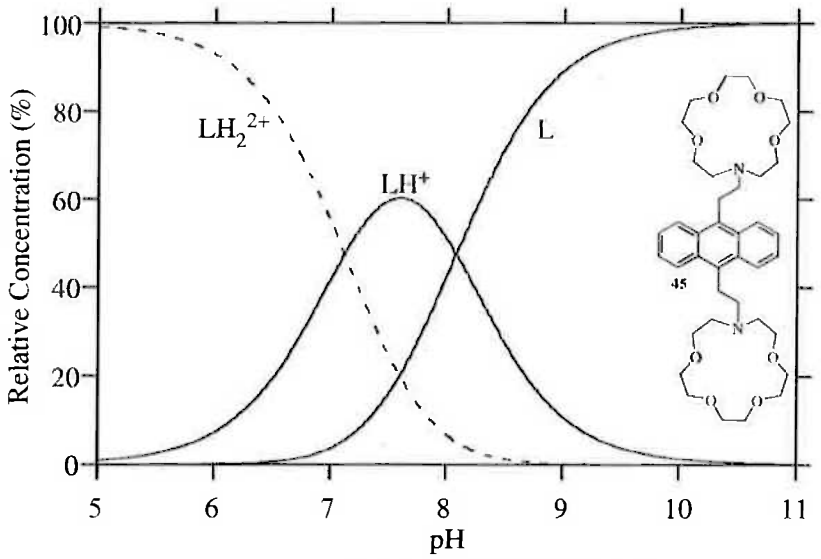

Species	L	LH^+	LH_2^{2+}
% at pH 7.36	10.9	56.7	32.4
% at pH 10.00	98.8	1.2	0.0

Figure 3.5. *Species distribution diagram of bis(azacrown)* ***45*** *as a function of pH. A dashed (- - - -) curve indicates a fluorescent species and % concentration is shown relative to the total concentration of ligand.*

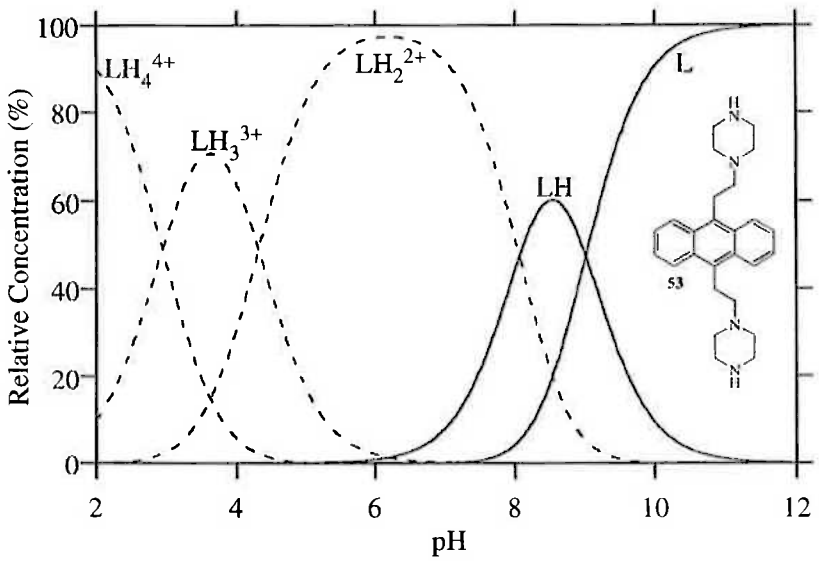

Species	L	LH^+	LH_2^{2+}	LH_3^{3+}	LH_4^{4+}
% at pH 7.36	0.4	16.6	82.9	0.1	0.0
% at pH 10.00	90.4	9.5	0.1	0.0	0.0

Figure 3.6. *Species distribution diagram of bis(piperazine)* ***53*** *as a function of pH. A dashed (- - - -) curve indicates a fluorescent species and % concentration is shown relative to the total concentration of ligand.*

Bis(piperazine) **45** is fluorescent despite two of its nitrogen existing as free amines. This is a result firstly of electrostatic repulsion causing each piperazine ring to accept a single proton. Secondly, even though nitrogen basicity would suggest that the protons are located on the secondary nitrogens,[123] this proton must be significantly 'shared' between the two nitrogens within each six-membered ring to halt the PET process. Support for this idea is found in a gas phase study utilising mass spectrometry which found clear evidence of intramolecular hydrogen bonding between the two heteroatoms in morpholine.[144] Consequently, the fluorescence of bis(piperazine) **53** only begins to diminish as the presence of this doubly protonated species also diminishes. Contrastingly, a 9-piperazinomethyl anthracene compound (**2**, Section 1.3.2) showed a quenching of fluorescence after one nitrogen was deprotonated.[25,145] The methylene spacer is obviously significant for this example, possibly sterically hindering the intramolecular hydrogen bonding.

The morpholine containing ligands with one, two and three carbon spacers (**38**, **36** and **42**, respectively) show no change in the magnitude of fluorescence at either buffer pH (Table

3.7). At pH 7.36 there is an insignificant amount of the doubly protonated species present for both bis(morpholinoethyl) **36** and bis(morpholinopropyl) **42** ligands (0% and 2%, respectively). Therefore, no further fluorescently important deprotonation occurs and there is no alteration in fluorescence.

The basis for this is that when a single amine nitrogen adjacent to the anthracene is deprotonated it is then able to quench the fluorescence by the mechanism described above. Consequently, a singly protonated diamine ligand is not fluorescent as although one amine is protonated there is a free amine nitrogen that can efficiently quench the fluorescence. The net result of this is that the two amine sites involved in PET quenching need to be protonated in order to switch on fluorescence, as has been previously observed for similar systems.[103,143]

A compound series utilising the 4-amino-1,8-naphthalimide fluorophore with two separate and independently operating PET pathways has further delineated this requirement.[146] The two PET pathways present were, from a pH-dependent donor to the fluorophore (PET input path), and from the fluorophore to an acceptor (PET output path). The input path was deactivated by protonation and the output path was deactivated by structural modification. It was found that if either pathway was operative (i.e. PET was ON), fluorescence was quenched.[146] See Sections 1.3.3 and 1.3.7 for further examples.

The magnitude of the basal fluorescence of the ligands at pH 10.00 also varies. This is significant as it is essentially a direct reflection of the efficiency of the PET process for each ligand.

Bis(azacrown) ligand **45** is less fluorescent (or more efficiently quenched) than the mono(azacrown) ligand **51** as the presence of two proximal amines allows more efficient quenching than a single amine. More successful electron transfer paths are available for quenching when two nitrogens are present[147] although as indicated above, one amine is sufficient for PET as the difference between the two is only small.

The variation in receptor also changes the fluorescence, such as between the azacrown receptor and morpholine receptor. All the six-membered ring containing receptor ligands have a similar level of fluorescence which is greater than that of the bis(azacrown) system **45**. This is due to the various oxidation potentials of the different receptor units and so their corresponding quenching efficiency.[148] Therefore, an amine receptor with a greater oxidation potential than those used in this study would have a higher baseline fluorescence.

The effect of spacer length on fluorescence efficiency is illustrated by the methyl **38**, ethyl **36**, and propyl **42** morpholine series of ligands. The fluorescence of bis(morpholino-methyl) **38** is negligible yet that of bis(morpholinopropyl) **42** is almost as large as that for the fully protonated methyl system **38**. The more distant the amine quencher is from the anthracene core, the less efficient the resulting PET quenching process.[141] Generally PET is considered to be a through bond process and the results described above are in accordance with this.[149,150] A series of structurally rigid, difunctional molecules of fixed distance and orientation have also been used to demonstrate this principle.[150]

Taken as a whole, these results show the universality of the Fluorophore-Spacer-Receptor design strategy where it is possible to alter components for varying targets and environments. Thus, some of the acidity related problems presented above can be ameliorated by using amine donors with different basicities affording the free amine as desired. For instance, de Silva and co-workers used an aniline-type nitrogen thereby negating protonic effects above pH 6.[151] Likewise, a substituted benzyl amine has also been utilised[29] or the nitrogen can even be removed completely.[152] The fluorophore sub-unit can also be altered (although not in this study) with coumarin[153] and squaraine[154] dyes, just two of many examples used (see Section 1.3). The spacer has been little altered in the literature[6,19] as generally only a methylene group is used. However, each subunit alteration can not be undertaken in isolation as each change influences other aspects of the molecule.

3.5 Summary and Conclusions

Photophysical measurements were performed in non-buffered 1,4-dioxane-water which initially appeared to afford some promising results. UV-visible absorbance spectra generally show only slight spectral changes for all ligands studied. The fluorescence response observed for the same ligands is much larger, with acid always producing the greatest effect of the analytes studied (Na^+, K^+, Mg^{2+}, Ca^{2+}, Al^{3+}, Zn^{2+}, Cd^{2+}, Pb^{2+} and H^+). This indicates that PET is indeed the quenching mechanism involved as desired by the molecular design.

The possibility of metal ion hydrolysis producing acid and thereby inducing fluorescence through protonation of the ligands was investigated by measurements in buffered solution. These studies show that none of the analytes added cause any observable change in the

fluorescence output. Therefore, the hypothesis of undesired acid production producing the fluorescence response was verified.

The obvious lesson to learn from this study is that this generic type of ligand is extremely sensitive to acid, ignoring this aspect is at the investigator's peril. Consequently, any solution used must be buffered to prevent the occurrence of erroneous, false positive, results. Indeed, the possibility of protonation must always be conclusively excluded before continuing with any study on this type of fluorescent sensor. An alternative method is to rigorously excluded water and hence negate the possibility of acid interfering with any measurements.

Clearly the basicity of these types of sensors is an important consideration when they are to be used in an aqueous environment, whether it is a buffered environment or not. This consideration arises because, as observed in the buffered study, the basal fluorescence level of a ligand is largely dependent upon the basicity of its amines. Thus, a more basic ligand would have a higher baseline fluorescence (at a larger range of pH values) thus reducing the degree to which the signal can be enhanced. Furthermore, the length of the spacer was found to also be a major factor responsible for the baseline level of fluorescence. When the spacer reaches the length of three carbons (propyl spacer) the significance of PET quenching is severely reduced. No meaningful comments can be made regarding the significance of the azacrown systems (i.e. one or two receptor units) since no metal ion complexation was involved for either system.

Since no (or negligible) metal ion complexation is observed in 1,4-dioxane-water solvent mixture it would be useful to attempt the same photophysical measurements in acetonitrile, a much less strongly coordinating solvent. In such a solvent metal ion complexation is more favourable and therefore it may be possible to further ascertain some properties of these fluorescent sensors. The following chapter will describe photophysical investigations towards this end.

Chapter 4 Fluorescence Sensing of Metal Ions by Anthracene Ligands in Acetonitrile Solution

4.1 Introduction

The solvent can have a very large influence on the stability and selectivity of metal ion complexation. This complexation involves substitution of several solvent molecules from the inner coordination sphere of the metal ion and may be regarded as a competition between the solvent and the ligand for coordination of the metal ion.

The stability constant of a complex generally increases as the solvating power of the solvent towards metal ions decreases.[155,156] For instance, two studies which obtained a series of stability constants for Na^+ with several crown systems in a range of water-methanol solvent mixtures found that as the proportion of methanol increased the complex stability also increased.[157,158] Frensdorff has similarly studied a range of univalent metal ions with a series of crown ether compounds in both water and methanol and found that the stability constants were generally at least two orders of magnitude greater in methanol.[159] Consequently, using acetonitrile in this investigation as the solvent for the photophysical studies should favour metal ion complexation, as compared to the studies described in the previous chapters using a 1,4-dioxane-water solvent mixture.

The majority of the ligands used in this study contain the hard ether oxygen donor group which generally shows a preference for binding with hard acid metal ions.[100,101] A useful series of metal ions to study are therefore the alkali (Group IA) metal ions Li^+, Na^+, K^+, Rb^+ and Cs^+, and the alkaline earth (Group IIA) metal ions Mg^{2+}, Ca^{2+}, Sr^{2+} and Ba^{2+} which are known to complex azacrowns.[29,41,117] Due to their closed shell, inert gas electronic structure, alkali and alkaline earth metal ions are not expected to show strong stereochemical requirements in complex formation (as do the transition metal ions) and so it is possible to observe complexation characteristics without being too concerned with any coordination directionality, other than that exerted by the multidentate ligand. Metal ion

size is an important consideration in complexation and so the ionic radii for these metal ions are collected in Table 4.1.

Table 4.1. Ionic radii of alkali and alkaline earth metal ions for various coordination numbers.[160]

	Ionic radii (Å) for coordination numbers 6-11					
Metal ion	6	7	8	9	10	11
Li^+	0.76		0.92			
Na^+	1.02	1.12	1.18	1.24		
K^+	1.38	1.46	1.51	1.55	1.59	
Rb^+	1.52	1.56	1.61	1.63	1.66	1.69
Cs^+	1.67		1.74	1.78	1.81	1.85
Mg^{2+}	0.72		0.89			
Ca^{2+}	1.00	1.06	1.12	1.18	1.23	
Sr^{2+}	1.18	1.21	1.26	1.31	1.36	
Ba^{2+}	1.35	1.38	1.42	1.47	1.52	1.57

Therefore, to further investigate the photophysical properties of the previously discussed ligands they were studied in acetonitrile solution with a range of alkali and alkaline earth metal ions. Where possible, complexation constants were determined for metal ion complexation by these ligands. These constants allow various design aspects of the ligands, such as the number of receptors and the nature of the complexing atoms, to be evaluated with respect to their likely influence on fluorescent signalling ability. Thus, these studies are intended to enhance the understanding of the underlying design principles required for PET based fluorescent sensors.

4.2 UV-Visible Absorbance Properties in the Presence of Metal Ions

Acetonitrile is a polar aprotic organic solvent with good UV transparency (> 213 nm for 1.0 cm path length)[134] in which all of the studied ligands are soluble. UV-visible absorbance spectra were measured over the 300-450 nm range for all of the ligands studied in the presence of 0.050 mol dm^{-3} tetraethylammonium perchlorate (NEt_4ClO_4) to maintain a constant ionic strength. The spectra were recorded for each ligand with a

variety of metal ions (Li^+, Na^+, K^+, Rb^+, Cs^+, Mg^{2+}, Ca^{2+}, Sr^{2+} and Ba^{2+}) to determine their influence on the substituted anthracene ligand absorption. The absorbance spectra of bis(azacrown) **45** alone and in the presence of Mg^{2+} is shown in Figure 4.1 as a typical example.

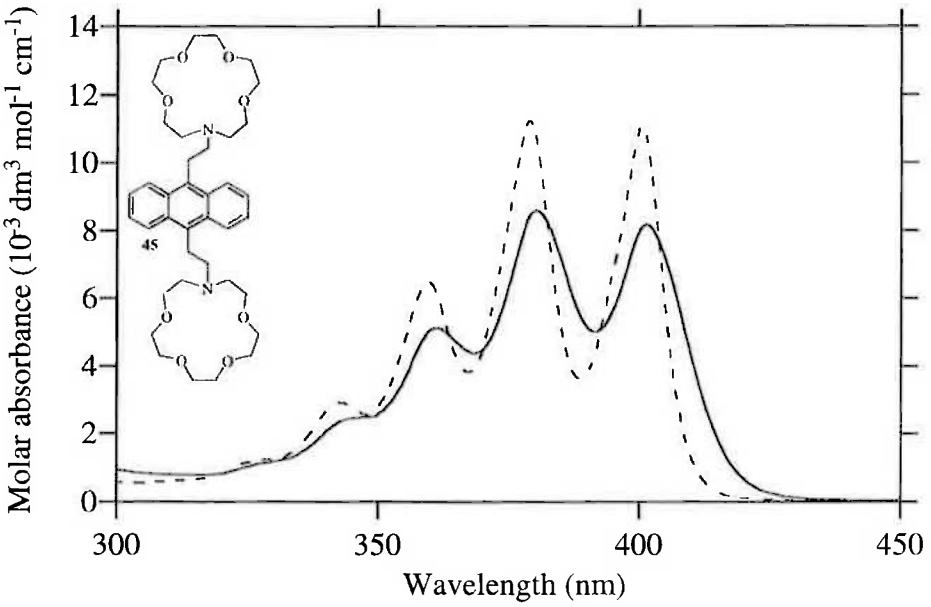

Figure 4.1. *UV-visible absorbance spectra of bis(azacrown) ligand* ***45*** *alone (——) and in the presence of* Mg^{2+} *(– – –) measured in acetonitrile.* ***[45]*** *= 6.6 x* 10^{-5} *mol* dm^{-3}, $[Mg(ClO_4)_2]$ *= 6.0 x* 10^{-4} *mol* dm^{-3}, *I = 0.050 mol* dm^{-3} (NEt_4ClO_4), *T = 298.2 K.*

The UV-visible absorbance spectra of the ligands are characteristic of 9,10-disubstituted alkyl anthracenes.[135] The absorption spectra of the bis(morpholinoethyl) ligand **36** displays four absorption bands with λ_{max} at 399.0, 378.0, 359.0 and 342.5 nm, and a shoulder at *ca.* 328 nm, essentially unchanged from those observed in 1,4-dioxane-water. Since the absorbance spectra undergo only small shifts with changing solvent polarity, this indicates that only a small difference between the dipole moments of the ground and excited states exists. Upon the addition of metal ions to the bis(morpholinoethyl) ligand **36**, little or no spectral changes are observed. The greatest spectral shift is observed in the presence of Mg^{2+} where a small hypsochromic shift of 4 nm and a slight increase in molar absorptivity are observed (Table 4.2).

Table 4.2. UV-visible molar absorbance (ε) values for the longest wavelength peak of various ligands alone and in the presence of Mg^{2+} in acetonitrile. [Ligand] = 6.6 x 10^{-5} mol dm^{-3}, [$Mg(ClO_4)_2$] = 6.0 x 10^{-4} mol dm^{-3}, I = 0.050 mol dm^{-3} (NEt_4ClO_4), T = 298.2 K.

	Maximum wavelength (nm) (ε x 10^{-3} (dm^3 mol^{-1} cm^{-1}))	
Ligand	Free ligand	Mg^{2+} Complex
Bis(morpholinomethyl) **38**	394.0 (11.6)	397.0 (10.5)
Bis(morpholinoethyl) **36**	399.0 (9.1)	395.0 (11.6)
Bis(morpholinopropyl) **42**	400.0 (11.8)	397.0 (12.8)
Bis(thiomorpholine) **52**[a]	400.0 (8.0)	395.0 (11.5)
Bis(piperazine) **53**[a]	399.5 (11.0)	398.0 (11.6)
Bis(azacrown) **45**	401.5 (8.2)	400.5 (11.1)
Mono(azacrown) **51**	399.5 (7.8)	399.5 (9.3)
Bis(propylamide) **41**	399.0 (10.0)	[b]
Bis(hydroxyethyl) **34**	398.0 (7.3)	[b]

[a] At 3.3 x 10^{-5} mol dm^{-3}. [b] Absorbance unchanged by the addition of Mg^{2+}.

The absorbance values for all the ligands studied, alone and in the presence of Mg^{2+}, are also shown in Table 4.2. The values in the presence Mg^{2+} are chosen as they display the largest spectral change of all the metal ions studied. The UV-visible absorption spectra generally show only small spectral changes, if any, upon the addition of the metal ions in acetonitrile. Typically a molar absorbance increase, of varying degree, is the major change observed (excluding **38**). Thus, the absorbance spectra of the ligands are only slightly perturbed by the presence of these metal ions in acetonitrile, as was similarly observed in 1,4-dioxane-water (Section 3.2.1).

4.3 Determination of Stability Constants from Fluorescence

The complexation of a metal ion (M^{n+}) by a ligand (L) may be expressed as;

$$M^{n+} + L \underset{}{\overset{K_1}{\rightleftharpoons}} [ML]^{n+} \qquad (4.1)$$

and if a second metal ion is then complexed;

$$M^{n+} + [ML]^{n+} \overset{K_2}{\rightleftharpoons} [M_2L]^{2n+} \tag{4.2}$$

where the stepwise stability constants, K_1 and K_2, are given by

$$K_1 = \frac{[ML^{n+}]}{[M^{n+}][L]} \tag{4.3}$$

$$K_2 = \frac{[M_2L]^{2n+}}{[M^{n+}][ML]^{n+}} \tag{4.4}$$

Furthermore, an overall stability constant, β_2, which is the product of the stepwise formation constants above, can be defined as;

$$2\,M^{n+} + L \overset{\beta_2}{\rightleftharpoons} [M_2L]^{2n+} \tag{4.5}$$

$$\beta_2 = \frac{[M_2L]^{2n+}}{[M^{n+}]^2[L]} = K_1.K_2 \tag{4.6}$$

A variety of methods can be utilised to study such complexation phenomena, for instance potentiometric titrations (Section 2.4), NMR spectroscopy and UV-visible or fluorescence spectroscopy, amongst others.[161,162] As fluorescence spectroscopy is often a very sensitive technique, it is ideal for studying low concentrations as in this study, and accordingly was the method chosen. Fluorescence spectroscopy can be used to study complexation phenomena provided that significant spectral differences exist between the ligand and any complex that may form.[161] The determination of values for K_1 and K_2 quantifies the ability of a ligand to complex a metal ion and also allows its specificity to be established.

For the quantitative determination of stability constants a common method used, and that employed for this work, is the mole ratio method whereby the ligand concentration is kept constant and the metal ion concentration is varied.[161,163] The metal ion concentrations usually vary in increments up to and including a concentration at which no further spectral change occurs such that formation of the complex is at, or approaches, completion. The data acquired from these solutions, containing a ligand with varying metal ion concentrations, were fitted to a particular algorithm using non-linear least-squares regression through the Matlab computer programme DATAFIT/SPECFIT[164] (see Section 6.6). Values obtained from non-linear regression methods are generally more reliable than

those obtained by linear fitting methods such as double reciprocal plots that place more weight on lower concentration values than on the higher ones.[165]

The SPECFIT programme allows different complexation stoichiometries to be investigated. Consequently, either an algorithm arising from the equilibrium shown in Equation 4.1 (i.e. formation of a (metal)•(ligand) complex alone) or an algorithm arising from the equilibria shown in Equations 4.1 and 4.2 (i.e. formation of both (metal)•(ligand) and $(metal)_2$•(ligand) complexes) were fitted. The two different models described will hereafter be referred to as the 1:1 binding model or the 2:1 binding model, respectively. The 2:1 binding model involves simultaneous fitting for both a (metal)•(ligand) complex and a $(metal)_2$•(ligand) complex as the formation of the latter species is necessarily preceded by (metal)•(ligand) complex formation. Also, SPECFIT displays the calculated emission spectrum for each of the species included in a particular binding model.

Finally, the use of matrices permitted simultaneous fitting of the data obtained at 0.5 nm intervals over the wavelength range 390-550 nm, in which a significant change in fluorescence intensity was observed. Therefore, the derived stability constants are based on between 3,220 and 8,000 data points (dependent upon the number of solutions used). The sum of the squared deviation (SSD) of each fit is for the best fit curve to all of the data points.

Due to the errors involved in spectral measurement and solution preparation, the actual errors on the derived stability constants are greater than the non-weighted standard deviations quoted (but they are unlikely exceed the non-weighted standard deviation by a factor of two in these systems).

4.4 Fluorescence Properties in the Presence of Metal Ions

Fluorescence emission spectra were measured over the 390-550 nm range for all ligands studied in the presence of 0.050 mol dm^{-3} tetraethylammonium perchlorate (NEt_4ClO_4) to maintain a constant ionic strength. The ligand concentration was constant at 3.0×10^{-6} mol dm^{-3}. The spectra were recorded for each ligand with a variety of metal perchlorate salts (Li^+, Na^+, K^+, Rb^+, Cs^+, Mg^{2+}, Ca^{2+}, Sr^{2+} and Ba^{2+}) to determine their effect, if any, on the substituted anthracene ligands fluorescence. The perchlorate salts were used since the perchlorate ion does not significantly complex to metal ions in solution. Where the

fluorescence change was spectrally significant a spectrofluorimetric titration was undertaken for that metal ion, as described in Section 4.3.

4.4.1 Metal Ion Complexation by Bis(morpholinomethyl) 38

Typical emission spectra for bis(morpholinomethyl) ligand **38** alone and in the presence of increasing concentrations of Mg^{2+} are shown in Figure 4.2. The emission spectra of the ligands are characteristic of 9,10-disubstituted alkyl anthracenes.[98] The fluorescence emission spectrum for bis(morpholinomethyl) ligand **38** alone is negligible under the measurement conditions with a quantum yield (Φ_F) of 0.001. However, upon the addition of Mg^{2+} an emission spectrum consisting of two intense bands at 405.5 and 429.0 nm, and a shoulder at *ca.* 451 nm is observed, the intensity of which increases with $[Mg^{2+}]$.

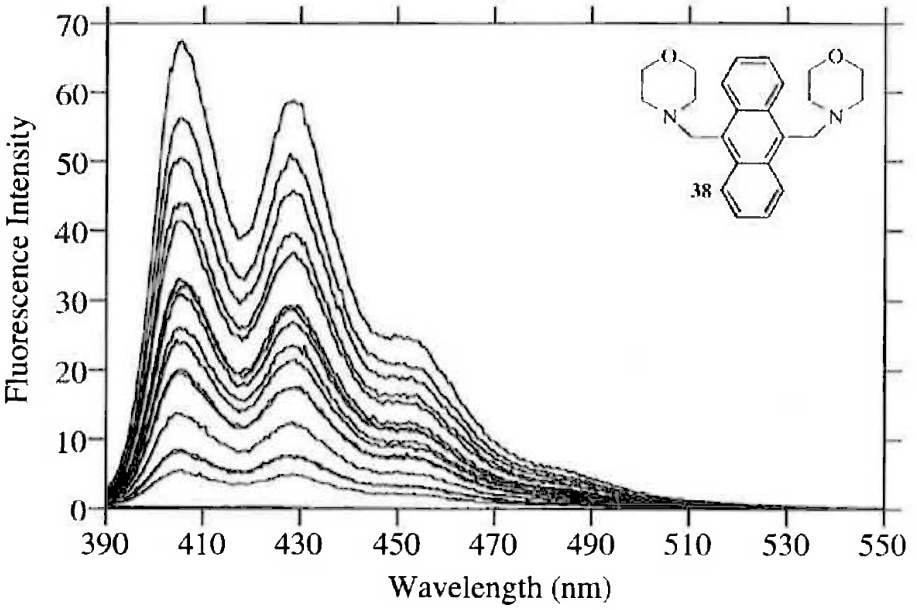

Figure 4.2. *Emission spectra of bis(morpholinomethyl)* ***38*** *alone (3.0 x 10^{-6} mol dm^{-3}) and in the presence of increasing concentrations of Mg^{2+} (ranging from 1.0 x 10^{-5} to 5.0 x 10^{-3} mol dm^{-3}) in acetonitrile (I = 0.050 mol dm^{-3}) at 298.2 K, when excited at 374.0 nm. The emission of* ***38*** *alone is coincident with the baseline.*

The general appearance of the emission spectra in the presence of Mg^{2+} remain the same apart from the alteration in intensity. The ligand shows a far greater spectral response for fluorescence than that witnessed for the UV-visible absorbance. The fluorescence enhancement observed for the addition of Mg^{2+} (Φ_F 0.31) is relatively large in comparison

with the free ligand **38**. This large increase is a direct result of the very low fluorescence of the free ligand.

The variation in ligand **38** fluorescence upon the addition of Mg^{2+} (ranging from 1.0×10^{-5} to 5.0×10^{-3} mol dm^{-3}) (Figure 4.2) was readily fitted to a 1:1 binding model (i.e. Equation 4.1). The binding curve for the complexation of Mg^{2+} by bis(morpholinomethyl) **38** at 405.0 nm displayed a reasonable visual fit as shown in Figure 4.3.

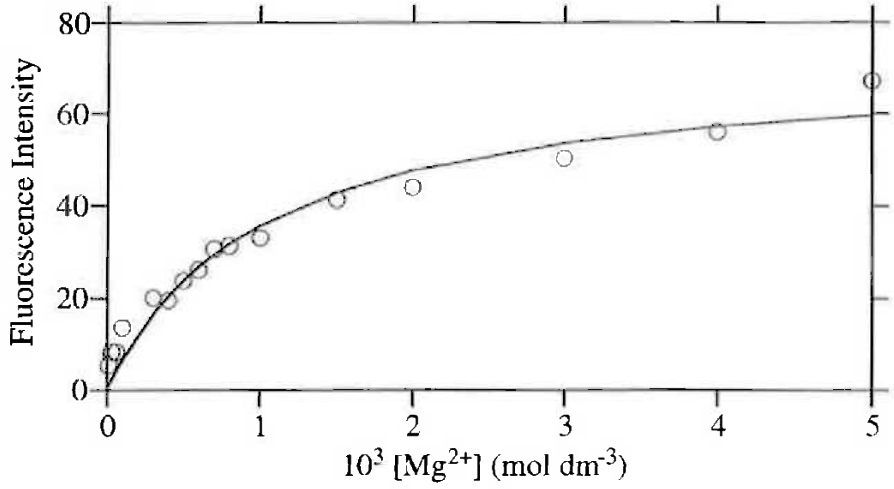

Figure 4.3. *Fluorescence variation of bis(morpholinomethyl) **38** (3.0×10^{-6} mol dm^{-3}) at 405.0 nm in the presence of increasing concentrations of Mg^{2+} (ranging from 1.0×10^{-5} to 5.0×10^{-3} mol dm^{-3}) in acetonitrile (I = 0.050 mol dm^{-3}) at 298.2 K, when excited at 374.0 nm. The circles represent experimentally obtained data points and the solid line represents the best fit of the data to a 1:1 binding model.*

Similarly, a fluorescence titration with ligand **38** and increasing concentrations of Ca^{2+} (ranging from 1.0×10^{-4} to 6.0×10^{-3} mol dm^{-3}) was performed (Appendix, Figure A.3). The resulting data could be fitted to a 1:1 binding model (Appendix, Figure A.4) to give a derived stability constant K_1. This value and the Φ_F of the complex is listed in Table 4.3.

Table 4.3. Stability constants (fitted to a 1:1 binding model) and quantum yields for the complexes of bis(morpholinomethyl) ligand **38** with metal ions in acetonitrile at 298.2 K.

Metal ion	K_1 ($dm^3\ mol^{-1}$)	SSD[a]	Φ_F[b]
None			0.001[c]
Mg^{2+}	$(1.10 \pm 0.01) \times 10^3$	1.8×10^4	0.31
Ca^{2+}	$(4.18 \pm 0.06) \times 10^2$	5.5×10^2	0.16
Sr^{2+}	[d]		[d]
Ba^{2+}	[d]		[d]

[a] Sum of the squared deviation. [b] Relative quantum yield determined from the calculated spectrum of the complex. [c] Experimentally determined value. [d] Spectral change too small to be determined.

The fluorescence response of the ligand in the presence of Sr^{2+} and Ba^{2+} is too small to allow the determination of any stability constants. Neither Mg^{2+} or Ca^{2+} data sets could be fitted to a 2:1 binding model. The bis(morpholinomethyl) ligand **38** displays no alteration in fluorescence emission in the presence of the alkali metal ions studied (Li^+, Na^+, K^+, Rb^+ and Cs^+).

4.4.2 Metal Ion Complexation by Bis(morpholinoethyl) 36

The fluorescence emission spectrum for bis(morpholinoethyl) ligand **36** alone shows two bands at 409.0 and 431.0 nm of low intensity when excited at 378.0 nm. Upon the addition of alkaline earth metal ions the emission intensity increases although the addition of alkali metal ions elicits no such response. The variation in ligand **36** fluorescence upon the addition of Ca^{2+} (ranging from 1.0×10^{-5} to 5.0×10^{-3} mol dm^{-3}) when excited at 365.0 nm is shown in Figure 4.4. For the metal ions that show a fluorescent response, the values obtained from fitting to a 1:1 binding model or to a 2:1 binding model are shown in Tables 4.4 and 4.5, respectively.

Table 4.4. Stability constants (fitted to a 1:1 binding model) and quantum yields for the complexes of bis(morpholinoethyl) ligand **36** with metal ions in acetonitrile at 298.2 K.

Metal ion	K_1 ($dm^3\ mol^{-1}$)	SSD[a]	Φ_F[b]
None			0.03[c]
Mg^{2+}	$(3.87 \pm 0.03) \times 10^4$	3.9×10^4	0.76
Ca^{2+}	$(1.65 \pm 0.01) \times 10^3$	1.7×10^4	0.75
Sr^{2+}	$(8.8 \pm 0.1) \times 10^2$	3.6×10^3	0.15
Ba^{2+}	$(4.96 \pm 0.07) \times 10^2$	1.8×10^3	0.11

[a] Sum of the squared deviation. [b] Relative quantum yield determined from the calculated spectrum of the complex. [c] Experimentally determined value.

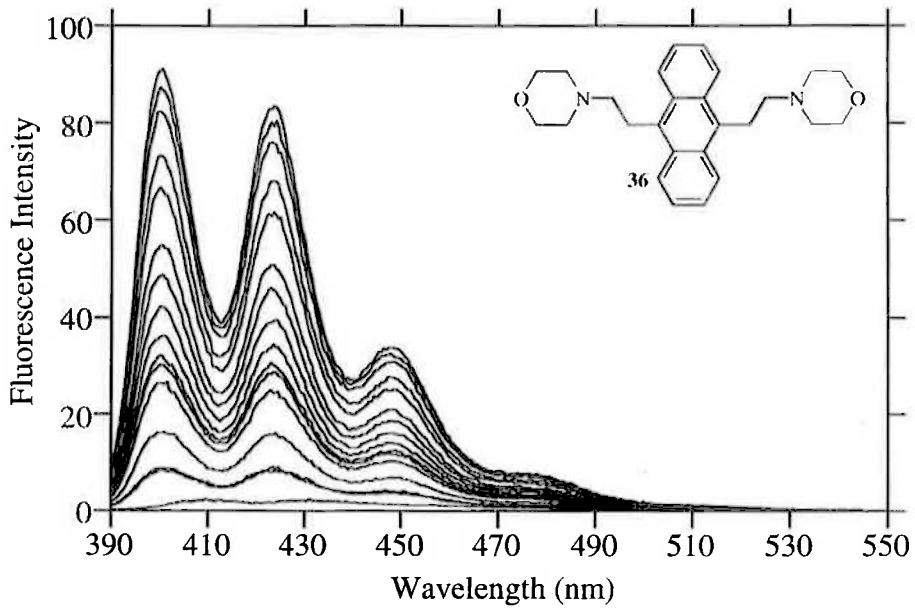

Figure 4.4. *Emission spectra of bis(morpholinoethyl)* ***36*** *alone (3.0×10^{-6} mol dm^{-3}) and in the presence of increasing concentrations of Ca^{2+} (ranging from 1.0×10^{-5} to 5.0×10^{-3} mol dm^{-3}) in acetonitrile (I = 0.050 mol dm^{-3}) at 298.2 K, when excited at 365.0 nm. The emission of* ***36*** *alone is the lowest intensity curve in the montage.*

Table 4.5. Stability constants (fitted to a 2:1 binding model) for the complexes of bis(morpholinoethyl) ligand **36** with metal ions in acetonitrile at 298.2 K.

Metal ion	K_1 (dm^3 mol^{-1})	Φ_F[a]	K_2 (dm^3 mol^{-1})	Φ_F[b]	SSD[c]
Mg^{2+}	$(9.19 \pm 0.07) \times 10^4$	0.58	$(1.19 \pm 0.01) \times 10^3$	0.92	9.9×10^3
Ca^{2+}	$(3.30 \pm 0.08) \times 10^4$	0.19	$(6.03 \pm 0.07) \times 10^2$	0.88	2.6×10^3
Sr^{2+}	$(1.57 \pm 0.04) \times 10^4$	0.06	$(1.17 \pm 0.03) \times 10^2$	0.26	4.5×10^2
Ba^{2+}	$(1.8 \pm 0.1) \times 10^5$	0.03	$(2.36 \pm 0.03) \times 10^2$	0.14	3.9×10^2

[a] Relative quantum yield determined from the calculated spectrum of the (metal)•(ligand) complex. [b] Relative quantum yield determined from the calculated spectrum of the $(metal)_2$•(ligand) complex. [c] Sum of the squared deviation.

The spectra in Figure 4.4 could be fitted to a 1:1 binding model to yield $K_1 = (1.65 \pm 0.01) \times 10^3$ dm^3 mol^{-1} (Figure 4.5a). Since some of the experimentally determined points do not coincide with the theoretical line, the spectra were also fitted to a 2:1 binding model which yielded $K_1 = (3.30 \pm 0.08) \times 10^4$ dm^3 mol^{-1} and $K_2 = (6.03 \pm 0.07) \times 10^2$ dm^3 mol^{-1} (Figure 4.5b). The errors for both fits are of similar magnitude indicating reliability in both calculations. The sum of the squared deviations (SSD) for this fit was 2.6×10^3, which is substantially less than the value of 1.7×10^4 for the 1:1 binding model. Although a decrease in the sum of the squared deviations is expected when the number of fitting parameters is increased, the magnitude of the change and the improved visual fit suggest that the 2:1 binding model is the most appropriate.

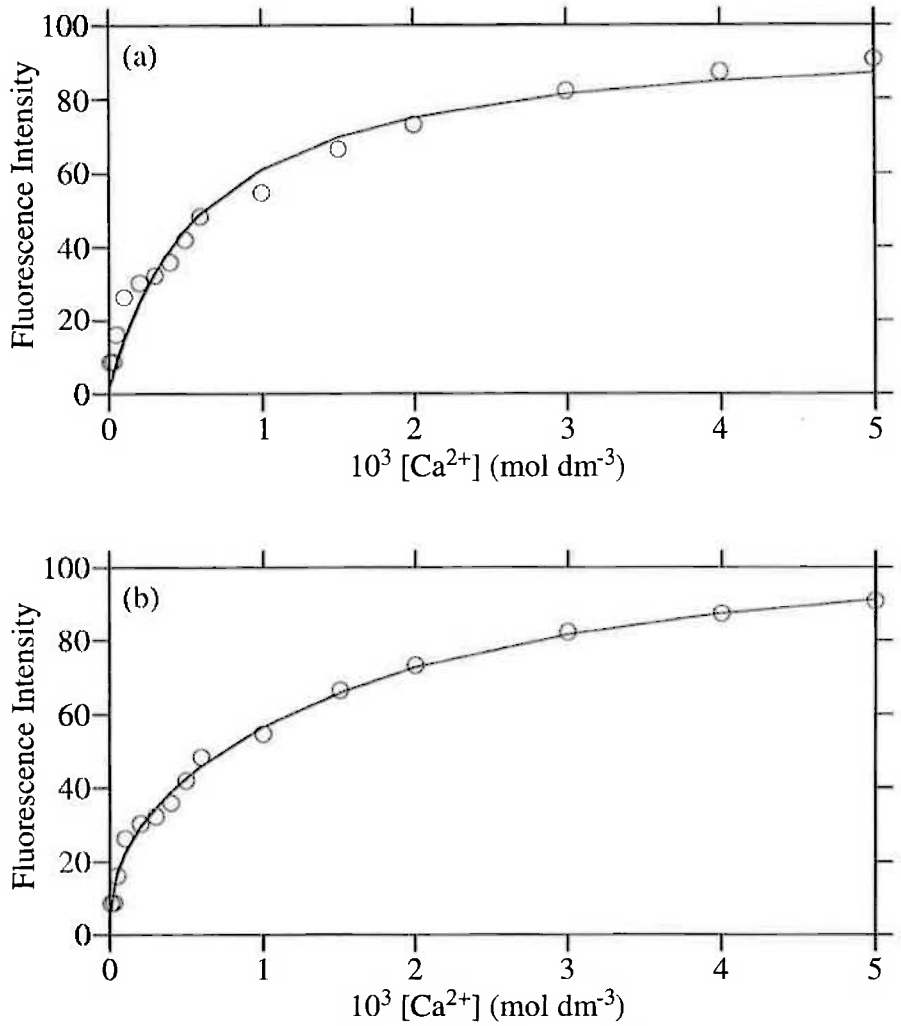

Figure 4.5. *Fluorescence variation of bis(morpholinoethyl)* ***36*** *(3.0 x 10^{-6} mol dm^{-3}) at 400.0 nm in the presence of increasing concentrations of Ca^{2+} (ranging from 1.0 x 10^{-5} to 5.0 x 10^{-3} mol dm^{-3}) in acetonitrile (I = 0.050 mol dm^{-3}) at 298.2 K, when excited at 365.0 nm. Graph (a) is the fit for a 1:1 binding model and (b) is the fit for a 2:1 binding model. The circles represent experimentally obtained data points and the solid line represents the best fit of the data.*

Likewise, the variation in ligand **36** fluorescence upon the addition of Sr^{2+} (ranging from 1.0 x 10^{-5} to 6.0 x 10^{-3} mol dm^{-3}) in acetonitrile when excited at 378.0 nm is shown in Figure 4.6. The emission intensity of Sr^{2+} (Φ_F 0.26) is significantly lower than that observed for Ca^{2+} (Φ_F 0.88).

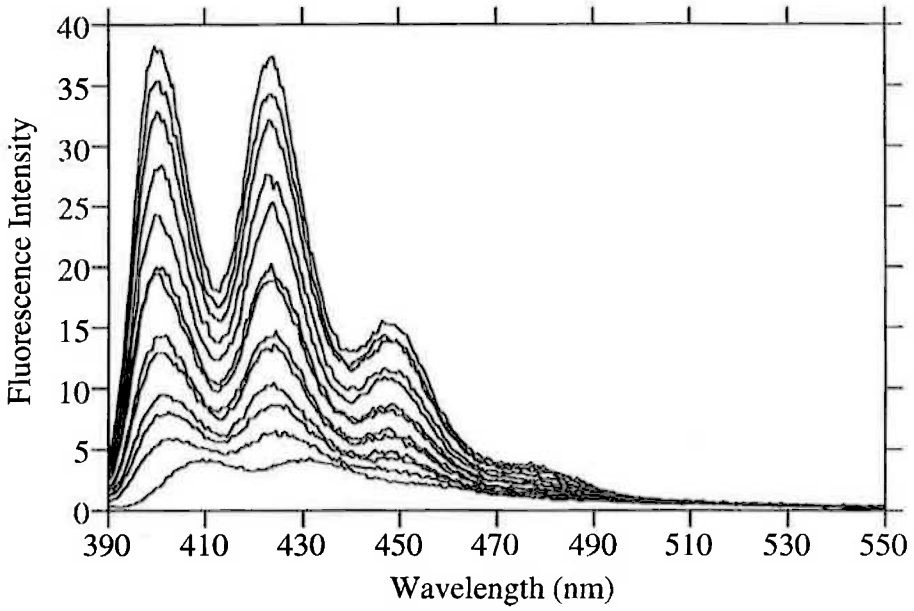

Figure 4.6. *Emission spectra of bis(morpholinoethyl)* ***36*** *alone (3.0 x 10^{-6} mol dm^{-3}) and in the presence of increasing concentrations of Sr^{2+} (ranging from 1.0 x 10^{-5} to 6.0 x 10^{-3} mol dm^{-3}) in acetonitrile (I = 0.050 mol dm^{-3}) at 298.2 K, when excited at 378.0 nm. The emission of* ***36*** *alone is the lowest intensity curve in the montage.*

The data could be fitted to a 1:1 binding model to yield K_1 = (8.8 ± 0.1) x 10^2 dm^3 mol^{-1} (Figure 4.7a). Although the emission spectra were successfully fitted to a 1:1 binding model they could also be fitted to 2:1 binding model which yielded K_1 = (1.57 ± 0.04) x 10^4 dm^3 mol^{-1} and K_2 = (1.17 ± 0.03) x 10^2 dm^3 mol^{-1} (Figure 4.7b). This fit had smaller errors than those observed when fitting for the (metal)•(ligand) complex alone. Also, two phases are now distinctly recognisable in the binding curve, corresponding to the formation of both (metal)•(ligand) and $(metal)_2$•(ligand) complexes. This, and the significantly improved visual fit, suggest that the 2:1 binding model is the most appropriate for Sr^{2+}.

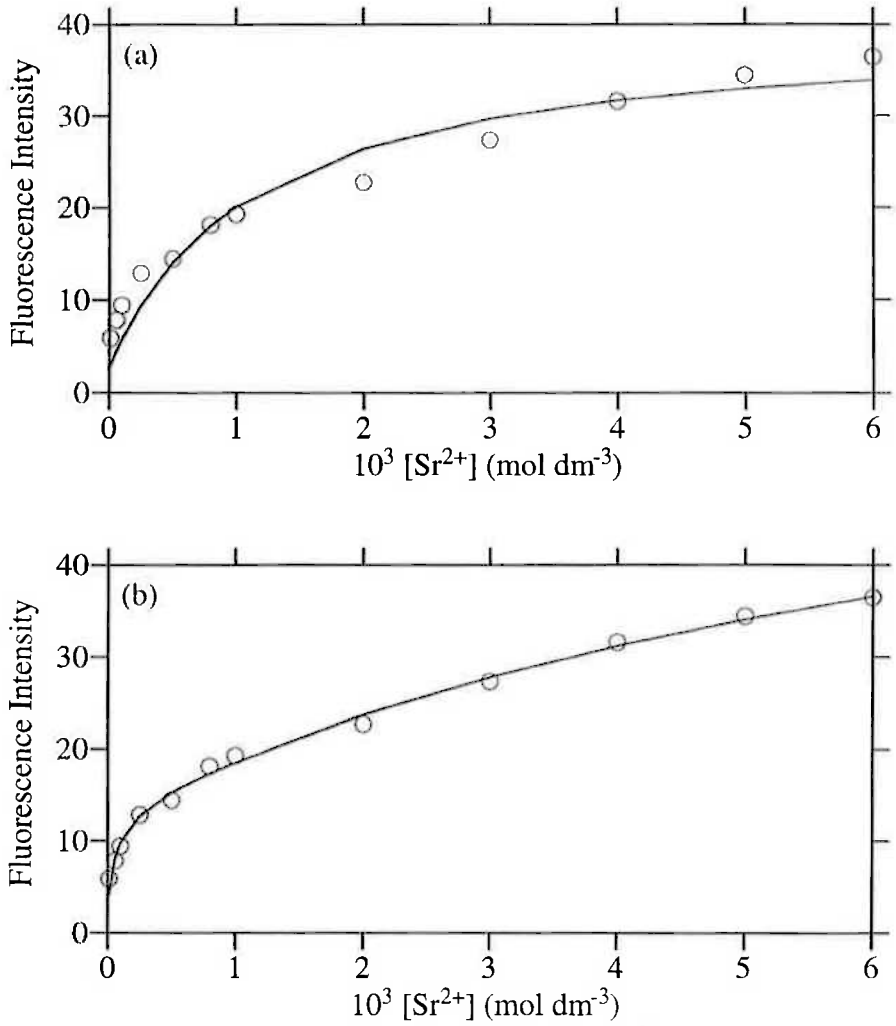

Figure 4.7. *Fluorescence variation of bis(morpholinoethyl)* ***36*** *(3.0 x 10^{-6} mol dm^{-3}) at 402.0 nm in the presence of increasing concentrations of Sr^{2+} (ranging from 1.0 x 10^{-5} to 6.0 x 10^{-3} mol dm^{-3}) in acetonitrile (I = 0.050 mol dm^{-3}) at 298.2 K, when excited at 378.0 nm. Graph (a) is the fit for a 1:1 binding model and (b) is the fit for a 2:1 binding model. The circles represent experimentally obtained data points and the solid line represents the best fit of the data.*

The emission spectra for the variation in ligand **36** fluorescence upon the addition of Mg^{2+} (ranging from 5.0 x 10^{-6} to 5.0 x 10^{-3} mol dm^{-3}) and in the presence of Ba^{2+} (ranging from 1.0 x 10^{-5} to 6.0 x 10^{-3} mol dm^{-3}) are shown in the Appendix, Figures A.5 and A.11, respectively.

The Mg^{2+} experimental data could be successfully fitted to both a 1:1 binding model and to a 2:1 binding model (Appendix, Figure A.6), the sum of the squared deviations for each fit was 3.9 x 10^4 and 9.9 x 10^3, respectively (Tables 4.4 and 4.5). This decrease in SSD is

slightly more than can be attributed simply to the introduction of an additional fitting parameter.[166] The errors for each model are of similar magnitude indicating reliability in both calculations yet the 2:1 binding model appears to give a better visual fit, particularly at higher Mg^{2+} concentrations. Therefore, the 2:1 complexation would again appear more likely.

The binding curve for Ba^{2+} (Appendix, Figure A.12) is similar to that observed for Sr^{2+} in displaying two distinct phases. Accordingly, the fit corresponding to the formation of both (metal)•(ligand) and $(metal)_2$•(ligand) complexes appeared superior, both visually and from the lower SSD value, when compared with a fit for the (metal)•(ligand) complex alone. The error in K_1 significantly increased when K_2 was also incorporated. This largely arises from the very small fluorescence increase over the region in which the (metal)•(ligand) complex forms which compounds the error for any value determined from it. Furthermore, the error in K_1 may be larger than that quoted (Table 4.5) due to the physical constraints of measuring small fluorescence increases.

The stability series for the 2:1 binding model with bis(morpholinoethyl) ligand **36** is $Mg^{2+} > Ca^{2+} > Sr^{2+} \leq Ba^{2+}$. Ligand **36** complexes Mg^{2+} most strongly as depicted by its binding curve (Appendix, Figure A.6) which shows maximum fluorescence from $[Mg^{2+}]$ *ca.* 1×10^{-3} mol dm^{-3} whereas the other metal ions studied do not reach a limiting fluorescence at the concentrations used. The Φ_F values (Table 4.5) generally follow the stability trend. Both Mg^{2+} and Ca^{2+} complexes are significantly more fluorescent than the Sr^{2+} and Ba^{2+} complexes.

4.4.3 Metal Ion Complexation by Bis(morpholinopropyl) 42

The fluorescence emission spectrum for bis(morpholinopropyl) ligand **42** alone is significantly greater in size than those for either the one or two carbon spacer systems, **38** and **36**, respectively. This is reflected in the quantum yield of bis(morpholinopropyl) ligand **42** (Φ_F 0.15) which is 5-fold larger than for the ethyl system **36** (Table 4.6). Upon the addition of alkaline earth metal ions the emission intensity of ligand **42** increases, although the addition of alkali metal ions elicits no such response. For example, the variation in emission of ligand **42** upon the addition of Mg^{2+} (ranging from 1.0×10^{-6} to 8.0×10^{-5} mol dm^{-3}) when excited at 377.0 nm is shown in Figure 4.8.

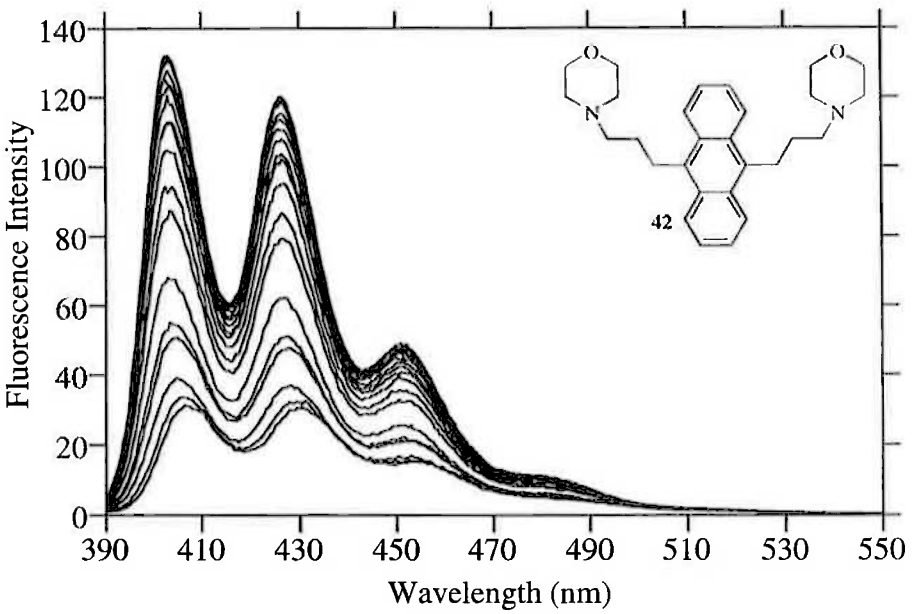

Figure 4.8. *Emission spectra of bis(morpholinopropyl)* ***42*** *alone (3.0 x 10^{-6} mol dm^{-3}) and in the presence of increasing concentrations of Mg^{2+} (ranging from 1.0 x 10^{-6} to 8.0 x 10^{-5} mol dm^{-3}) in acetonitrile (I = 0.050 mol dm^{-3}) at 298.2 K, when excited at 377.0 nm. The emission of* ***42*** *alone is the lowest intensity curve in the montage.*

The Mg^{2+} spectral data could be fitted to a 1:1 binding model to yield K_1 = (3.89 ± 0.04) x 10^5 dm^3 mol^{-1} (Figure 4.9a) although with a poor visual fit. The same data could also be fitted to the formation of both (metal)•(ligand) and $(metal)_2$•(ligand) complexes (Figure 4.9b) to yield K_1 = (1.2 ± 0.2) x 10^7 dm^3 mol^{-1} and K_2 = (5.7 ± 0.3) x 10^6 dm^3 mol^{-1} (Table 4.7). There was a small decrease in the sum of the squared deviations when a $(metal)_2$•(ligand) complex was incorporated into the fitting yet the error in the values of K_1 and K_2 increase. As K = 10^7 dm^3 mol^{-1} is the upper limit that is quantifiable using this method (*vide infra*), the observed error increase is expected. The visual fit suggested however, that the 2:1 binding model is more likely with both complexes having high stability.

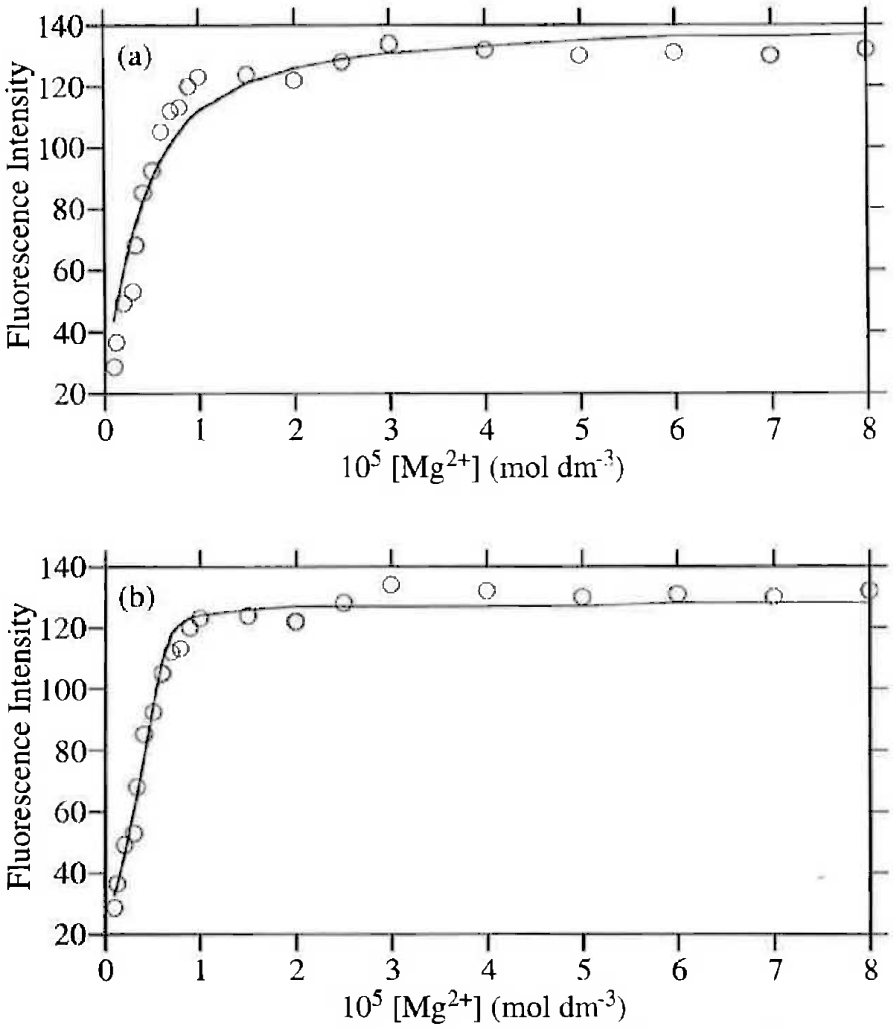

Figure 4.9. *Fluorescence variation of bis(morpholinopropyl)* ***42*** *(3.0 x 10^{-6} mol dm^{-3}) at 403.0 nm in the presence of increasing concentrations of Mg^{2+} (ranging from 1.0 x 10^{-6} to 8.0 x 10^{-5} mol dm^{-3}) in acetonitrile (I = 0.050 mol dm^{-3}) at 298.2 K, when excited at 377.0 nm. Graph (a) is the fit for a 1:1 binding model and (b) is the fit for a 2:1 binding model. The circles represent experimentally obtained data points and the solid line represents the best fit of the data.*

In a similar manner, a spectrofluorimetric titration with Ca^{2+} (ranging from 5.0 x 10^{-6} to 5.0 x 10^{-3} mol dm^{-3}) was performed (Appendix, Figure A.15). The data could be fitted to both a 1:1 binding model and to a 2:1 binding model with equally good visual fits (Appendix, Figure A.16). The values obtained are collated in Tables 4.6 and 4.7, respectively. The errors for both fits were of similar magnitude indicating reliability in both calculations. The SSD decrease for the 2:1 binding model is of the size which can be attributed to the introduction of an additional fitting parameter.[166] Consequently, arguments for one model over the other are inconclusive on the basis of calculated errors

although the 2:1 binding model is more likely in accordance with the complexation of the other metal ions.

Table 4.6. Stability constants (fitted to a 1:1 binding model) and quantum yields for the complexes of bis(morpholinopropyl) ligand **42** with metal ions in acetonitrile at 298.2 K.

Metal ion	K_1 (dm^3 mol^{-1})	SSD[a]	Φ_F[b]
None			0.15[c]
Mg^{2+}	$(3.89 \pm 0.04) \times 10^5$	7.5×10^4	0.45
Ca^{2+}	$(2.71 \pm 0.01) \times 10^4$	2.4×10^4	0.49
Sr^{2+}	$(1.27 \pm 0.02) \times 10^3$	1.4×10^4	0.27
Ba^{2+}	$(8.2 \pm 0.2) \times 10^2$	5.6×10^3	0.20

[a] Sum of the squared deviation. [b] Relative quantum yield determined from the calculated spectrum of the complex. [c] Experimentally determined value.

Table 4.7. Stability constants (fitted to a 2:1 binding model) for the complexes of bis(morpholinopropyl) ligand **42** with metal ions in acetonitrile at 298.2 K.

Metal ion	K_1 (dm^3 mol^{-1})	Φ_F[a]	K_2 (dm^3 mol^{-1})	Φ_F[b]	SSD[c]
Mg^{2+}	$(1.2 \pm 0.2) \times 10^7$	0.15	$(5.7 \pm 0.3) \times 10^6$	0.42	2.2×10^4
Ca^{2+}	$(1.17 \pm 0.06) \times 10^5$	0.28	$(1.12 \pm 0.01) \times 10^4$	0.50	1.5×10^4
Sr^{2+}	$(7.3 \pm 0.2) \times 10^4$	0.17	$(2.97 \pm 0.04) \times 10^2$	0.33	1.6×10^3
Ba^{2+}	$(1.03 \pm 0.02) \times 10^5$	0.14	$(2.31 \pm 0.04) \times 10^2$	0.24	1.0×10^3

[a] Relative quantum yield determined from the calculated spectrum of the (metal)•(ligand) complex. [b] Relative quantum yield determined from the calculated spectrum of the $(metal)_2$•(ligand) complex. [c] Sum of the squared deviation.

The variation in ligand **42** fluorescence upon the addition of Sr^{2+} (ranging from 5.0×10^{-6} to 5.0×10^{-3} mol dm^{-3}) when excited at 377.0 nm is shown in the Appendix, Figure A.17. The data was fitted to both a 1:1 binding model and to a 2:1 binding model (Figure 4.10). Two phases are distinctly recognisable in the binding curve, corresponding to the formation of both (metal)•(ligand) and $(metal)_2$•(ligand) complexes and the significant decrease in the SSD upon the incorporation of the $(metal)_2$•(ligand) complex reflects this. The biphasic curve and the significantly improved visual fit suggest that the 2:1 binding model is the most appropriate for Sr^{2+}, as was similarly observed for Sr^{2+} with bis(morpholinoethyl) **36**.

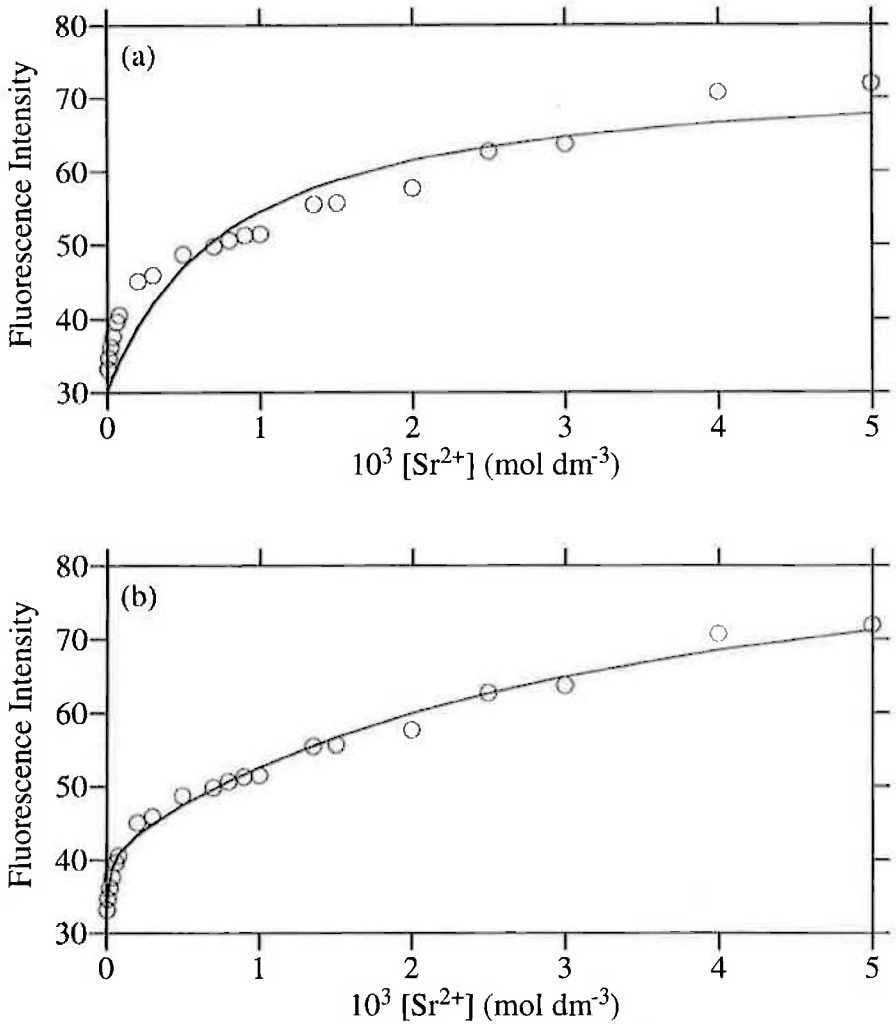

Figure 4.10. *Fluorescence variation of bis(morpholinopropyl)* ***42*** *(3.0 x 10^{-6} mol dm^{-3}) at 404.0 nm in the presence of increasing concentrations of Sr^{2+} (ranging from 5.0 x 10^{-6} to 5.0 x 10^{-3} mol dm^{-3}) in acetonitrile (I = 0.050 mol dm^{-3}) at 298.2 K, when excited at 377.0 nm. Graph (a) is the fit for a 1:1 binding model and (b) is the fit for a 2:1 binding model. The circles represent experimentally obtained data points and the solid line represents the best fit of the data.*

A spectrofluorimetric titration with Ba^{2+} (ranging from 1.0 x 10^{-4} to 6.0 x 10^{-3} mol dm^{-3}) (Appendix, Figure A.19) was performed and the binding curve for Ba^{2+} (Appendix, Figure A.20) is similar to that observed for Sr^{2+} in displaying two distinct phases. Accordingly, the fit corresponding to the formation of both (metal)•(ligand) and $(metal)_2$•(ligand) complexes appeared superior both visually and from the SSD value when compared to a fit for the (metal)•(ligand) complex alone. The value for K_1 significantly increased when K_2 was also incorporated. This is a result of the 2:1 binding model accounting for the initial

sharp increase in emission when Ba^{2+} is added. However, due to the very small fluorescence increase over the region in which the (metal)•(ligand) complex forms the error in the value calculated for K_1 may be larger than that quoted in Table 4.7.

The general series of overall stability (β_2) observed for this ligand is $Mg^{2+} > Ca^{2+} > Sr^{2+} \approx Ba^{2+}$. The M^{2+} complexes with bis(morpholinopropyl) ligand **42** are significantly more stable than those observed for the ligands with the shorter methyl and ethyl spacers. This effect is particularly pronounced for the Mg^{2+} complex which is over 100-fold more stable than with the ethyl system. The quantum yield values also reflect the altered spacer as the Mg^{2+} complex (Φ_F 0.42) is approximately half as fluorescent as the corresponding ethyl system.

4.4.4 Metal Ion Complexation by Bis(thiomorpholine) 52

The ethylene spaced bis(thiomorpholine) ligand **52** (emission peaks at 415.5 and 434.5 nm) displays a similar fluorescence intensity to that observed for bis(morpholinoethyl) ligand **36** alone. A typical change in the fluorescence of ligand **52** in the presence of alkaline earth metal ions is shown in Figure 4.11 with the addition of Ca^{2+} (ranging from 3.0×10^{-6} to 5.0×10^{-3} mol dm^{-3}). In contrast to the morpholine containing ligands, the emission wavelength peaks display a large hypsochromic shift to 400.5, 423.5 and 448.0 nm with a shoulder at *ca.* 476 nm when in the presence of Ca^{2+}. This is a general phenomenon for the alkaline earth metal ions and **52**. No significant spectral changes are observed in the presence of the alkali metal ions.

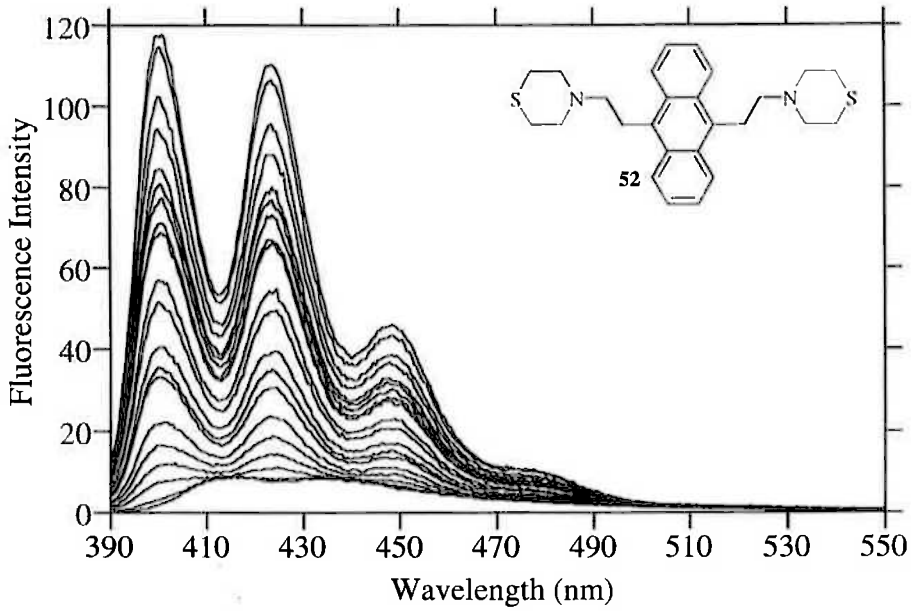

Figure 4.11. *Emission spectra of bis(thiomorpholine)* ***52*** *alone (3.0 x 10^{-6} mol dm^{-3}) and in the presence of increasing concentrations of Ca^{2+} (ranging from 3.0 x 10^{-6} to 5.0 x 10^{-3} mol dm^{-3}) in acetonitrile (I = 0.050 mol dm^{-3}) at 298.2 K, when excited at 378.0 nm. The emission of* ***52*** *alone is the lowest intensity curve in the montage.*

A spectrofluorimetric titration with Mg^{2+} (ranging from 1.0 x 10^{-6} to 3.0 x 10^{-3} mol dm^{-3}) was performed and the spectra arising from it appear in the Appendix, Figure A.21. The attempts to fit the data obtained to either a 1:1 binding model or to a 2:1 binding model are also shown in the Appendix, Figure A.22. The data was readily fitted to both models and the observed decrease in the SSD when a $(metal)_2$•(ligand) complex was incorporated is of the order attributable to an additional fitting parameter (Tables 4.8 and 4.9). The value for K_1 increased slightly when a $(metal)_2$•(ligand) complex was included and the errors in the stability values decreased. In accordance with the improved visual fit to the data, the 2:1 binding model is the most likely.

Table 4.8. Stability constants (fitted to a 1:1 binding model) and quantum yields for the complexes of bis(thiomorpholine) ligand **52** with metal ions in acetonitrile at 298.2 K.

Metal ion	K_1 (dm^3 mol^{-1})	SSD[a]	Φ_F[b]
None			0.07[c]
Mg^{2+}	$(7.69 \pm 0.05) \times 10^4$	4.6×10^4	0.53
Ca^{2+}	$(3.10 \pm 0.02) \times 10^3$	3.7×10^4	0.48
Sr^{2+}	$(4.9 \pm 0.1) \times 10^2$	8.7×10^3	0.25
Ba^{2+}	$(8.37 \pm 0.06) \times 10^2$	8.6×10^2	0.21

[a] Sum of the squared deviation. [b] Relative quantum yield determined from the calculated spectrum of the complex. [c] Experimentally determined value.

Table 4.9. Stability constants (fitted to a 2:1 binding model) for the complexes of bis(thiomorpholine) ligand **52** with metal ions in acetonitrile at 298.2 K.

Metal ion	K_1 (dm^3 mol^{-1})	Φ_F[a]	K_2 (dm^3 mol^{-1})	Φ_F[b]	SSD[c]
Mg^{2+}	$(1.20 \pm 0.01) \times 10^5$	0.46	$(8.28 \pm 0.01) \times 10^2$	0.63	2.2×10^4
Ca^{2+}	$(2.29 \pm 0.05) \times 10^4$	0.20	$(8.0 \pm 0.1) \times 10^2$	0.57	7.2×10^3
Sr^{2+}	$(7.5 \pm 0.5) \times 10^4$	0.08	$(1.23 \pm 0.04) \times 10^2$	0.40	2.0×10^3
Ba^{2+}	$(2.9 \pm 0.3) \times 10^3$	0.10	$(5.2 \pm 0.3) \times 10^2$	0.22	6.0×10^2

[a] Relative quantum yield determined from the calculated spectrum of the (metal)•(ligand) complex. [b] Relative quantum yield determined from the calculated spectrum of the $(metal)_2$•(ligand) complex. [c] Sum of the squared deviation.

The spectra in Figure 4.11, from the spectrofluorimetric titration with Ca^{2+}, could be fitted to a 1:1 binding model to yield $K_1 = (3.10 \pm 0.02) \times 10^3$ (Figure 4.12a). Since some of the experimentally determined points do not coincide with the theoretical line, the data was also fitted to a 2:1 binding model (Figure 4.12b). As the SSD was lower for this model and the visual fit was improved, particularly in the early phase of the binding curve, the 2:1 binding model seems the most appropriate.

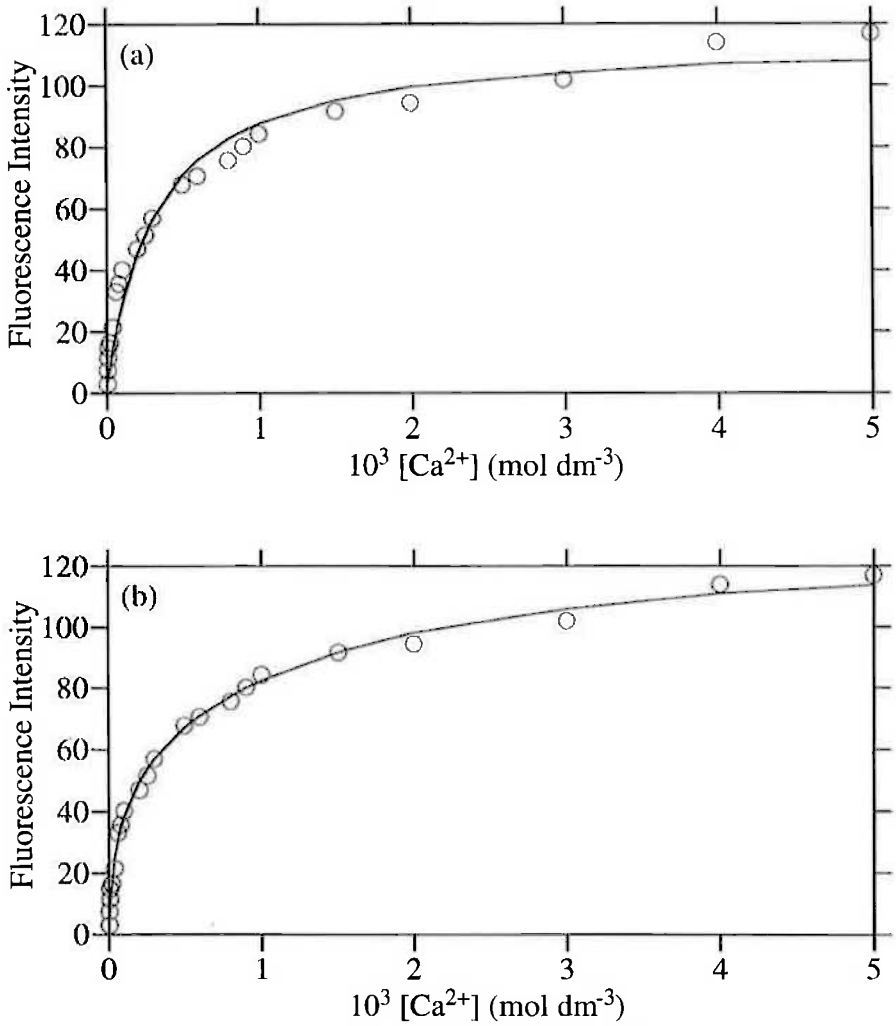

Figure 4.12. *Fluorescence variation of bis(thiomorpholine)* ***52*** *(3.0 x 10^{-6} mol dm^{-3}) at 400.0 nm in the presence of increasing concentrations of Ca^{2+} (ranging from 3.0 x 10^{-6} to 5.0 x 10^{-3} mol dm^{-3}) in acetonitrile (I = 0.050 mol dm^{-3}) at 298.2 K, when excited at 378.0 nm. Graph (a) is the fit for a 1:1 binding model and (b) is the fit for a 2:1 binding model. The circles represent experimentally obtained data points and the solid line represents the best fit of the data.*

A spectrofluorimetric titration of Sr^{2+} (ranging from 1.0 x 10^{-5} to 6.0 x 10^{-3} mol dm^{-3}) with ligand **52** was performed and the spectra, and the fits arising from them, are shown in the Appendix, Figures A.25 and A.26, respectively. The binding curve shows two distinct phases and consequently the 1:1 binding model displayed a poor visual fit to the data. Fitting the data to a 2:1 binding model gave a better visual fit and SSD value. This is a result of the 2:1 binding model accounting for the initial sharp increase in emission when Sr^{2+} was added. However, due to the extremely small fluorescence increase over the

region in which the (metal)•(ligand) complex forms the error in the value calculated for K_1 may be larger than that quoted in Table 4.9.

The spectrofluorimetric titration of Ba^{2+} (ranging from 5.0×10^{-5} to 6.0×10^{-3} mol dm^{-3}) with ligand **52**, and the fits obtained from that data, are shown in the Appendix, Figures A.27 and A.28, respectively. The binding curve for Ba^{2+} shows that the fits for the 1:1 and 2:1 binding models are almost indistinguishable and both models gave stability constant values of similar magnitude. The SSD decreases for the 2:1 binding model, however, this decrease is of the size which can be attributed to the introduction of an additional fitting parameter.[166] The choice of binding models is inconclusive on the basis of errors, although the calculated fluorescence emission spectra for the 2:1 binding model more closely resembles the emission curves for the data obtained. This, and the mode of binding observed for Ba^{2+} with the other ligands, consequently suggests a 2:1 binding model.

The stability constant values obtained (Tables 4.8 and 4.9) for bis(thiomorpholine) ligand **52** also follow the previously observed trend in overall stability of $Mg^{2+} > Ca^{2+} > Sr^{2+} > Ba^{2+}$. All the derived values for K_2 are lower than those for K_1 and are of the 10^2 order of magnitude, independent of the size of K_1. The Φ_F values also decrease in the order $Mg^{2+} \approx Ca^{2+} > Sr^{2+} > Ba^{2+}$ which is similar to the ethyl and propyl morpholine ligands, **36** and **42**. However, the magnitude of the Φ_F values are more related to the three carbon spacer containing bis(morpholinopropyl) **42** than the structurally related bis(morpholinoethyl) **36**.

4.4.5 Metal Ion Complexation by Bis(piperazine) 53

The fluorescence emission spectrum for bis(piperazine) ligand **53** alone shows two bands at 408.0 and 430.5 nm of very low intensity when excited at 378.0 nm. Upon the addition of alkali and alkaline earth metal ions the emission intensity significantly increases, with Cs^+ the only exception by not causing any spectral change. The variation in fluorescence of ligand **53** upon the addition of Li^+ (ranging from 1.0×10^{-5} to 5.0×10^{-3} mol dm^{-3}) when excited at 378.0 nm is shown in Figure 4.13. In the presence of Li^+ the emission spectrum exhibits two bands at 408.0 and 431.0 nm and a shoulder at *ca.* 452 nm which is unchanged from the free ligand (Na^+, K^+ and Rb^+ similarly unaltered).

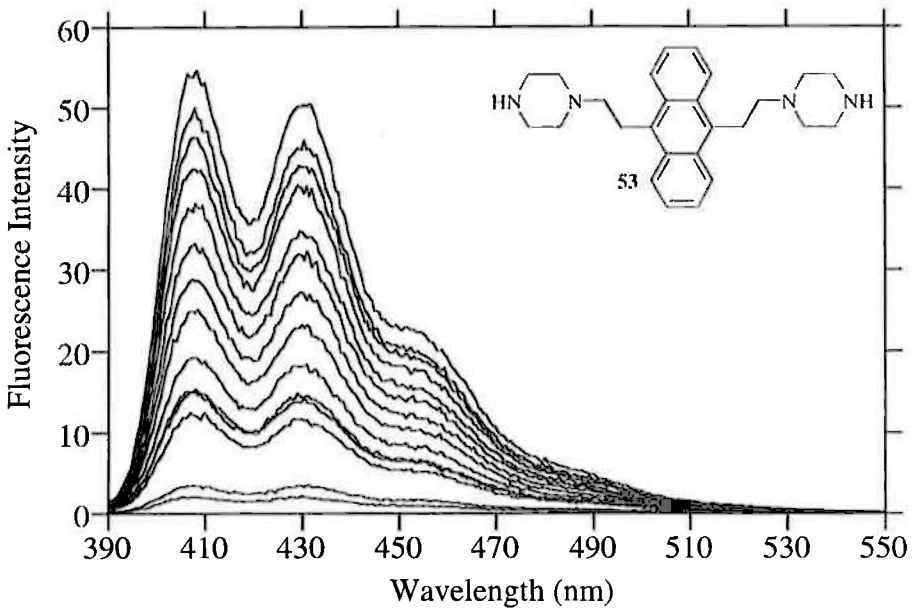

Figure 4.13. *Emission spectra of bis(piperazine)* ***53*** *alone (3.0 x 10^{-6} mol dm^{-3}) and in the presence of increasing concentrations of Li^+ (ranging from 1.0 x 10^{-5} to 5.0 x 10^{-3} mol dm^{-3}) in acetonitrile (I = 0.050 mol dm^{-3}) at 298.2 K, when excited at 378.0 nm. The emission of* ***53*** *alone is the lowest intensity curve in the montage.*

The spectra in Figure 4.13 could be fitted to a 1:1 binding model yielding K_1 = (1.25 ± 0.01) x 10^3 dm^3 mol^{-1}. Since some of the experimentally determined points do not coincide with the theoretical line, the spectra were also fitted to a 2:1 binding model which yielded K_1 = (5.3 ± 0.3) x 10^4 dm^3 mol^{-1} and K_2 = (5.45 ± 0.07) x 10^2 dm^3 mol^{-1} (Figure 4.14). The sum of the squared deviations (SSD) for this fit was 1.9 x 10^3, which is less than the value of 7.8 x 10^3 for the 1:1 binding model. Although a decrease in the sum of the squared deviations is expected when the number of fitting parameters is increased, the magnitude of the change and the improved visual fit suggest that the 2:1 binding model is the most appropriate.

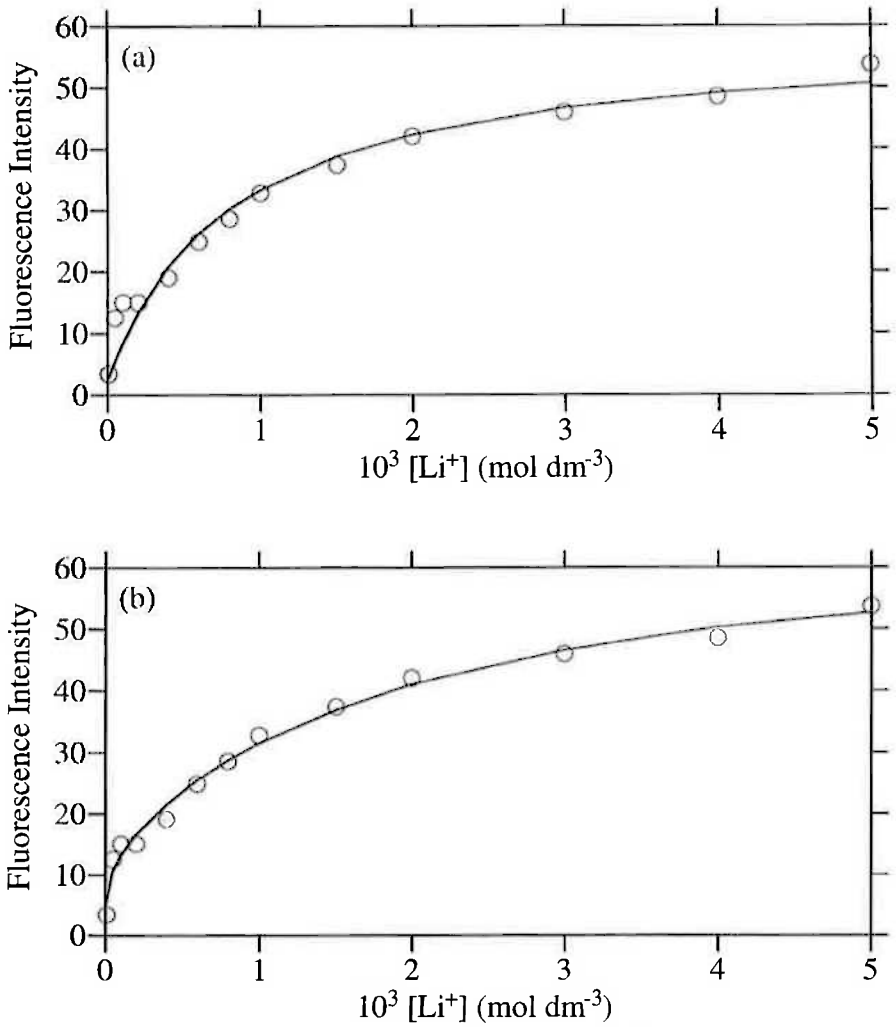

Figure 4.14. *Fluorescence variation of bis(piperazine)* ***53*** *(3.0×10^{-6} mol dm^{-3}) at 407.0 nm in the presence of increasing concentrations of Li^+ (ranging from 1.0×10^{-5} to 5.0×10^{-3} mol dm^{-3}) in acetonitrile ($I = 0.050$ mol dm^{-3}) at 298.2 K, when excited at 378.0 nm. Graph (a) is the fit for a 1:1 binding model and (b) is the fit for a 2:1 binding model. The circles represent experimentally obtained data points and the solid line represents the best fit of the data.*

A spectrofluorimetric titration with Na^+ (ranging from 1.0×10^{-5} to 5.0×10^{-3} mol dm^{-3}) was performed and the spectra arising from it appear in the Appendix, Figure A.31. The attempts to fit the spectra obtained to either a 1:1 binding model or to a 2:1 binding model are also shown in the Appendix, Figure A.32. The 1:1 binding model displayed a poor visual fit whereas the fit for the 2:1 binding model accounted for the two distinct phases in the binding curve and yielded $K_1 = (1.33 \pm 0.05) \times 10^5$ dm^3 mol^{-1} and $K_2 = (4.20 \pm 0.09) \times 10^2$ dm^3 mol^{-1} (Table 4.11). The SSD when a (metal)$_2$•(ligand) complex was incorporated

into the fit also significantly decreased. The value for K_1 may have a larger error than that quoted due to the small number of data points and slight fluorescence increase for the emission region in which the (metal)•(ligand) complex is most predominant, as previously described. Nevertheless, the 2:1 binding model appears the most appropriate.

A spectrofluorimetric titration with K^+ (ranging from 5.0×10^{-5} to 5.0×10^{-3} mol dm^{-3}) was performed and the spectra arising from it appear in the Appendix, Figure A.33. The attempts to fit the data obtained to either a 1:1 binding model or to a 2:1 binding model are also shown in the Appendix, Figure A.34. The 1:1 binding model displayed a reasonable visual fit to yield $K_1 = (2.31 \pm 0.04) \times 10^3$ dm^3 mol^{-1}. When a $(metal)_2$•(ligand) complex was incorporated into the fitting process an improved visual fit resulted and the size of the sum of the squared deviations also decreased. The 2:1 binding model seems the most appropriate yet the low emission again increases the possible errors.

For the metal ions that show a fluorescent response, the values obtained from fitting to a 1:1 binding model are shown in Table 4.10 and from fitting to a 2:1 binding model are shown in Table 4.11.

Table 4.10. Stability constants (fitted to a 1:1 binding model) and quantum yields for the complexes of bis(piperazine) ligand **53** with metal ions in acetonitrile at 298.2 K.

Metal ion	K_1 (dm^3 mol^{-1})	SSD[a]	Φ_F[b]
None			0.01[c]
Li^+	$(1.25 \pm 0.01) \times 10^3$	7.8×10^3	0.24
Na^+	$(4.25 \pm 0.08) \times 10^3$	1.4×10^3	0.05
K^+	$(2.31 \pm 0.04) \times 10^3$	1.8×10^3	0.09
Rb^+	$(5.59 \pm 0.09) \times 10^2$	1.2×10^3	0.12
Cs^+	[d]		[d]
Mg^{2+}	$(2.67 \pm 0.03) \times 10^6$	3.7×10^4	0.51
Ca^{2+}	$(4.47 \pm 0.05) \times 10^5$	1.2×10^5	0.48
Sr^{2+}	$(2.16 \pm 0.02) \times 10^5$	9.5×10^4	0.46
Ba^{2+}	$(8.5 \pm 0.1) \times 10^4$	1.4×10^5	0.40

[a] Sum of the squared deviation. [b] Relative quantum yield determined from the calculated spectrum of the complex. [c] Experimentally determined value. [d] Spectral change too small to be determined.

Table 4.11. Stability constants (fitted to a 2:1 binding model) for the complexes of bis(piperazine) ligand **53** with metal ions in acetonitrile at 298.2 K.

Metal ion	K_1 (dm^3 mol^{-1})	Φ_F[a]	K_2 (dm^3 mol^{-1})	Φ_F[b]	SSD[c]
Li^+	$(5.3 \pm 0.3) \times 10^4$	0.04	$(5.45 \pm 0.07) \times 10^2$	0.26	1.9×10^3
Na^+	$(1.33 \pm 0.05) \times 10^5$	0.02	$(4.20 \pm 0.09) \times 10^2$	0.07	2.0×10^2
K^+	$(6.27 \pm 0.08) \times 10^3$	0.04	$(5.16 \pm 0.06) \times 10^2$	0.10	3.3×10^2
Rb^+	$(2.2 \pm 0.2) \times 10^4$	0.03	$(9.4 \pm 0.7) \times 10^1$	0.25	5.2×10^2
Cs^+	[d]	[d]	[d]	[d]	
Mg^{2+}	$\geq 10^7$	0.38	$\approx 10^6$	0.50	[e]
Ca^{2+}	$(3.2 \pm 0.1) \times 10^6$	0.34	$(1.32 \pm 0.03) \times 10^4$	0.54	2.4×10^4
Sr^{2+}	$(1.71 \pm 0.05) \times 10^6$	0.29	$(1.37 \pm 0.03) \times 10^4$	0.50	1.6×10^4
Ba^{2+}	$(4.91 \pm 0.06) \times 10^5$	0.25	$(2.77 \pm 0.03) \times 10^3$	0.50	8.3×10^3

[a] Relative quantum yield determined from the calculated spectrum of the (metal)•(ligand) complex. [b] Relative quantum yield determined from the calculated spectrum of the $(metal)_2$•(ligand) complex. [c] Sum of the squared deviation. [d] Spectral change too small to be determined. [e] Not applicable.

The change in fluorescence of bis(piperazine) **53** when Rb^+ (ranging from 5.0×10^{-5} to 4.0×10^{-3} mol dm^{-3}) was added is shown in the Appendix, Figure A.35. In a similar manner to K^+, the fluorescence increase observed is small. Accordingly, the data from the spectrofluorimetric titration could be fitted to a 1:1 binding model to yield $K_1 = (5.59 \pm 0.09) \times 10^2$ (dm^3 mol^{-1}), a low stability constant. Since some of the experimentally determined points do not coincide with the theoretical line, particularly at low [Rb^+], the data was also fitted to a 2:1 binding model (Appendix, Figure A.36b) which yielded $K_1 = (2.2 \pm 0.2) \times 10^4$ dm^3 mol^{-1} and $K_2 = (9.4 \pm 0.7) \times 10^1$ dm^3 mol^{-1}. The improved visual fit and the decrease in the SSD value support the 2:1 binding model. However, as stated above, the error in K_1 may be larger than that stated due to both the small fluorescence increase and the small extent of spectral change observed upon the addition of Rb^+. As the spectral change of the ligand in the presence of Cs^+ is even smaller than that for Rb^+, no derived stability constants could be obtained.

In direct contrast to the alkali metal ions, the alkaline earth metal ions all show large fluorescence increases with bis(piperazine) **53.** For example, the spectrofluorimetric titration with Ba^{2+} (ranging from 1.0×10^{-6} to 3.0×10^{-3} mol dm^{-3}) (Figure 4.15) results in a relative quantum yield almost double that of the most fluorescent alkali metal ion (Li^+)

(Table 4.11). Consequently, the trend in Φ_F is Mg^{2+}, Ca^{2+}, Sr^{2+}, Ba^{2+} > Li^+, Rb^+ > Na^+ and K^+.

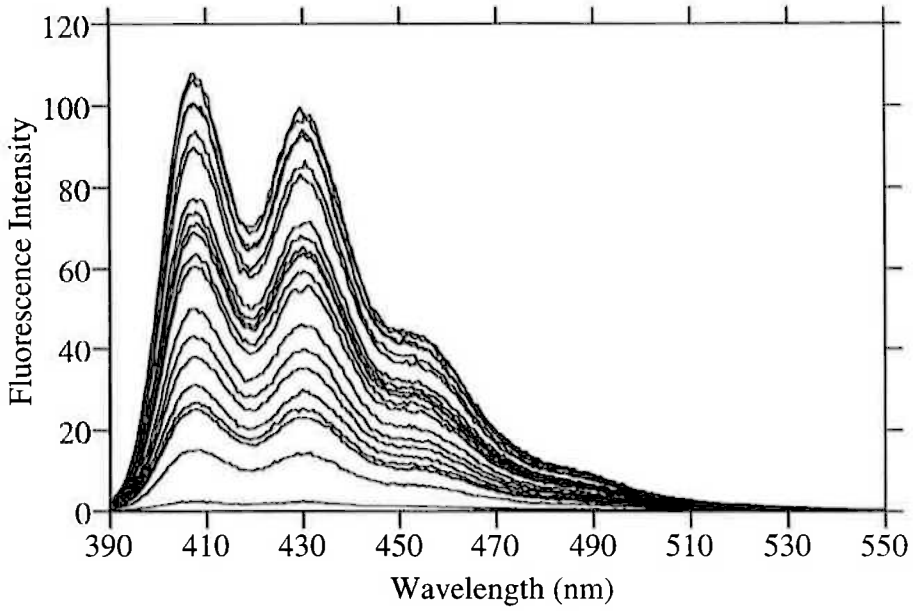

Figure 4.15. *Emission spectra of bis(piperazine)* ***53*** *alone (3.0 x 10^{-6} mol dm^{-3}) and in the presence of increasing concentrations of Ba^{2+} (ranging from 1.0 x 10^{-6} to 3.0 x 10^{-3} mol dm^{-3}) in acetonitrile (I = 0.050 mol dm^{-3}) at 298.2 K, when excited at 377.0 nm. The emission of* ***53*** *alone is the lowest intensity curve in the montage.*

A spectrofluorimetric titration with Mg^{2+} (ranging from 1.0 x 10^{-6} to 1.0 x 10^{-4} mol dm^{-3}) (Appendix, Figure A.37) was performed and the spectra thus obtained could be readily fitted to both a 1:1 binding model and to a 2:1 binding model (Appendix, Figure A.38). Both fits gave large derived stability constants although little distinguishes the visual fits of the data for each model. As K = 10^7 dm^3 mol^{-1} is the upper limit of stability that is quantifiable using this method (*vide infra*) any difference in the SSD is not really applicable. In accordance with the fits obtained for other metal ions, the 2:1 binding model appears the most appropriate.

A spectrofluorimetric titration with Ca^{2+} (ranging from 1.0 x 10^{-6} to 8.0 x 10^{-4} mol dm^{-3}) was similarly performed and the spectra thus produced appear in the Appendix (Figure A.39) and the fits derived from the data are shown in Figure 4.16. The spectra could be fitted to a 1:1 binding model to yield K_1 = (4.47 ± 0.05) x 10^5 dm^3 mol^{-1} (Figure 4.16a). Since some of the experimentally determined points do not coincide with the theoretical line, the data was also fitted to a 2:1 binding model which yielded K_1 = (3.2 ± 0.1) x 10^6

$dm^3\ mol^{-1}$ and $K_2 = (1.32 \pm 0.03) \times 10^4\ dm^3\ mol^{-1}$ (Figure 4.5b). The errors for both fits are of similar magnitude indicating reliability in both calculations. The sum of the squared deviations for this fit was 2.4×10^4, which is substantially less than the value of 1.2×10^5 for the 1:1 binding model. Although a decrease in the sum of the squared deviations is expected when the number of fitting parameters is increased the magnitude of the change remains significant. This and the improved visual fit, particularly at the inflection point, suggest that the 2:1 binding model is the most appropriate.

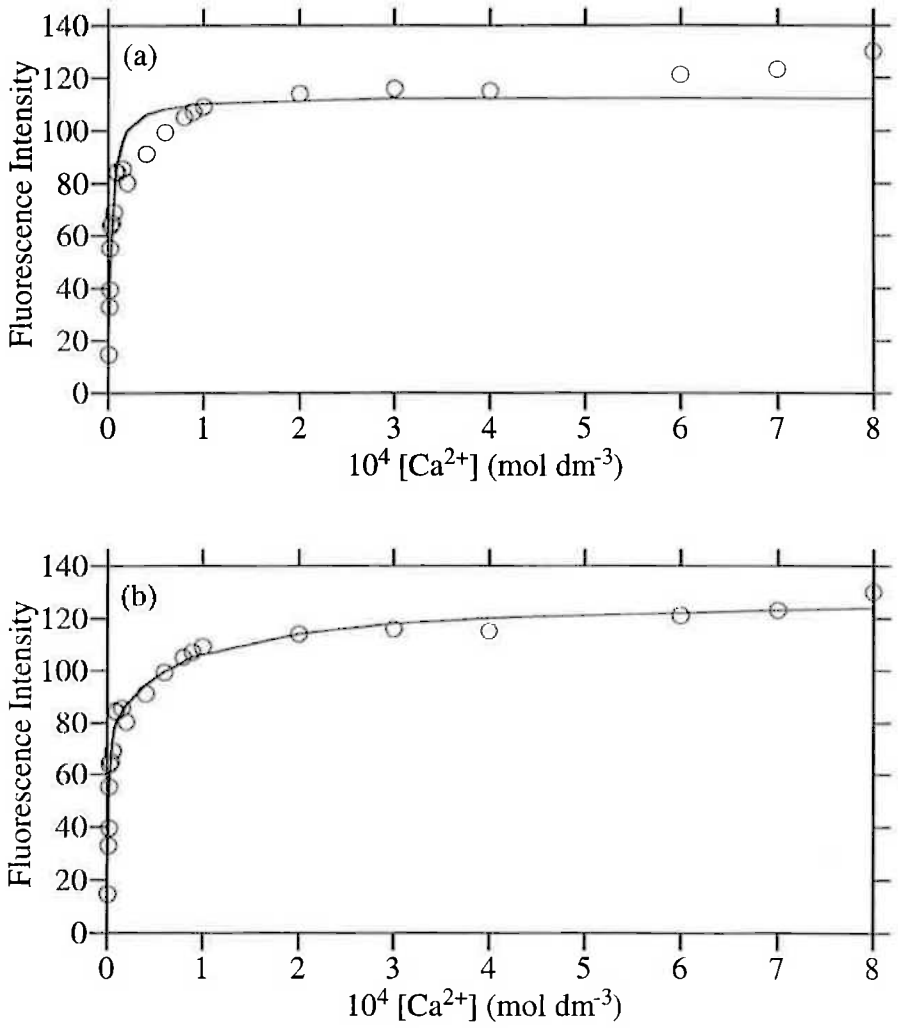

Figure 4.16. *Fluorescence variation of bis(piperazine)* ***53*** *(3.0×10^{-6} mol dm^{-3}) at 408.0 nm in the presence of increasing concentrations of Ca^{2+} (ranging from 1.0×10^{-6} to 8.0×10^{-4} mol dm^{-3}) in acetonitrile ($I = 0.050$ mol dm^{-3}) at 298.2 K, when excited at 380.0 nm. Graph (a) is the fit for a 1:1 binding model and (b) is the fit for a 2:1 binding model. The circles represent experimentally obtained data points and the solid line represents the best fit of the data.*

A spectrofluorimetric titration with Sr^{2+} (ranging from 1.0×10^{-6} to 3.0×10^{-3} mol dm^{-3}) was performed and the spectra thus produced, and the fits derived from the data, are shown in the Appendix, Figures A.41 and Figure A.42, respectively. Similarly, the data shown in Figure 4.15 for the emission of bis(piperazine) **53** in the presence of Ba^{2+} was fitted to both a 1:1 and 2:1 binding model as shown in the Appendix, Figure A.44. Both Sr^{2+} and Ba^{2+} display very similar binding curves to that of Ca^{2+}, described above. Therefore, the 2:1 binding model is the most appropriate for Sr^{2+} and Ba^{2+} for the same reasons as described for bis(piperazine) **53** and Ca^{2+}. The derived stability constants for Sr^{2+} are similar to Ca^{2+}, with Ba^{2+} having slightly lower values for K_1 and K_2 (Table 4.11).

The stability series obtained for the 2:1 binding model with the alkaline earth metal ions and bis(piperazine) ligand **53** is $Mg^{2+} > Ca^{2+} \approx Sr^{2+} > Ba^{2+}$. The alkali metal ions show a less noticeable trend, in part due to their low Φ_F values, and because they display similar derived stability constants. Furthermore, the divalent metal ions are at least one order of magnitude more stable than the univalent metal ions.

4.4.6 Metal Ion Complexation by Mono(azacrown) 51

The fluorescence emission spectrum for mono(azacrown) ligand **51** alone shows two bands at 405.5 and 429.0 nm (and a shoulder at *ca.* 452 nm) of relatively high intensity when excited at 381.0 nm. Upon the addition of any of the alkali and alkaline earth metal ions studied, the emission intensity of the ligand significantly increases. The variation in ligand **51** fluorescence upon the addition of Na^+ (ranging from 1.0×10^{-6} to 4.0×10^{-4} mol dm^{-3}) when excited at 381.0 nm, shown in Figure 4.17, is typical of the alkali metal ions. In the presence of Na^+, the emission spectrum shows three bands at 408.0, 430.5 and 454.0 nm (and a small shoulder at *ca.* 485 nm), a small bathochromic shift from the free ligand.

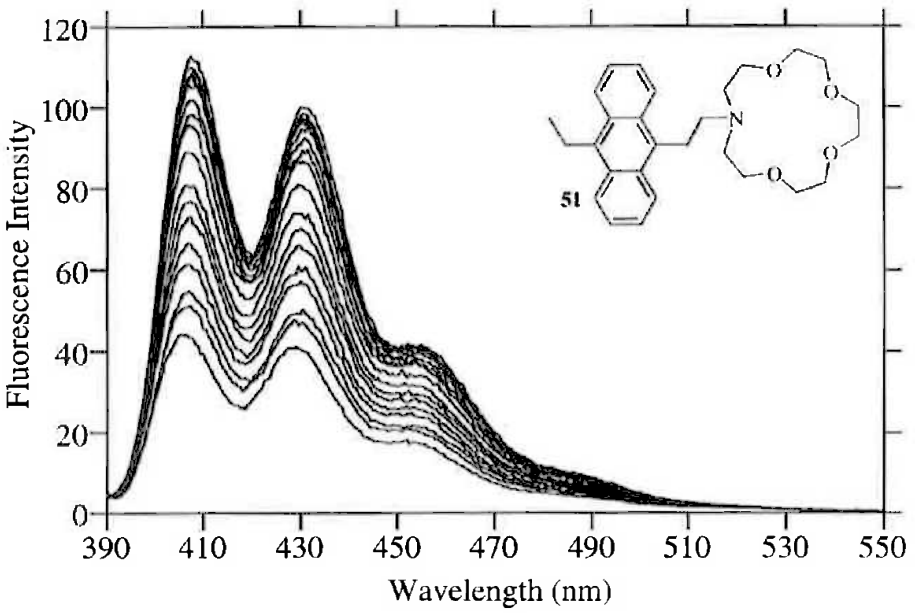

Figure 4.17. *Emission spectra of mono(azacrown)* ***51*** *alone (3.0 x 10^{-6} mol dm^{-3}) and in the presence of increasing concentrations of Na^+ (ranging from 1.0 x 10^{-6} to 4.0 x 10^{-4} mol dm^{-3}) in acetonitrile (I = 0.050 mol dm^{-3}) at 298.2 K, when excited at 381.0 nm. The emission of* ***51*** *alone is the lowest intensity curve in the montage.*

The quantum yield of mono(azacrown) **51** (Φ_F 0.25) is the highest recorded for any of the amine containing ligands studied. The highest quantum yield in the presence of a metal ion is Mg^{2+} (Φ_F 0.78), a three-fold increase from the free ligand, which is the smallest observed for any of the ligands studied. This increase is similar to the quantum yields obtained for the bis(morpholinopropyl) ligand **42**. The divalent metal ions all display a similar and high relative quantum yield (Φ_F *ca.* 0.7). However, the quantum yield values of the alkali metal ions are lower and decrease as the metal ion size increases, such that the difference between the uncomplexed ligand and the Cs^+ complex (Φ_F 0.34) is marginal (Table 4.12).

A spectrofluorimetric titration with Li^+ (ranging from 1.0 x 10^{-6} to 8.0 x 10^{-4} mol dm^{-3}) (Appendix, Figure A.45) was performed which produced a very similar series of emission curves to those shown for Na^+ above. The data obtained could be readily fitted to a 1:1 binding model (Appendix, Figure A.46) to yield K_1 = (1.28 ± 0.01) x 10^5 dm^3 mol^{-1} and the sum of the squared deviations was 7.4 x 10^3 (Table 4.12).

Table 4.12. Stability constants (fitted to a 1:1 binding model) and quantum yields for the complexes of mono(azacrown) ligand **51** with metal ions in acetonitrile at 298.2 K.

Metal ion	K_1 (dm^3 mol^{-1})	SSD[a]	Φ_F[b]
None			0.25[c]
Li^+	$(1.28 \pm 0.01) \times 10^5$	7.4×10^3	0.71
Na^+	$(9.27 \pm 0.04) \times 10^4$	4.4×10^3	0.64
K^+	$(1.73 \pm 0.02) \times 10^4$	1.0×10^4	0.60
Rb^+	$(3.08 \pm 0.05) \times 10^3$	3.8×10^3	0.53
Cs^+	$(2.17 \pm 0.04) \times 10^3$	6.8×10^2	0.34
Mg^{2+}	$\geq 10^7$	d	0.78
Ca^{2+}	$\geq 10^7$	d	0.67
Sr^{2+}	$\geq 10^7$	d	0.66
Ba^{2+}	$\geq 10^7$	d	0.67

[a] Sum of the squared deviation. [b] Relative quantum yield determined from the calculated spectrum of the complex. [c] Experimentally determined value. [d] Not applicable.

The data shown in Figure 4.17 could be fitted to a 1:1 binding model that showed an excellent visual fit to the data which is depicted in Figure 4.18. The derived stability constant K_1 is only slightly lower than that obtained for Li^+ (Table 4.12). The error in the K_1 value obtained is also low indicating reliability in the calculation.

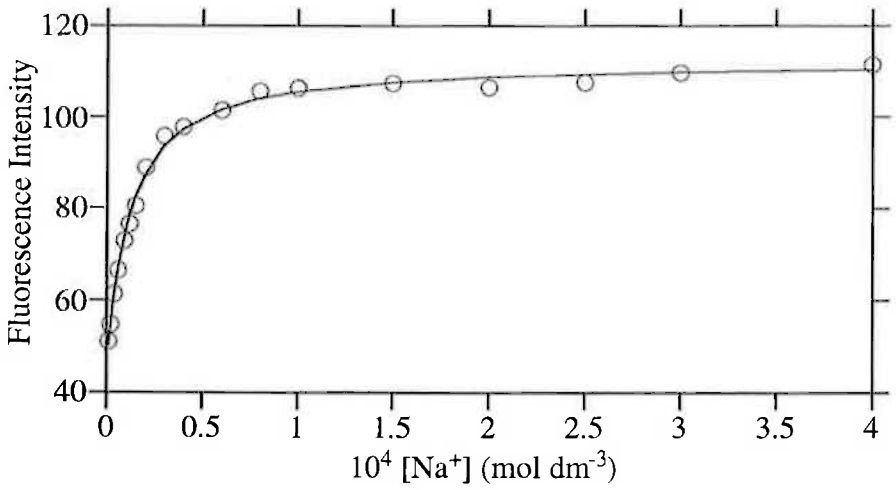

Figure 4.18. *Fluorescence variation of mono(azacrown)* ***51*** *(3.0×10^{-6} mol dm^{-3}) at 407.0 nm in the presence of increasing concentrations of Na^+ (ranging from 1.0×10^{-6} to 4.0×10^{-4} mol dm^{-3}) in acetonitrile (I = 0.050 mol dm^{-3}) at 298.2 K, when excited at 381.0 nm. The circles represent experimentally obtained data points and the solid line represents the best fit of the data to a 1:1 binding model.*

In a similar manner, spectrofluorimetric titrations with K^+, Rb^+ and Cs^+ were also completed, as shown in the Appendix, Figures A.49, A.51, and A.53, respectively. The fit of the data obtained for K^+ was good and resembled that for Na^+ above and is shown in the Appendix, Figure A.50. The higher concentration of K^+ required to reach maximum fluorescence, compared to Li^+ and Na^+, is reflected in the lowered K_1 value.

Both the Rb^+ and Cs^+ series of spectra could be fitted to 1:1 binding models with reasonable visual fits (Appendix, Figures A.52 and A.54, respectively). The fluorescence variation depicts a smooth, gradually increasing emission intensity as the $[M^+]$ increases, as expected from the low stability constants calculated for each metal ion. Due to the small fluorescence variation observed for these two metal ions, the error in the stability constant may be larger than that actually quoted, as discussed above. Thus, the stability series observed for the alkali metal ions with the mono(azacrown) ligand **51** is $Li^+ \approx Na^+ > K^+ > Rb^+ \approx Cs^+$ and the Li^+ complex is *ca.* 60-fold more stable than the Cs^+ complex.

Spectrofluorimetric titrations with Mg^{2+}, Ca^{2+}, Sr^{2+} and Ba^{2+} were performed, as shown in the Appendix, Figures A.55, A.57, A.59 and A.61, respectively. The emission spectra are similar to the ligand in the presence of the alkali metal ions displaying the same small bathochromic shift.

The spectra obtained from the addition of Sr^{2+} (ranging from 1.0×10^{-7} to 9.0×10^{-6} mol dm^{-3}) to mono(azacrown) ligand **51** could be fitted to a 1:1 binding model, as shown in Figure 4.19, to yield $K_1 = (2.01 \pm 0.07) \times 10^7$ dm^3 mol^{-1}. There is an almost linear increase in fluorescence up to a sharp end-point at $[Sr^{2+}] \approx 3 \times 10^{-6}$ mol dm^{-3}, which is equivalent to the ligand concentration employed, indicating a very stable complex.

The SPECFIT programme can not adequately fit stability constants of this magnitude and so the best approximation is $K_1 \geq 10^7$ dm^3 mol^{-1}. This arises because in the added $[M^{2+}]$ range where the (metal)•(ligand) complex concentration varies, the free $[M^{2+}]$ is very low such that small experimental errors produce large variations in the ratio of complexed ligand to unbound ligand and large errors in the data fits. That is, as the stability constant becomes larger (i.e. $\geq 10^7$ dm^3 mol^{-1}), it becomes increasingly difficult to determine an accurate value using this method since any experimental errors are amplified. In addition, for a stability constant of this magnitude, the observed fluorescence emission of the (metal)•(ligand) complex is limited only by the quantity of added metal ion at

concentrations below the total ligand concentration. A species distribution diagram for (metal)•(ligand) complex formation (K_1 = 10^7 mol dm^{-3}) is shown in Figure 4.20 for comparative purposes.

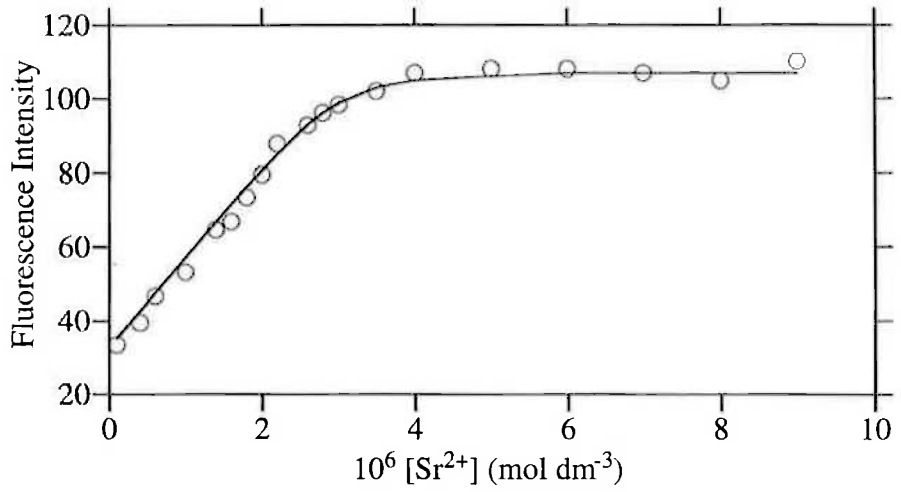

Figure 4.19. *Fluorescence variation of mono(azacrown)* ***51*** *(3.0 x 10^{-6} mol dm^{-3}) at 406.0 nm in the presence of increasing concentrations of Sr^{2+} (ranging from 1.0 x 10^{-7} to 9.0 x 10^{-6} mol dm^{-3}) in acetonitrile (I = 0.050 mol dm^{-3}) at 298.2 K, when excited at 375.0 nm. The circles represent experimentally obtained data points and the solid line represents the best fit of the data to a 1:1 binding model.*

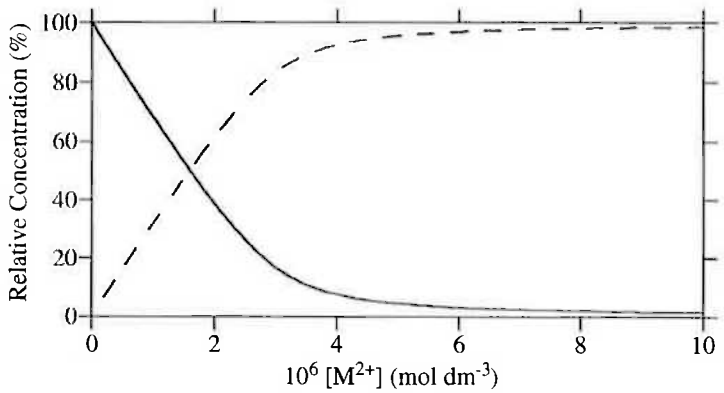

Figure 4.20. *Species distribution diagram of mono(azacrown) ligand* ***51*** *(——) (3.0 x 10^{-6} mol dm^{-3}) and (M^{2+})•(**51**) complex (– – –) as a function of M^{2+} concentration for K_1 = 10^7 dm^3 mol^{-1}. Species are shown as percentages where 100% = $[\mathbf{51}]_{total}$*

In a similar manner, Mg^{2+}, Ca^{2+} and Ba^{2+} display identical binding variation with increasing metal ion concentration, within experimental limitations, to the Sr^{2+} titration (Appendix, Figures A.56, A.58 and A.62). As a consequence, a stability series for the

alkaline earth metal ions can not be established as no definitive values could be determined by the method used.

4.4.7 Metal Ion Complexation by Bis(azacrown) 45

The fluorescence emission spectrum for bis(azacrown) ligand **45** alone shows two bands at 411.0 and 434.5 nm of low intensity, when excited at 385.0 nm. Upon the addition of Li^+ (ranging from 1.0×10^{-6} to 8.0×10^{-4} mol dm^{-3}) an emission spectrum consisting of two intense bands at an unchanged 411.5 and 434.5 nm (and a shoulder at *ca.* 458 nm) are observed, the intensity of which increases with [Li^+] (Figure 4.21). Furthermore, upon the addition of the alkali and alkaline earth metal ions studied, with the exception of Cs^+, the emission intensity of ligand **45** significantly increases.

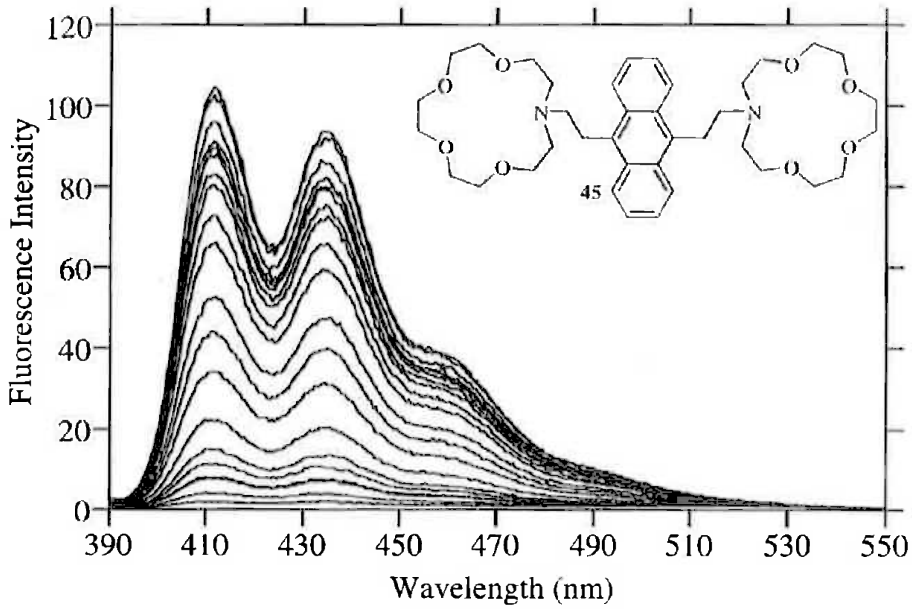

Figure 4.21. *Emission spectra of bis(azacrown)* ***45*** *alone (3.0×10^{-6} mol dm^{-3}) and in the presence of increasing concentrations of Li^+ (ranging from 1.0×10^{-6} to 8.0×10^{-4} mol dm^{-3}) in acetonitrile (I = 0.050 mol dm^{-3}) at 298.2 K, when excited at 385.0 nm. The emission of* ***45*** *alone is the lowest intensity curve in the montage.*

The spectra shown above could be readily fitted to a 1:1 binding model to yield K_1 = (4.60 ± 0.02) x 10^4 dm^3 mol^{-1}. The spectra could also be fitted to a 2:1 binding model yielding K_1 = (7.1 ± 0.3) x 10^5 dm^3 mol^{-1} and K_2 = (6.41 ± 0.01) x 10^4 dm^3 mol^{-1} (Figure 4.22). The magnitude of the difference between the sum of the squared deviations for this fit (2.7 x 10^3) and that of the 1:1 binding model (1.8 x 10^4), implies that the formation of both

(metal)•(ligand) and (metal)$_2$•(ligand) complexes is more likely. The error in K_1 increases for the 2:1 binding model, although this arises from the very low fluorescence attributed to the (metal)•(ligand) complex in the calculated emission spectra, as shown in Figure 4.24. There was little difference in the visual fits for the two models as shown in Figure 4.22 although when the scale is expanded to only show [Li$^+$] $\leq$ 8.0 x 10^{-4} mol dm^{-3} (Figure 4.23) the slight biphasic character of the binding curve is revealed. Consequently, the 2:1 binding model exhibits the better visual fit and appears to be the most appropriate.

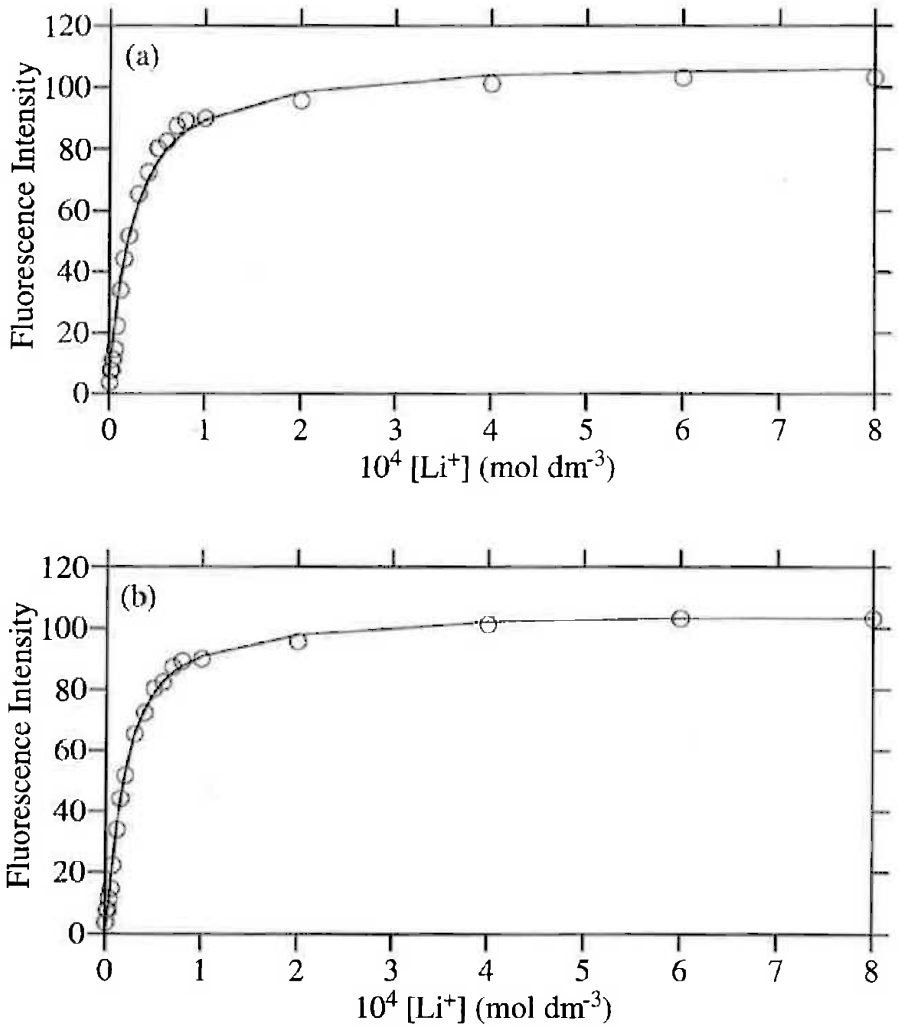

Figure 4.22. *Fluorescence variation of bis(azacrown)* ***45*** *(3.0 x 10^{-6} mol dm^{-3}) at 411.0 nm in the presence of increasing concentrations of Li$^+$ (ranging from 1.0 x 10^{-6} to 8.0 x 10^{-4} mol dm^{-3}) in acetonitrile (I = 0.050 mol dm^{-3}) at 298.2 K, when excited at 385.0 nm. Graph (a) is the fit for a 1:1 binding model and (b) is the fit for a 2:1 binding model. The circles represent experimentally obtained data points and the solid line represents the best fit of the data.*

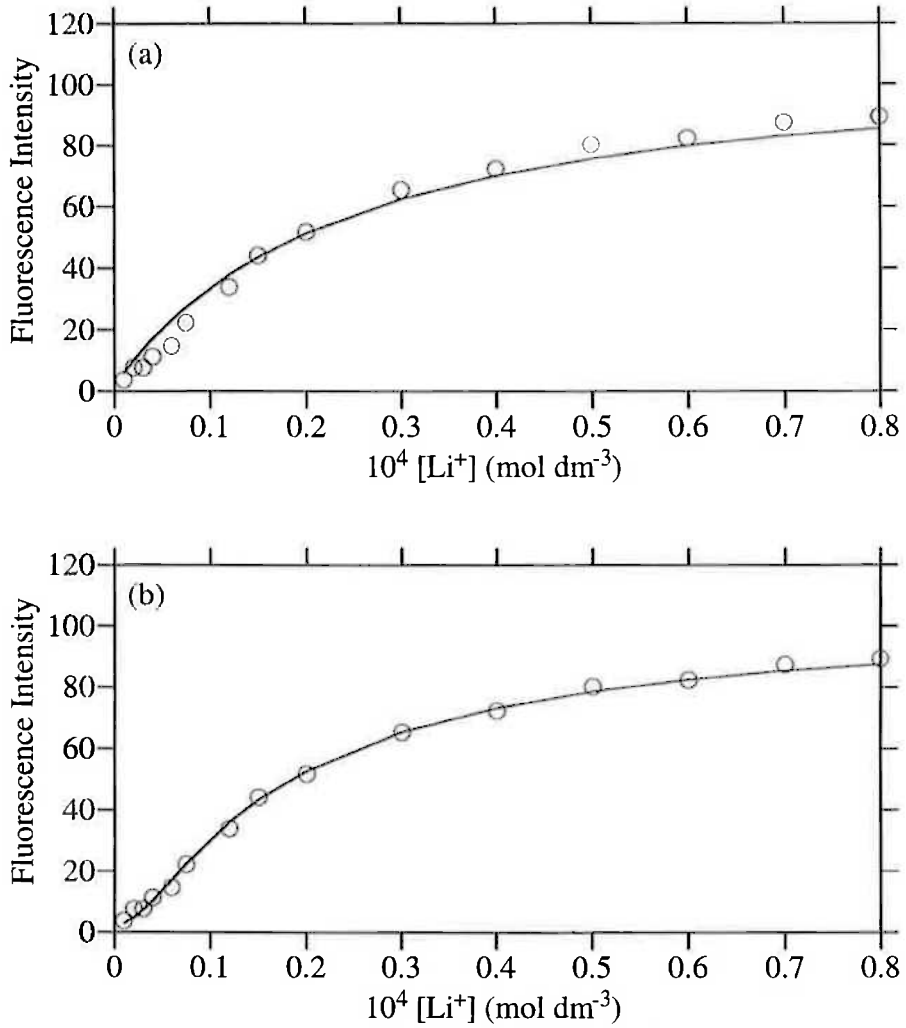

Figure 4.23. *Expansion of the binding curve in Figure 4.22 showing the fluorescence variation of bis(azacrown)* ***45*** *in the presence of increasing concentrations of* Li^+ *(1.0 x* 10^{-6} *to 8.0 x* 10^{-5} *mol* dm^{-3} *displayed) in acetonitrile. Graph (a) is the fit for a 1:1 binding model and (b) is the fit for a 2:1 binding model. The circles represent experimentally obtained data points and the solid line represents the best fit of the data.*

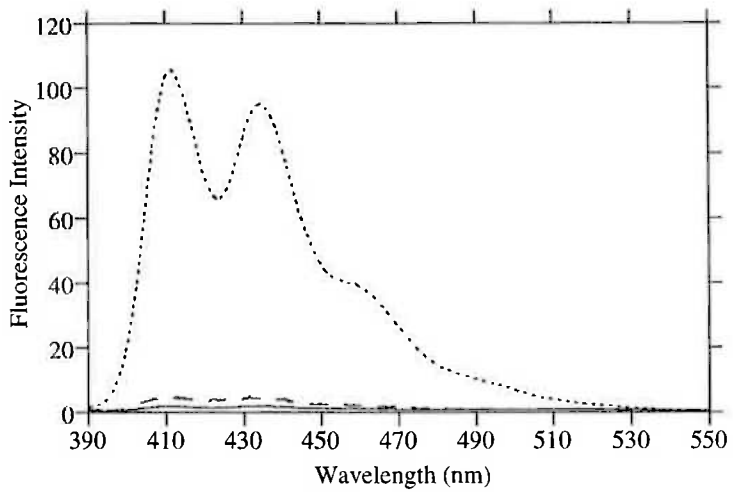

Figure 4.24. *Calculated emission spectra of bis(azacrown)* ***45*** *alone (——), (Li^+)•(**45**) complex (– – –) and $(Li^+)_2$•(**45**) complex (- - -). The spectra for the complexes are derived from the best fit of the data in Figure 4.21.*

A spectrofluorimetric titration with Na^+ (ranging from 1.0×10^{-6} to 3.0×10^{-3} mol dm^{-3}) (Appendix, Figure A.65) was performed and the data obtained could be fitted to both a 1:1 binding model and to a 2:1 binding model (Appendix, Figure A.66). As observed for Li^+, the binding curve displays a slightly biphasic character upon expansion of the region containing low [Na^+] that was more adequately fitted by the 2:1 binding model. Therefore, the 2:1 binding model appears the most appropriate and the values obtained for the stability constants are included in Table 4.13 and Table 4.14.

Table 4.13. Stability constants (fitted to a 1:1 binding model) and quantum yields for the complexes of bis(azacrown) ligand **45** with metal ions in acetonitrile at 298.2 K.

Metal ion	K_1 (dm^3 mol^{-1})	SSD[a]	Φ_F[b]
None			0.03[c]
Li^+	$(4.60 \pm 0.02) \times 10^4$	1.8×10^4	0.76
Na^+	$(3.91 \pm 0.01) \times 10^4$	9.9×10^3	0.54
K^+	$(4.08 \pm 0.02) \times 10^3$	3.6×10^3	0.41
Rb^+	$(9.8 \pm 0.1) \times 10^2$	5.5×10^3	0.15
Cs^+	d		d
Mg^{2+}	$\geq 10^7$	e	0.99[f]
Ca^{2+}	$\geq 10^7$	e	0.90[f]
Sr^{2+}	$\geq 10^7$	e	0.85[f]
Ba^{2+}	$\geq 10^7$	e	0.94[f]

[a] Sum of the squared deviation. [b] Relative quantum yield determined from the calculated spectrum of the complex. [c] Experimentally determined value. [d] Spectral change too small to be determined. [e] Not applicable. [f] Approximate value only.

Table 4.14. Stability constants (fitted to a 2:1 binding model) for the complexes of bis(azacrown) ligand **45** with metal ions in acetonitrile at 298.2 K.

Metal ion	K_1 (dm^3 mol^{-1})	Φ_F[a]	K_2 (dm^3 mol^{-1})	Φ_F[b]	SSD[c]
Li^+	$(7.1 \pm 0.3) \times 10^5$	0.04	$(6.41 \pm 0.01) \times 10^4$	0.73	2.7×10^3
Na^+	$(5.2 \pm 0.3) \times 10^5$	0.06	$(4.84 \pm 0.01) \times 10^4$	0.53	2.4×10^3
K^+	$(1.00 \pm 0.03) \times 10^4$	0.02	$(1.59 \pm 0.06) \times 10^3$	0.39	1.8×10^3
Rb^+	$(1.8 \pm 0.2) \times 10^4$	0.05	$(6.8 \pm 0.1) \times 10^2$	0.15	2.9×10^2
Cs^+	d	d	d	d	
Mg^{2+}	$\geq 10^7$	0.04[e]	$\geq 10^7$	0.95[e]	f
Ca^{2+}	$\geq 10^7$	0.04[e]	$\geq 10^7$	0.80[e]	f
Sr^{2+}	$\geq 10^7$	0.03[e]	$\geq 10^7$	0.77[e]	f
Ba^{2+}	$\geq 10^7$	0.12[e]	$\geq 10^7$	0.86[c]	f

[a] Relative quantum yield determined from the calculated spectrum of the (metal)•(ligand) complex. [b] Relative quantum yield determined from the calculated spectrum of the $(metal)_2$•(ligand) complex. [c] Sum of the squared deviation. [d] Spectral change too small to be determined. [e] Approximate value only. [f] Not applicable.

Likewise, a spectrofluorimetric titration with K^+ (ranging from 1.5×10^{-5} to 3.0×10^{-3} mol dm^{-3}) (Appendix, Figure A.67) was performed and the data obtained could be fitted to both a 1:1 binding model and to a 2:1 binding model (Appendix, Figure A.68). The SSD

decreased with the incorporation of a $(metal)_2$•(ligand) complex into the fit but of the order attributable to the inclusion of an additional fitting parameter. The visual fit slightly improved however, and in accordance with the previous fits the 2:1 binding model appears slightly more appropriate.

The fluorescence emission increase of bis(azacrown) ligand **45** with increasing $[Rb^+]$ (ranging from 1.5×10^{-5} to 3.0×10^{-3} mol dm^{-3}) is significantly smaller than for the other alkali metal ions, when excited at 376.0 nm (Appendix, Figure A.69). The spectra in the presence of Rb^+ also show an 8 nm bathochromic shift. The emission spectra obtained could be fitted to both a 1:1 and a 2:1 binding model with very similar visual fits (Appendix, Figure A.70). The errors in the derived stability constants for either model are larger than for the other alkali metal ions due to the lower fluorescence variation involved. The SSD decreased with the incorporation of a $(metal)_2$•(ligand) complex into the fitting process, and in accordance with the previous fits the 2:1 binding model appears the most appropriate. The reason the maximum $[Rb^+]$ used was 3.0×10^{-3} mol dm^{-3} is a direct result of the low solubility of the metal perchlorate salt in acetonitrile.

Thus, from the overall stability constants obtained, the stability series for the bis(azacrown) ligand **45** with the alkali metal ions is $Li^+ \approx Na^+ > K^+ \approx Rb^+$. This order is mirrored in the Φ_F values obtained which decrease as the metal ion size increase, such that no change is observed in the presence of Cs^+. Contrastingly, the alkaline earth metal ions all show a similar and high relative quantum yield ($\Phi_F > 0.7$) (Table 4.14). In view of the inadequate fits obtained for the divalent metal ions (*vide infra*), the experimentally determined Φ_F values for Mg^{2+} (Φ_F 0.81), Ca^{2+} (Φ_F 0.77), Sr^{2+} (Φ_F 0.71) and Ba^{2+} (Φ_F 0.80) complexes are probably more meaningful than those quoted in Tables 4.13 and 4.14.

Spectrofluorimetric titrations with Mg^{2+}, Ca^{2+}, Sr^{2+} and Ba^{2+} were performed, as shown in the Appendix, Figures A.71, A.73, A.75 and A.77, respectively. The fit arising from the spectra obtained in the presence Ba^{2+} (ranging from 1.0×10^{-6} to 1.0×10^{-4} mol dm^{-3}) is shown in Figure 4.25.

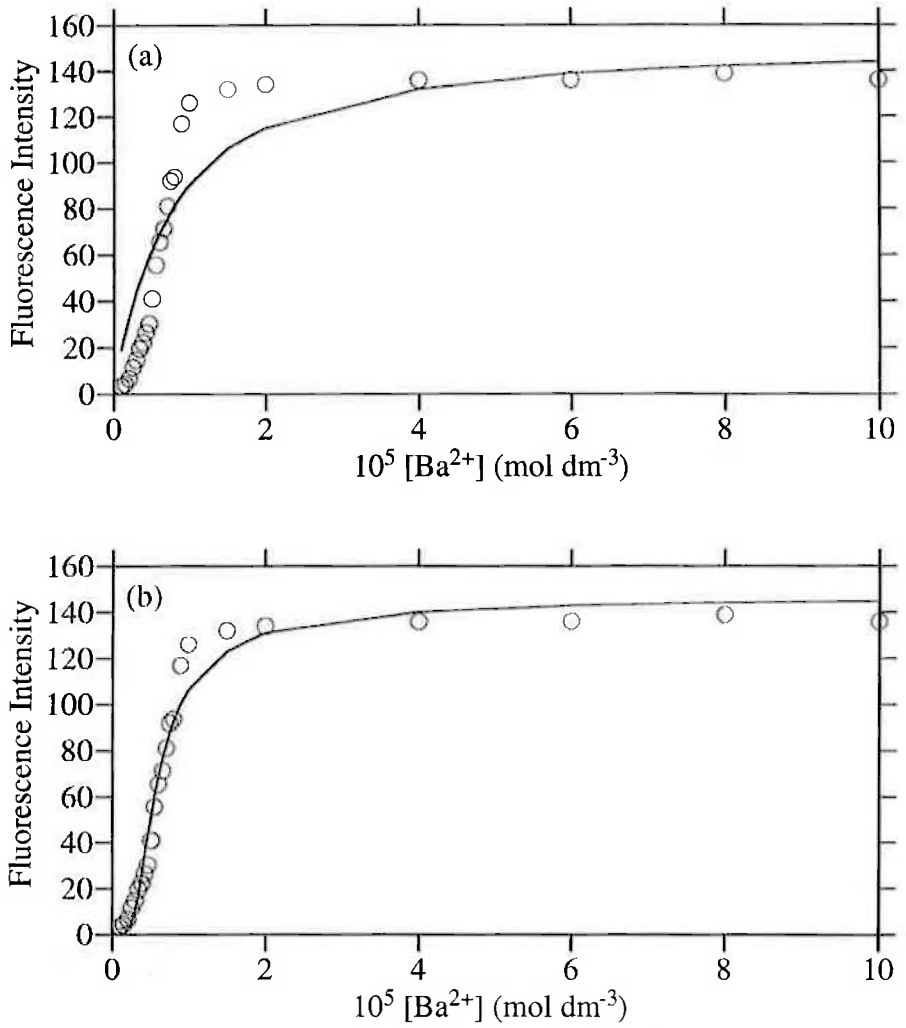

Figure 4.25. *Fluorescence variation of bis(azacrown)* ***45*** *(3.0 x 10^{-6} mol dm^{-3}) at 410.0 nm in the presence of increasing concentrations of Ba^{2+} (ranging from 1.0 x 10^{-6} to 1.0 x 10^{-4} mol dm^{-3}) in acetonitrile (I = 0.050 mol dm^{-3}) at 298.2 K, when excited at 386.0 nm. Graph (a) is the fit for a 1:1 binding model and (b) is the fit for a 2:1 binding model. The circles represent experimentally obtained data points and the solid line represents the best fit of the data.*

The fluorescence variation of bis(azacrown) **45** in the presence of Ba^{2+} shows two distinct phases and so consequently the 1:1 binding model displays a poor visual fit to the data obtained. The 2:1 binding model shows an improved visual fit, particularly at lower Ba^{2+} concentrations, although the overall fit remains inadequate. The cause for this is that, as observed for the mono(azacrown) ligand **51** above, the complexes that form are highly stable and so K_1 and K_2 are at least of the order of 10^7 dm^3 mol^{-1}. Consequently, the

SPECFIT programme can not adequately fit the data and the best approximation is $K_1 \geq 10^7$ dm^3 mol^{-1} and $K_2 \geq 10^7$ dm^3 mol^{-1}.

Attempts to fit the spectra obtained for Mg^{2+}, Ca^{2+} and Sr^{2+} (Appendix, Figures A.72, A.74 and A.76, respectively) yielded similar binding curves and poor visual fits. The derived emission spectra for the metal ion complexes formed in the presence of Sr^{2+} are shown in Figure 4.26 which depicts the low fluorescence ascribed to the (metal)•(ligand) complex and the high fluorescence due to the (metal)$_2$•(ligand) complex.

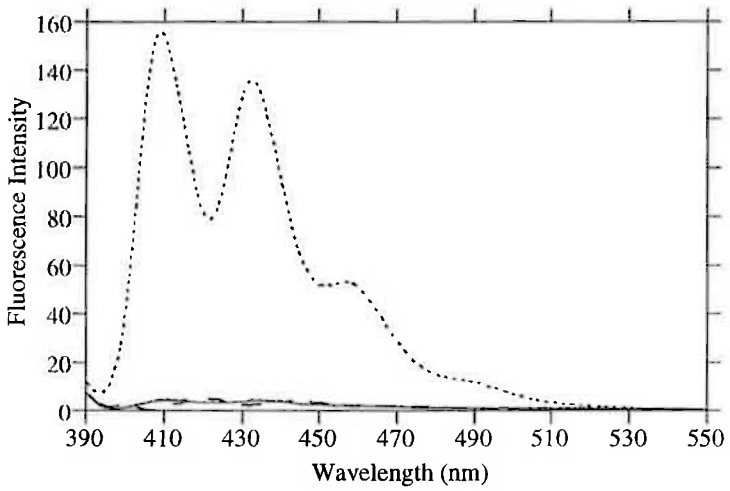

Figure 4.26. *Calculated emission spectra of bis(azacrown)* ***45*** *alone (——), (Sr^{2+})•(**45**) complex (– – –) and (Sr^{2+})$_2$•(**45**) complex (-----). The spectra for the complexes are derived from a fit of the spectra in Figure A.76 (Appendix).*

The derived spectra obtained, and the biphasic nature of the fluorescence variation, suggest that a 2:1 binding model is most likely for Mg^{2+}, Ca^{2+}, Sr^{2+} and Ba^{2+}. Also, the (metal)•(ligand) complex formed is of low fluorescence, the (metal)$_2$•(ligand) complex is highly fluorescent, and both complexes are highly stable. A species distribution diagram for a divalent metal ion and ligand forming a (metal)$_2$•(ligand) complex of high stability via a (metal)•(ligand) complex also of high stability, is shown in Figure 4.27. The formation of the (metal)$_2$•(ligand) complex appears to mirror the fluorescence observed for the alkaline earth metal ions with bis(azacrown) ligand **45**.

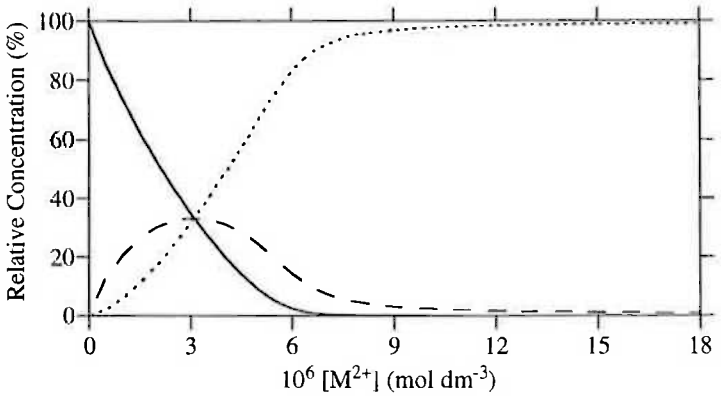

Figure 4.27. *Species distribution diagram of bis(azacrown) ligand* ***45*** *(——) (3.0 x 10^{-6} mol dm^{-3}), (M^{2+})•(**45**) complex (– – –) and $(M^{2+})_2$•(**45**) complex (-----) as a function of M^{2+} concentration for $K_1 = 10^7$ dm^3 mol^{-1} and $K_2 = 10^7$ dm^3 mol^{-1}. Species are shown as percentages where 100% = $[\mathbf{45}]_{total}$.*

4.4.8 Emission Spectra of Bis(hydroxyethyl) 34 and Bis(propyl-amide) 41

The fluorescence emission spectrum of bis(hydroxyethyl) ligand **34** shows three bands at 405.0, 427.5 and 452.0 nm (and a shoulder at *ca.* 481 nm) of moderate intensity (Φ_F 0.67) when excited at 379.0 nm. Likewise, the fluorescence emission spectrum of bis(propyl-amide) ligand **41** displays three similar bands of slightly higher intensity (Φ_F 0.57) at 405.5, 429.0 and 453.5 nm (and a shoulder at *ca.* 481 nm) when excited at 377.0 nm. The emission spectra are shown in Figure 4.28. The quantum yield values reflect the higher absorbance of bis(propylamide) **41** (Table 4.2). Neither ligand displays any spectral change in the presence of any of the alkali or alkaline earth metal ions studied, again as was reflected in their UV-visible absorbance properties

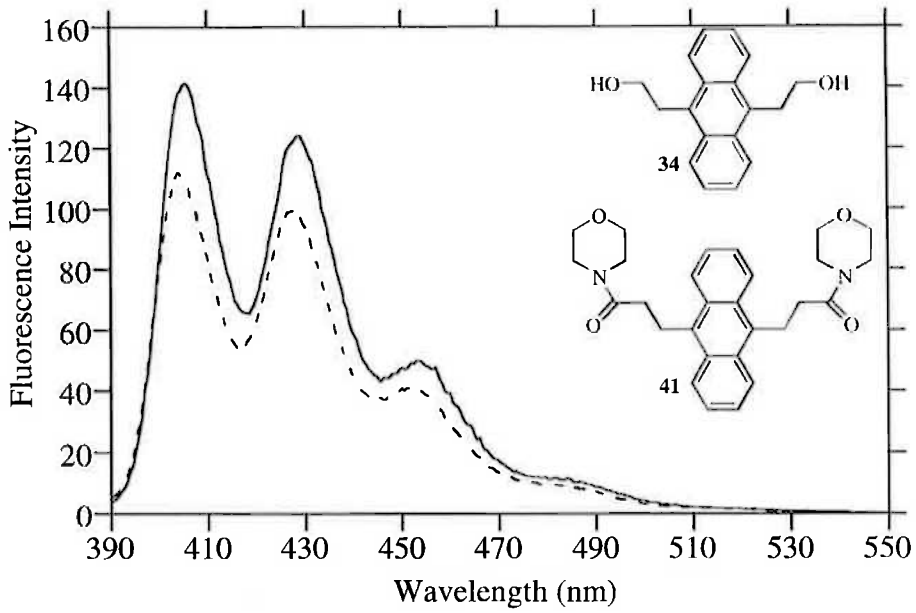

Figure 4.28. *Emission spectra of bis(hydroxyethyl) ligand* ***34*** *(– – –) (3.0 x 10^{-6} mol dm^{-3}) and bis(propylamide) ligand* ***41*** *(——) (3.0 x 10^{-6} mol dm^{-3}) in acetonitrile (I = 0.050 mol dm^{-3}) at 298.2 K, when excited at 379.0 nm and 377.0 nm, respectively.*

4.5 Fluorescence Quantum Yields for the Calculated Spectra Obtained from Data Fitting

The experimental quantum yield values for the ligands listed in the previous section were determined relative to quinine sulphate[167,168] using the optically dilute solution method,[169] as described in Section 6.7. However, comparison between the quantum yield values of the different ligand systems and the complexes they form should be treated with some caution as different excitation wavelengths, which may be of different intensity, were used.

Combined in Tables 4.15 and 4.16, for the purposes of discussion and ease of comparison, are the quantum yields of the calculated complexes for a 2:1 binding model for the ligands studied (1:1 binding model for **38** and **51** only).

Table 4.15 Fluorescence quantum yield (Φ_F) values for the derived spectra obtained from the fits for bis(morpholinomethyl) **38**, bis(morpholinoethyl) **36**, bis(morpholinopropyl) **42** and bis(thiomorpholine) **52** ligands in acetonitrile.

Complex[a]	Mg^{2+}	Ca^{2+}	Sr^{2+}	Ba^{2+}
Bis(morpholinomethyl) **38** (Φ_F 0.001)				
ML	0.31	0.16		
Bis(morpholinoethyl) **36** (Φ_F 0.03)				
ML	0.58	0.19	0.06	0.03
M_2L	0.92	0.88	0.26	0.14
Bis(morpholinopropyl) **42** (Φ_F 0.15)				
ML	0.15	0.28	0.17	0.14
M_2L	0.42	0.50	0.33	0.24
Bis(thiomorpholine) **52** (Φ_F 0.07)				
ML	0.46	0.20	0.08	0.10
M_2L	0.63	0.57	0.40	0.22

[a] ML = (metal)•(ligand) and M_2L = $(metal)_2$•(ligand) complexes.

Table 4.16 Fluorescence quantum yield (Φ_F) values for the derived spectra obtained from the fits for mono(azacrown) **51**, bis(azacrown) **45** and bis(piperazine) **53** ligands in acetonitrile.

Complex[a]	Li^+	Na^+	K^+	Rb^+	Cs^+	Mg^{2+}	Ca^{2+}	Sr^{2+}	Ba^{2+}
Mono(azacrown) **51** (Φ_F 0.25)									
ML	0.71	0.64	0.60	0.53	0.34	0.78	0.67	0.66	0.67
Bis(azacrown) **45**[b] (Φ_F 0.03)									
ML	0.04	0.06	0.02	0.05		0.04	0.04	0.03	0.12
M_2L	0.73	0.53	0.39	0.15		0.95	0.80	0.77	0.86
Bis(piperazine) **53** (Φ_F 0.01)									
ML	0.04	0.02	0.04	0.03		0.38	0.34	0.29	0.25
M_2L	0.26	0.07	0.10	0.25		0.50	0.54	0.50	0.50

[a] ML = (metal)•(ligand) and M_2L = $(metal)_2$•(ligand) complexes. [b] Approximate values for alkaline earth metal ions.

4.6 Discussion

Changing the solvent to acetonitrile from 1,4-dioxane-water markedly increased the stability constants of the metal ion complexes, as expected. For instance, no complexation of mono(azacrown) ligand **51** with Ca^{2+} was detected by potentiometric titration in 1,4-dioxane-water (Section 2.4) yet in acetonitrile a highly stable complex is observed. As was described above (Section 4.1) this is a consequence of decreased solvation of the metal ion and so the ligand is able to compete for the metal ion more effectively.

The influence of the spacer on the fluorescence quantum yield was readily apparent. Bis(morpholinomethyl) ligand **38** (one carbon) is almost non-fluorescent (Φ_F 0.001), in the absence of metal ions, under the measurement conditions, whereas bis(morpholinoethyl) ligand **36** is 30-fold more fluorescent (Φ_F 0.03). The inclusion of an extra carbon to give a propyl spacer (Φ_F 0.15) further increases the fluorescence, although only 5-fold that of the ethyl system. This displays how the efficiency of PET mediated fluorescence quenching drops off rapidly with increasing distance, as was similarly observed in the buffered solution study (Section 3.4).

The direct role that the number of nitrogen donors involved in PET fluorescence quenching plays is shown by the two azacrown containing ligands, **45** and **51**. The bis(azacrown) ligand **45** (Φ_F 0.03) displays the same quantum yield as bis(morpholinoethyl) ligand **36**. However, when only one azacrown receptor was present (mono(azacrown) ligand **51**), the fluorescence is almost 10-fold greater (Φ_F 0.25). This is because more efficient electron transfer paths are available for PET quenching when two nitrogens are present.[147] Although other factors such as decreased vibrational relaxation for the single receptor system due to its smaller size are in operation, the major controlling force is the lowered efficiency of PET quenching. This is evident from the similarity in Φ_F for bis(morpholinoethyl) **36** and bis(azacrown) **45** despite their overall size differences. The presence of two amine containing receptors has other consequences in relation to both complexation and fluorescence, which will be discussed later. In addition, the presence of other heteroatoms in the receptor does not appear to have any influence on the quantum yield as all the ditopic ligands with ethyl spacers have similar Φ_F values.

As was also observed in 1,4-dioxane-water solution, bis(hydroxyethyl) ligand **34** and bis(propylamide) ligand **42** exemplify the fact that an amine nitrogen is required for PET

quenching of fluorescence, at least with this ligand design. These two ligands also illustrate the requirement of metal ion complexation to cause a fluorescence variation, as the presence of a metal ion alone does not alter the fluorescence of the anthracene subunit.

The Φ_F values obtained in the absence or presence of metal ions (Section 4.5) exemplifies the principle of the PET quenching mechanism for fluorescent sensing. That is, metal ion complexation switches the fluorescence ON as compared with the unbound ligand, which is in the fluorescence OFF state. Before the discussion of the metal ion complexation of the different ligands, it is worthwhile examining the various possible binding modes available for these ligands and their respective photophysical outcomes. A schematic representation of these structural binding modes appears in Figure 4.29.

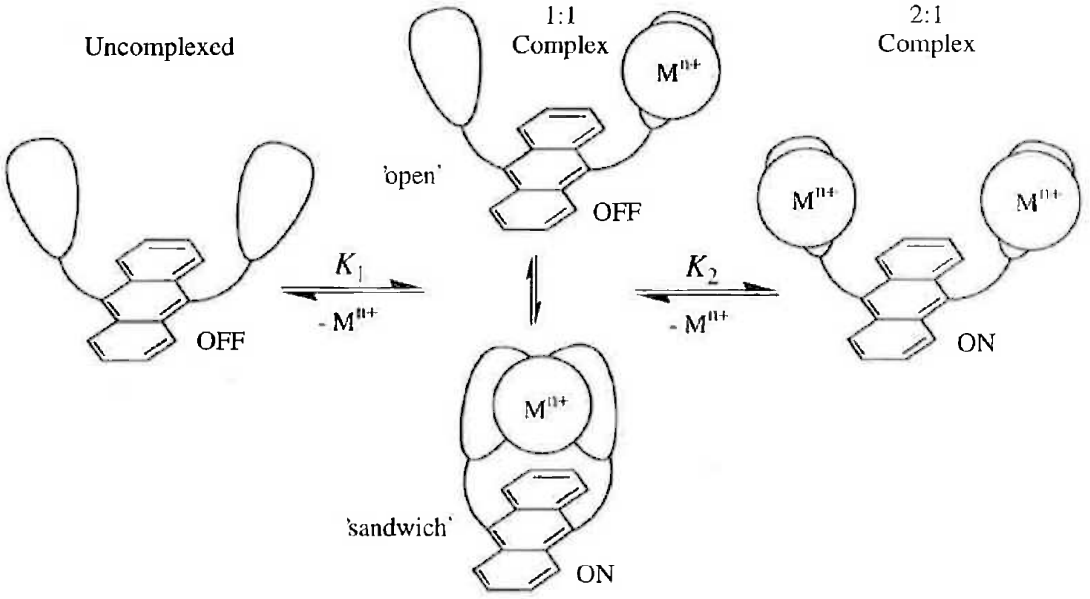

Figure 4.29. *Schematic diagram illustrating the inter-relationship between some of the possible binding modes of a ligand with two distinct receptor groups and the corresponding photophysical outcomes: ON represents a fluorescent species and OFF a non-fluorescent species.*

For metal ion complexation involving the formation of both (metal)•(ligand) and $(metal)_2$•(ligand) complexes with the ditopic ligands in this study, the binding route depends on how the different binding modes are utilised. The formation of a $(metal)_2$•(ligand) complex necessarily requires that a metal ion be bound to each receptor subunit. A (metal)•(ligand) complex has the possibility of forming two different structures than can interconvert. Thus, a metal ion can be bound solely by one receptor ('open' 1:1 complex in Figure 4.29) or equally bound by both receptors in an intramolecular sandwich type structure ('sandwich' 1:1 complex in Figure 4.29). The difference between the two

structures is that the sandwich structure engages both nitrogen lone pairs in metal ion complexation and is consequently fluorescent, whereas the open structure is less fluorescent as an amine nitrogen lone pair is still available for PET mediated quenching of fluorescence. Thus, the formation of a $(metal)_2$•(ligand) complex is predicated upon the formation of a (metal)•(ligand) complex whose fluorescence is reliant upon its binding mode, which may also depend upon the metal ion concerned.

Of course a $(metal)_2$•(ligand) complex need not form. Formation of a (metal)•(ligand) complex only, as observed for bis(morpholinomethyl) ligand **38**, is possible. In that case some of the complex was the fluorescent sandwich complex. However, only an open (metal)•(ligand) complex may form, although its detection is difficult due to the lack of fluorescence difference with the free ligand.

Other binding stoichiometries such as more than one ligand with a single metal ion or a $(metal)_2$•$(ligand)_2$ complex are unlikely due to the low concentration of ligand that was employed in the fluorescence measurements. Also, attempts to fit the spectra obtained to other models were unsuccessful. Finally, a lack of fluorescence variation in the presence of a metal ion does not necessarily signify that no complexation occurs, just that if it does, it results in no alteration in the fluorescence spectrum of the ligand. Some information about the different binding routes described above can be derived from the quantum yields for the spectra calculated from the fitting process, as will be discussed below.

For all ligands studied (excluding **38** and **51** as they only form (metal)•(ligand) complexes) the K_2 value obtained is lower than K_1, as expected from statistical and entropic factors. The complexation of a second metal ion is made sterically and electrostatically more difficult by the presence of an already bound metal ion. In addition, the $(metal)_2$•(ligand) complex is always of higher fluorescence than the (metal)•(ligand) complex for several reasons. As shown in Figure 4.29, due to interconversion of binding modes, not all (metal)•(ligand) complexes are fluorescent. Also, when two tertiary nitrogen amines are complexed to a single metal ion it is less likely that they will be as efficiently engaged as in a $(metal)_2$•(ligand) complex, and so a lower Φ_F results for the (metal)•(ligand) complex.

The proximity of the amine nitrogen to the fluorophore influences the Φ_F of the ligand not only in the free state but also when the ligand complexes a metal ion. The fluorescence quantum yield of the Mg^{2+} complex of bis(morpholinomethyl) ligand **38** is low (Φ_F 0.31) and only the formation of (metal)•(ligand) complexes could be detected for this ligand.

This is most likely a result of the small separation between the two morpholine receptors as the simultaneous complexation of two metal ions would result in too large an electrostatic repulsion, consequently no $(metal)_2$•(ligand) complex formation is observed. One reason for the low quantum yield could be due to an oscillation between an open and sandwich complex structure of which only one is fluorescent and thus observed. Also, as described above, a sandwich (metal)•(ligand) complex is generally expected to be less fluorescent than a $(metal)_2$•(ligand) complex, particularly when sterically strained.

Upon the addition of an extra methylene unit in the spacer arm the situation changes. Firstly, the bis(morpholinoethyl) ligand **36** forms more stable complexes with Mg^{2+} and Ca^{2+} (*ca.* 100-fold) in addition to complexing Sr^{2+} and Ba^{2+}. However, the quantum yields in the presence of Sr^{2+} and Ba^{2+} are quite small, particularly when compared with Mg^{2+} and Ca^{2+}, despite the similarity in overall stability of the complexes. This is possibly a result of their decreased charge density (Table 4.17) and so they consequently engage the nitrogen lone pair less effectively than Mg^{2+} and Ca^{2+}. This also explains the lack of complexation observed with the alkali metal ions (*vide infra*).

Thus, the fit for Mg^{2+} with bis(morpholinoethyl) **36** calculated a (metal)•(ligand) complex with high fluorescence (Φ_F 0.58) which suggests that it is complexing predominantly via the sandwich mode described above, preceding a less stable, more fluorescent $(metal)_2$•(ligand) complex. This may be due to a good size fit across the aromatic cavity of the ligand allowing formation of a sandwich type structure with Mg^{2+}. Conversely, the fits for the other alkaline earth metal ions attributed very little fluorescence to the (metal)•(ligand) complex suggesting that there was little sandwich structure binding of these metal ions. This reflects a size discrimination whereby the formation of a sandwich structure is possibly sterically more difficult with the larger metal ions and therefore is not observed.

As described in Section 4.4.2, two distinct phases are present in the binding curves for Sr^{2+} and Ba^{2+} with bis(morpholinoethyl) **36**. A very similar binding curve for another fluorophore, although it involved fluorescence quenching, has been observed by Leray and co-workers.[170] They obtained metal ion complexation constants with at least two orders of magnitude between K_1 and K_2 values ($K_1 > K_2$) and large differences in the Φ_F for each complex, as was found in this study. The biphasic curve arises largely from the much

lower stability of K_2 compared with K_1, the Φ_F difference between complexes, and is diagnostic of a 2:1 binding model.

The role of the cavity size across the aromatic ring in complexation is further portrayed by the bis(morpholinopropyl) ligand **42** as the stability constants obtained are higher than with the shorter spacer systems, although no complexation with any alkali metal ion is observed. The stability constants increased such that for Mg^{2+} with a 2:1 binding model K_1 is $\geq 10^7$ dm^3 mol^{-1}, much stronger than the ethyl spacer system **36**. The K_2 values also significantly increase reflecting the lower electrostatic repulsion between metal ions that increased distance affords. The stability change is most noticeable for Mg^{2+} and Ca^{2+} whereas Sr^{2+} and Ba^{2+} are little changed for the propyl ligand. For this ligand the Ca^{2+} complex shows evidence of sandwich structure formation, as indicated by the fluorescence of the calculated (metal)•(ligand) spectrum (Φ_F 0.28). This probably results from the sandwich type complex of the ligand with a propyl spacer now being more accommodating for the larger Ca^{2+}. Again, Sr^{2+} and Ba^{2+} display distinctly biphasic binding curves. The trend in the Φ_F values is similar to bis(morpholinoethyl) **36**, most likely for the same charge density reasons. The higher free ligand Φ_F and the lower metal ion complex Φ_F exemplify the decreased quenching ability of the amine nitrogen as the spacer distance increases.

Thus, the role of spacer length is important in the Fluorophore-Spacer-Receptor design strategy for fluorescent sensors.[141] The ligand with a methyl spacer is the best quenched but it is harder to fully switch the fluorescence on. Conversely, the propyl spacer system is so inefficiently quenched that when it is switched on the fluorescence increase is marginal. Hence, the ethyl spacer system strikes a useful balance between these two extreme situations, as uncomplexed it is efficiently quenched however when complexed, the fluorescence increase is large and of high Φ_F.

The influence of changing sulphur for oxygen in the receptor ring was investigated with the bis(thiomorpholine) ligand **52**. The influence on the stability constants was minimal as the overall stability (β_2) is almost unchanged for the sulphur containing ligand when compared with bis(morpholinoethyl) ligand **36**. In contrast, the quantum yields are different with Mg^{2+} and Ca^{2+} complexes much lower, and Sr^{2+} and Ba^{2+} complexes slightly higher. That is, there is less disparity between the two sets of metal ions than existed in the ethyl system. The reduced range of the Φ_F values, without significant

alteration of complex stability, may possibly arise due to the larger sulphur atom (a C-S bond is longer than a C-O bond)[171] reducing the extent of nitrogen lone pair involvement in complexation. The relatively large hypsochromic shift upon complexation for this ligand may also reflect an altered binding geometry. Again, the Mg^{2+} complex displays a significant amount of sandwich structure formation with the Ca^{2+} complex showing slightly less, as suggested by the Φ_F of the (metal)•(ligand) complex in the 2:1 binding model.

These results were surprising in that the Hard and Soft Acids and Bases (HSAB) principle[100,101] would suggest that metal ion complexation of the alkaline earth metal ions should be significantly stronger with an oxygen donor system rather than its sulphur containing analogue. However, the results show that metal ion complexation is dependent upon many varied and competing forces, each of which may contribute different proportions to the overall stability for different metal ions and ligands. Consequently, no one factor is controlling or absolute in defining stability. For example, the struggle between the binding strength and any electrostatic effect of the metal ions on the amine nitrogen is important in determining the magnitude of the emission observed upon complexation, although this is more important when there are more donor atoms available for complexation. Thus, a complex may be stable but not necessarily highly fluorescent. Further contributors such as the degree of solvation of the metal ions and ligands, structural changes of the ligands, deformation of the ligands during complexation, and interactions between donor atoms of the ligands and the complexed metal ions, must also be considered.

Changing oxygen (in **36**) for nitrogen to give the bis(piperazine) ligand **53** displayed a striking consequence on the fluorescence emission. With ligand **53** the alkaline earth metal ions form complexes at least two orders of magnitude more stable, with stability decreasing with increasing size, than with the morpholine ligand **36**. The quantum yields are similar (Φ_F *ca.* 0.5) and comparatively low, considering the high stability. The interaction of the metal ion with the lone pair of the tertiary nitrogen must be less than in the analogous bis(morpholinoethyl) **36** and so the effective suppression of PET is reduced resulting in lower Φ_F values. The calculated spectra suggested significant formation of a sandwich structure for the (metal)•(ligand) complex with all the divalent metal ions. This reflects the increased flexibility of the piperazine ring.[172,173]

The formation of sandwich type structures for a (metal)•(ligand) complex has been noted in the literature.[174-176] A compound similar in structure to bis(azacrown) **45** containing a bis(15-crown-5) moiety and a diboronic acid cleft found that there was an optimum metal ion size for sandwich structure formation as metal ion sizes above or below displayed open structure formation only.[174] Similarly, with an alkyl linked bis(monoaza-15-crown-5) ligand sandwich formation was observed with Na^+ and K^+ although none with the larger monoaza-18-crown-6 ring.[175] Consequently, the lack of any distinct trend in the formation of sandwich type structures for the ligands in this study is not surprising.

The stronger complexation for bis(piperazine) **53** is most likely due to the increased flexibility of the nitrogen centre in contrast to sulphur and oxygen. It is known that nitrogen containing macrocycles in a small ring have a high degree of conformational mobility[172,173] and that the nitrogen itself can undergo inversion[177] thereby significantly changing the position of the lone pairs. Such properties should facilitate metal ion complexation as dictated by the metal ion involved. This flexibility may be more important because the ring is small and so much more restricted than the larger nitrogen containing crowns which generally follow the HSAB principle. However, as stated above, many factors are involved in complexation. Consequently, Φ_F values lower than those observed for bis(morpholinoethyl) ligand **36** may be a result of more effective complexation by the other heteroatom for bis(piperazine) **53,** thereby reducing the electrostatic effect on the tertiary amine nitrogen.

Compared with the oxygen and sulphur containing six-membered receptors there was a response to the alkali metal ions for the piperazine containing ligand **53**. Albeit the fluorescence variation and consequently the Φ_F values are low with little distinguishing the overall formation constants. The lowered response is due to the smaller charge density of these metal ions (Table 4.17) which may also be the reason for the low fluorescence attributed to the (metal)•(ligand) complex for these ions, thereby suggesting the open structure predominates. The univalent ions have such low fluorescence for the $(metal)_2$•(ligand) complex that a sandwich structured (metal)•(ligand) complex would probably be poorly fluorescent anyway.

The complex stability constants examined above show a good correlation to the so-called class A or ionic index (ratio of formal charge and ionic radius, n^2/r^{n+}, as a measure for electrostatic attraction) (Table 4.17).[178]

Table 4.17 Charge densities (z^2 Å^{-1}) of the ions studied for a coordination number of six, using the class A or ionic index.[178]

Metal ion	Li^+	Na^+	K^+	Rb^+	Cs^+	Mg^{2+}	Ca^{2+}	Sr^{2+}	Ba^{2+}
n^2/r^{n+}	1.32	0.98	0.72	0.66	0.60	5.56	4.00	3.39	2.96

The complex stabilities observed in this study suggest that as the ionic radius of the metal ion decreases, there is a corresponding increase in the electrostatic attraction between metal ion and the ligand as indicated by the increase in quantum yield. This charge density relationship has been previously observed for Li^+, Na^+, K^+, Mg^{2+}, Ca^{2+}, Sr^{2+} and Ba^{2+} for monoaza-15-crown-5 appended fluorophores.[23,41]

The strength of the electrostatic attraction of the metal ion to the tertiary amine nitrogen is the reason a Mg^{2+} complex generally has a higher Φ_F than a Ba^{2+} complex, for example. Also, the large difference in Φ_F between the alkali and alkaline earth metal ions suggests that the stronger electrostatic interaction between the divalent metal ions and the lone pair of the nitrogen atom of the receptor more efficiently suppresses the PET quenching process, a result observed by others.[29]

The complexation characteristics observed for the three ligands, bis(morpholinoethyl) **36**, bis(thiomorpholine) **52** and bis(piperazine) **53**, illustrates the influence of how small changes in the ligand structure can cause significant changes in fluorescence signalling properties. The oxygen containing ligand is the most specific as it complexes Mg^{2+} and Ca^{2+} with moderate strength and very high Φ_F. Conversely, the inclusion of nitrogen (bis(piperazine) **53**) increases the complex stability yet decreases the specificity.

The influence of a receptor with more donor atoms, mono(azacrown) ligand **51**, was large as the alkaline earth metal ions gave stability constants that are too high to be determined with acceptable accuracy by the method used (i.e. $K_1 \geq 10^7$ dm^3 mol^{-1}). This again shows the large influence of solvent as no complexation with metal ions is observed in 1,4-dioxane-water (Section 2.4). The alkali metal ions show that as the size increases (and so charge density decreases) the stability constant (and Φ_F) decreases. The increased number of hard oxygen donors in the receptor favours the strong complexation of the hard alkali and alkaline earth metal ions. The simplicity of the binding curves and the lack of any biphasic character exhibit the sole (metal)•(ligand) complex formation, as expected with

only one receptor. Despite the large difference between the divalent and univalent ions in regards to complex stability, little difference was correspondingly observed in the maximum Φ_F values.

With the addition of an extra azacrown receptor, bis(azacrown) ligand **45**, the binding curves for the alkaline earth metal ions changed significantly with a distinctly biphasic nature. The binding curves for the univalent metal ions appear similar to those obtained for mono(azacrown) **51** although some biphasic character is evident. All the derived K_1 values that were obtained for a 1:1 binding model for the univalent metal ions with bis(azacrown) **45** ligand are lower than those obtained for the mono(azacrown) ligand **51**, despite the extra receptor. This is further suggestive of the inappropriate nature of the 1:1 binding model for the bis(azacrown) **45** ligand, notwithstanding the distinctly biphasic nature of the binding curves observed for the alkaline earth metal ions.

The biphasic nature of the binding curves for the divalent metal ions implies the formation of a predominantly open structure (metal)•(ligand) complex of high stability that precedes the formation of an equally stable $(metal)_2$•(ligand) complex (at least by the limitations of the method used). Thus, the initial phase of very low fluorescence at low $[M^{2+}]$ is due to the formation of a poorly fluorescent (metal)•(ligand) complex (Figure 4.26). It is only when the $(metal)_2$•(ligand) complex forms that the fluorescence immediately begins to increase. The species distribution diagram in Figure 4.27 shows the formation of a $(metal)_2$•(ligand) complex of high stability and its formation reflects the appearance of the binding curves for the divalent metal ions with bis(azacrown) **45**. This effect was also observed for some of the alkali metal ions (Figure 4.23) although it was less conspicuous due to the lower stability of the corresponding complexes. This lack of cooperativity between the two receptors is further shown by the minimal increase observed in K_1 (for the 2:1 binding model) when compared with the single receptor ligand, mono(azacrown) **51**.

The lack of cooperativity was also reflected in the binding mode, as there was no evidence of sandwich formation since negligible fluorescence arose from a (metal)•(ligand) complex of **45**. The cause for this is most likely due to too many unfavourable steric interactions between the bulky receptors. In contrast to the smaller six-membered ring receptors (e.g. **36**), the value of K_2 for bis(azacrown) **45** is generally only a factor of 10 smaller than K_1. In the presence of more donor atoms (i.e. monoaza-15-crown-5) the stability of a $(metal)_2$•(ligand) complex is higher as each receptor can more effectively act in an

independent manner. Therefore, due to the inherently greater stability of the larger crown, the small decrease observed in K_2 arises largely from statistical and electrostatic effects, not lack of receptor binding strength.

The magnitude of the stability constants for the azacrown receptor ligands compare reasonably well with values obtained in acetonitrile for fluorescent sensors, of varying designs, containing the monoaza-15-crown-5 receptor.[23,29,41,75,179-181] It is not feasible to compare any trend within the alkaline earth metal ion series as their stability could not be accurately determined in this study. From the stability values above and literature values it appears that as the steric hindrance near the nitrogen centre in the crown decreases, the stability constants increase in magnitude. Thus, the magnitude of K_1 increases as the spacer size increases (i.e. methyl < ethyl < propyl). However, as mentioned above, as the spacer becomes larger other less desirable effects become important, such as reduced Φ_F variation on metal ion binding.

The stability constant values obtained for the azacrown containing ligands (**51** and **45**) correlate well with the charge density of the metal ion (Table 4.17), as was similarly observed for the other ligands in this study. The diameter of the monoaza-15-crown-5 receptor is 1.7-2.2 Å[159,182] and so Na^+ and Ca^{2+} should be the best fit to the crown based on size. The basis of complex stability primarily derived from the relative size-fit of crown and metal ion has been much discussed.[156,183] However, a recent study in the gas phase using guided ion beam mass spectrometry suggests it is not of primary importance.[184] In that study it was found that the intrinsic metal ion complexation of the alkali metal ions with oxygen containing crowns (12-crown-4, 15-crown-5 and 18-crown-6) was determined principally by the charge density of the metal ion and not by the ratio of the ionic radius to the cavity size.[184] Thus, as mentioned above, the determinants of macrocycle complex stability are many and varied. A recent review examines some of these aspects.[31]

The inclusion of an extra receptor did not confer any real benefit for complexation of the alkali metal ions, at least in acetonitrile as studied here. Two receptors may have actually delayed the point at which maximum saturated fluorescence was attained. This results from the maximum fluorescence response only being attained when both receptors are complexed. Hence, higher metal ion concentrations are required for this to occur when two receptors are present, particularly as the binding constant for the second metal ion complexed is lower than the first. Similarly, the concentration of an alkaline earth metal ion required for maximum fluorescence was essentially increased by the incorporation of

the additional receptor. The effect is accentuated for bis(azacrown) **45** as minimal fluorescence is observable until the second metal ion is complexed. This could be useful in allowing fine-tuning of the effective concentration range of the receptor depending on its desired usage as a practical fluorescent sensor. In this case, the lack of benefit from the introduction of a second receptor arises largely from the lack of cooperativity between the two receptors. The binding of ditopic molecular analytes may allow such cooperativity to be observed and utilised.

Chapter 5 Conclusions and Future Directions

This thesis describes a comprehensive investigation of a group of photoinduced electron transfer (PET) based fluorescent sensors and their UV-visible absorption and fluorescence emission behaviour.

The desired series of 9,10-disubstituted anthracene ligands were synthesised in moderate yields through modification of existing literature procedures. Anthracene proved to be an effective scaffold for construction of the fluorescent sensors. A large degree of synthetic simplicity arose from the use of only one nitrogen in the receptor (excluding bis(piperazine) ligand **53**) which obviated the need for the use of protecting groups. However, the synthetic routes used remain amenable to further functionalisation of the receptor.

The pK_a values for the ligands soluble in 1,4-dioxane-water solution were determined by potentiometric titration. The values obtained were within the range of those expected for substituted aliphatic amines and showed some evidence of intramolecular hydrogen-bonding within an individual receptor. None of the studied metal ions (Na^+, Ca^{2+} and Pb^{2+}) showed any evidence of complex formation in aqueous solution.

The UV-visible absorption and fluorescence emission behaviour of all the ligands synthesised was studied in 1,4-dioxane-water solution. Only slight changes in the absorption spectra upon the addition of metal ions were observed which is consistent with the mechanism of action for PET based fluorescent sensors. The fluorescence emission spectra initially showed large enhancement upon the addition of metal ions. However, through the use of buffered solutions, this was found to result from the liberation of acid from metal ion hydrolysis in aqueous solution. The protonation behaviour as it related to fluorescence emission was also studied. Protonation of one nitrogen amine of a dual receptor system was found to be insufficient to restore fluorescence. Interestingly, the bis(piperazine) ligand **53** showed that it only required a single proton bound to each receptor unit for the PET quenching of fluorescence to be suppressed. These results emphasised the importance of the basicity of PET quenching nitrogen atom for studies in aqueous solution and its role in determining basal fluorescence levels. The spacer length

was also found to influence the level of baseline fluorescence for the morpholine containing ligands (**38**, **36** and **42**).

To further study the photophysical properties of the ligands in the absence of metal ion hydrolysis, their complexation of metal ions was examined in anhydrous acetonitrile (a solvent more favourable for metal ion complexation). Accordingly, ligand fluorescence increases were observed, of varying degree, in the presence of alkali or alkaline earth metal ions. Stability constants, K_1 and K_2 (if applicable), for relevant metal ions inducing altered ligand fluorescence were determined from spectrofluorimetric titration. Only bis-(piperazine) ligand **53**, bis(azacrown) ligand **45** and mono(azacrown) ligand **51** showed any change in fluorescence with the univalent metal ions. The necessity of a tertiary amine nitrogen for PET quenching was shown by the insensitivity to metal ions and the high quantum yields of bis(hydroxyethyl) ligand **34** and bis(propylamide) ligand **41**.

The length of the alkyl spacer was found to have a major influence on the stability and composition of the alkaline earth metal ion complexes. Complex stability increased with the lengthening of the spacer although quantum yield differences decreased. Bis-(morpholinomethyl) **38** only showed evidence of (metal)•(ligand) complex formation of low stability. In contrast, the longer ethyl **36** and propyl **42** systems formed both (metal)•(ligand) and $(metal)_2$•(ligand) complexes. The stability of the (metal)•(ligand) complex formed was always greater than that of the corresponding $(metal)_2$•(ligand) complex. The relative charge densities of the metal ions was found to impinge upon both the stability and the quantum yield of the complex formed, with Mg^{2+} more fluorescent than Ba^{2+} complexes. The likelihood of formation of fluorescent 'sandwich' type structures (metal ion coordinating both receptors simultaneously) for the (metal)•(ligand) complexes increased as the spacer length increased.

Changing the constitution of the morpholine receptor in **36** to that of thiomorpholine (**52**) caused little change in the stability constant although the fluorescence quantum yield decreased significantly. A similar substitution of morpholine for piperazine (**53**) gave the same lowered quantum yields yet complexation was appreciably improved with high stability constants observed for the alkaline earths metal ions. Alkali metal ion complexation for **53** was also observed. Again, the charge density of the metal ion had a strong influence on the level of complexation and observed quantum yield as the

complexes with alkaline earth metal ions were more fluorescent than the alkali metal ions. This trend was also observed for the azacrown containing ligands **45** and **51**.

The complexation of bis(azacrown) **45** and mono(azacrown) **51** with alkaline earth metal ions was too strong to be accurately determined by the spectrofluorimetric method used. Bis(azacrown) **45** displayed distinctly biphasic binding curves as the (metal)•(ligand) complex formed was of low fluorescence and the $(metal)_2$•(ligand) complex was highly fluorescent. This shows the lack of cooperativity for simultaneous binding of a single metal ion between the two receptors. The mono(azacrown) ligand **51** with a single receptor displayed high sensitivity with the ability to detect metal ion concentrations below 10^{-6} mol dm^{-3}. The complex stability constants for the azacrown containing ligands were higher than related systems in the literature due to the increased spacer length.

The results described show the universality of the Fluorophore-Spacer-Receptor design strategy where altering the various components, even minimally, significantly alters the specificity and selectivity of a fluorescent sensor for metal ions. This study provides valuable insight into some of the factors controlling fluorescence complex stability that can be incorporated into more sophisticated sensor systems.

The ligands described here show insufficient selectivity between metal ions to be employed in selective systems and the low stability of their complexes in water renders them unsuitable for use in the solvent of greatest analytical interest, water. Hence, further elaboration of these fluorescent sensors is required in order to fully investigate their potential use as viable fluorescent sensors.

Of prime importance is increasing the metal ion complex stability in water by the introduction of hydrophilic pendant arms, which could also improve the aqueous solubility. It should be emphasised that the desired selectivity towards a given metal ion in a specific concentration range can be very different according to the ultimate application. Introduction of other appropriate hydrophilic moieties could also enhance the aqueous solubility of the ligand system. However, depending upon the end-usage of the fluorescent sensor, limited water solubility can be advantageous as it prevents leaching of the sensor from thin-films or immobilised in gel.

Altering the basicity of the PET quenching nitrogen such that it is less pH sensitive would also be of use in an aqueous environment. Aniline analogues may be of benefit in that regard although its rigidity could hinder complexation.

Examining the synthesised ligands through time-resolved photophysical studies in order to determine both excited state lifetimes and decay rates would be of interest. Furthermore, complexation of molecular analytes that may utilise the dual receptors in a cooperative manner would be of interest.

Future fluorescent sensor designs for a particular analyte should focus on the utilisation of pre-existing knowledge of an analyte-specific receptor with subsequent alteration of the receptor to achieve a specific and favourable photophysical response.

Chapter 6 Experimental

6.1 General Physical Methods

Deionised water used was ultrapurified with a Milli-Q Reagent system to produce water with a specific resistance of >15 MΩ cm, boiled for 1 h to remove dissolved gases and protected from carbon dioxide by storage in a closed vessel under a drying tube containing soda lime. 1,4-Dioxane was purified by standing over potassium hydroxide pellets overnight, then passed through oven dried basic alumina before it was distilled under nitrogen from sodium/benzophenone. Acetonitrile was purified by standing over 3Å molecular sieves overnight, then passed through oven-dried basic alumina before it was distilled under nitrogen from anhydrous potassium carbonate.

Tetraethylammonium perchlorate (NEt_4ClO_4) was prepared by the addition of a slight excess of aqueous 1.0 mol dm^{-3} perchloric acid (600 cm^3) to tetraethylammonium bromide (100 g, 0.48 mol)(Aldrich) in water (150 cm^3). The crude NEt_4ClO_4 that precipitated was repeatedly recrystallised from aqueous ethanol until free from acid and bromide. Finally, the white crystalline NEt_4ClO_4 was dried over phosphorus pentoxide containing indicator (Sicapent) under vacuum overnight and then used immediately. All solutions were prepared in 0.050 mol dm^{-3} supporting electrolyte (NEt_4ClO_4) in the appropriate solvent.

Chemicals used were of analytical reagent grade and all glassware was A-grade. All sample solutions were thermostatted to 298.2 ± 0.2 K.

HEPES (*N*-2-hydroxyethylpiperazine-*N*'-2-ethanesulphonic acid, pK_a 7.55) buffer solution was prepared as described in the literature,[185] using a calibrated pH-electrode (see Section 6.3) in a 1,4-dioxane-water solvent mixture (40:60, v/v). The pH was adjusted by the addition of $HClO_4$ until the desired solution pH was obtained (0.050 mol dm^{-3}, pH 7.36, I = 0.050 mol dm^{-3} (NEt_4ClO_4)). Likewise, boric acid/borate (pK_a 9.23) buffer was prepared in a 1,4-dioxane-water solvent mixture (40:60, v/v). The pH was adjusted by the addition of NEt_4OH until the desired solution was obtained (0.050 mol dm^{-3}, pH 10.00, I = 0.050 mol dm^{-3} (NEt_4ClO_4)).[185]

The 4-(2-{10-[2-(1,4-thiazinan-4-yl)ethyl]-9-anthryl}ethyl)thiomorpholine **52** and 1-{2-[10-(2-piperazinoethyl)-9-anthryl]ethyl}piperazine **53** ligands were supplied by Dr. Nicholas J. Head.[122] All other ligands used were prepared as described in Section 6.9. The ligands studied were dried over phosphorus pentoxide containing indicator (Sicapent) under vacuum for a minimum of 6 h before use. The metal perchlorate salts (Aldrich) were used as received after drying. All metal salts were vacuum dried at room temperature for 24 hours over phosphorus pentoxide containing indicator (Sicapent) and then used immediately. For non-aqueous measurements the required metal salts were further dried in a vacuum oven (120°C at 0.05 mm Hg),[41] to remove water of hydration, and then used immediately.

6.2 Standardisation of Metal Ion Solutions

All the metal perchlorate salts used were standardised in triplicate using cation exchange chromatography. A Dowex AG 50W-X2 ion exchange column (2x20 cm) was washed twice with hydrochloric acid (1.0 mol dm^{-3}) to ensure complete protonation of the column, and then rinsed thoroughly with Milli-Q water. The column was then loaded with 1.00 cm^3 of a 0.1 mol dm^{-3} aqueous solution of the metal salt to be standardised, and eluted with purified Milli-Q water until the eluant became neutral. Bromothymol Blue (2 drops) was then added to the eluant, and the solution was titrated against sodium hydroxide (0.1 mol dm^{-3}, previously standardised against potassium hydrogen phthalate) to determine the total number of moles of hydrochloric acid eluted from the column. This in turn allowed the number of moles of the metal ion to be determined accurately, since one mole of the metal(I) salt displaces one equivalent of protons form the column. Alternatively, one mole of a metal(II) salt displaces two equivalents of protons from the column.

6.3 Potentiometric Titrations in 1,4-Dioxane-Water Solution

1,4-Dioxane, Milli-Q water and NEt_4ClO_4 were prepared as described in Section 6.1. All titration solutions were prepared in a 1,4-dioxane-water solvent mixture (40:60, v/v).

Potentiometric titrations were carried out using a Metrohm E665 Dosimat Autoburette that was equipped with a 5.0 cm^3 burette interfaced to an Acer Power 466d IBM compatible

personal computer. Changes in hydrogen ion concentration were monitored using an Orion Ross Sureflow 81-72 BN combination pH electrode (filled with 0.050 mol dm^{-3} NEt_4ClO_4 in 1,4-dioxane-water (40:60, v/v)) connected to an Orion Research SA 720 pH meter. All titration solutions were magnetically stirred and thermostatted at 298.2 ± 0.2 K in a water jacketed 20 cm^3 vessel. The solutions were saturated with high purity nitrogen by passing a fine stream of nitrogen bubbles through them for at least 15 min before commencement of any titration. Prior to entering the vessel, the nitrogen was bubbled through a solution of 0.050 mol dm^{-3} NEt_4ClO_4 in the solvent mixture, in order to prevent evaporation from the titration vessel. During the titrations a similar stream of nitrogen bubbles was passed through the titration solution to prevent the ingress of atmospheric carbon dioxide.

The pK_a values were determined by the titration of a solution of 0.1 mol dm^{-3} NEt_4OH (standardised by titration against potassium hydrogen phthalate) with 10.00 cm^3 of a solution containing the ligand of interest and $HClO_4$. The following ligand (and $HClO_4$) concentrations were used; bis(azacrown) **45**, 8.0 x 10^{-4} mol dm^{-3} (0.0068 mol dm^{-3}); mono(azacrown) **51**, 9.0 x 10^{-4} mol dm^{-3} (0.0060 mol dm^{-3}); bis(morpholinoethyl) **36** and bis(morpholinopropyl) **42**, 9.0 x 10^{-4} mol dm^{-3} (0.0050 mol dm^{-3}); and bis(piperazine) **53**, 6.4 x 10^{-4} mol dm-3 (0.0040 mol dm^{-3}), respectively. The ligand and $HClO_4$ solutions were 0.050 mol dm^{-3} in NEt_4ClO_4. For titrations in the presence of a metal ion, a sufficient quantity of a metal salt solution (*ca.* 0.1 mol dm^{-3} $NaClO_4$, $Ca(ClO_4)_2$ or $Pb(ClO_4)_2$) was added directly to the acidic titration solution to give a final metal ion to ligand ratio of 2:1. The addition of titrant was computer controlled so that either constant volume aliquots could be delivered, or successive additions of titrant were added to cause a decrease in potential of approximately 4 mV. For all titrations, a maximum delay of 300 seconds between each titrant addition was sufficient for equilibrium to be established.

The pH electrode was regularly calibrated by the titration of 0.1 mol dm^{-3} NEt_4OH from the autoburette with 10.00 cm^3 of 0.005 mol dm^{-3} $HClO_4$ (0.050 mol dm^{-3} in NEt_4ClO_4). The resulting data was fitted to the Nernst equation (Equation 6.1);

$$E = E_O + \frac{RT}{F} \ln[H^+] \quad (6.1)$$

where E is the observed potential (V)

E_0 is the standard potential for the electrode (V)

R is the ideal gas constant (8.314 J mol^{-1} K^{-1})

T is the temperature (K)

F is Faraday's constant (9.6487 x 10^4 Coulombs mol^{-1})

$[H^+]$ is the hydrogen ion concentration

At 298.2 K, with E in millivolts and converting to logarithm base 10, Equation 6.1 becomes;

$$pH = \frac{E_O - E}{59.15} \quad (6.2)$$

where E is the observed potential (mV)

pH = -log[H+]

When considering pK_w = pH + pOH and pOH = $-\log[OH^-]$, Equation 6.2 becomes;

$$pK_W = \frac{E_O - E}{59.15} + pOH \quad (6.3)$$

The programme MacCalib[186] was used to calculate the endpoint of the titration (and hence the exact concentration of H^+ used) and the calibration parameters E_0 and pK_w. The ligand protonation constants were determined by fitting the titration data using the programme SUPERQUAD.[187] At least three runs were performed for each system, and at least two of these runs were averaged; the criterion for selection for this averaging being that χ^2 for each run was less than 12.6 at the 95% confidence level.[187] Averaging was performed using the Matlab programme ERRORS.[188]

6.4 Ultraviolet-Visible Spectroscopy

UV-visible absorbance spectra were recorded using a Varian CARY 300 Bio spectrophotometer equipped with matched 1.0 cm path length quartz cells over the wavelength range 300-450 nm at 0.5 nm intervals, with a scan rate of 300 nm min^{-1}. Each solution was run against a blank containing all components of the solution of interest except the ligand and metal salt (if applicable). Baseline correction measurements were used for all spectra. Solutions were pre-equilibrated at 298.2 ± 0.2 K and maintained at this temperature during measurement by means of a thermostatted block.

The concentration of all ligands studied was 6.6 x 10^{-5} mol dm^{-3}. However, when the ligand of interest was of insufficient solubility in the solvent used, a concentration of 3.3 x 10^{-5} mol dm^{-3} was utilised. All solutions were freshly prepared prior to measurement.

6.5 Fluorescence Spectroscopy

Fluorescence measurements were obtained with a Perkin-Elmer LS-50B spectrofluorimeter equipped with a 1.0 cm path length quartz cell. Spectra were acquired between 390 and 550 nm with excitation and emission slit widths of 10 nm and 5 nm, respectively, using a 1% transmittance emission filter. Two scans at 0.5 nm intervals, with a scan rate of 200 nm min^{-1}, were recorded and averaged. Emission spectra obtained were not corrected for instrumental factors. Solutions were pre-equilibrated at 298.2 ± 0.2 K and maintained at this temperature during measurement by means of a thermostatted block. Fluorescence, if any, due to the solvent and supporting electrolyte alone was measured and subtracted from each spectrum. The concentration of all ligands studied was 3.0 x 10^{-6} mol dm^{-3}. All solutions were freshly prepared prior to measurement.

The excitation wavelength for each system studied was selected from within the second longest wavelength absorption band. The wavelength chosen was either an isosbestic point or, in its absence, the wavelength where the absorbance difference between the species of interest was at a minimum. This was designed to ensure that all species in solution absorbed an identical, or at least comparable, number of photons.

6.6 Stability Constants from Fluorescence

The observed fluorescence of a single (metal)•(ligand) complex is given by Equation 6.4, where F represents the total fluorescence, ε_L, ε_M and $\varepsilon_{M\bullet L}$ the molar fluorescences of the ligand, metal and (metal)•(ligand) complex, and [ligand], [metal] and [(metal)•(ligand)] represent the equilibrium ligand, metal and (metal)•(ligand) complex concentrations, respectively.

$$F = \varepsilon_L[\text{ligand}] + \varepsilon_M[\text{metal}] + \varepsilon_{M\bullet L}[(\text{metal})\bullet(\text{ligand})] \quad (6.4)$$

When an additional $(\text{metal})_2$•(ligand) complex is present, the observed fluorescence is given by Equation 6.5.

$$F = \varepsilon_L[\text{ligand}] + \varepsilon_M[\text{metal}] + \varepsilon_{M\bullet L}[(\text{metal})\bullet(\text{ligand})] + \varepsilon_{(M)_2\bullet L}[(\text{metal})_2\bullet(\text{ligand})] \quad (6.5)$$

Stability constants were determined by a simultaneous fit of the entire range of spectral data recorded to Equations 6.4 and 6.5 using a non-linear least-squares regression routine based on Method 5 of Pitha and Jones[189] through the Matlab programme DATAFIT/SPECFIT.[164] SPECFIT is designed to calculate stability constants and their standard deviations from fluorescence spectra followed by the emission spectra of each species. Physical constraints, such as the fact that neither the stability constants nor the derived complex fluorescence could be negative, are incorporated in the fitting process. The data was not weighted.

6.7 Relative Quantum Yields

The relative quantum yield (Φ_F) values were determined using the optically dilute solution method,[169] whereby the quantum yield of an unknown is related to that of a reference standard by Equation 6.6.[169,190]

$$\Phi_x = \Phi_r \cdot \frac{A_r}{A_x} \cdot \frac{F_x}{F_r} \cdot \frac{(n_x)^2}{(n_r)^2} \quad (6.6)$$

where x refers to the unknown

r refers to the reference standard

Φ is the quantum yield

A is the absorbance of the solution at the excitation wavelength

F is the integrated area under the emission spectrum

n is the index of refraction of the solvent

The reference standard used was quinine sulphate (Φ_r = 0.546 in 1.0 N sulphuric acid).[167,168] The refractive index values used were, n = 1.342 for acetonitrile and n = 1.333 for water, at 25°C at the sodium D line.[171] Standard solutions were prepared in aqueous 0.50 mol dm^{-3} (1.0 N) sulphuric acid (Convol, BDH) using analytical reagent grade anhydrous quinine (Fluka). All ligand containing solutions were prepared in anhydrous acetonitrile containing 0.050 mol dm^{-3} NEt_4ClO_4.

UV-visible absorbance spectra of quinine sulphate (1.0×10^{-5} mol dm^{-3} and 5.0×10^{-6} mol dm^{-3} solutions) were recorded as described in Section 6.4. Similarly, fluorescence spectra of quinine sulphate (1.0×10^{-5} mol dm^{-3} and 5.0×10^{-6} mol dm^{-3} solutions) were recorded as described in Section 6.5. The excitation wavelength used for the quinine standard was matched to that used for the unknown so as to ensure that the relative intensity of the exciting light was identical. The concentrations used for the fluorescence measurements corresponded to absorbances of < 0.03 at the excitation wavelength. Therefore, corrections for self-absorption, of incident and emitted light, on the emission intensities were not made. The area under the emission spectrum between 390 and 550 nm was calculated by computerised integration. Errors in quantum yield values obtained are approximately 10%.

6.8 General Synthetic Methods

All solvents and reagents were purified using standard literature procedures.[191] Reactions were generally performed under an anhydrous nitrogen atmosphere. Flash chromatography was performed using Merck $60PF_{254}$ silica gel 230-400 mesh or Fluka neutral alumina (type 507 C, 100-125 mesh). Thin layer chromatography (TLC) analysis of reaction mixtures was performed on aluminium-backed Merck $60PF_{254}$ silica or alumina (neutral) plates.

Melting points were determined on a Kofler hot-stage apparatus equipped with a Reichert microscope and are uncorrected. ^1H and ^{13}C NMR spectra were recorded as solutions with tetramethylsilane as the internal standard using a Varian Gemini-2000 spectrometer

operating at 300.145 MHz (^{1}H) and 75.4 MHz (^{13}C). Chemical shifts are cited as parts per million (ppm) downfield from the internal standard and coupling constants (*J*) are given in Hertz (Hz). The multiplicity of signals are reported as being: s, singlet; d, doublet; t, triplet; q, quartet; m, an unassignable multiplicity or overlapping signals; br, broadened signal.

Combustion analyses were carried out by the Microanalytical Division of the Chemistry Department, University of Otago, New Zealand. The conventional electron impact mass spectra were recorded on a VG ZAB 2HF mass spectrometer. Electrospray ionisation mass spectra (ESI-MS) were recorded on a Finnigan MAT ion trap LC-Q octapole mass spectrometer.

6.9 Syntheses

Lithioanthracene.[115]

9,10-Dibromoanthracene (200 mg, 0.89 mmol) and anhydrous diethyl ether (10 cm^3) were stirred under nitrogen, cooled to 0°C and *n*-butyl lithium (0.9 cm^3 of a 2.3 mol dm^{-3} solution in hexane, 2.07 mmol) was added over 5 min. Stirring was continued for a further 20 min and the resulting mixture of 9,10-dilithioanthracene was used directly in subsequent reactions.

9-Lithio-10-ethylanthracene was similarly prepared from 9-bromo-10-ethylanthracene **48**.

2-[10-(2-Hydroxyethyl)-9-anthryl]-1-ethanol, 34.[105]

To freshly prepared 9,10-dilithioanthracene (30.0 mmol) was added ethylene oxide (excess) dropwise via direct condensation of the gas into the reaction mixture (using a dry-ice/acetone condenser) until a yellow colour persisted within the reaction mixture. The mixture was then allowed to warm to room temperature and poured onto ice (25 g). The precipitate that formed was filtered, washed with diethyl ether (20 cm^3) followed by a large amount of water (100 cm^3), and then recrystallised from ethanol to obtain the title compound **34** as bright yellow needles (3.0 g, 38 %). mp 222-225°C (lit.[105] 221-225°C). δ_H(d_6-DMSO) 3.75 (s, 8H, Ar$\mathbf{CH_2CH_2}$OH), 4.92 (br s, 2H ,OH), 7.54 (m, 4H, ArH), 8.37 (m, 4H, ArH). δ_C(d_6-DMSO) 31.48, 61.71, 125.09, 125.16, 129.50, 130.12. *m/z* (%); 266 ($M^{+\cdot}$, 84), 235 (54), 205 (100), 191 (34).

2-[10-(2-{[(4-Methylphenyl)sulfonyl]oxy}ethyl)-9-anthryl]ethyl 4-methyl-1-benzene-sulfonate, 35.

To a solution of 2-[10-(2-hydroxyethyl)-9-anthryl]-1-ethanol **34** (520 mg, 1.95 mmol) and pyridine (15 cm^3) at 0°C was added *p*-toluenesulfonyl chloride (810 mg, 4.24 mmol). The resulting solution was allowed to warm to room temperature and was stirred for 24h. The reaction was quenched with an aqueous saturated ammonium chloride solution (25 cm^3). The product was collected and then washed with cold ethanol (35 cm^3) to obtain the title compound **35** as a pale white powder (1.07 g, 95%). mp 200-202°C. $\delta_H(CDCl_3)$ 2.39 (s, 6H, $ArCH_3$), 4.01 (t, 4H, *J* 8.1 Hz, $ArCH_2$), 4.35 (t, 4H, *J* 8.1 Hz, CH_2O), 7.19 (AA' portion of AA'XX', 4H, ArH), 7.50 (m, 4H, ArH), 7.64 (XX' portion of AA'XX', 4H, ArH), 8.14 (m, 4H, ArH). $\delta_C(CDCl_3)$ 21.58, 27.90, 69.17, 124.42, 125.95, 127.55, 127.73, 129.65, 129.92, 132.96, 144.62. *m/z* (%); 574 ($M^{+\cdot}$, 34), 402 (25), 230 (100), 203 (62), 172 (24).

4-{2-[10-(2-Morpholinoethyl)-9-anthryl]ethyl}morpholine, 36.

To 2-[10-(2-{[(4-methylphenyl)sulfonyl]oxy}ethyl)-9-anthryl]ethyl 4-methyl-1-benzene-sulfonate **35** (200 mg, 0.35 mmol) and sodium hydrogencarbonate (120 mg, 1.4 mmol) in *N,N*-dimethylformamide (6 cm^3) was added morpholine (0.12 cm^3, 1.39 mmol) at room temperature and the mixture was heated for 24 h at 80°C. After cooling for 20 h, the white-yellow precipitate that formed was filtered and recrystallised from dichloromethane/methanol to give pale yellow crystals of the title compound **36** (95 mg, 67%). mp 224-226°C. $\delta_H(CDCl_3)$ 2.75 (m, 12H, CH_2N), 3.84 (m, 12H, CH_2O and $ArCH_2$), 7.54 (m, 4H, ArH), 8.32 (m, 4H, ArH). $\delta_C(CDCl_3)$ 25.52, 53.77, 59.32, 67.02, 124.92, 125.29, 129.68, 131.04. *m/z* (%); 404 ($M^{+\cdot}$, 9), 208 (38), 152 (29). Analysis Calcd for $C_{26}H_{32}N_2O_2$: C, 77.19; H, 7.97; N, 6.92. Found: C, 77.00; H, 7.97; N, 6.96.

9,10-Di(chloromethyl)anthracene, 37.[106]

A solution of 1,4-dioxane (220 cm^3) and concentrated hydrochloric acid (32 cm^3) was saturated for 12 min with hydrogen chloride gas. Anthracene (25.0 g, 140 mmol) and para-formaldehyde (23.0 g, 767 mmol) were then added, and to the resultant solution at reflux, hydrogen chloride was bubbled in for 2 h. The mixture was then slowly stirred at reflux for a further 3 h without the addition of hydrogen chloride before it was left overnight to precipitate. The yellow solid that formed was collected by filtration. The solid was

resuspended and refiltered from 1,4-dioxane (1 x 80 cm^3, 1 x 50 cm^3) before a final wash with 1,4-dioxane (80 cm^3) and thorough drying gave the title compound **37** as a bright yellow powder (19.73 g, 51%). mp 255°C dec. (lit.[106] mp 253-255°C dec.). $\delta_H(CDCl_3)$ 5.61 (s, 4H, CH_2Cl), 7.66 (m, 4H, ArH), 8.38 (m, 4H, ArH). $\delta_C(CDCl_3)$ 38.79, 124.36, 126.71, 129.80, 130.25. *m/z* (%); 273 ($MH^{+\cdot}$, 29), 241 (37), 239 (100), 204 (98), 101 (36).

4-{[10-(Morpholinomethyl)-9-anthryl]methyl}morpholine, 38.[107]

To 9,10-di(chloromethyl)anthracene **37** (500 mg, 1.82 mmol) in benzene (8 cm^3) was added morpholine (0.6 cm^3, 6.9 mmol) and the resultant mixture was refluxed for 3 h and left to cool overnight. The benzene was removed *in vacuo* and the solid redissolved in dichloromethane (20 cm^3). The organic phase was extracted with a 10% hydrochloric acid solution (2 x 20 cm^3) and the aqueous phase was then basified with sodium hydroxide to give a white precipitate. The solid was recrystallised from ethanol to give the title compound **38** as pale yellow plates (211 mg, 31%). mp 240°C dec. (lit.[107] mp 243°C dec.). $\delta_H(CDCl_3)$ 2.63 (m, 8H, NCH_2CH_2O), 3.64 (m, 8H, CH_2O), 4.46 (s, 4H, $ArCH_2N$), 7.53 (m, 4H, ArH), 8.54 (m, 4H, ArH). $\delta_C(CDCl_3)$ 53.67, 54.72, 67.19, 125.13, 125.57, 129.81, 131.13. *m/z* (%); 376 ($M^{+\cdot}$, 41), 290 (100), 204 (44), 191 (43).

Diethyl 2-({10-[3-ethoxy-2-(ethoxycarbonyl)-3-oxopropyl]-9-anthryl}methyl)-malonate, 39.[109]

Sodium hydride (222 mg, 60% dispersion in oil, 5.6 mmol) was washed with hexane (three times) and toluene to remove the oil. The washed sodium hydride was then resuspended in toluene (7 cm^3) and at 70°C, diethyl malonate (0.8 cm^3, 5.3 mmol) was added. After stirring for 1.5 h, 9,10-di(chloromethyl)anthracene **37** (400 mg, 1.45 mmol) was added portionwise to the clear solution at 70°C. The solution was then left to stir at 70°C for 2 h. After cooling, the solution was poured into water (10 cm^3), neutralised with a 10% hydrochloric acid solution, and the solid present in the organic phase was filtered. The filtered solid was washed with water and a little ethanol before recrystallisation from dichloromethane/ethanol gave the title compound **39** as yellow plates (317 mg, 42%). mp 170-171°C (lit.[109] mp 173°C). $\delta_H(CDCl_3)$ 1.05 (t, 12H, *J* 7.2 Hz, CH_3CH_2O), 3.84 (t, 2H, *J* 7.4 Hz, $ArCH_2CH$), 4.05 (m, 8H, CH_3CH_2O), 4.21 (d, 4H, *J* 7.4 Hz, $ArCH_2CH$), 7.52 (m, 4H, ArH), 8.32 (m, 4H, ArH). $\delta_C(CDCl_3)$ 13.76, 26.69, 53.14, 61.52, 125.04, 125.50, 129.97, 130.38, 169.18. *m/z* (%); 522 ($M^{+\cdot}$, 100), 363 (53), 289 (51), 215 (82).

1-Morpholino-3-[10-(3-morpholino-3-oxopropyl)-9-anthryl]-1-propanone, 41.

Diisopropylamine (0.64 cm^3, 4.54 mmol) in anhydrous tetrahydrofuran (5 cm^3) under nitrogen was cooled to 0°C, *n*-butyl lithium (2.05 cm^3 of a 2.25 mol dm^{-3} solution in hexane, 4.54 mmol) was added and the mixture was left to stir for 30 min. 4-Acetylmorpholine (0.53 cm^3, 4.54 mmol) was then added and the mixture was left to stir at 0°C for 2 h. 9,10-Di(chloromethyl)anthracene **37** (400 mg, 1.45 mmol) was then added as a solid, and after 10 min, anhydrous tetrahydrofuran (10 cm^3) was added. The yellow suspension was stirred at 0°C for 2 h. The resultant solution was quenched with water (10 cm^3) and the tetrahydrofuran was removed *in vacuo*. The aqueous layer was extracted with dichloromethane (2 x 30 cm^3), dried ($MgSO_4$) and the solvent was removed *in vacuo* to give a yellow solid. The solid was recrystallised from ethanol to give the title compound **41** as yellow needles (395 mg, 59%). mp 200-203°C. $\delta_H(CDCl_3)$ 2.78 (m, 4H, $ArCH_2CH_2$), 3.09 (AA' portion of AA'XX', 4H, CH_2N), 3.23 (BB' portion of BB'YY', 4H, CH_2N), 3.52 (XX' portion of AA'XX', 4H, CH_2O), 3.61 (YY' portion of BB'YY', 4H, CH_2O), 4.03 (m, 4H, $ArCH_2$), 7.55 (m, 4H, ArH), 8.32 (m, 4H, ArH). $\delta_C(CDCl_3)$ 23.44, 33.76, 42.00, 45.82, 66.19, 66.69, 124.96, 125.62, 129.50, 132.53, 170.96. *m/z* (%); 460 ($M^{+\cdot}$, 100), 332 (31), 217 (21). Analysis Calcd for $C_{28}H_{32}N_2O_4$: C, 73.02; H, 7.00; N, 6.08. Found: C, 73.03; H, 7.23; N, 5.91.

4-{3-[10-(3-Morpholinopropyl)-9-anthryl]propyl}morpholine, 42.

To 1-morpholino-3-[10-(3-morpholino-3-oxopropyl)-9-anthryl]-1-propanone **41** (300 mg, 0.65 mmol) in anhydrous tetrahydrofuran (10 cm^3) at 0°C was added borane-tetrahydrofuran complex (5.2 cm^3 of a 1.0 mol dm^{-3} solution in tetrahydrofuran, 5.2 mmol) and the clear solution was stirred at room temperature for 1 h and then refluxed for 2 h. After cooling, the excess borane was hydrolysed with a water-methanol mixture (3 cm^3, 1:1) and the solvents were evaporated. The residue was then refluxed in 6 mol dm^{-3} hydrochloric acid (10 cm^3) for 3 h and left to cool overnight. The mixture was neutralised by the addition of sodium hydroxide pellets (pH > 10) and the aqueous layer was extracted with chloroform (2 x 25 cm^3), dried ($MgSO_4$), and the solvent removed *in vacuo* to give a yellow solid. The solid was recrystallised from methanol/dichloromethane to give the title compound **42** as yellow cubes (140 mg, 50%). mp 156-158°C. $\delta_H(CDCl_3)$ 2.00 (m, 4H, $ArCH_2CH_2$), 2.49 (m, 8H, CH_2N), 2.56 (m, 4H, $ArCH_2CH_2CH_2N$), 3.66 (m, 4H,

$ArCH_2CH_2$), 3.77 (m, 8H, CH_2O), 7.49 (m, 4H, ArH), 8.36 (m, 4H, ArH). $\delta_C(CDCl_3)$ 25.56, 28.09, 53.84, 58.68, 67.09, 124.90, 125.24, 129.56, 133.44. *m/z* (%); 432 ($M^{+\cdot}$, 43), 332 (23), 306 (34), 126 (77), 100 (100). Analysis Calcd for $C_{28}H_{36}N_2O_2$: C, 77.74; H, 8.39; N, 6.48. Found: C, 77.33; H, 8.34; N, 6.45.

3-[10-(3-Hydroxy-1-propynyl)-9-anthryl]-2-propyn-1-ol, 43.

Nitrogen was bubbled through a solution of chloroform (15 cm^3) and triethylamine (0.83 cm^3, 5.95 mmol) for 15 min at 0°C. 9,10-Diiodoanthracene[115] (1.00 g, 2.33 mmol), propargyl alcohol (0.52 cm^3, 8.9 mmol), tetrakis(triphenylphosphine)palladium(0) (69 mg, 0.06 mmol) and finally copper(I) iodide (12 mg, 0.06 mmol) were added to the deoxygenated solution which was then heated at 60°C for 21 h. More propargyl alcohol (0.50 cm^3, 8.6 mmol) was added to the reaction mixture after 6 h. Hot dichloromethane was added and the resultant mixture was filtered through Celite. The filter cake was further washed with hot dichloromethane (4 x 50 cm^3) and the solvent was removed *in vacuo*. Flash chromatography (silica; diethyl ether:dichloromethane, 1:4) gave a fraction that predominantly contained the title compound **43** as a brownish-yellow solid (134 mg, 20%). $\delta_H(CDCl_3)$ 4.86 (s, 4H, CH_2OH), 7.61 (m, 4H, ArH), 8.75 (m, 4H, ArH). *m/z* (%); 287 ($MH^{+\cdot}$, 100), 229 (66), 105 (99).

13-(2-{10-[2-(1,4,7,10-Tetraoxa-13-azacyclopentadecanyl)ethyl]-9-anthryl}ethyl)-1,4,7,10-tetraoxa-13-azacyclopentadecane, 45.

1,4,7,10-Tetraoxa-13-azacyclopentadecane (404 mg, 1.84 mmol) was added to 9,10-di(2-iodoethyl)anthracene **44**[105] (208 mg, 0.43 mmol) in dry toluene (10 cm^3) and the solution was heated under reflux for 2 days. After cooling, the solvent was removed *in vacuo*, and dichloromethane (15 cm^3) was added to the brown residue. The organic solution was extracted with hydrochloric acid (4 x 10 cm^3, 0.10 mol dm^{-3}) and the aqueous layer was then basified to pH 11 with potassium carbonate. The aqueous layer was extracted with chloroform (5 x 10 cm^3), the solvent was removed *in vacuo*, and a 1.8 mol dm^{-3} hydrogen chloride in methanol solution (2 cm^3) was added. The solvent was again removed *in vacuo* to give a yellow powder that contained the desired compound and unreacted monoaza-15-crown-5 as an impurity. An aqueous 10% sodium carbonate solution (4 cm^3) was added to the crude solid and it was extracted with dichloromethane (3 x 6 cm^3). The combined organic layers were washed with water (5 x 3 cm^3), the solvent was removed, and a 1.8

mol dm^{-3} hydrogen chloride in methanol solution (2 cm^3) was added. The solvent was removed in vacuo to afford the title compound **45**.2HCl as yellow-brown microcrystals (154 mg, 48%). mp 153°C dec. $\delta_H(CDCl_3)$ 3.49-3.77 (m, 36H, 16 x CH_2O and 2 x $ArCH_2$), 4.02 (m, 4H, 2 x $ArCH_2CH_2N$, 4.34 (m, 8H, 4 x NCH_2CH_2O), 7.60 (m, 4H, ArH), 8.61 (m, 4H, ArH). $\delta_C(CDCl_3)$ 23.68, 52.21, 54.31, 65.95, 69.96, 70.76, 70.87, 125.05, 126.35, 128.66, 129.92. ESI-MS *m/z* (%); 669 ($MH^{+\cdot}$, 52), 691 ($(M+Na)^+$, 68), 335 ($(MH_2)^{2+}$, 100). Analysis Calcd for $C_{38}H_{56}N_2O_8$.HCl.NaCl.$2H_2O$: C, 57.07; H, 7.69; N, 3.50. Found: C, 56.74; H, 7.74; N, 3.35.

9-Ethylanthracene, 47.[119]

To dry magnesium turnings (5.638 g, 0.23 mol) in diethyl ether (100 cm^3), a crystal of iodine and a few drops of a solution of bromoethane (17.3 cm^3, 0.23 mol) in diethyl ether (10 cm^3) were added. After the reaction commenced (disappearance of the brown iodine colour), the remaining bromoethane solution was added dropwise at such a rate so as to maintain reflux. The reaction was then heated under reflux for a further 40 min before it was cooled to 0°C and anthrone (15.08 g, 077 mol) was added portionwise. The resultant mixture was stirred overnight at room temperature, then carefully poured onto ice, acidified with dilute hydrochloric acid and the organic phase was separated. The aqueous phase was extracted with diethyl ether (3 x 30 cm^3) and the combined organic layers were washed with an aqueous saturated sodium hydrogencarbonate solution (3 x 60 cm^3), dried ($MgSO_4$), and the solvent removed *in vacuo* to give a crude brown oil. To the crude product was added toluene (100 cm^3) and *p*-toluenesulphonic acid monohydrate (600 mg, ca. 5 mol%) and the solution was heated under refluxed for 17 h in a Dean-Stark apparatus. The solution was cooled and the organic layer was washed with an aqueous saturated sodium hydrogencarbonate solution (2 x 35 cm^3), dried ($MgSO_4$), and the solvent removed *in vacuo*. The residue was dissolved in dichloromethane and adsorbed onto silica before addition to a squat column that was eluted with hexane to give a yellow product that was recrystallised from methanol to give the title compound **47** as pale yellow needles (6.162 g, 42%). mp 57-58°C (lit.[119] mp 59°C). $\delta_H(CDCl_3)$ 1.45 (t, 3H, *J* 7.5 Hz, CH_2CH_3), 3.65 (q, 2H, *J* 7.5 Hz, CH_2CH_3), 7.43-7.53 (m, 4H, ArH), 8.00 (m, 2H, ArH), 8.29 (m, 3H, ArH). $\delta_C(CDCl_3)$ 15.48, 21.09, 124.31, 124.78, 125.37, 125.47, 129.22, 131.71, 136.64 (one Ar peak hidden). *m/z* (%); 206 ($M^{+\cdot}$, 41), 191 (100), 94 (26).

9-Bromo-10-ethylanthracene, 48.[121]

A mixture of 9-ethylanthracene **47** (5.0 g, 0.024 mol) and copper(II) bromide (10.827g, 0.048 mol) in dry benzene (200 cm^3) was heated under reflux for 5 h until the evolution of hydrogen bromide ceased. After cooling, the reaction mixture was filtered through Celite and the solvent was removed *in vacuo*. The crude product was purified by flash chromatography (silica; hexane) to afford the title compound **48** as a yellow powder (3.263 g, 48%). mp 103-105°C (lit.[121] mp 104-105°C). $\delta_H(CDCl_3)$ 1.46 (t, 3H, *J* 7.5 Hz, CH_2CH_3), 3.65 (q, 2H, *J* 7.5 Hz, CH_2CH_3), 7.55-7.61 (m, 4H, ArH), 8.31 (m, 2H, ArH), 8.60 (m, 2H, ArH). $\delta_C(CDCl_3)$ 15.45, 21.41, 124.16, 124.64, 125.68, 126.65, 128.72, 130.03, 130.46, 137.36. *m/z* (%); 285 ($M^{+\cdot}$, 64), 270 (100), 190 (50), 95 (28).

2-(10-Ethyl-9-anthryl)-1-ethanol, 49.

To freshly prepared 9-lithio-10-ethylanthracene (5.43 mmol) (prepared in an analogous manner to dilithioanthracene) at 0°C was added ethylene oxide (0.7 cm^3, excess) dropwise via cold syringe. The resultant yellow mixture was then allowed to warm to room temperature before it was poured onto ice (15 g). The precipitate that formed was filtered, washed with diethyl ether (10 cm^3) and water (30 cm^3), then recrystallised from ethanol to afford the title compound **49** as fluorescent yellow needles (562 mg, 41%). mp 148-150°C. $\delta_H(CDCl_3)$ 1.44 (t, 3H, *J* 7.8 Hz, CH_2CH_3), 3.60 (q, 2H, *J* 7.8 Hz, CH_2CH_3), 3.95 (m, 2H, CH_2CH_2OH), 4.10 (m, 2H, CH_2CH_2OH), 7.53 (m, 4H, ArH), 8.32-8.38 (m, 4H, ArH). $\delta_C(CDCl_3)$ 15.48, 21.27, 31.12, 63.50, 125.00, 125.09, 125.13, 125.30, 128.54, 129.05, 130.30, 136.18. *m/z* (%); 250 ($M^{+\cdot}$, 27), 219 (86), 204 (24), 41 (100). Analysis Calcd for $C_{18}H_{18}O$: C, 86.36; H, 7.25. Found: C, 86.02; H, 7.45.

9-Ethyl-10-(2-iodoethyl)anthracene, 50.

To 2-(10-ethyl-9-anthryl)-1-ethanol **49** (376 mg, 1.5 mmol) in dry *N,N*-dimethylformamide (5 cm^3) at 15°C was added methyltriphenoxyphosphonium iodide[192] (1.55 g, 3.4 mmol) with stirring. After 1 h, methanol (5 cm^3), followed by water (5 cm^3), were added and the precipitate was filtered, washed with methanol, then recrystallised from benzene to give the title compound **50** as yellow needles (414 mg, 77%). mp 130-132°C. $\delta_H(CDCl_3)$ 1.43 (t, 3H, *J* 7.5 Hz, CH_2CH_3), 3.43 (m, 2H, CH_2I), 3.61 (q, 2H, *J* 7.5 Hz, $ArCH_2CH_3$), 4.16 (m, 2H, $ArCH_2CH_2I$), 7.47-7.57 (m, 4H, ArH), 8.21 (m, 2H, ArH), 8.32 (m, 2H, ArH).

$\delta_C(CDCl_3)$ 3.19, 15.40, 21.34, 33.50, 124.44, 125.12, 125.18, 125.72, 129.12, 129.23, 131.51, 136.79. *m/z* (%); 360 ($M^{+\cdot}$, 35), 233 (100), 204 (100), 189 (30). Analysis Calcd for $C_{18}H_{17}I$: C, 60.02; H, 4.76. Found: C, 60.17; H, 4.95.

13-[2-(10-Ethyl-9-anthryl)ethyl]-1,4,7,10-tetraoxa-13-azacyclopentadecane, 51.

To 9-ethyl-10-(2-iodoethyl)anthracene **50** (100 mg, 0.28 mmol) in dry toluene (8 cm^3) was added 1,4,7,10-tetraoxa-13-azacyclopentadecane (150 mg, 0.62 mmol) and the solution was heated under reflux for 2 days. After cooling, the mixture was filtered and the solvent was removed *in vacuo*. The brown residue was redissolved in methanol (3 cm^3) and a 1.8 mol dm^{-3} hydrogen chloride in methanol solution (1 cm^3) was added and the solvent was removed *in vacuo* to give a yellow powder (98 mg) which contained unreacted monoaza-15-crown-5 as an impurity. An aqueous 10% sodium carbonate solution (2 cm^3) was added to the crude solid and it was extracted with dichloromethane (6 cm^3). The organic layer was washed with water (5 x 3 cm^3), the solvent was removed, and a 1.8 mol dm^{-3} hydrogen chloride in methanol solution (1 cm^3) was added and the solvent was removed *in vacuo* to afford the title compound **51**.HCl as pale yellow powder (67 mg, 49%). mp 166-168°C. $\delta_H(CDCl_3)$ 1.41 (t, 3H, *J* 7.5 Hz, CH_2CH_3), 3.46-3.76 (m, 20H, 8 x CH_2O and 2 x $ArCH_2$), 4.00 (m, 2H, $ArCH_2CH_2N$), 4.32 (m, 4H, 2 x NCH_2CH_2O), 7.48-7.60 (m, 4H, ArH), 8.30 (d, 2H, ArH), 8.58 (d, 2H, ArH). $\delta_C(CDCl_3)$ 15.37, 21.17, 23.44, 52.09, 54.26, 65.79, 69.82, 70.60, 70.71, 124.89, 124.94, 125.05, 125.94, 126.49, 128.88, 129.86, 136.87. ESI-MS *m/z* (%); 453 (MH^+, 3), 233 (100), 205 (29), 100 (31), 43 (86). Analysis Calcd for $C_{28}H_{37}NO_4$.HCl: C, 68.91; H, 7.85; N, 2.87. Found: C, 68.61; H, 7.94; N, 2.83.

Appendix A Fluorescence Spectra and Derived Binding Curves for Ligands in Acetonitrile Solution

A.1 Bis(morpholinomethyl) 38

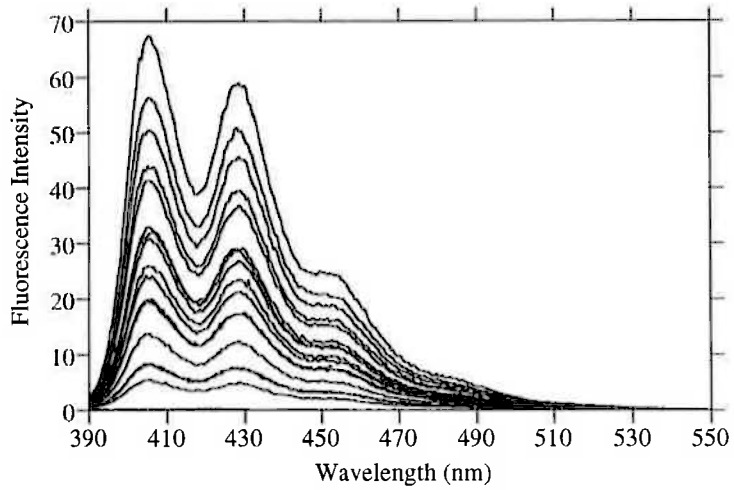

Figure A.1. *Emission spectra of bis(morpholinomethyl)* ***38*** *alone (3.0 x 10^{-6} mol dm^{-3}) and in the presence of increasing concentrations of Mg^{2+} (ranging from 1.0 x 10^{-5} to 5.0 x 10^{-3} mol dm^{-3}) in acetonitrile (I = 0.050 mol dm^{-3}) at 298.2 K, when excited at 374.0 nm. The emission of* ***38*** *alone is coincident with the baseline.*

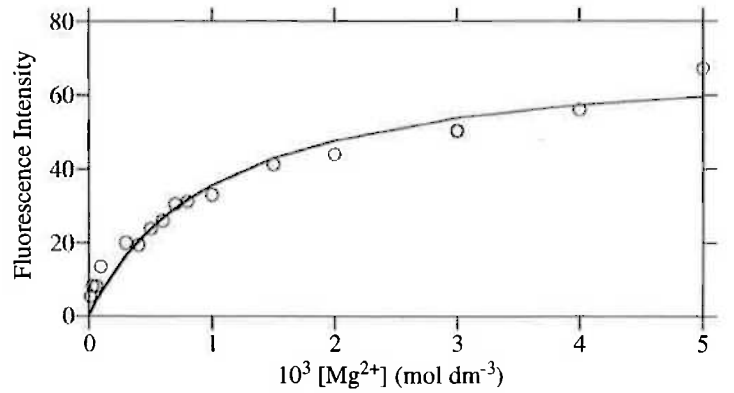

Figure A.2. *Fluorescence variation of bis(morpholinomethyl)* ***38*** *at 405.0 nm in the presence of increasing concentrations of Mg^{2+} when excited at 374.0 nm. The circles represent experimentally obtained data points and the solid line represents the best fit of the data to a 1:1 binding model.*

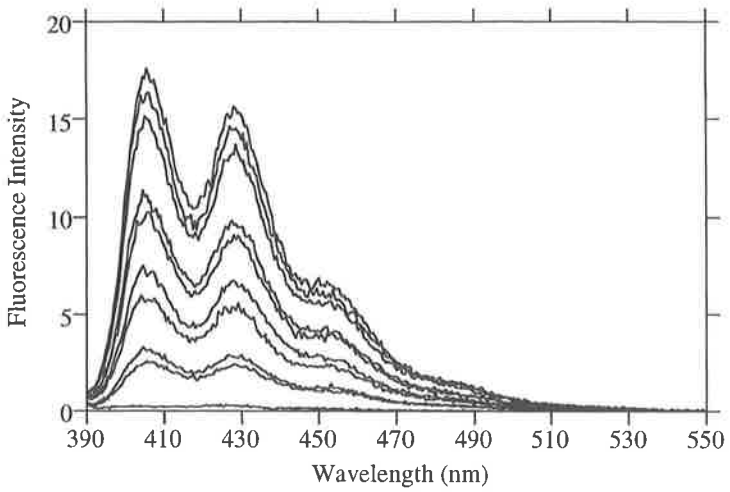

Figure A.3. *Emission spectra of bis(morpholinomethyl)* ***38*** *alone (3.0 x 10^{-6} mol dm^{-3}) and in the presence of increasing concentrations of Ca^{2+} (ranging from 1.0 x 10^{-4} to 6.0 x 10^{-3} mol dm^{-3}) in acetonitrile (I = 0.05 mol dm^{-3}) at 298.2 K, when excited at 378.0 nm. The emission of* ***38*** *alone is the lowest intensity curve in the montage.*

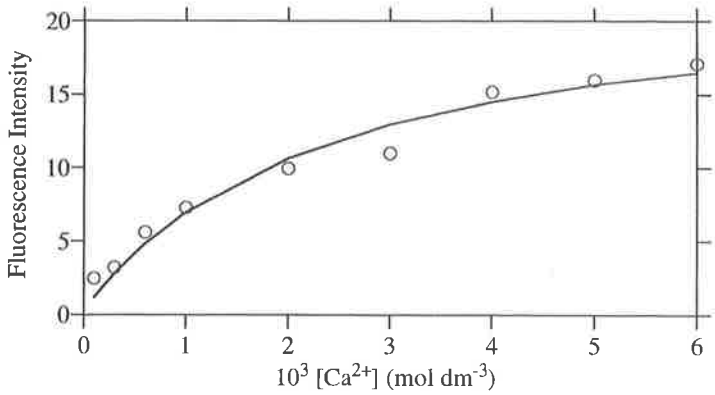

Figure A.4. *Fluorescence variation of bis(morpholinomethyl)* ***38*** *at 405.0 nm in the presence of increasing concentrations of Ca^{2+} when excited at 378.0 nm. The circles represent experimentally obtained data points and the solid line represents the best fit of the data to a 1:1 binding model.*

A.2 Bis(morpholinoethyl) 36

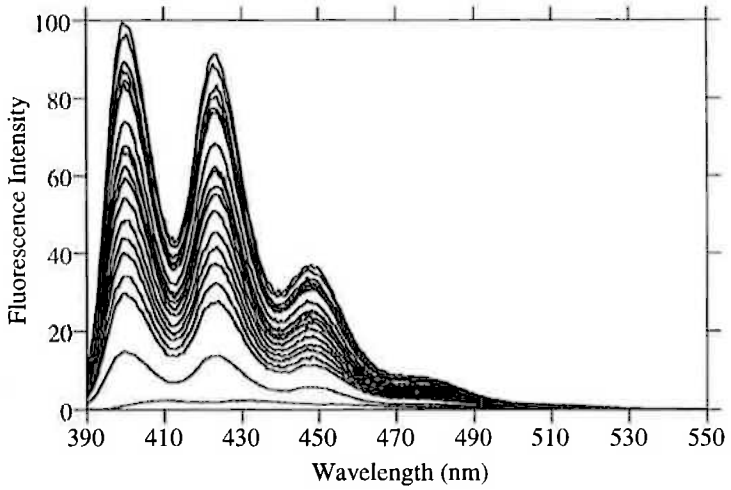

Figure A.5. *Emission spectra of bis(morpholinomethyl)* ***36*** *alone (3.0 x 10^{-6} mol dm^{-3}) and in the presence of increasing concentrations of Mg^{2+} (ranging from 5.0 x 10^{-6} to 5.0 x 10^{-3} mol dm^{-3}) in acetonitrile (I = 0.050 mol dm^{-3}) at 298.2 K, when excited at 365.0 nm. The emission of* ***36*** *alone is the lowest intensity curve in the montage.*

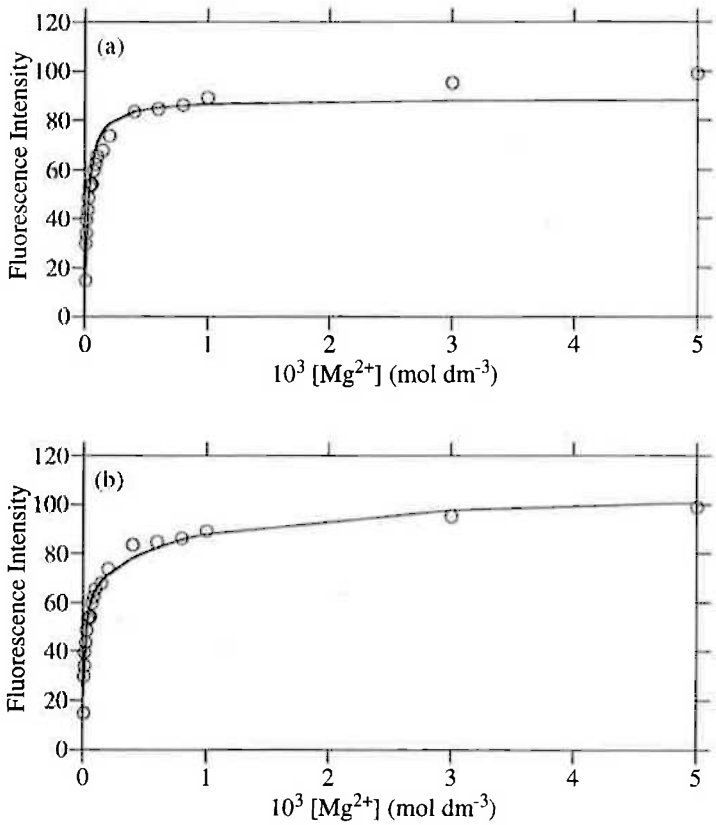

Figure A.6. *Fluorescence variation of bis(morpholinoethyl)* ***36*** *at 400.0 nm in the presence of increasing concentrations of Mg^{2+} when excited at 365.0 nm. Graph (a) is the fit for a 1:1 binding model and (b) is the fit for a 2:1 binding model. The circles represent experimentally obtained data points and the solid line represents the best fit of the data.*

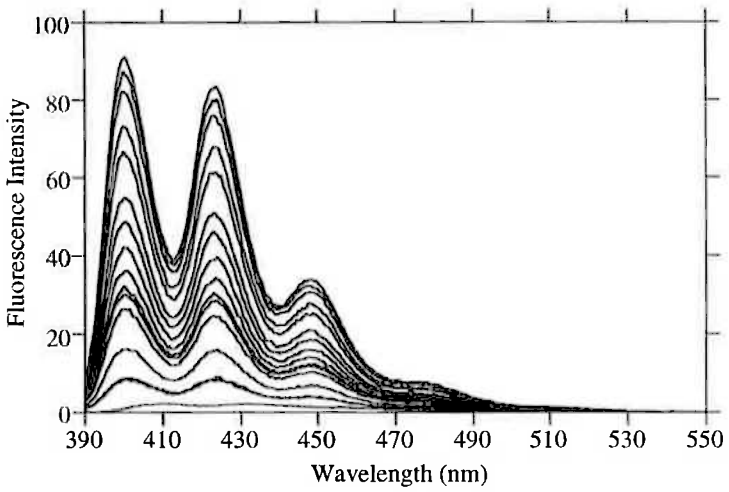

Figure A.7. *Emission spectra of bis(morpholinoethyl)* ***36*** *alone (3.0 x 10^{-6} mol dm^{-3}) and in the presence of increasing concentrations of Ca^{2+} (ranging from 1.0 x 10^{-5} to 5.0 x 10^{-3} mol dm^{-3}) in acetonitrile (I = 0.050 mol dm^{-3}) at 298.2 K, when excited at 365.0 nm. The emission of* ***36*** *alone is the lowest intensity curve in the montage.*

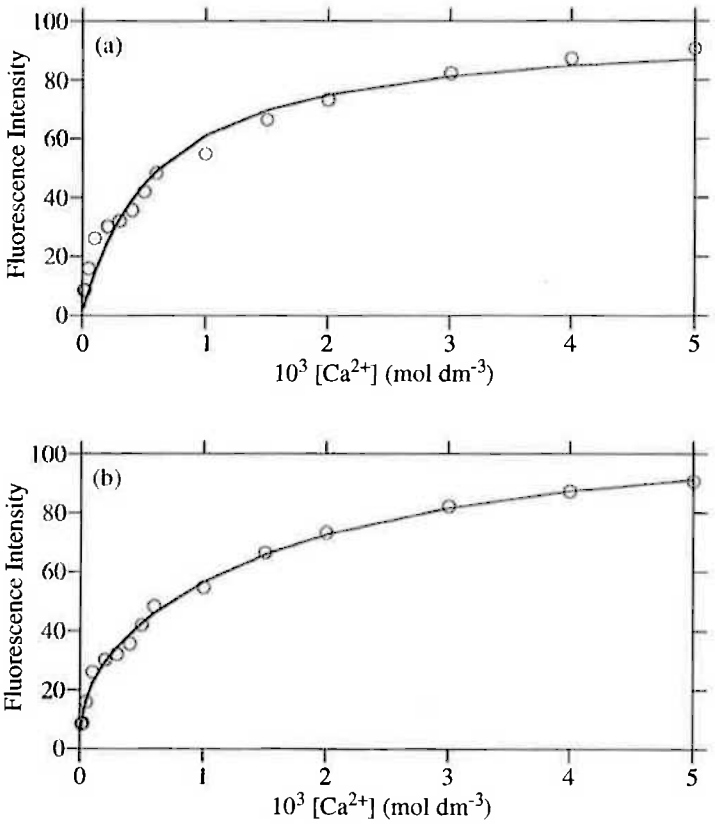

Figure A.8. *Fluorescence variation of bis(morpholinoethyl)* ***36*** *at 400.0 nm in the presence of increasing concentrations of Ca^{2+} when excited at 365.0 nm. Graph (a) is the fit for a 1:1 binding model and (b) is the fit for a 2:1 binding model. The circles represent experimentally obtained data points and the solid line represents the best fit of the data.*

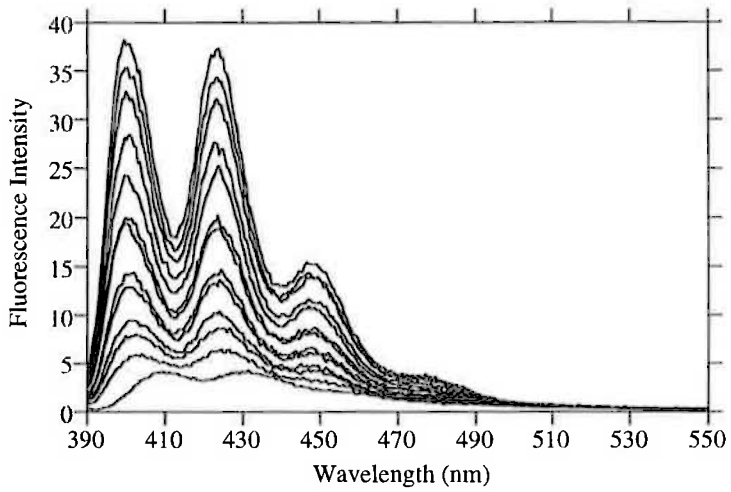

Figure A.9. *Emission spectra of bis(morpholinoethyl)* ***36*** *alone (3.0 x 10^{-6} mol dm^{-3}) and in the presence of increasing concentrations of Sr^{2+} (ranging from 1.0 x 10^{-5} to 6.0 x 10^{-3} mol dm^{-3}) in acetonitrile (I = 0.050 mol dm^{-3}) at 298.2 K, when excited at 378.0 nm. The emission of* ***36*** *alone is the lowest intensity curve in the montage.*

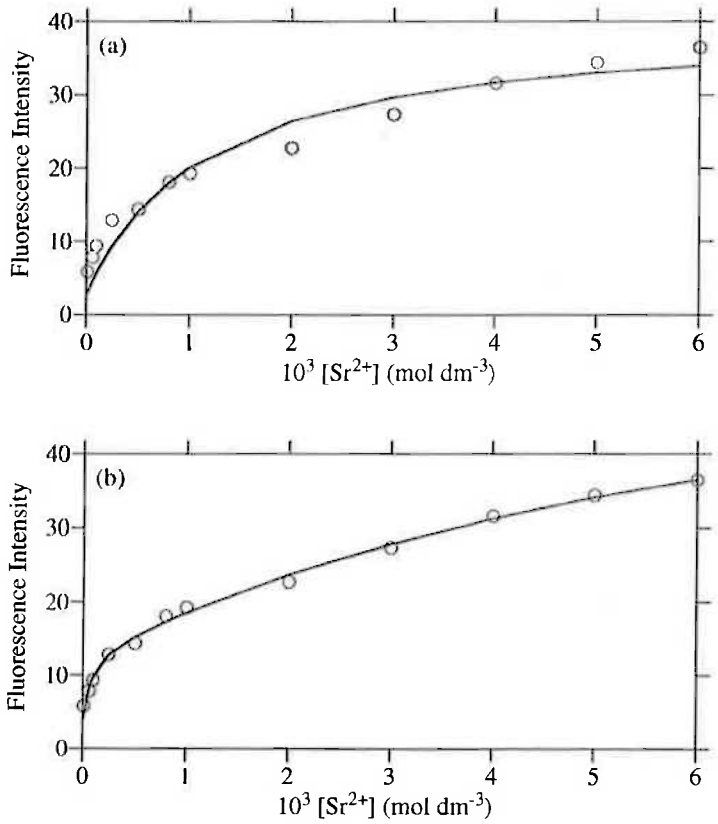

Figure A.10. *Fluorescence variation of bis(morpholinoethyl)* ***36*** *at 402.0 nm in the presence of increasing concentrations of Sr^{2+} when excited at 378.0 nm. Graph (a) is the fit for a 1:1 binding model and (b) is the fit for a 2:1 binding model. The circles represent experimentally obtained data points and the solid line represents the best fit of the data.*

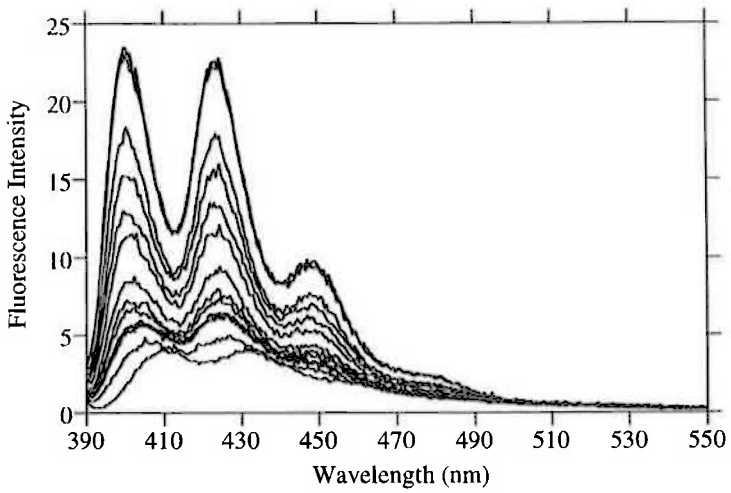

Figure A.11. *Emission spectra of bis(morpholinoethyl)* ***36*** *alone (3.0 x 10^{-6} mol dm^{-3}) and in the presence of increasing concentrations of Ba^{2+} (ranging from 1.0 x 10^{-5} to 6.0 x 10^{-3} mol dm^{-3}) in acetonitrile (I = 0.050 mol dm^{-3}) at 298.2 K, when excited at 379.0 nm. The emission of* ***36*** *alone is the lowest intensity curve in the montage.*

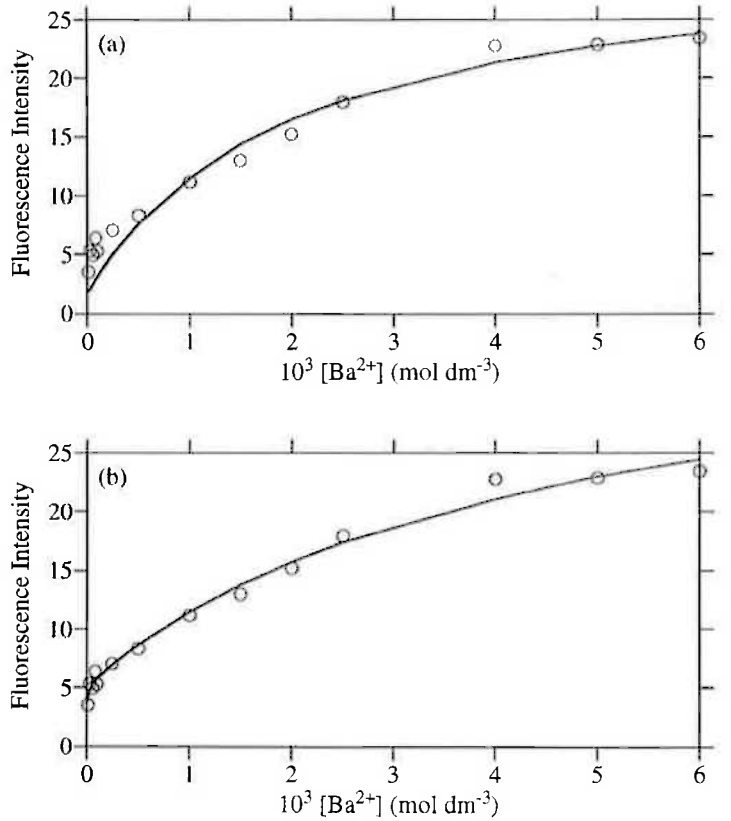

Figure A.12. *Fluorescence variation of bis(morpholinoethyl)* ***36*** *at 400.0 nm in the presence of increasing concentrations of Ba^{2+} when excited at 379.0 nm. Graph (a) is the fit for a 1:1 binding model and (b) is the fit for a 2:1 binding model. The circles represent experimentally obtained data points and the solid line represents the best fit of the data.*

A.3 Bis(morpholinopropyl) 42

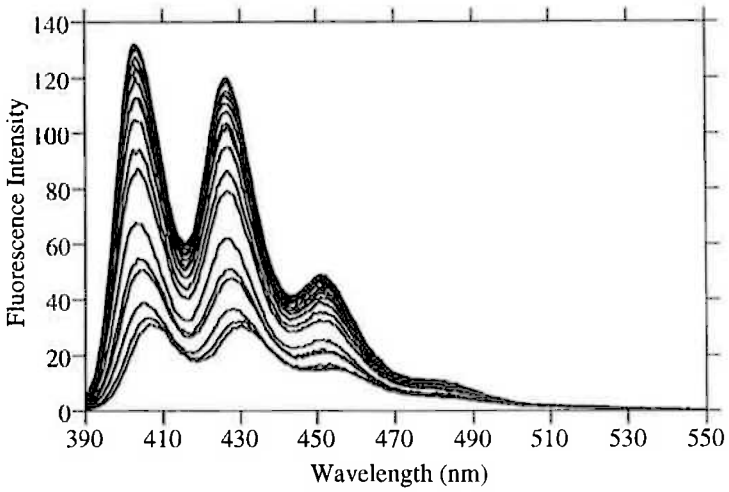

Figure A.13. *Emission spectra of bis(morpholinopropyl)* ***42*** *alone (3.0 x 10^{-6} mol dm^{-3}) and in the presence of increasing concentrations of Mg^{2+} (ranging from 1.0 x 10^{-6} to 8.0 x 10^{-5} mol dm^{-3}) in acetonitrile (I = 0.050 mol dm^{-3}) at 298.2 K, when excited at 377.0 nm. The emission of* ***42*** *alone is the lowest intensity curve in the montage.*

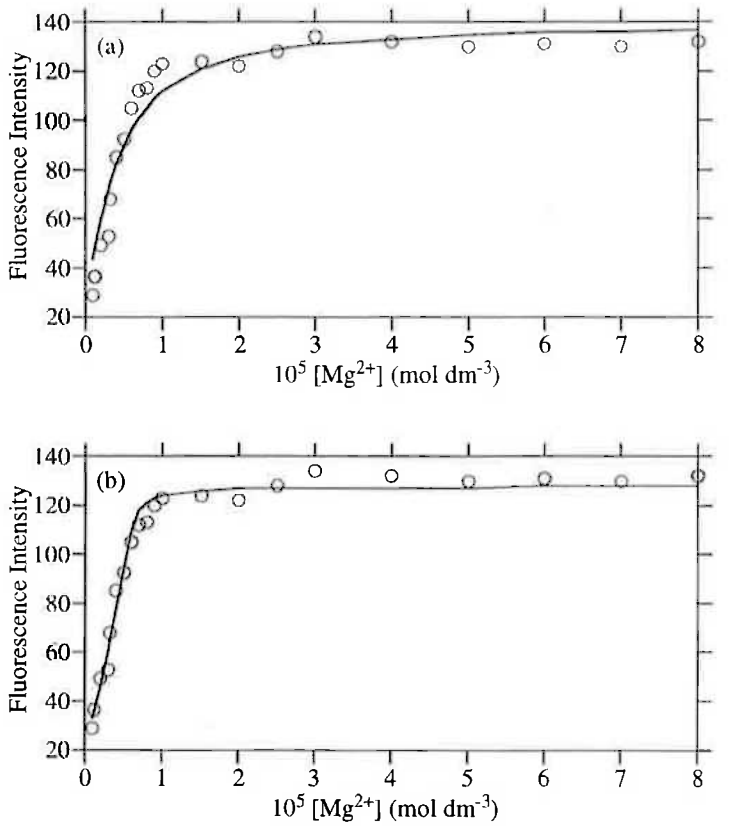

Figure A.14. *Fluorescence variation of bis(morpholinopropyl)* ***42*** *at 403.0 nm in the presence of increasing concentrations of Mg^{2+} when excited at 377.0 nm. Graph (a) is the fit for a 1:1 binding model and (b) is the fit for a 2:1 binding model. The circles represent experimentally obtained data points and the solid line represents the best fit of the data.*

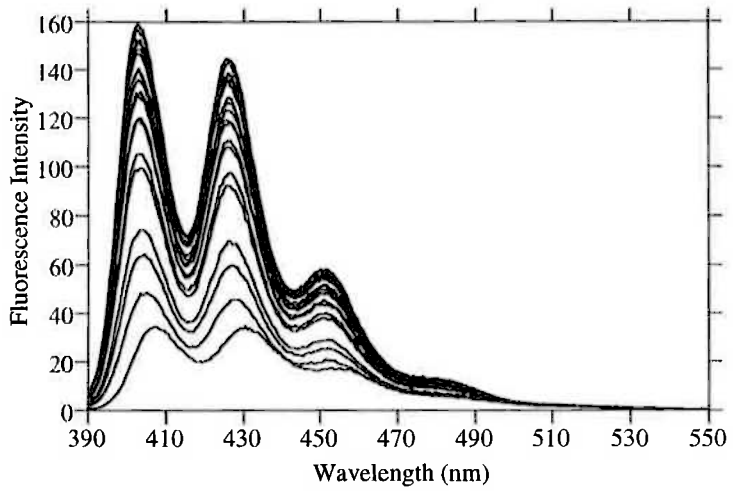

Figure A.15. *Emission spectra of bis(morpholinopropyl)* ***42*** *alone (3.0 x 10^{-6} mol dm^{-3}) and in the presence of increasing concentrations of Ca^{2+} (ranging from 5.0 x 10^{-6} to 5.0 x 10^{-3} mol dm^{-3}) in acetonitrile (I = 0.050 mol dm^{-3}) at 298.2 K, when excited at 378.0 nm. The emission of* ***42*** *alone is the lowest intensity curve in the montage.*

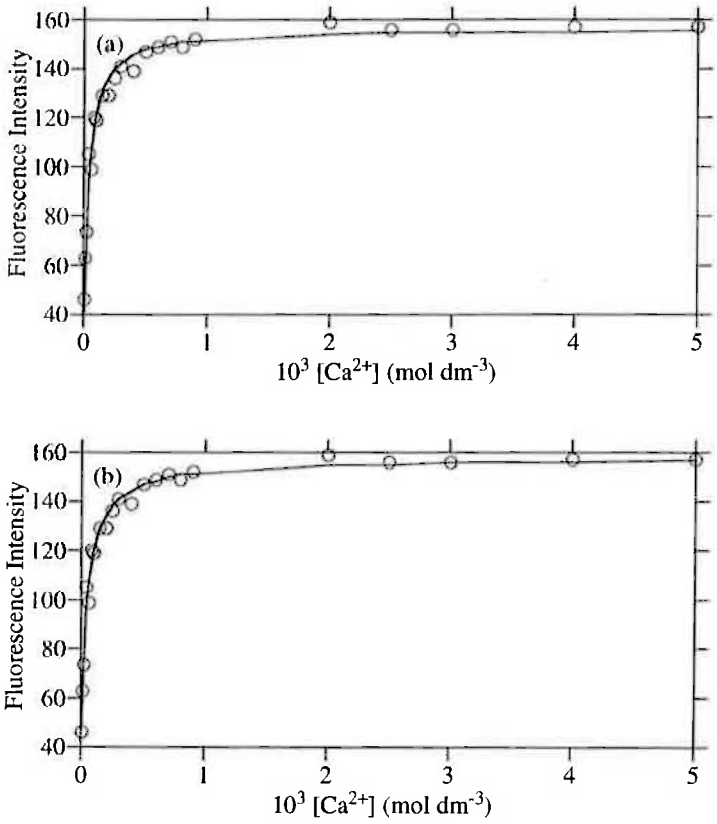

Figure A.16. *Fluorescence variation of bis(morpholinopropyl)* ***42*** *at 403.0 nm in the presence of increasing concentrations of Ca^{2+} when excited at 378.0 nm. Graph (a) is the fit for a 1:1 binding model and (b) is the fit for a 2:1 binding model. The circles represent experimentally obtained data points and the solid line represents the best fit of the data.*

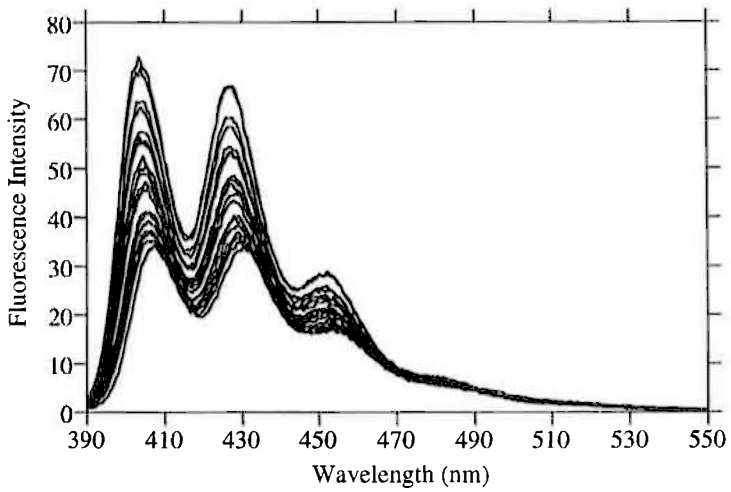

Figure A.17. *Emission spectra of bis(morpholinopropyl)* ***42*** *alone (3.0 x 10^{-6} mol dm^{-3}) and in the presence of increasing concentrations of Sr^{2+} (ranging from 5.0 x 10^{-6} to 5.0 x 10^{-3} mol dm^{-3}) in acetonitrile (I = 0.050 mol dm^{-3}) at 298.2 K, when excited at 377.0 nm. The emission of* ***42*** *alone is the lowest intensity curve in the montage.*

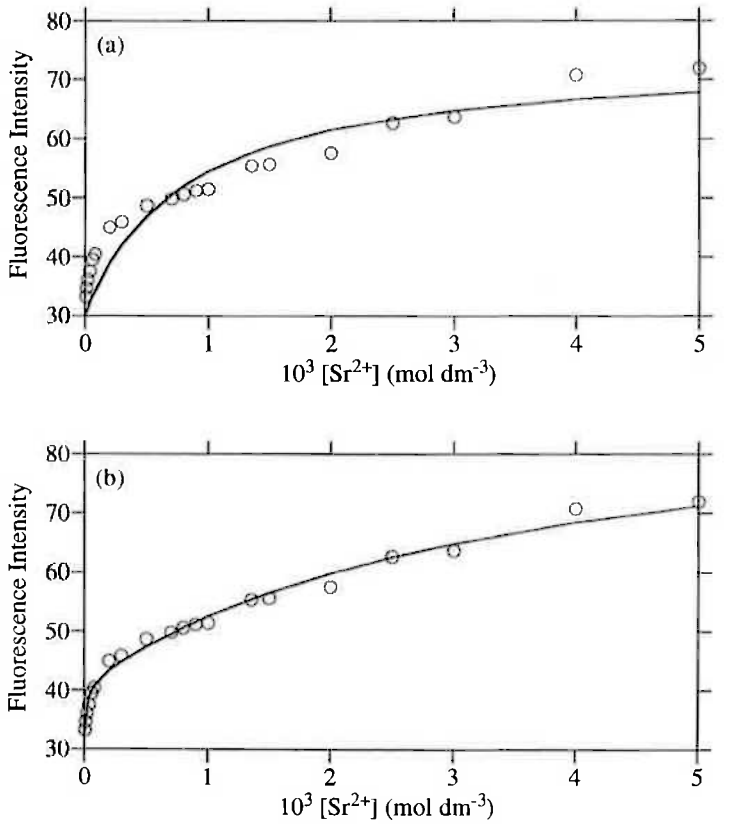

Figure A.18. *Fluorescence variation of bis(morpholinopropyl)* ***42*** *at 404.0 nm in the presence of increasing concentrations of Sr^{2+} when excited at 377.0 nm. Graph (a) is the fit for a 1:1 binding model and (b) is the fit for a 2:1 binding model. The circles represent experimentally obtained data points and the solid line represents the best fit of the data.*

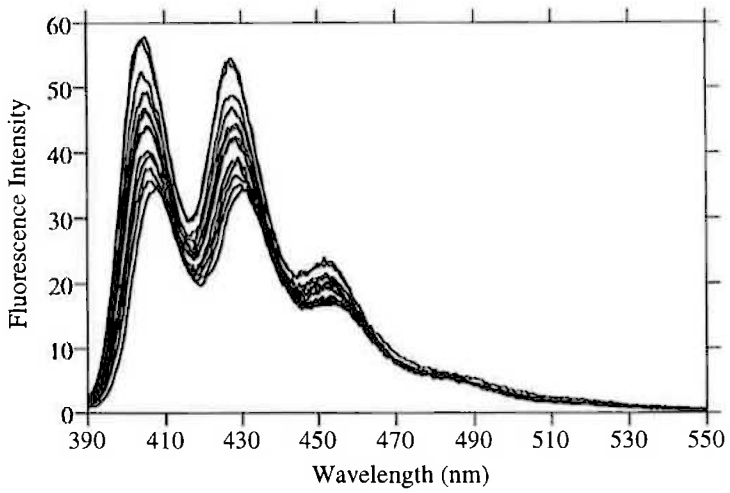

Figure A.19. *Emission spectra of bis(morpholinopropyl)* ***42*** *alone (3.0 x 10^{-6} mol dm^{-3}) and in the presence of increasing concentrations of Ba^{2+} (ranging from 1.0 x 10^{-4} to 6.0 x 10^{-3} mol dm^{-3}) in acetonitrile (I = 0.050 mol dm^{-3}) at 298.2 K, when excited at 378.0 nm. The emission of* ***42*** *alone is the lowest intensity curve in the montage.*

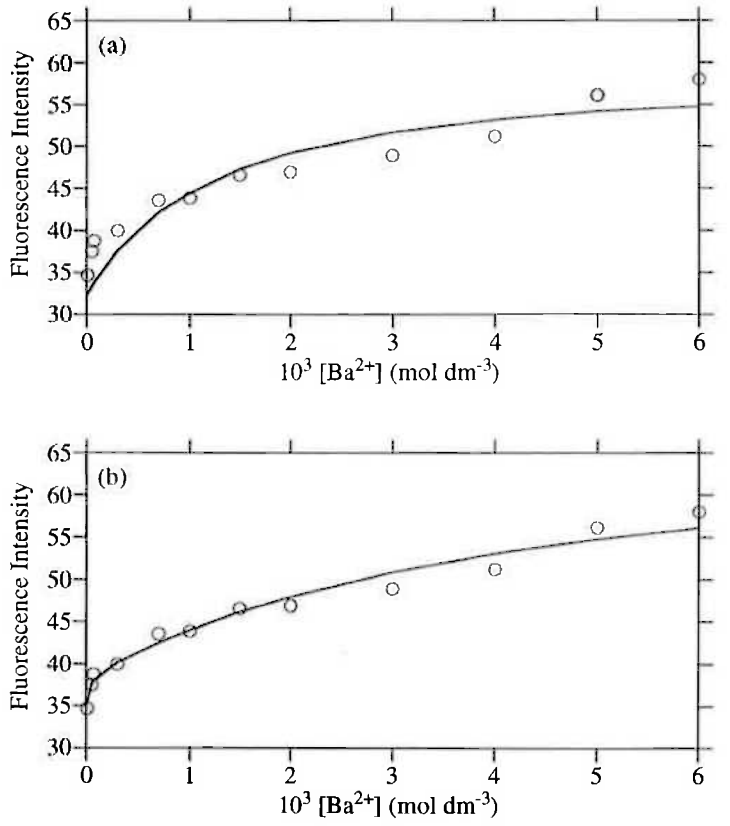

Figure A.20. *Fluorescence variation of bis(morpholinopropyl)* ***42*** *at 405.0 nm in the presence of increasing concentrations of Ba^{2+} when excited at 378.0 nm. Graph (a) is the fit for a 1:1 binding model and (b) is the fit for a 2:1 binding model. The circles represent experimentally obtained data points and the solid line represents the best fit of the data.*

A.4 Bis(thiomorpholine) 52

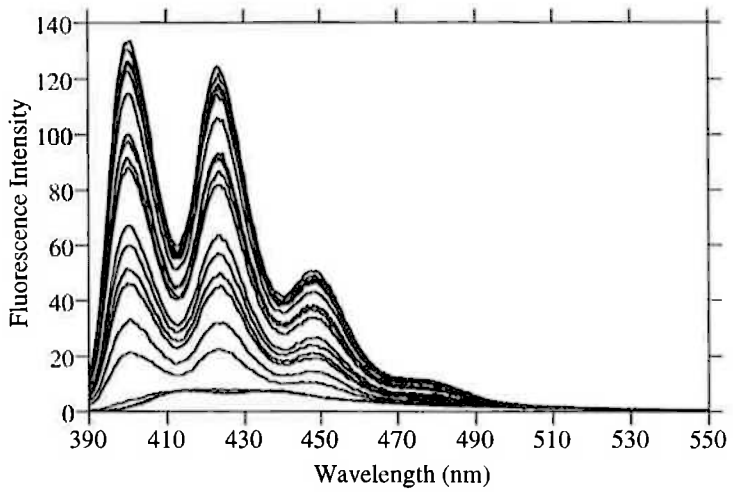

Figure A.21. *Emission spectra of bis(thiomorpholine)* ***52*** *alone (3.0 x 10^{-6} mol dm^{-3}) and in the presence of increasing concentrations of Mg^{2+} (ranging from 1.0 x 10^{-6} to 3.0 x 10^{-3} mol dm^{-3}) in acetonitrile (I = 0.050 mol dm^{-3}) at 298.2 K, when excited at 377.0 nm. The emission of* ***52*** *alone is the lowest intensity curve in the montage.*

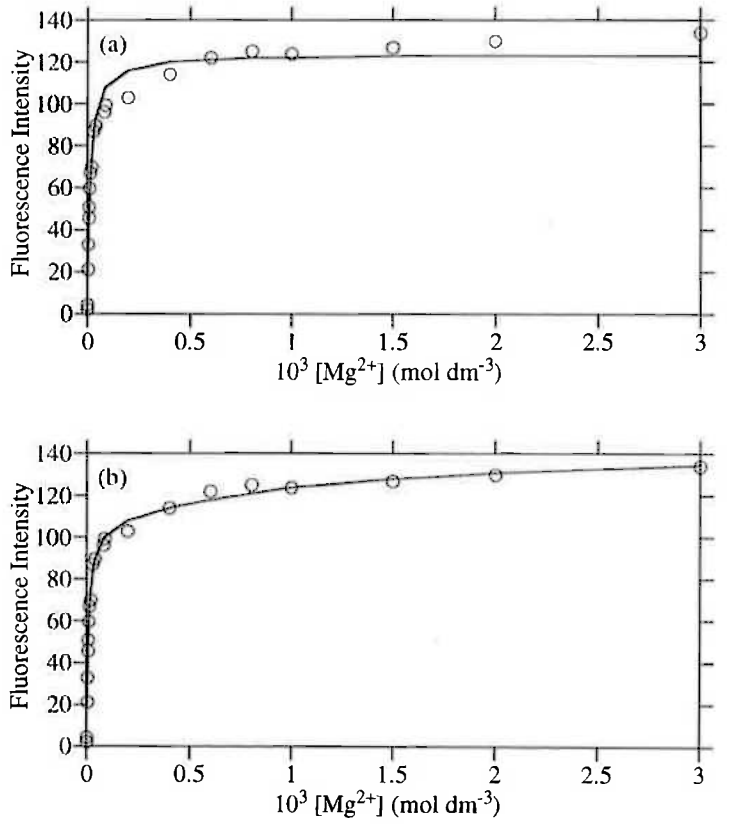

Figure A.22. *Fluorescence variation of bis(thiomorpholine)* ***52*** *at 401.0 nm in the presence of increasing concentrations of Mg^{2+} when excited at 377.0 nm. Graph (a) is the fit for a 1:1 binding model and (b) is the fit for a 2:1 binding model. The circles represent experimentally obtained data points and the solid line represents the best fit of the data.*

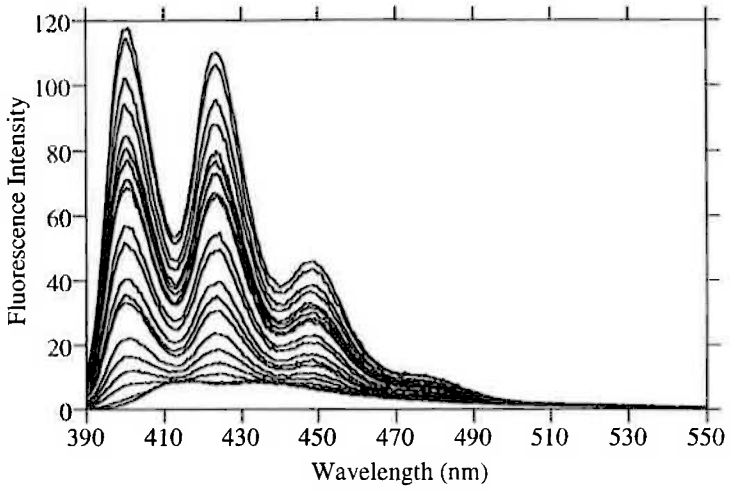

Figure A.23. *Emission spectra of bis(thiomorpholine)* ***52*** *alone (3.0 x 10^{-6} mol dm^{-3}) and in the presence of increasing concentrations of Ca^{2+} (ranging from 3.0 x 10^{-6} to 5.0 x 10^{-3} mol dm^{-3}) in acetonitrile (I = 0.050 mol dm^{-3}) at 298.2 K, when excited at 378.0 nm. The emission of* ***52*** *alone is the lowest intensity curve in the montage.*

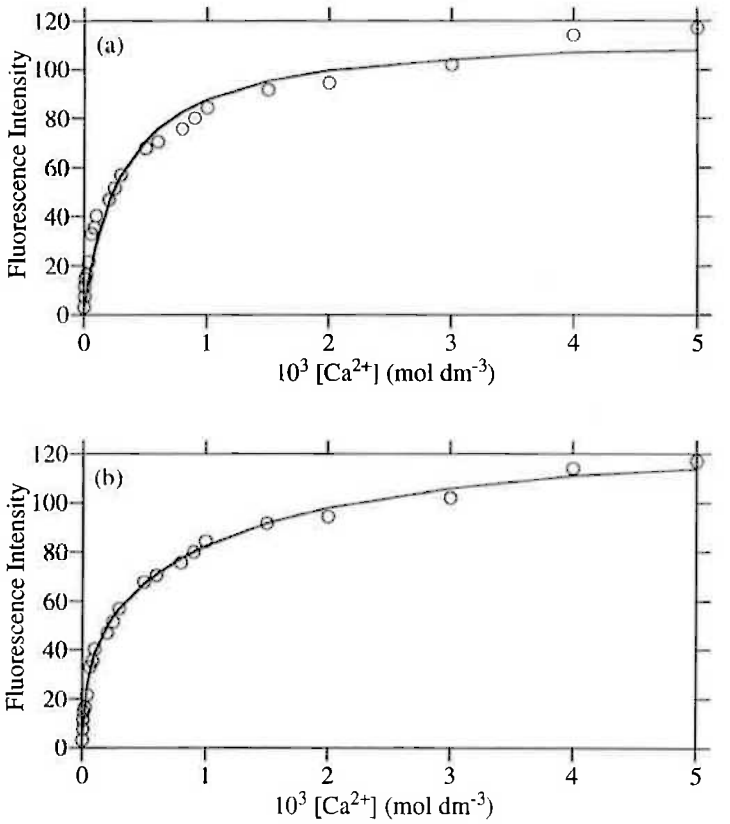

Figure A.24. *Fluorescence variation of bis(thiomorpholine)* ***52*** *at 400.0 nm in the presence of increasing concentrations of Ca^{2+} when excited at 378.0 nm. Graph (a) is the fit for a 1:1 binding model and (b) is the fit for a 2:1 binding model. The circles represent experimentally obtained data points and the solid line represents the best fit of the data.*

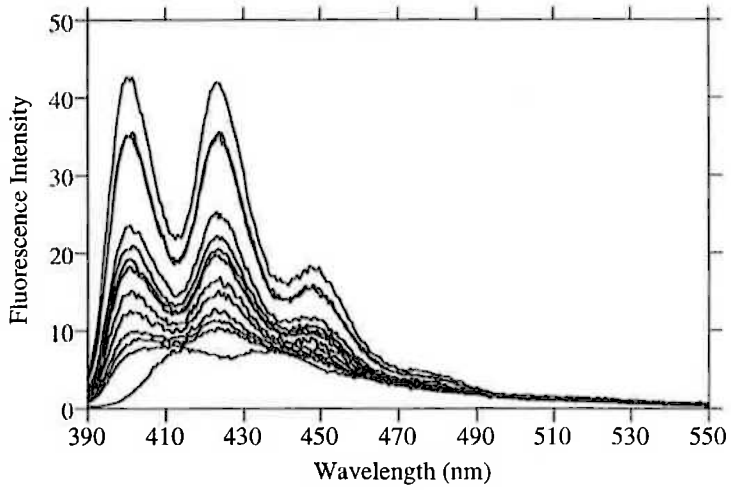

Figure A.25. *Emission spectra of bis(thiomorpholine)* ***52*** *alone (3.0 x 10^{-6} mol dm^{-3}) and in the presence of increasing concentrations of Sr^{2+} (ranging from 1.0 x 10^{-5} to 6.0 x 10^{-3} mol dm^{-3}) in acetonitrile (I = 0.050 mol dm^{-3}) at 298.2 K, when excited at 377.0 nm. The emission of* ***52*** *alone is the lowest intensity curve in the montage.*

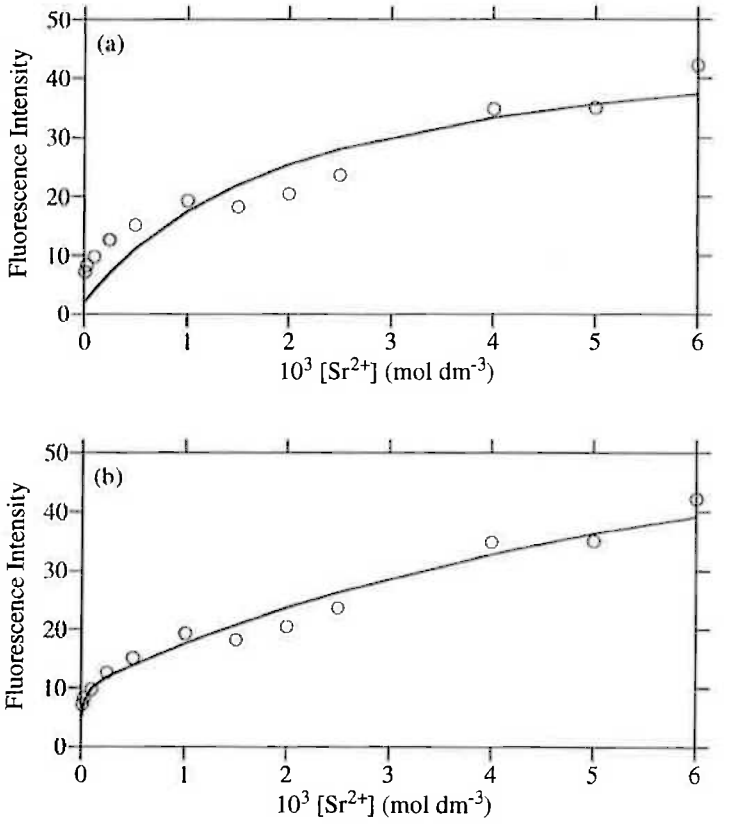

Figure A.26. *Fluorescence variation of bis(thiomorpholine)* ***52*** *at 401.0 nm in the presence of increasing concentrations of Sr^{2+} when excited at 377.0 nm. Graph (a) is the fit for a 1:1 binding model and (b) is the fit for a 2:1 binding model. The circles represent experimentally obtained data points and the solid line represents the best fit of the data.*

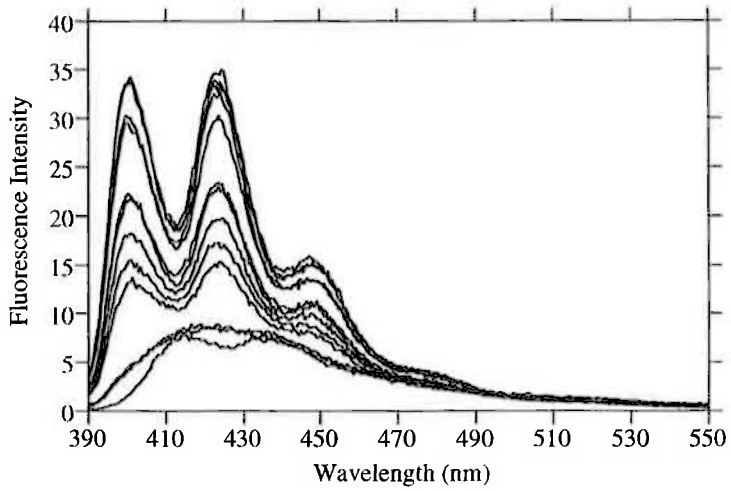

Figure A.27. *Emission spectra of bis(thiomorpholine)* ***52*** *alone (3.0 x 10^{-6} mol dm^{-3}) and in the presence of increasing concentrations of Ba^{2+} (ranging from 5.0 x 10^{-5} to 6.0 x 10^{-3} mol dm^{-3}) in acetonitrile (I = 0.050 mol dm^{-3}) at 298.2 K, when excited at 377.0 nm. The emission of* ***52*** *alone is the lowest intensity curve in the montage.*

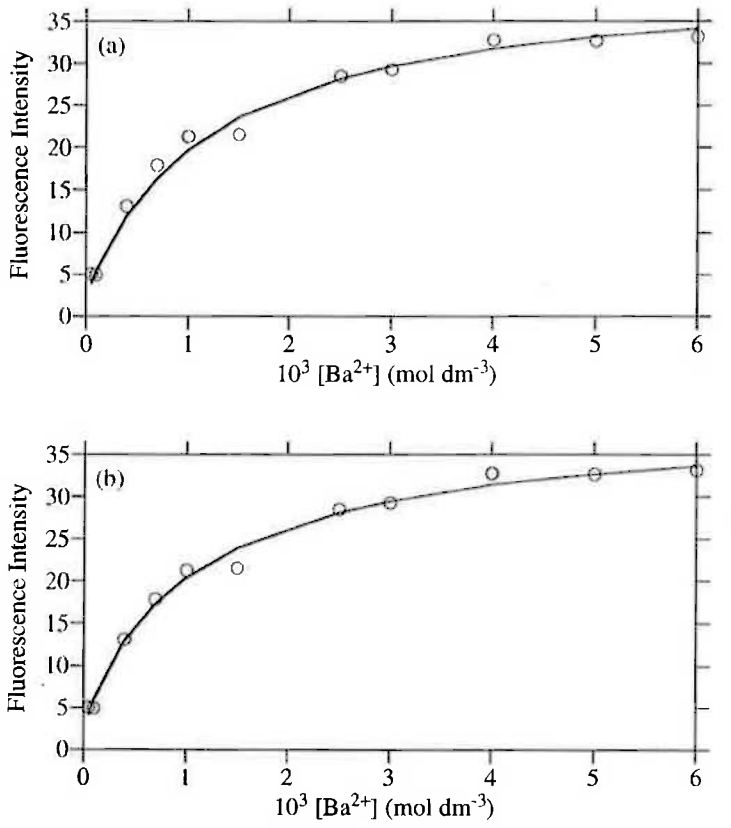

Figure A.28. *Fluorescence variation of bis(thiomorpholine)* ***52*** *at 402.0 nm in the presence of increasing concentrations of Ba^{2+} when excited at 377.0 nm. Graph (a) is the fit for a 1:1 binding model and (b) is the fit for a 2:1 binding model. The circles represent experimentally obtained data points and the solid line represents the best fit of the data.*

A.5 Bis(piperazine) 53

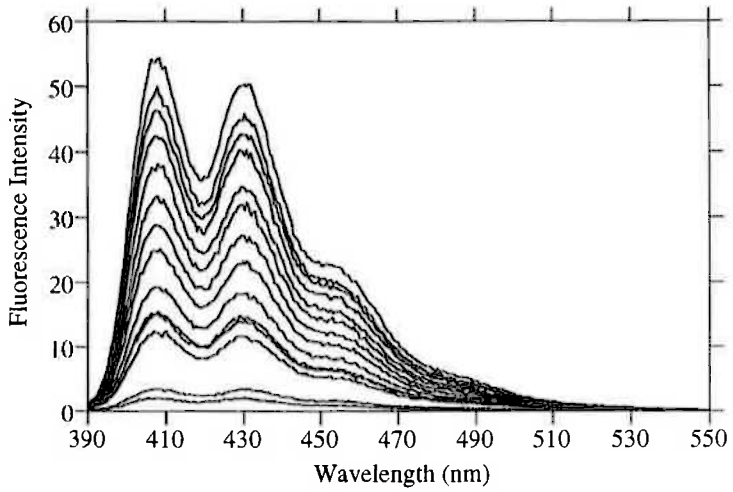

Figure A.29. *Emission spectra of bis(piperazine)* ***53*** *alone (3.0 x 10^{-6} mol dm^{-3}) and in the presence of increasing concentrations of Li^+ (ranging from 1.0 x 10^{-5} to 5.0 x 10^{-3} mol dm^{-3}) in acetonitrile (I = 0.050 mol dm^{-3}) at 298.2 K, when excited at 378.0 nm. The emission of* ***53*** *alone is the lowest intensity curve in the montage.*

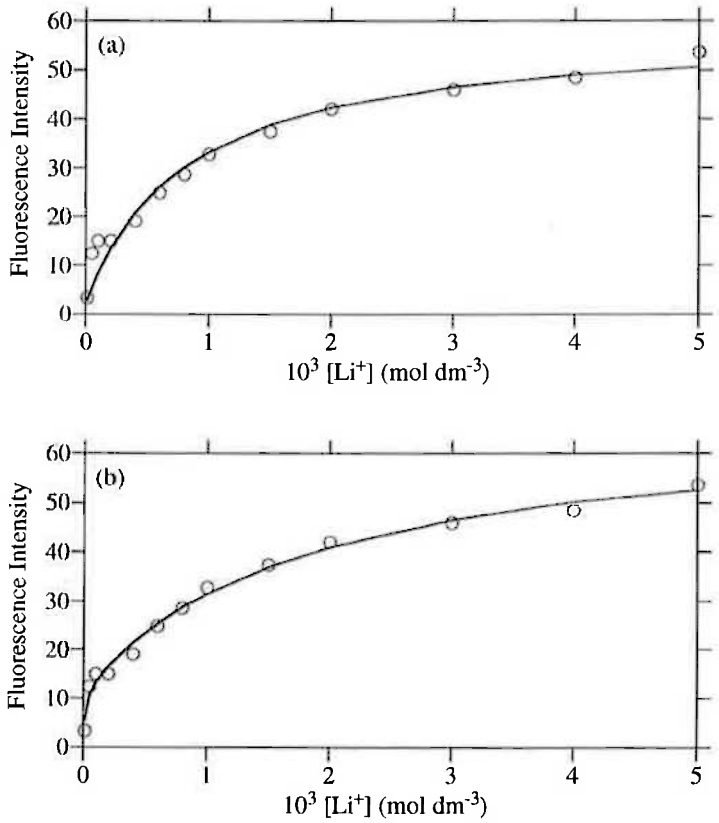

Figure A.30. *Fluorescence variation of bis(piperazine)* ***53*** *at 407.0 nm in the presence of increasing concentrations of Li^+ when excited at 378.0 nm. Graph (a) is the fit for a 1:1 binding model and (b) is the fit for a 2:1 binding model. The circles represent experimentally obtained data points and the solid line represents the best fit of the data.*

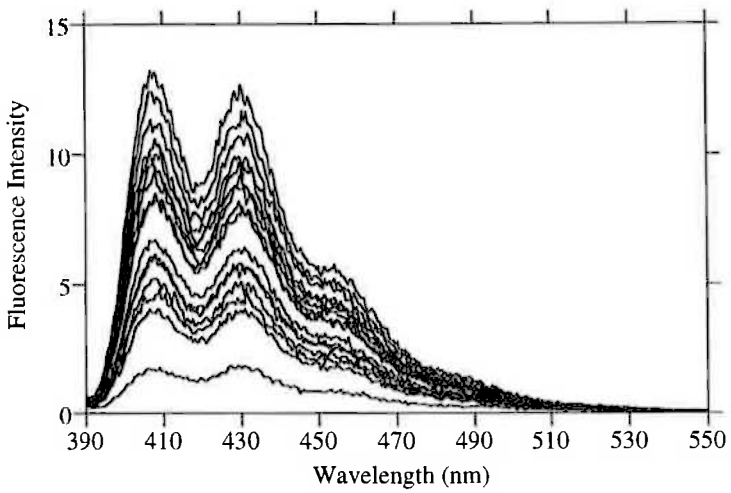

Figure A.31. *Emission spectra of bis(piperazine)* ***53*** *alone (3.0 x 10^{-6} mol dm^{-3}) and in the presence of increasing concentrations of Na^+ (ranging from 1.0 x 10^{-5} to 5.0 x 10^{-3} mol dm^{-3}) in acetonitrile (I = 0.050 mol dm^{-3}) at 298.2 K, when excited at 378.0 nm. The emission of* ***53*** *alone is the lowest intensity curve in the montage.*

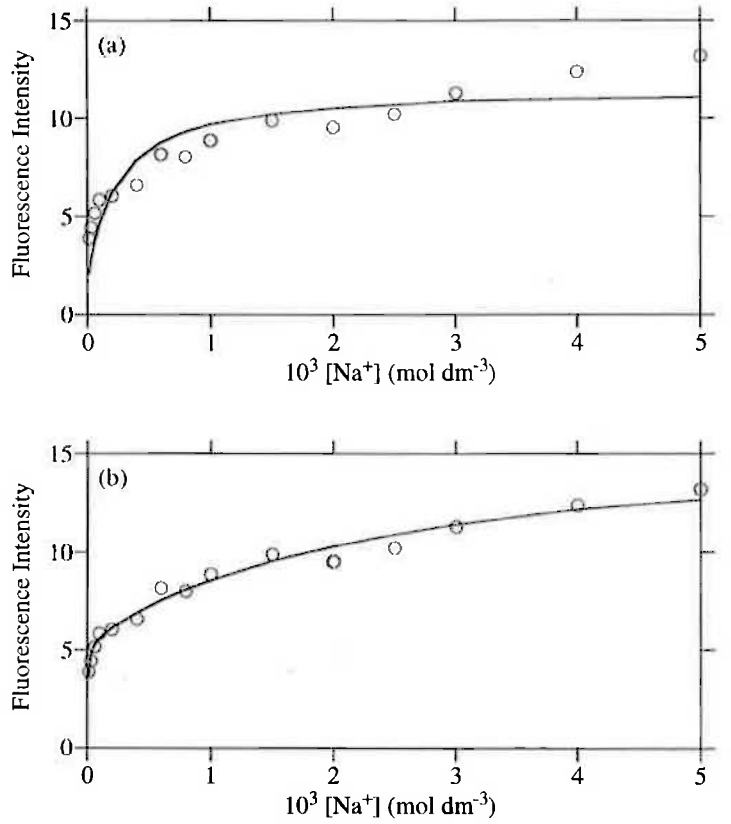

Figure A.32. *Fluorescence variation of bis(piperazine)* ***53*** *at 407.0 nm in the presence of increasing concentrations of Na^+ when excited at 378.0 nm. Graph (a) is the fit for a 1:1 binding model and (b) is the fit for a 2:1 binding model. The circles represent experimentally obtained data points and the solid line represents the best fit of the data.*

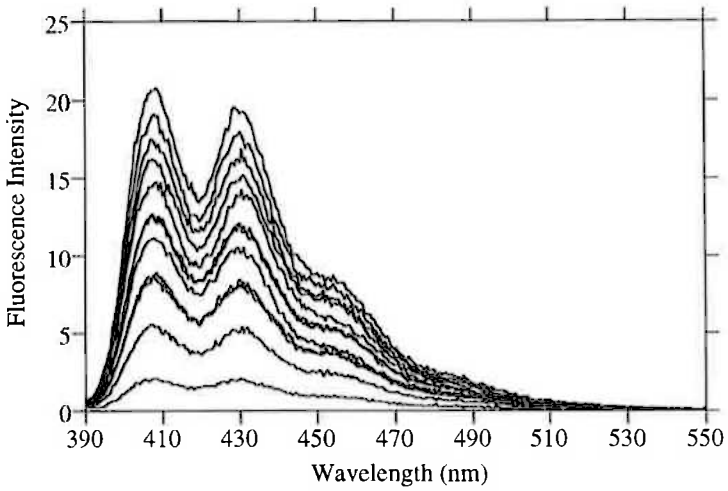

Figure A.33. *Emission spectra of bis(piperazine)* ***53*** *alone (3.0 x 10^{-6} mol dm^{-3}) and in the presence of increasing concentrations of K^+ (ranging from 5.0 x 10^{-5} to 5.0 x 10^{-3} mol dm^{-3}) in acetonitrile (I = 0.050 mol dm^{-3}) at 298.2 K, when excited at 377.0 nm. The emission of* ***53*** *alone is the lowest intensity curve in the montage.*

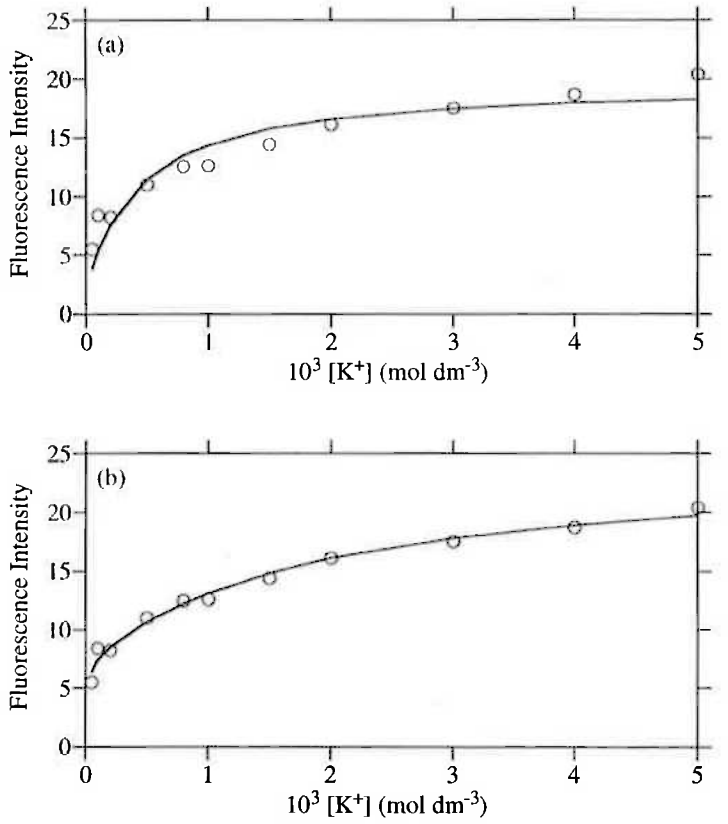

Figure A.34. *Fluorescence variation of bis(piperazine)* ***53*** *at 407.0 nm in the presence of increasing concentrations of K^+ when excited at 377.0 nm. Graph (a) is the fit for a 1:1 binding model and (b) is the fit for a 2:1 binding model. The circles represent experimentally obtained data points and the solid line represents the best fit of the data.*

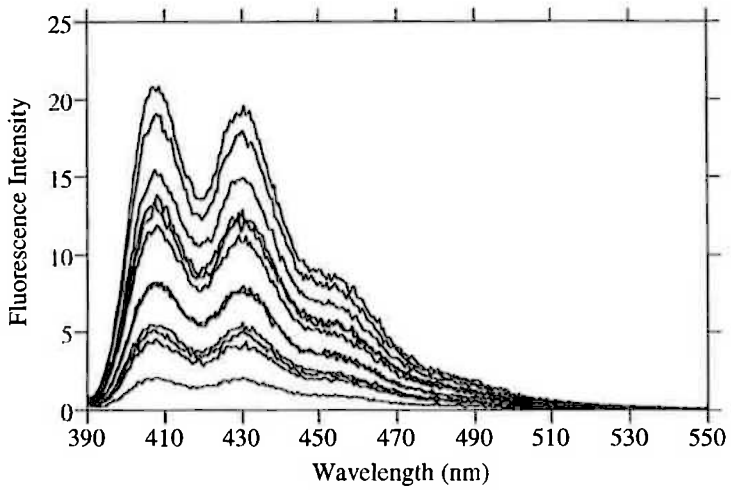

Figure A.35. *Emission spectra of bis(piperazine)* ***53*** *alone (3.0 x 10^{-6} mol dm^{-3}) and in the presence of increasing concentrations of Rb^+ (ranging from 5.0 x 10^{-5} to 4.0 x 10^{-3} mol dm^{-3}) in acetonitrile (I = 0.050 mol dm^{-3}) at 298.2 K, when excited at 377.0 nm. The emission of* ***53*** *alone is the lowest intensity curve in the montage.*

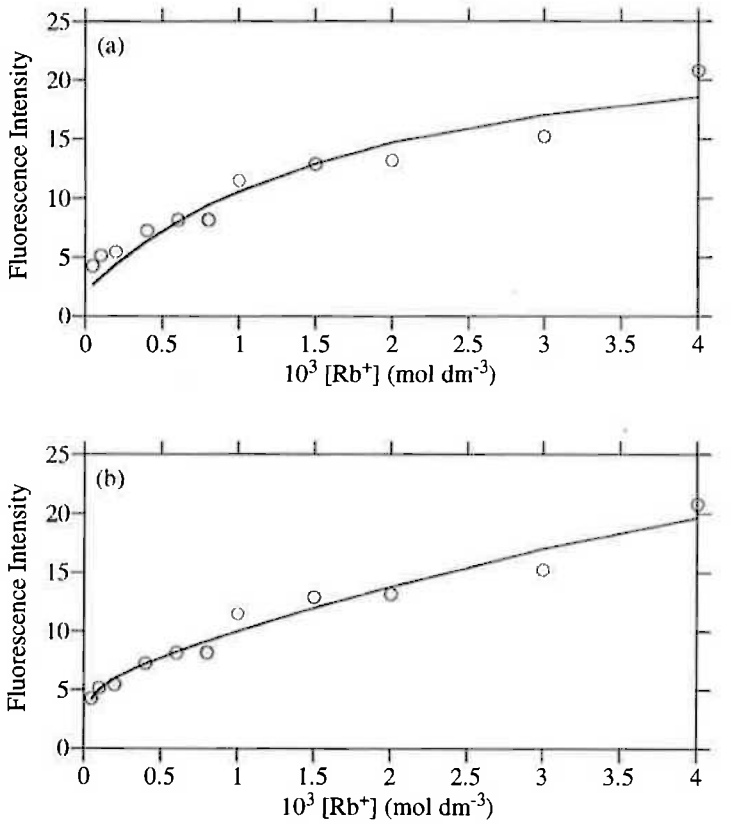

Figure A.36. *Fluorescence variation of bis(piperazine)* ***53*** *at 407.0 nm in the presence of increasing concentrations of Rb^+ when excited at 377.0 nm. Graph (a) is the fit for a 1:1 binding model and (b) is the fit for a 2:1 binding model. The circles represent experimentally obtained data points and the solid line represents the best fit of the data.*

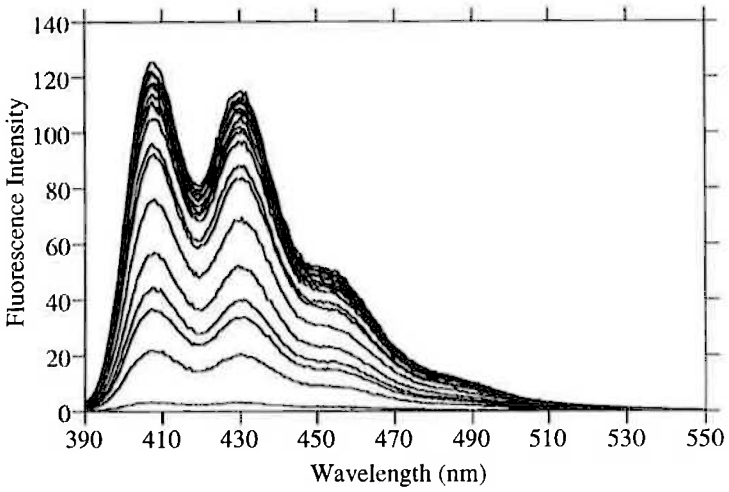

Figure A.37. *Emission spectra of bis(piperazine)* ***53*** *alone (3.0 x 10^{-6} mol dm^{-3}) and in the presence of increasing concentrations of Mg^{2+} (ranging from 1.0 x 10^{-6} to 1.0 x 10^{-4} mol dm^{-3}) in acetonitrile (I = 0.050 mol dm^{-3}) at 298.2 K, when excited at 379.0 nm. The emission of* ***53*** *alone is the lowest intensity curve in the montage.*

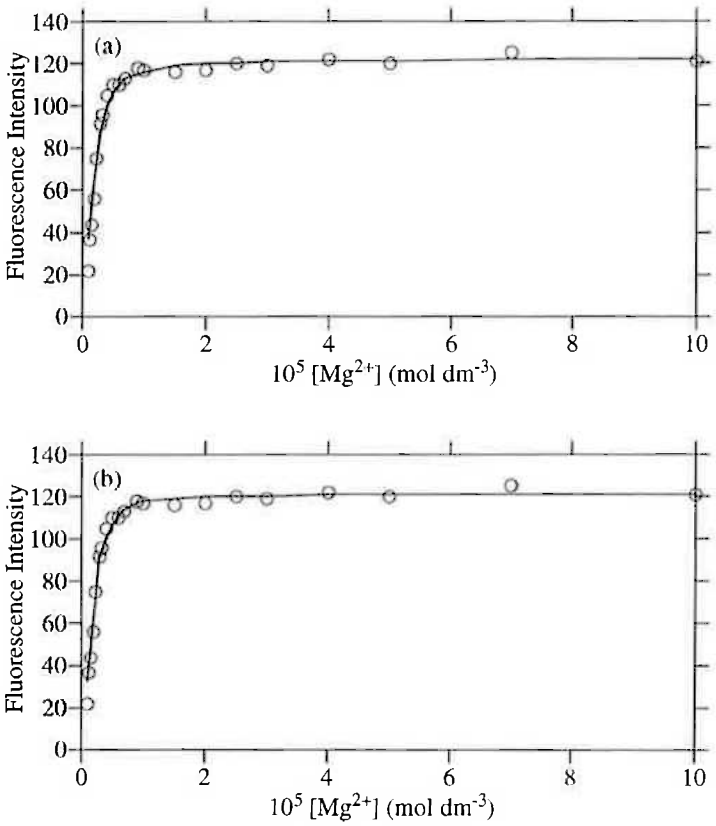

Figure A.38. *Fluorescence variation of bis(piperazine)* ***53*** *at 407.0 nm in the presence of increasing concentrations of Mg^{2+} when excited at 379.0 nm. Graph (a) is the fit for a 1:1 binding model and (b) is the fit for a 2:1 binding model. The circles represent experimentally obtained data points and the solid line represents the best fit of the data.*

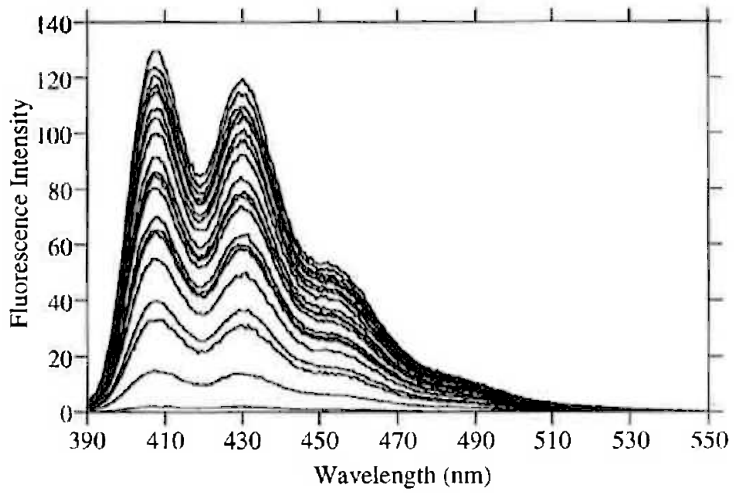

Figure A.39. *Emission spectra of bis(piperazine)* ***53*** *alone (3.0 x 10^{-6} mol dm^{-3}) and in the presence of increasing concentrations of Ca^{2+} (ranging from 1.0 x 10^{-6} to 8.0 x 10^{-4} mol dm^{-3}) in acetonitrile (I = 0.050 mol dm^{-3}) at 298.2 K, when excited at 380.0 nm. The emission of* ***53*** *alone is the lowest intensity curve in the montage.*

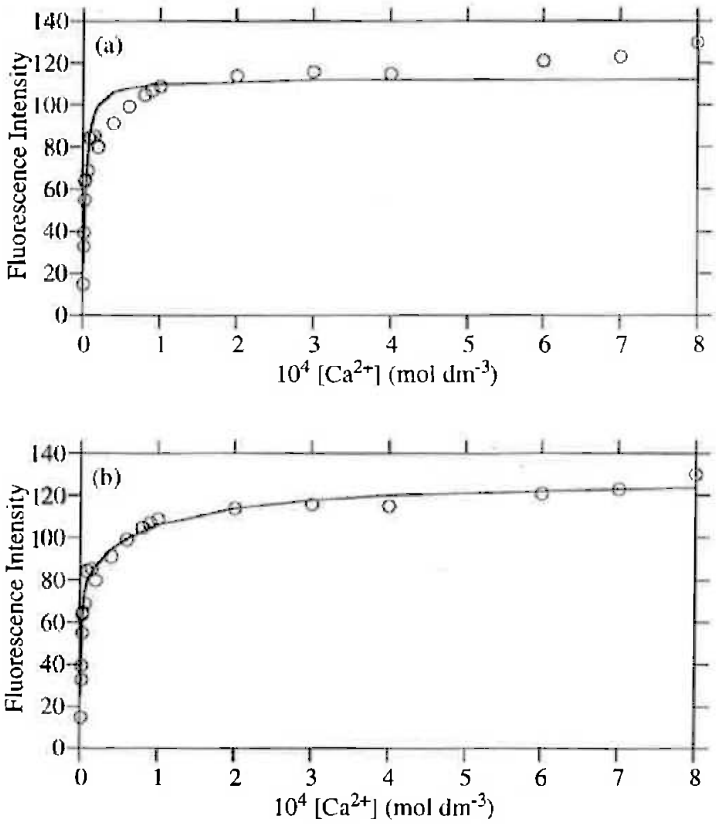

Figure A.40. *Fluorescence variation of bis(piperazine)* ***53*** *at 408.0 nm in the presence of increasing concentrations of Ca^{2+} when excited at 380.0 nm. Graph (a) is the fit for a 1:1 binding model and (b) is the fit for a 2:1 binding model. The circles represent experimentally obtained data points and the solid line represents the best fit of the data.*

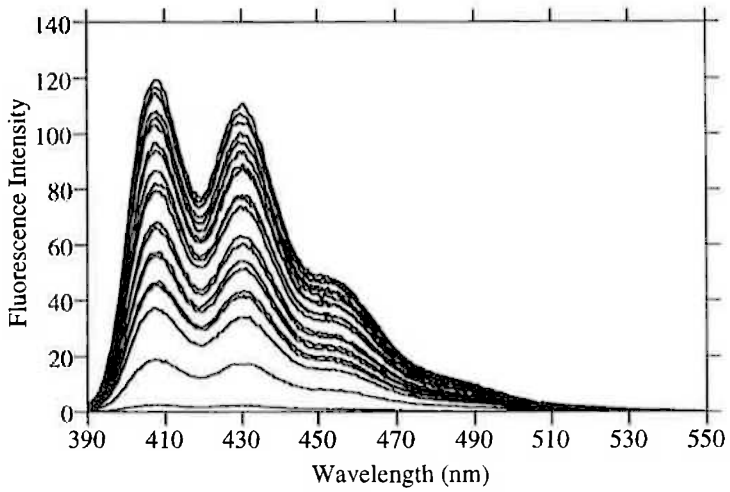

Figure A.41. *Emission spectra of bis(piperazine)* ***53*** *alone (3.0 x 10^{-6} mol dm^{-3}) and in the presence of increasing concentrations of Sr^{2+} (ranging from 1.0 x 10^{-6} to 3.0 x 10^{-3} mol dm^{-3}) in acetonitrile (I = 0.050 mol dm^{-3}) at 298.2 K, when excited at 377.0 nm. The emission of* ***53*** *alone is the lowest intensity curve in the montage.*

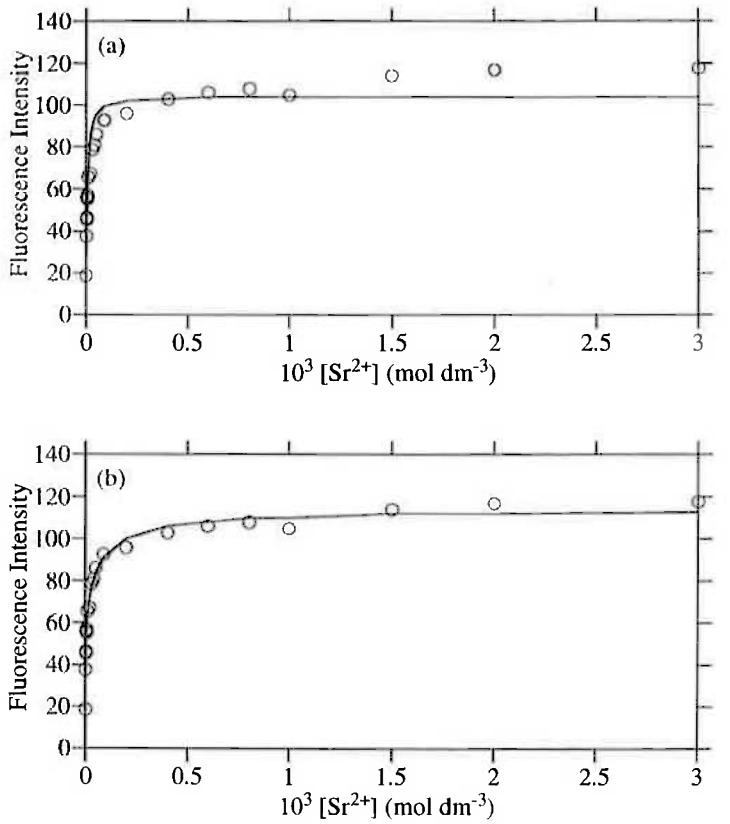

Figure A.42. *Fluorescence variation of bis(piperazine)* ***53*** *at 407.0 nm in the presence of increasing concentrations of Sr^{2+} when excited at 377.0 nm. Graph (a) is the fit for a 1:1 binding model and (b) is the fit for a 2:1 binding model. The circles represent experimentally obtained data points and the solid line represents the best fit of the data.*

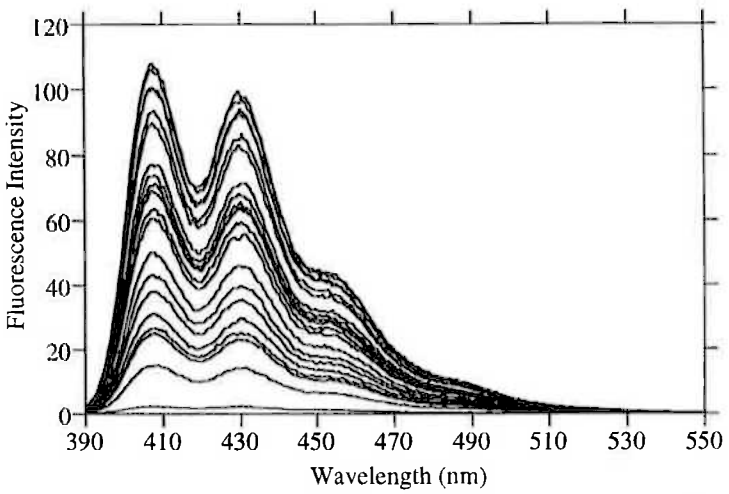

Figure A.43. *Emission spectra of bis(piperazine)* ***53*** *alone (3.0 x 10^{-6} mol dm^{-3}) and in the presence of increasing concentrations of Ba^{2+} (ranging from 1.0 x 10^{-6} to 3.0 x 10^{-3} mol dm^{-3}) in acetonitrile (I = 0.050 mol dm^{-3}) at 298.2 K, when excited at 377.0 nm. The emission of* ***53*** *alone is the lowest intensity curve in the montage.*

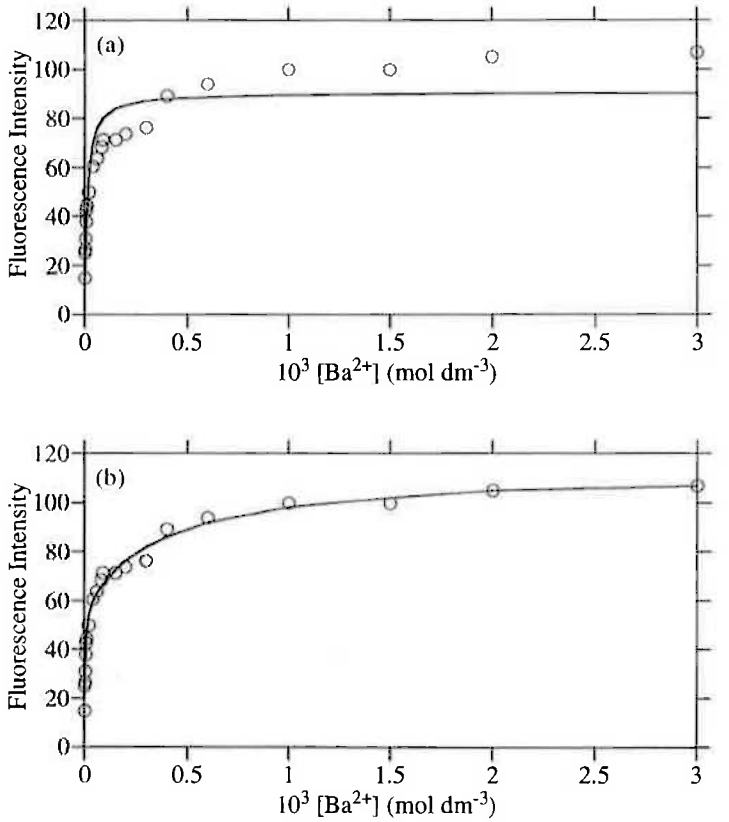

Figure A.44. *Fluorescence variation of bis(piperazine)* ***53*** *at 408.0 nm in the presence of increasing concentrations of Ba^{2+} when excited at 377.0 nm. Graph (a) is the fit for a 1:1 binding model and (b) is the fit for a 2:1 binding model. The circles represent experimentally obtained data points and the solid line represents the best fit of the data.*

A.6 Mono(azacrown) 51

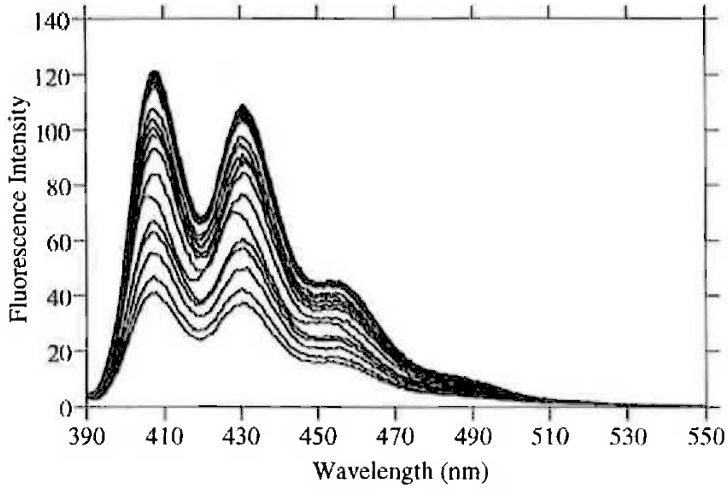

Figure A.45. *Emission spectra of mono(azacrown)* ***51*** *(3.0 x 10^{-6} mol dm^{-3}) and in the presence of increasing concentrations of Li^+ (ranging from 1.0 x 10^{-6} to 8.0 x 10^{-4} mol dm^{-3}) in acetonitrile (I = 0.050 mol dm^{-3}) at 298.2 K, when excited at 381.0 nm. The emission of* ***51*** *alone is the lowest intensity curve in the montage.*

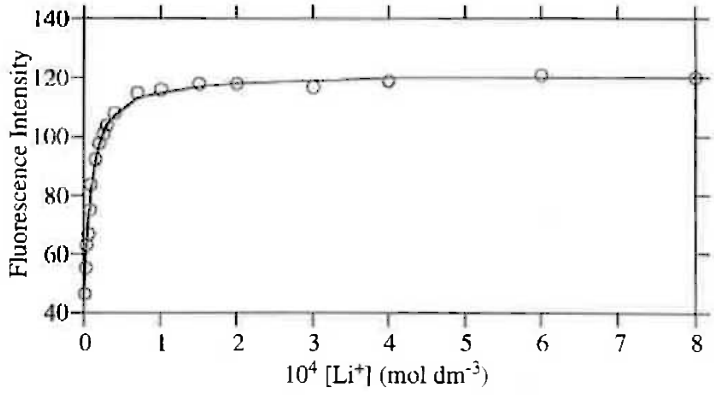

Figure A.46. *Fluorescence variation of mono(azacrown)* ***51*** *at 407.0 nm in the presence of increasing concentrations of Li^+ when excited at 381.0 nm. The circles represent experimentally obtained data points and the solid line represents the best fit of the data to a 1:1 binding model.*

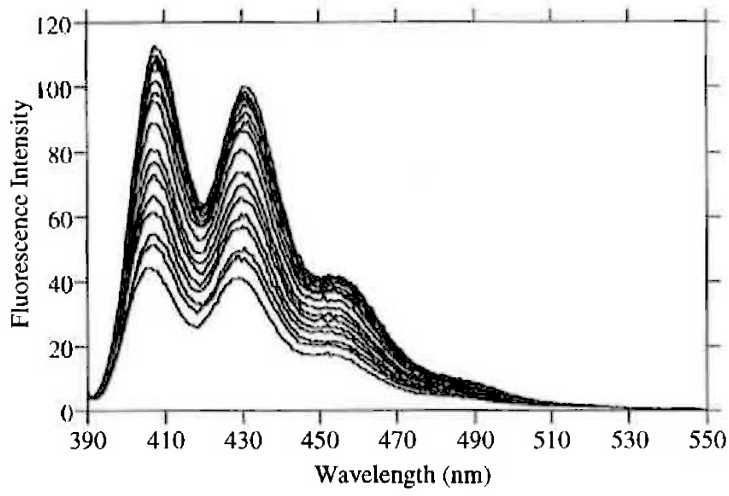

Figure A.47. *Emission spectra of mono(azacrown)* ***51*** *alone (3.0 x 10^{-6} mol dm^{-3}) and in the presence of increasing concentrations of Na^+ (ranging from 1.0 x 10^{-6} to 4.0 x 10^{-4} mol dm^{-3}) in acetonitrile (I = 0.050 mol dm^{-3}) at 298.2 K, when excited at 381.0 nm. The emission of* ***51*** *alone is the lowest intensity curve in the montage.*

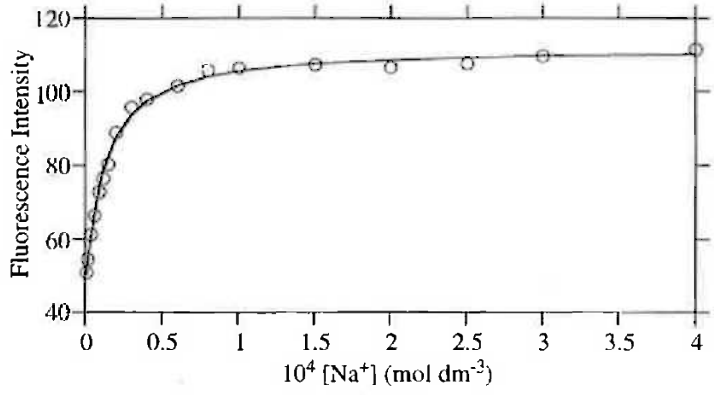

Figure A.48. *Fluorescence variation of mono(azacrown)* ***51*** *at 407.0 nm in the presence of increasing concentrations of Na^+ when excited at 381.0 nm. The circles represent experimentally obtained data points and the solid line represents the best fit of the data to a 1:1 binding model.*

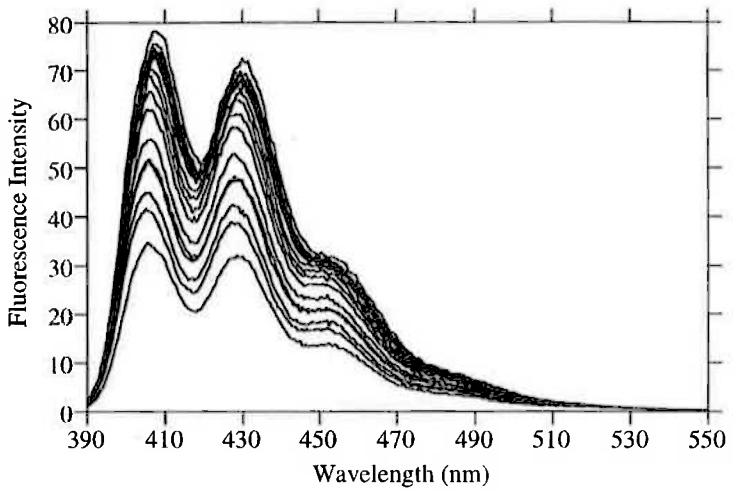

Figure A.49. *Emission spectra of mono(azacrown)* ***51*** *alone (3.0 x 10^{-6} mol dm^{-3}) and in the presence of increasing concentrations of K^+ (ranging from 5.0 x 10^{-6} to 5.0 x 10^{-3} mol dm^{-3}) in acetonitrile (I = 0.050 mol dm^{-3}) at 298.2 K, when excited at 375.0 nm. The emission of* ***51*** *alone is the lowest intensity curve in the montage.*

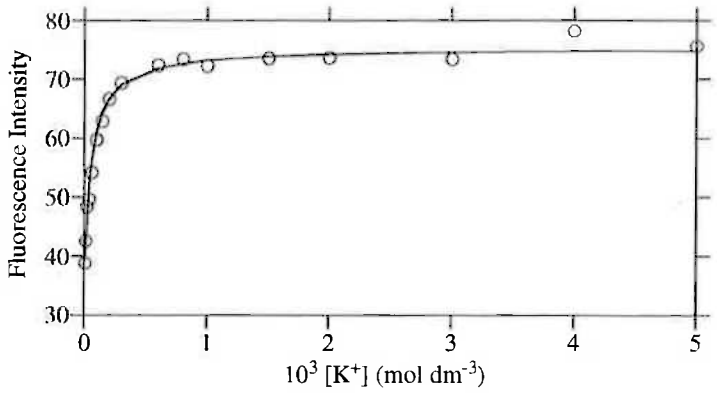

Figure A.50. *Fluorescence variation of mono(azacrown)* ***51*** *at 408.0 nm in the presence of increasing concentrations of K^+ when excited at 375.0 nm. The circles represent experimentally obtained data points and the solid line represents the best fit of the data to a 1:1 binding model.*

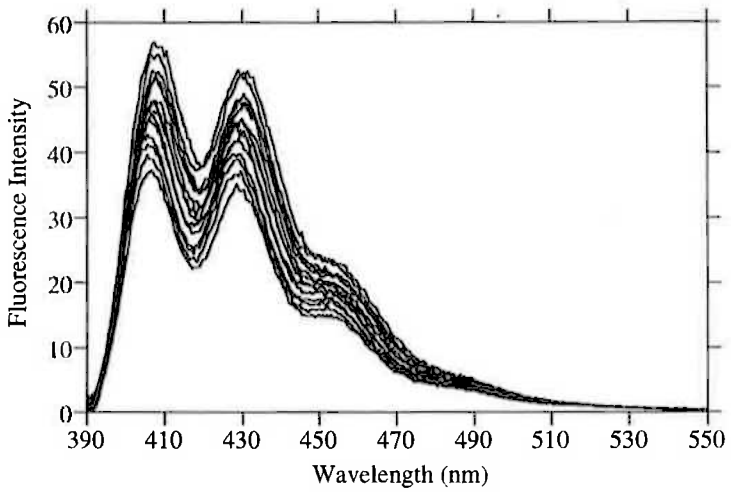

Figure A.51. *Emission spectra of mono(azacrown)* ***51*** *alone (3.0 x 10^{-6} mol dm^{-3}) and in the presence of increasing concentrations of Rb^+ (ranging from 2.0 x 10^{-5} to 3.0 x 10^{-3} mol dm^{-3}) in acetonitrile (I = 0.050 mol dm^{-3}) at 298.2 K, when excited at 386.0 nm. The emission of* ***51*** *alone is the lowest intensity curve in the montage.*

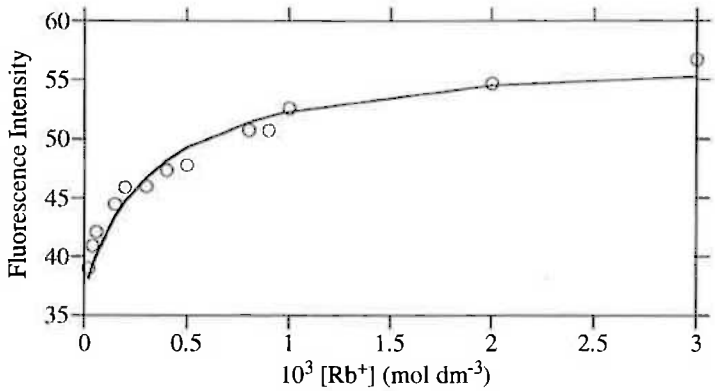

Figure A.52. *Fluorescence variation of mono(azacrown)* ***51*** *at 407.0 nm in the presence of increasing concentrations of Rb^+ when excited at 386.0 nm. The circles represent experimentally obtained data points and the solid line represents the best fit of the data to a 1:1 binding model.*

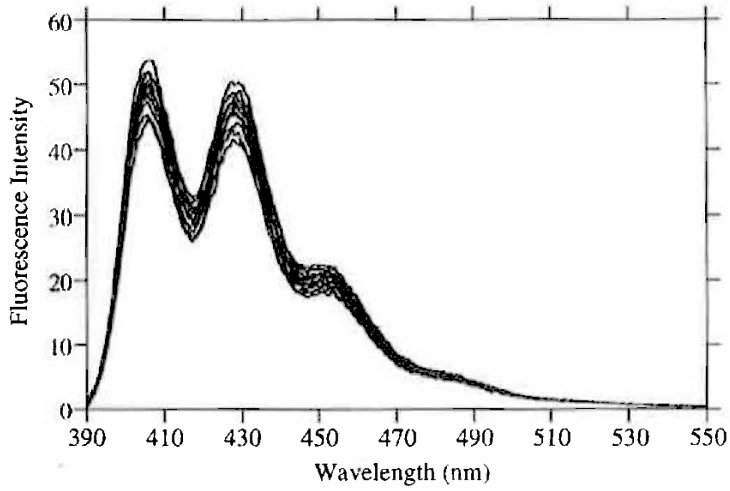

Figure A.53. *Emission spectra of mono(azacrown)* ***51*** *alone (3.0 x 10^{-6} mol dm^{-3}) and in the presence of increasing concentrations of Cs^+ (ranging from 5.0 x 10^{-5} to 4.0 x 10^{-3} mol dm^{-3}) in acetonitrile (I = 0.050 mol dm^{-3}) at 298.2 K, when excited at 382.0 nm. The emission of* ***51*** *alone is the lowest intensity curve in the montage.*

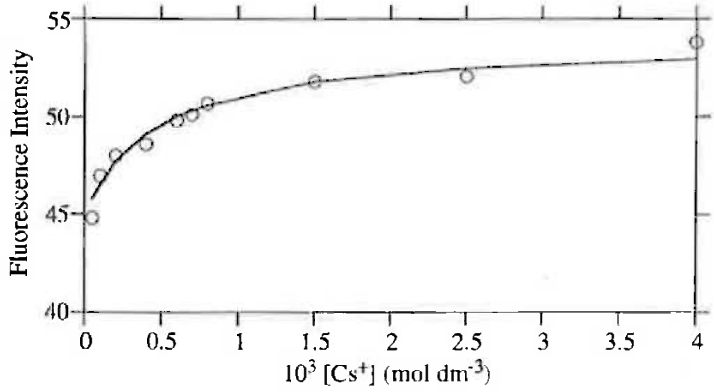

Figure A.54. *Fluorescence variation of mono(azacrown)* ***51*** *at 406.0 nm in the presence of increasing concentrations of Cs^+ when excited at 382.0 nm. The circles represent experimentally obtained data points and the solid line represents the best fit of the data to a 1:1 binding model.*

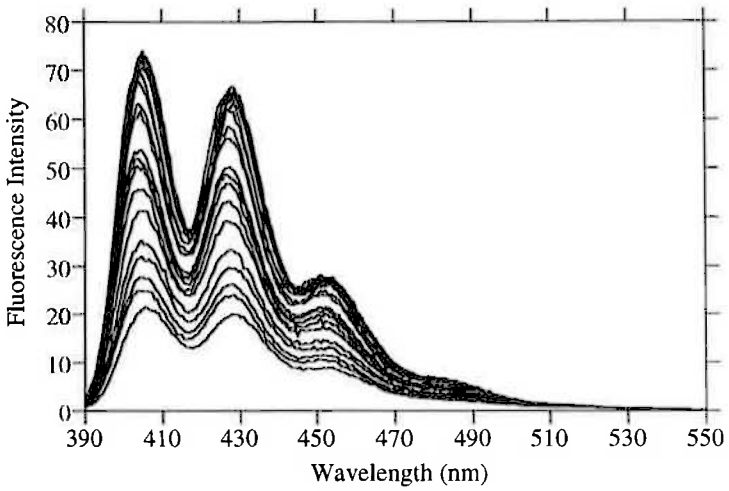

Figure A.55. *Emission spectra of mono(azacrown)* ***51*** *alone (3.0 x 10^{-6} mol dm^{-3}) and in the presence of increasing concentrations of Mg^{2+} (ranging from 1.0 x 10^{-7} to 9.0 x 10^{-6} mol dm^{-3}) in acetonitrile (I = 0.050 mol dm^{-3}) at 298.2 K, when excited at 369.0 nm. The emission of* ***51*** *alone is the lowest intensity curve in the montage.*

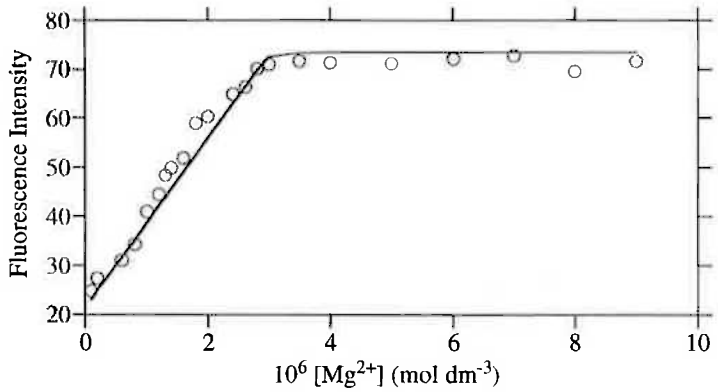

Figure A.56. *Fluorescence variation of mono(azacrown)* ***51*** *at 406.0 nm in the presence of increasing concentrations of Mg^{2+} when excited at 369.0 nm. The circles represent experimentally obtained data points and the solid line represents the best fit of the data to a 1:1 binding model.*

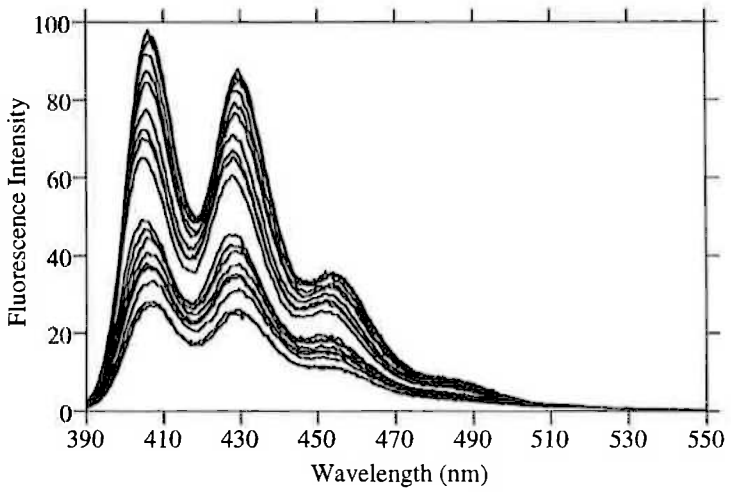

Figure A.57. *Emission spectra of mono(azacrown)* ***51*** *alone (3.0 x 10^{-6} mol dm^{-3}) and in the presence of increasing concentrations of Ca^{2+} (ranging from 6.0 x 10^{-8} to 8.0 x 10^{-6} mol dm^{-3}) in acetonitrile (I = 0.050 mol dm^{-3}) at 298.2 K, when excited at 374.0 nm. The emission of* ***51*** *alone is the lowest intensity curve in the montage.*

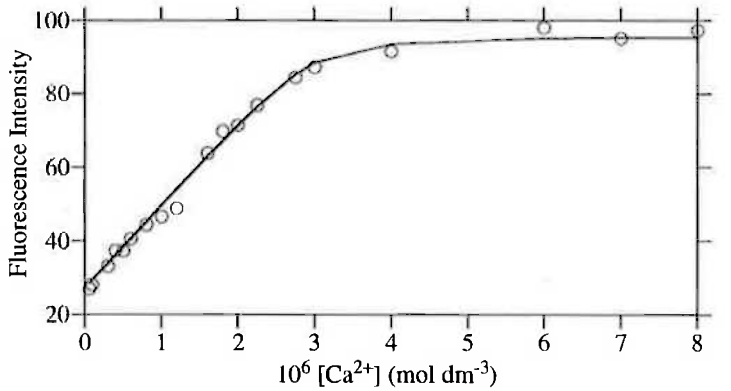

Figure A.58. *Fluorescence variation of mono(azacrown)* ***51*** *at 406.0 nm in the presence of increasing concentrations of Ca^{2+} when excited at 374.0 nm. The circles represent experimentally obtained data points and the solid line represents the best fit of the data to a 1:1 binding model.*

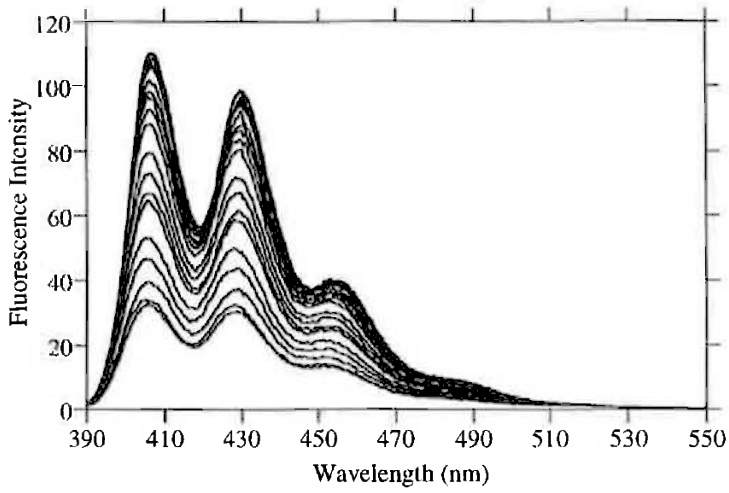

Figure A.59. *Emission spectra of mono(azacrown)* ***51*** *alone (3.0 x 10^{-6} mol dm^{-3}) and in the presence of increasing concentrations of Sr^{2+} (ranging from 1.0 x 10^{-7} to 9.0 x 10^{-6} mol dm^{-3}) in acetonitrile (I = 0.050 mol dm^{-3}) at 298.2 K, when excited at 375.0 nm. The emission of* ***51*** *alone is the lowest intensity curve in the montage.*

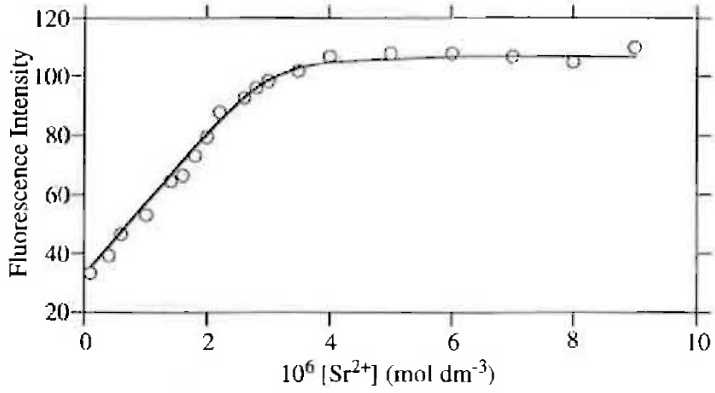

Figure A.60. *Fluorescence variation of mono(azacrown)* ***51*** *at 406.0 nm in the presence of increasing concentrations of Sr^{2+} when excited at 375.0 nm. The circles represent experimentally obtained data points and the solid line represents the best fit of the data to a 1:1 binding model.*

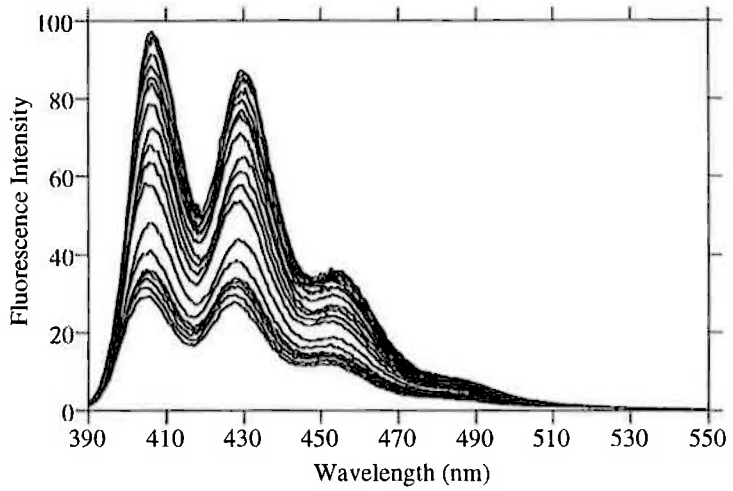

Figure A.61. *Emission spectra of mono(azacrown)* ***51*** *alone (3.0 x 10^{-6} mol dm^{-3}) and in the presence of increasing concentrations of Ba^{2+} (ranging from 1.0 x 10^{-7} to 9.0 x 10^{-6} mol dm^{-3}) in acetonitrile (I = 0.050 mol dm^{-3}) at 298.2 K, when excited at 374.0 nm. The emission of* ***51*** *alone is the lowest intensity curve in the montage.*

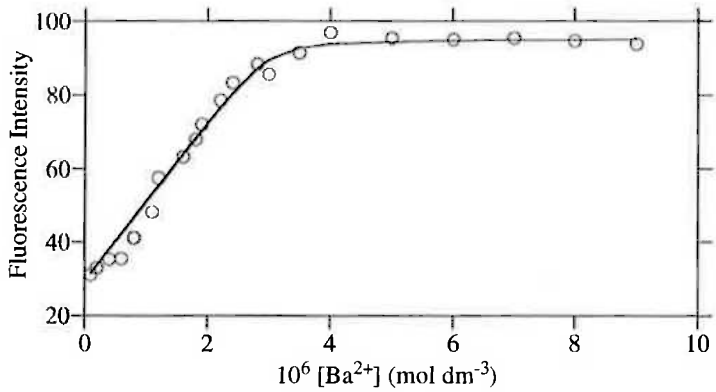

Figure A.62. *Fluorescence variation of mono(azacrown)* ***51*** *at 406.0 nm in the presence of increasing concentrations of Ba^{2+} when excited at 374.0 nm. The circles represent experimentally obtained data points and the solid line represents the best fit of the data to a 1:1 binding model.*

A.7 Bis(azacrown) 45

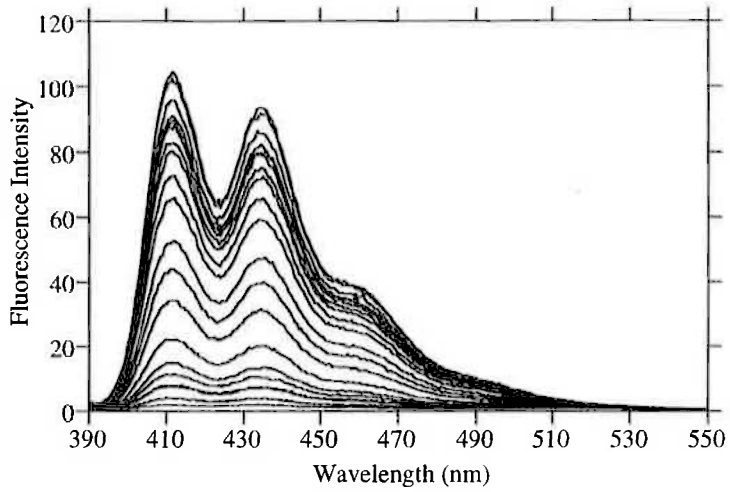

Figure A.63. *Emission spectra of bis(azacrown)* ***45*** *alone (3.0 x 10^{-6} mol dm^{-3}) and in the presence of increasing concentrations of Li^+ (ranging from 1.0 x 10^{-6} to 8.0 x 10^{-4} mol dm^{-3}) in acetonitrile (I = 0.050 mol dm^{-3}) at 298.2 K, when excited at 385.0 nm. The emission of* ***45*** *alone is the lowest intensity curve in the montage.*

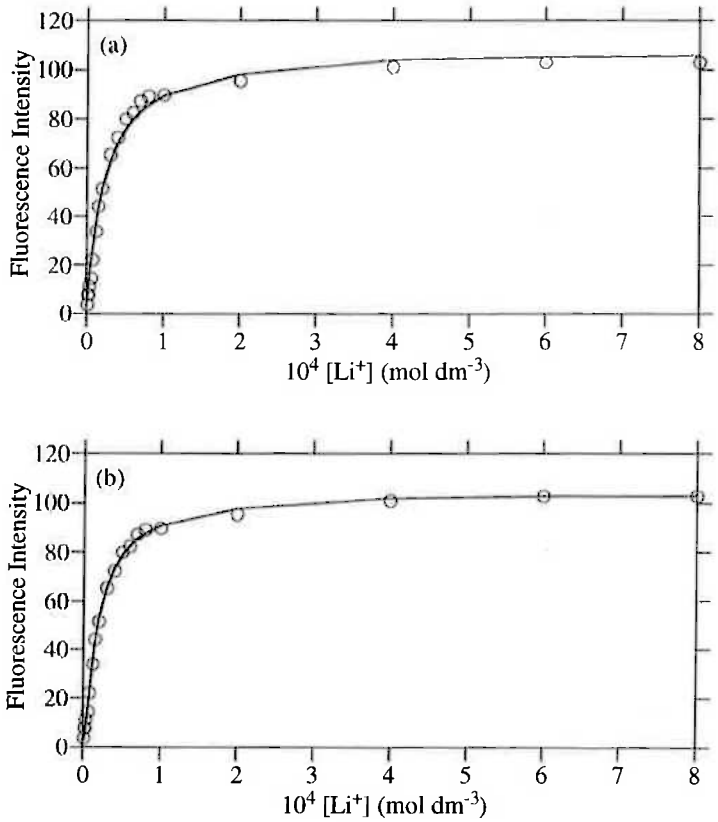

Figure A.64. *Fluorescence variation of bis(azacrown)* ***45*** *at 411.0 nm in the presence of increasing concentrations of Li^+ when excited at 385.0 nm. Graph (a) is the fit for a 1:1 binding model and (b) is the fit for a 2:1 binding model. The circles represent experimentally obtained data points and the solid line represents the best fit of the data.*

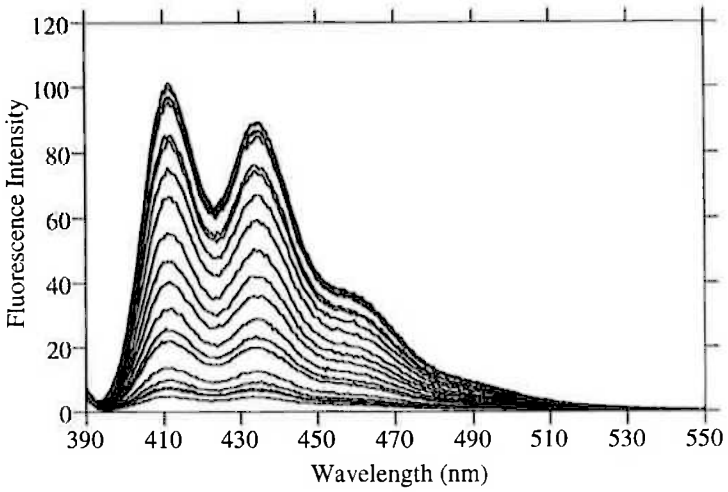

Figure A.65. *Emission spectra of bis(azacrown)* ***45*** *alone (3.0 x 10^{-6} mol dm^{-3}) and in the presence of increasing concentrations of Na^+ (ranging from 1.0 x 10^{-6} to 3.0 x 10^{-3} mol dm^{-3}) in acetonitrile (I = 0.050 mol dm^{-3}) at 298.2 K, when excited at 382.0 nm. The emission of* ***45*** *alone is the lowest intensity curve in the montage.*

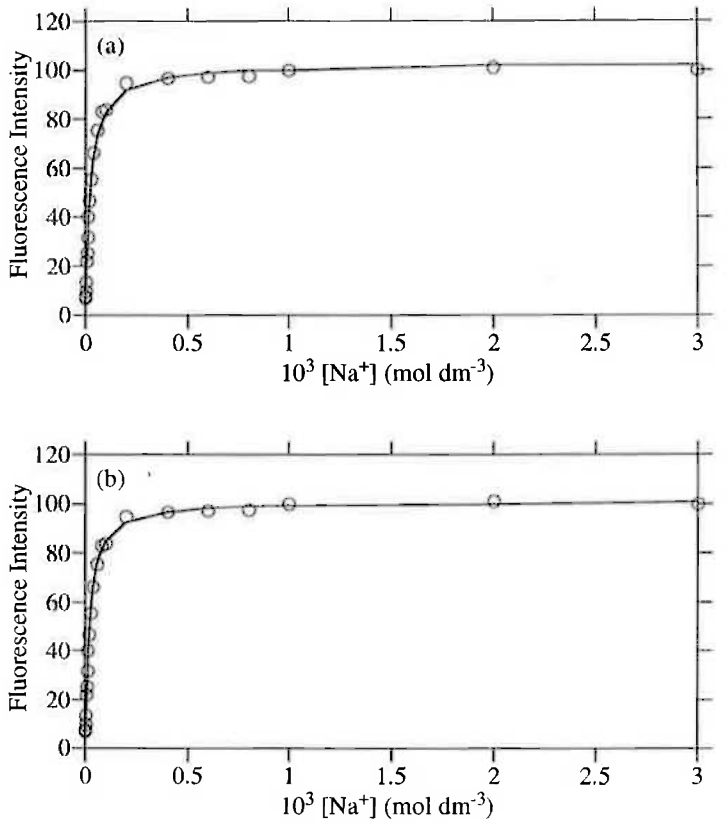

Figure A.66. *Fluorescence variation of bis(azacrown)* ***45*** *at 411.0 nm in the presence of increasing concentrations of Na^+ when excited at 382.0 nm. Graph (a) is the fit for a 1:1 binding model and (b) is the fit for a 2:1 binding model. The circles represent experimentally obtained data points and the solid line represents the best fit of the data.*

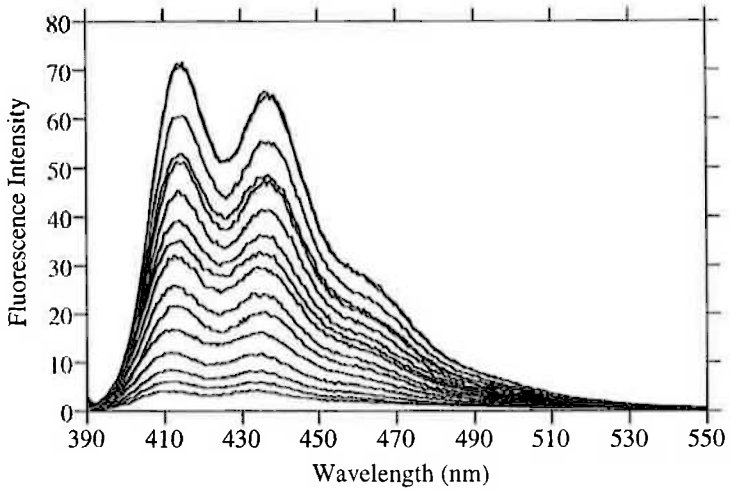

Figure A.67. *Emission spectra of bis(azacrown)* ***45*** *alone (3.0 x 10^{-6} mol dm^{-3}) and in the presence of increasing concentrations of K^+ (ranging from 1.5 x 10^{-5} to 3.0 x 10^{-3} mol dm^{-3}) in acetonitrile (I = 0.050 mol dm^{-3}) at 298.2 K, when excited at 380.0 nm. The emission of* ***45*** *alone is the lowest intensity curve in the montage.*

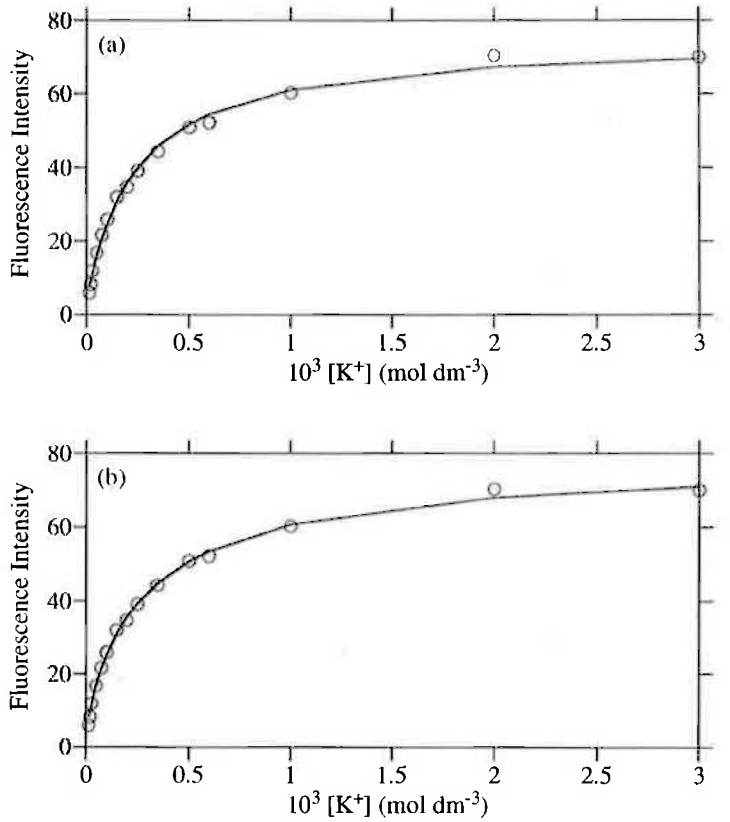

Figure A.68. *Fluorescence variation of bis(azacrown)* ***45*** *at 413.0 nm in the presence of increasing concentrations of K^+ when excited at 380.0 nm. Graph (a) is the fit for a 1:1 binding model and (b) is the fit for a 2:1 binding model. The circles represent experimentally obtained data points and the solid line represents the best fit of the data.*

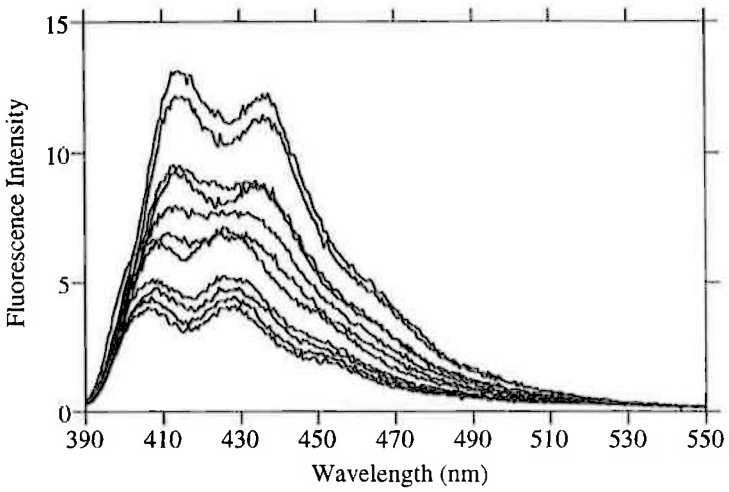

Figure A.69. *Emission spectra of bis(azacrown)* ***45*** *alone (3.0 x 10^{-6} mol dm^{-3}) and in the presence of increasing concentrations of Rb^+ (ranging from 1.0 x 10^{-5} to 3.0 x 10^{-3} mol dm^{-3}) in acetonitrile (I = 0.050 mol dm^{-3}) at 298.2 K, when excited at 376.0 nm. The emission of* ***45*** *alone is the lowest intensity curve in the montage.*

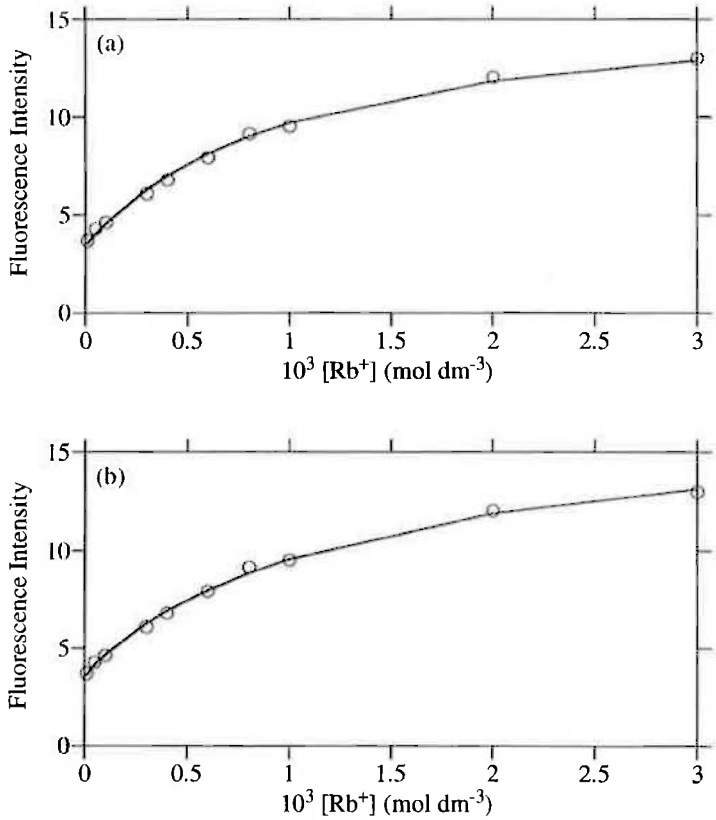

Figure A.70. *Fluorescence variation of bis(azacrown)* ***45*** *at 413.0 nm in the presence of increasing concentrations of Rb^+ when excited at 376.0 nm. Graph (a) is the fit for a 1:1 binding model and (b) is the fit for a 2:1 binding model. The circles represent experimentally obtained data points and the solid line represents the best fit of the data.*

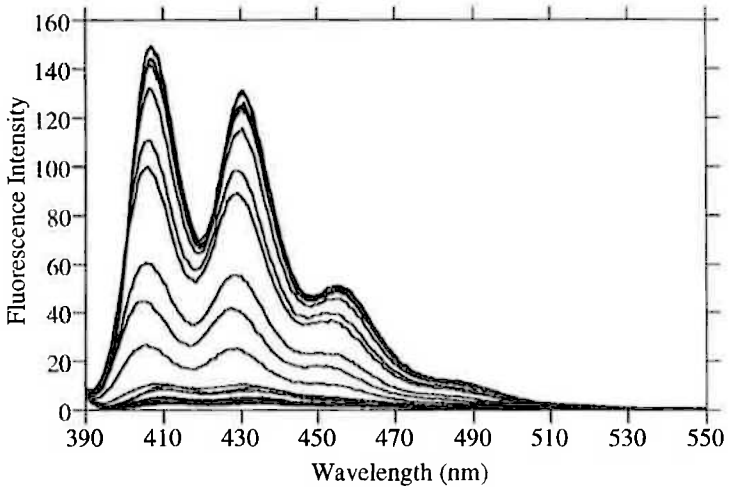

Figure A.71. *Emission spectra of bis(azacrown)* ***45*** *alone (3.0 x 10^{-6} mol dm^{-3}) and in the presence of increasing concentrations of Mg^{2+} (ranging from 5.0 x 10^{-7} to 1.0 x 10^{-4} mol dm^{-3}) in acetonitrile (I = 0.050 mol dm^{-3}) at 298.2 K, when excited at 383.0 nm. The emission of* ***45*** *alone is the lowest intensity curve in the montage.*

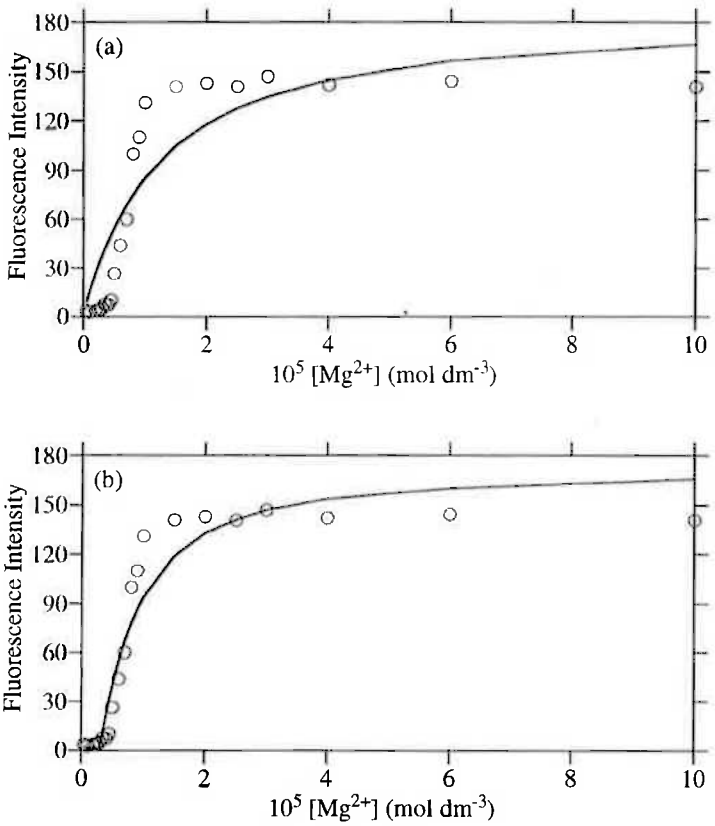

Figure A.72. *Fluorescence variation of bis(azacrown)* ***45*** *at 406.0 nm in the presence of increasing concentrations of Mg^{2+} when excited at 383.0 nm. Graph (a) is the fit for a 1:1 binding model and (b) is the fit for a 2:1 binding model. The circles represent experimentally obtained data points and the solid line represents the best fit of the data.*

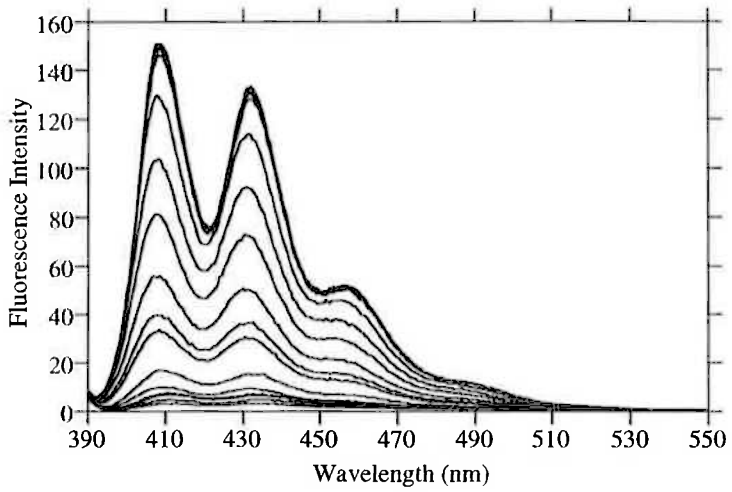

Figure A.73. *Emission spectra of bis(azacrown)* ***45*** *alone (3.0 x 10^{-6} mol dm^{-3}) and in the presence of increasing concentrations of Ca^{2+} (ranging from 5.0 x 10^{-7} to 8.0 x 10^{-5} mol dm^{-3}) in acetonitrile (I = 0.050 mol dm^{-3}) at 298.2 K, when excited at 383.0 nm. The emission of* ***45*** *alone is the lowest intensity curve in the montage.*

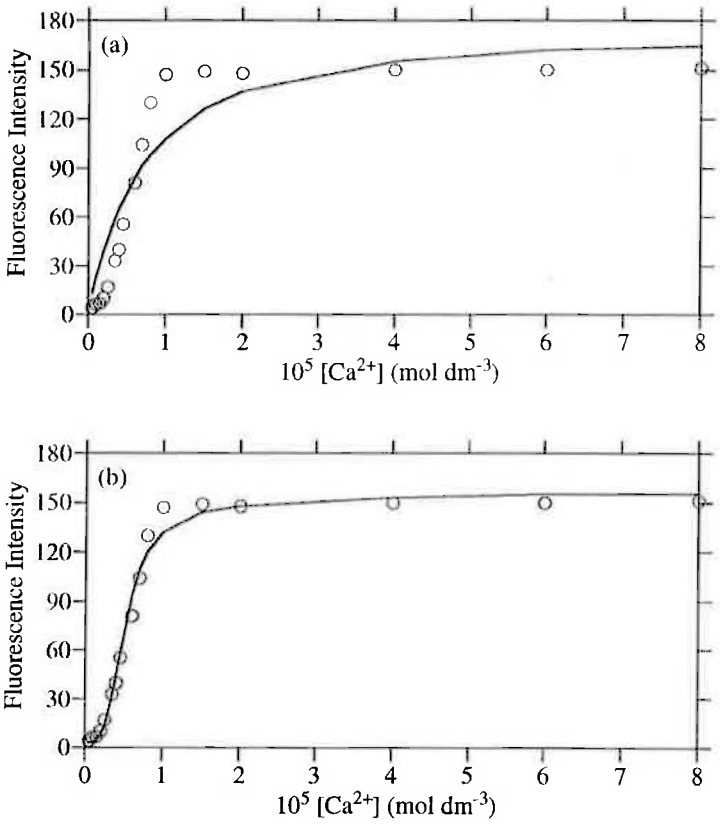

Figure A.74. *Fluorescence variation of bis(azacrown)* ***45*** *at 408.0 nm in the presence of increasing concentrations of Ca^{2+} when excited at 383.0 nm. Graph (a) is the fit for a 1:1 binding model and (b) is the fit for a 2:1 binding model. The circles represent experimentally obtained data points and the solid line represents the best fit of the data.*

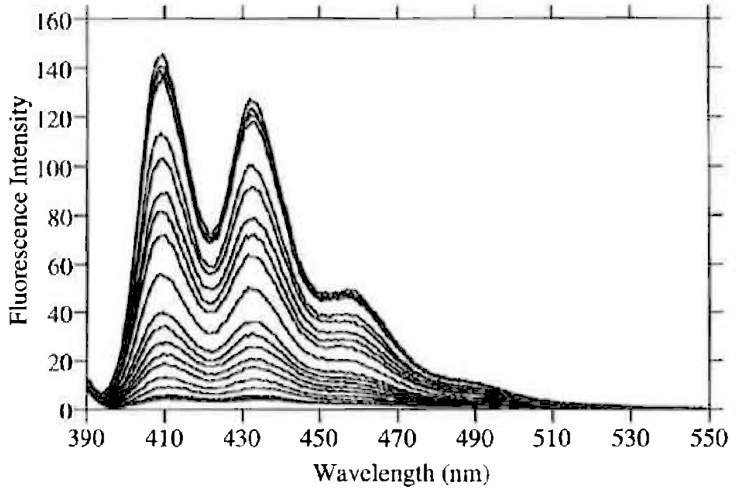

Figure A.75. *Emission spectra of bis(azacrown)* ***45*** *alone (3.0 x 10^{-6} mol dm^{-3}) and in the presence of increasing concentrations of Sr^{2+} (ranging from 5.0 x 10^{-7} to 8.0 x 10^{-5} mol dm^{-3}) in acetonitrile (I = 0.050 mol dm^{-3}) at 298.2 K, when excited at 384.0 nm. The emission of* ***45*** *alone is the lowest intensity curve in the montage.*

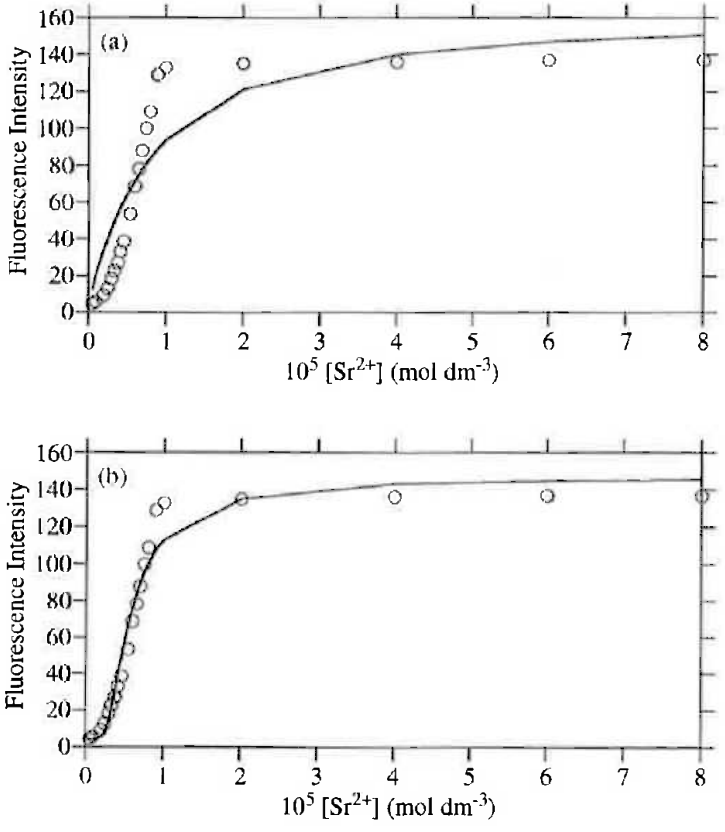

Figure A.76. *Fluorescence variation of bis(azacrown)* ***45*** *at 411.0 nm in the presence of increasing concentrations of Sr^{2+} when excited at 384.0 nm. Graph (a) is the fit for a 1:1 binding model and (b) is the fit for a 2:1 binding model. The circles represent experimentally obtained data points and the solid line represents the best fit of the data.*

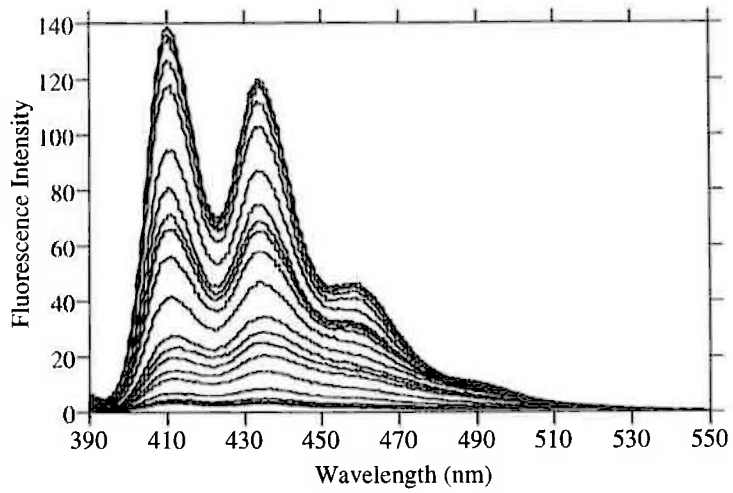

Figure A.77. *Emission spectra of bis(azacrown)* ***45*** *alone (3.0 x 10^{-6} mol dm^{-3}) and in the presence of increasing concentrations of Ba^{2+} (ranging from 1.0 x 10^{-6} to 1.0 x 10^{-4} mol dm^{-3}) in acetonitrile (I = 0.050 mol dm^{-3}) at 298.2 K, when excited at 386.0 nm. The emission of* ***45*** *alone is the lowest intensity curve in the montage.*

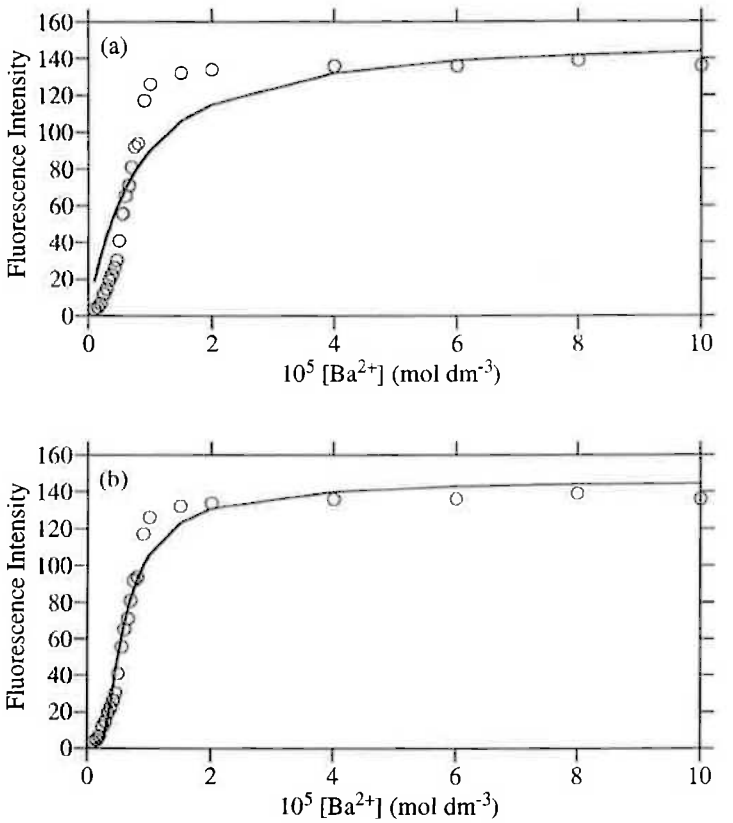

Figure A.78. *Fluorescence variation of bis(azacrown)* ***45*** *at 410.0 nm in the presence of increasing concentrations of Ba^{2+} when excited at 386.0 nm. Graph (a) is the fit for a 1:1 binding model and (b) is the fit for a 2:1 binding model. The circles represent experimentally obtained data points and the solid line represents the best fit of the data.*

Bibliography

1. Valeur, B.; Bardez, E. *Chem. Brit.* **1995**, 216-220.
2. Kaim, W.; Schwederski, B. *Bioinorganic Chemistry: Inorganic Elements in the Chemistry of Life*; John Wiley & Sons: Chichester, 1994.
3. Needleman, H. L. *Human Lead Exposure*; CRC Press: Boca Raton, 1992.
4. Czarnik, A. W. *Chem. Biol.* **1995**, *2*, 423-428.
5. Willard, H. H.; Merritt, L. L., Jr.; Merritt, L. L.; Dean, J. A. *Instrumental Methods of Analysis*; 6th ed.; Wadsworth Publishing Co.: Belmont, 1981.
6. de Silva, A. P.; Gunaratne, H. Q. N.; Gunnlaugsson, T.; Huxley, A. J. M.; McCoy, C. P.; Rademacher, J. T.; Rice, T. E. *Chem. Rev.* **1997**, *97*, 1515-1556.
7. Goodwin, P. M.; Ambrose, W. P.; Keller, R. A. *Acc. Chem. Res.* **1996**, *29*, 607-613.
8. Ambrose, W. P.; Goodwin, P. M.; Jett, J. H.; Van Orden, A.; Werner, J. H.; Keller, R. A. *Chem. Rev.* **1999**, *99*, 2929-2956.
9. *Luminescence Techniques in Chemical and Biochemical Analysis*; Baeyens, W. R. G.; De Keukeleire, D.; Korkidis, K., Eds.; Marcel Dekker: New York, 1991.
10. *Fluorescent and Luminescent Probes for Biological Activity*; Mason, W. T., Ed.; Academic Press: London, 1993.
11. Lehn, J.-M. *Angew. Chem. Int. Ed.* **1988**, *27*, 89-112.
12. Quici, S.; Manfredi, A.; Buttafava, M. *J. Org. Chem.* **1996**, *61*, 3870-3873.
13. Prodi, L.; Bolletta, F.; Montalti, M.; Zaccheroni, N. *Coord. Chem. Rev.* **2000**, *205*, 59-83.
14. Fabbrizzi, L.; Licchelli, M.; Parodi, L.; Poggi, A.; Taglietti, A. *Eur. J. Inorg. Chem.* **1999**, 35-39.
15. *Handbook of Fluorescent Probes and Research Products*; 9th ed.; Haugland, R. P., Ed.; Molecular Probes, Inc.: Eugene, 2002.

16. Slavik, J. *Fluorescent Probes in Cellular and Molecular Biology*; CRC Press: Boca Raton, 1994.

17. Bissell, R. A.; de Silva, A. P.; Gunaratne, H. Q. N.; Lynch, P. L. M.; Maguire, G. E. M.; McCoy, C. P.; Sandanayake, K. R. A. S. *Top. Curr. Chem.* **1993**, *168*, 223-264.

18. *Chemosensors of Ion and Molecule Recognition*; Desvergne, J.-P.; Czarnik, A. W., Eds.; Kluwer Academic: Dordrecht, 1997.

19. de Silva, A. P.; Fox, D. B.; Moody, T. S.; Weir, S. M. In *Optical Sensors and Switches*; Ramamurthy, V., Schanze, K. S., Eds.; Marcel Dekker: New York, 2001; Vol. 7.

20. Kavarnos, G. J. *Top. Curr. Chem.* **1990**, *156*, 23-58.

21. Valeur, B.; Leray, I. *Coord. Chem. Rev.* **2000**, *205*, 3-40.

22. Kawai, S. H.; Nagamura, T.; Mori, T.; Yoshida, K. *J. Phys. Chem. A* **1999**, *103*, 660-664.

23. Kollmannsberger, M.; Rurack, K.; Resch-Genger, U.; Daub, J. *J. Phys. Chem. A* **1998**, *102*, 10211-10220.

24. de Silva, A. P.; de Silva, S. A. *J. Chem. Soc., Chem. Commun.* **1986**, 1709-1710.

25. Akkaya, E. U.; Huston, M. E.; Czarnik, A. W. *J. Am. Chem. Soc.* **1990**, *112*, 3590-3593.

26. Huston, M. E.; Haider, K. W.; Czarnik, A. W. *J. Am. Chem. Soc.* **1988**, *110*, 4460-4462.

27. Chae, M.-Y.; Cherian, X. M.; Czarnik, A. W. *J. Org. Chem.* **1993**, *58*, 5797-5801.

28. Hancock, R. D.; Evers, A.; Ngwenya, M. P.; Wade, P. W. *J. Chem. Soc., Chem. Commun.* **1987**, 1129-1130.

29. Yoshida, K.; Mori, T.; Watanabe, S.; Kawai, H.; Nagamura, T. *J. Chem. Soc., Perkin Trans. 2* **1999**, 393-397.

30. Shen, Y.; Sullivan, B. P. *J. Chem. Ed.* **1997**, *74*, 685-689.

31. Hancock, R. D.; Maumela, H.; de Sousa, A. S. *Coord. Chem. Rev.* **1996**, *148*, 315-347.

32. Fages, F.; Desvergne, J.-P.; Bouas-Laurent, H.; Marsau, P.; Lehn, J.-M.; Kotzyba-Hibert, F.; Allbrecht-Gary, A.-M.; Al-Joubbeh, M. *J. Am. Chem. Soc.* **1989**, *111*, 8672-8680.

33. Kastenholz, F.; Grell, E.; Bats, J. W.; Quinkert, G.; Brand, K.; Lanig, H.; Schneider, F. W. *J. Fluoresc.* **1994**, *4*, 243-246.

34. Buet, P.; Kastenholz, F.; Grell, E.; Kaeb, G.; Haefner, A.; Schneider, F. W. *J. Phys. Chem. A* **1999**, *103*, 5871-5881.

35. Ghosh, P.; Bharadwaj, P. K.; Roy, J.; Ghosh, S. *J. Am. Chem. Soc.* **1997**, *119*, 11903-11909.

36. Masuhara, H.; Shioyama, H.; Saito, T.; Hamada, K.; Yasoshima, S.; Mataga, N. *J. Phys. Chem.* **1984**, *88*, 5868-5873.

37. Birks, J. B. *Photophysics of Aromatic Molecules*; Wiley-Interscience: London, 1970.

38. Ramachandram, B.; Samanta, A. *Chem. Commun.* **1997**, 1037-1038.

39. Hampe, E. M.; Rudkevich, D. M. *Chem. Commun.* **2002**, 1450-1451.

40. Rurack, K.; Resch-Genger, U. *Chem. Soc. Rev.* **2002**, *31*, 116-127.

41. Rurack, K.; Bricks, J. L.; Schulz, B.; Maus, M.; Reck, G.; Resch-Genger, U. *J. Phys. Chem. A* **2000**, *104*, 6171-6188.

42. Suppan, P. *Chemistry and Light*; Royal Society of Chemistry: London, 1994.

43. Fabbrizzi, L.; Licchelli, M.; Pallavicini, P.; Perotti, A.; Taglietti, A.; Sacchi, D. *Chem. Eur. J.* **1996**, *2*, 75-82.

44. Turfan, B.; Akkaya, E. U. *Org. Lett.* **2002**, *4*, 2857-2859.

45. Aoki, I.; Sakaki, T.; Shinkai, S. *J. Chem. Soc., Chem. Commun.* **1992**, 730-732.

46. de Silva, A. P.; Fox, D. B.; Huxley, A. J. M.; Moody, T. S. *Coord. Chem. Rev.* **2000**, *205*, 41-57.

47. Xu, H.; Xu, X.; Ji, H.-F. *Chem. Commun.* **2001**, *2001*, 2092-2093.

48. Ji, H.-F.; Dabestani, R.; Brown, G. M. *J. Am. Chem. Soc.* **2000**, *122*, 9306-9307.

49. Xu, H.; Xu, X.; Dabestani, R.; Brown, G. M.; Fan, L.; Ji, H.-F. *J. Chem. Soc., Perkin Trans. 2* **2002**, 636-643.

50. de Silva, S. A.; Amorelli, B.; Isidor, D. C.; Loo, K. C.; Crooker, K. E.; Pena, Y. E. *Chem. Commun.* **2002**, 1360-1361.

51. de Silva, A. P.; Gunaratne, H. Q. N.; McCoy, C. P. *J. Am. Chem. Soc.* **1997**, *119*, 7891-7892.

52. de Silva, S. A.; Zavaleta, A.; Baron, D. E.; Allam, O.; Isidor, E. V.; Kashimura, N.; Percarpio, J. M. *Tetrahedron Lett.* **1997**, *38*, 2237-2240.

53. Fabbrizzi, L.; Francese, G.; Pallavicini, P.; Parodi, L. *New J. Chem.* **1998**, 1403-1407.

54. Gawley, R. E.; Zhang, Q.; Higgs, P. I.; Wang, S.; Leblanc, R. M. *Tetrahedron Lett.* **1999**, *40*, 5461-5465.

55. Wang, S.; Zhang, Q.; Datta, P. K.; Gawley, R. E.; Leblanc, R. M. *Langmuir* **2000**, *16*, 4607-4612.

56. James, T. D.; Sandanayake, K. R. A. S.; Shinkai, S. *Angew. Chem. Int. Ed.* **1994**, *33*, 2207-2209.

57. James, T. D.; Sandanayake, K. R. A. S.; Shinkai, S. *Angew. Chem. Int. Ed.* **1996**, *35*, 1910-1922.

58. Cooper, C. R.; James, T. D. *J. Chem. Soc., Perkin Trans. 1* **2000**, 963-969.

59. James, T. D.; Sandanayake, K. R. A. S.; Shinkai, S. *J. Chem. Soc., Chem. Commun.* **1994**, 477-478.

60. Gunnlaugsson, T.; Davis, A. P.; Glynn, M. *Chem. Commun.* **2001**, 2556-2557.

61. Gunnlaugsson, T.; Davis, A. P.; O'Brien, J. E.; Glynn, M. *Org. Lett.* **2002**, *4*, 2449-2452.

62. Fabbrizzi, L.; Francese, G.; Licchelli, M.; Perotti, A.; Taglietti, A. *Chem. Commun.* **1997**, 581-582.

63. De Santis, G.; Fabbrizzi, L.; Faravelli, I.; Licchelli, M.; Poggi, A.; Taglietti, A. *Angew. Chem. Int. Ed.* **1996**, *35*, 202-204.

64. Ojida, A.; Mito-oka, Y.; Inoue, M.; Hamachi, I. *J. Am. Chem. Soc.* **2002**, *124*, 6256-6258.

65. Rurack, K. *Spectrochim. Acta, Part A* **2001**, *57*, 2161-2195.

66. Martin, M. M.; Plaza, P.; Dai Hung, N.; Meyer, Y. H.; Bourson, J.; Valeur, B. *Chem. Phys. Lett.* **1993**, *202*, 425-430.

67. Dumon, P.; Jonusauskas, G.; Dupuy, F.; Pée, P.; Rullière, C.; Létard, J.-F.; Lapouyade, R. *J. Phys. Chem.* **1994**, *98*, 10391-10396.

68. Rettig, W. *Top. Curr. Chem.* **1994**, *169*, 254-299.

69. Bhattacharyya, K.; Chowdhury, M. *Chem. Rev.* **1993**, *93*, 507-535.

70. Bourson, J.; Valeur, B. *J. Phys. Chem.* **1989**, *93*, 3871-3876.

71. Rurack, K.; Rettig, W.; Resch-Genger, U. *Chem. Commun.* **2000**, 407-408.

72. Bricks, J. L.; Slominskii, J. L.; Kudinova, M. A.; Tolmachev, A. I.; Rurack, K.; Resch-Genger, U.; Rettig, W. *J. Photochem. Photobiol. A: Chem* **2000**, *132*, 193-208.

73. Minta, A.; Tsien, R. Y. *J. Biol. Chem.* **1989**, *264*, 19449-19457.

74. Grynkiewicz, G.; Poenie, M.; Tsien, R. Y. *J. Biol. Chem.* **1985**, *260*, 3440-3450.

75. Bourson, J.; Pouget, J.; Valeur, B. *J. Phys. Chem.* **1993**, *97*, 4552-4557.

76. Marquis, D.; Desvergne, J.-P.; Bouas-Laurent, H. *J. Org. Chem.* **1995**, *60*, 7984-7996.

77. Krauss, R.; Weinig, H.-G.; Seydack, M.; Bendig, J.; Koert, U. *Angew. Chem. Int. Ed.* **2000**, *39*, 1835-1837.

78. Glass, T. E. *J. Am. Chem. Soc.* **2000**, *122*, 4522-4523.

79. Raker, J.; Glass, T. E. *J. Org. Chem.* **2001**, *66*, 6505-6512.

80. Raker, J.; Glass, T. E. *Tetrahedron* **2001**, *57*, 10233-10240.

81. McFarland, S. A.; Finney, N. S. *J. Am. Chem. Soc.* **2001**, *123*, 1260-1261.

82. Mello, J. V.; Finney, N. S. *Angew. Chem. Int. Ed.* **2001**, *40*, 1536-1538.

83. Hendrickson, K. M.; Rodopoulos, T.; Pittet, P.-A.; Mahadevan, I.; Lincoln, S. F.; Ward, A. D.; Kurucsev, T.; Duckworth, P. A.; Forbes, I. J.; Zalewski, P. D.; Betts, W. H. *J. Chem. Soc., Dalton Trans.* **1997**, 3879-3882.

84. Deo, S.; Godwin, H. A. *J. Am. Chem. Soc.* **2000**, *122*, 174-175.

85. Fenniri, H.; Hosseini, M. W.; Lehn, J.-M. *Helv. Chim. Acta* **1997**, *80*, 786-803.

86. Dhaenens, M.; Lehn, J.-M.; Vigneron, J.-P. *J. Chem. Soc., Pekin Trans. 2* **1993**, 1379-1381.

87. Winkler, J. D.; Bowen, C. M.; Michelet, V. *J. Am. Chem. Soc.* **1998**, *120*, 3237-3242.

88. Raymo, F. M.; Giordani, S. *Org. Lett.* **2001**, *3*, 3475-3478.

89. Raymo, F. M.; Giordani, S. *J. Am. Chem. Soc.* **2001**, *123*, 4651-4652.

90. Malval, J.-P.; Gosse, I.; Morand, J.-P.; Lapouyade, R. *J. Am. Chem. Soc.* **2002**, *124*, 904-905.

91. Wiskur, S. L.; Ait-Haddou, H.; Lavigne, J. J.; Anslyn, E. V. *Acc. Chem. Res.* **2001**, *34*, 963-972.

92. Fabbrizzi, L.; Leone, A.; Taglietti, A. *Angew. Chem. Int. Ed.* **2001**, *40*, 3066-3069.

93. Metzger, A.; Anslyn, E. V. *Angew. Chem. Int. Ed.* **1998**, *37*, 649-652.

94. Fabbrizzi, L.; Licchelli, M.; Pallavicini, P. *Acc. Chem. Res.* **1999**, *32*, 846-853.

95. Czarnik, A. W. *Acc. Chem. Res.* **1994**, *27*, 302-308.

96. Yoon, J.; Ohler, N. E.; Vance, D. H.; Aumiller, W. D.; Czarnik, A. W. In *Chemosensors of Ion and Molecule Recognition*; Desvergne, J. P., Czarnik, A. W., Eds.; Kluwer Academic: Dordrecht, 1997.

97. Becker, H. D. *Chem. Rev.* **1993**, *93*, 145-172.

98. Schoof, S.; Güsten, H.; von Sonntag, C. *Ber. Bunsenges. Phys. Chem.* **1978**, *82*, 1068-1073.

99. Badger, G. M. *Structures and Reactions of the Aromatic Compounds*; Cambridge University Press: Cambridge, 1957.

100. Hancock, R. D.; Martell, A. E. *J. Chem. Ed.* **1996**, *73*, 654-661.

101. *Hard and Soft Acids and Bases*; Pearson, R. G., Ed.; Dowden, Hutchinson & Ross: Stroudsburg, 1973.

102. Fabbrizzi, L.; Licchelli, M.; Perotti, A.; Poggi, A.; Rabaioli, G.; Sacchi, D.; Taglietti, A. *J. Chem. Soc., Perkin Trans. 2* **2001**, 2108-2113.

103. Amendola, V.; Fabbrizzi, L.; Pallavicini, P.; Parodi, L.; Perotti, A. *J. Chem. Soc., Dalton Trans.* **1998**, 2053-2057.

104. Lehn, J.-M.; Sauvage, J. P. *J. Am. Chem. Soc.* **1975**, *97*, 6700-6707.

105. Evans, D. F.; Upton, M. W. *J. Chem. Soc., Dalton Trans.* **1985**, 1141-1145.

106. Miller, M. W.; Amidon, R. W.; Tawney, P. O. *J. Am. Chem. Soc.* **1955**, *77*, 2845-2848.

107. Beckett, A. H.; Walker, J. *Tetrahedron* **1963**, *19*, 545-556.

108. Benn, R.; Bogdanovíc, B.; Brüning, M.; Grondey, H.; Herrmann, W.; Kinzelmann, H.-G.; Seevogel, K. *Chem. Ber.* **1993**, *126*, 225-237.

109. Postovskii, I. Y.; Bednyagin, N. P. *J. Gen. Chem. (U.S.S.R.)* **1937**, *7*, 2919-2925.

110. Guoqiang, L.; Hjalmarsson, M.; Högberg, H.-E.; Jernstedt, K.; Norin, T. *Acta Chem. Scand.* **1984**, *B38*, 795-801.

111. Friebolin, H. *Basic One- and Two-Dimensional NMR Spectroscopy*; VCH Publishers: New York, 1991.

112. Konopelski, J. P.; Kotzyba-Hibert, F.; Lehn, J.-M.; Desvergne, J.-P.; Fages, F.; Castellan, A.; Bouas-Laurent, H. *J. Chem. Soc., Chem. Commun.* **1985**, 433-436.

113. Brandès, S.; Denat, F.; Lacour, S.; Rabiet, F.; Barbette, F.; Pullumbi, P.; Guilard, R. *Eur. J. Org. Chem.* **1998**, 2349-2360.

114. Tsuji, J. *Palladium Reagents and Catalysts: Innovations in Organic Synthesis*; Wiley & Sons: Chichester, 1996.

115. Duerr, B. F.; Chung, Y.-S.; Czarnik, A. W. *J. Org. Chem.* **1988**, *53*, 2120-2122.

116. Bumagin, N. A.; Ponomaryov, A. B.; Beletskaya, I. P. *Synthesis* **1984**, 728-729.

117. Gunnlaugsson, T.; Nieuwenhuyzen, M.; Richard, L.; Thoss, V. *J. Chem. Soc., Perkin Trans. 2* **2002**, 141-150.

118. Krakowiak, K. E.; Bradshaw, J. S.; Dalley, N. K.; Zhu, C.; Yi, G.; Curtis, J. C.; Izatt, R. M. *J. Org. Chem.* **1992**, *57*, 3166-3173.

119. Sieglitz, A.; Marx, R. *Ber. dtsch. chem. Ges.* **1923**, *56*, 1619-1621.

120. Mosnaim, D.; Nonhebel, D. C.; Russel, J. A. *Tetrahedron* **1969**, *25*, 3485-3492.

121. Rigaudy, J.; Seuleiman, A. M.; Cuong, N. K. *Tetrahedron* **1982**, *38*, 3151-3155.

122. Geue, J. P.; Head, N. J.; Lincoln, S. F.; Ward, A. D. **2002**, *Manuscript in preparation.*

123. Bencini, A.; Bianchi, A.; Garcia-España, E.; Micheloni, M.; Ramirez, J. A. *Coord. Chem. Rev.* **1999**, *188*, 97-156.

124. Martell, A. E.; Smith, R. M. *Critical Stability Constants*; Plenum Press: New York, 1974.

125. Alder, R. W. *Chem. Rev.* **1989**, *89*, 1215.

126. Hart, S. M.; Boeyens, J. C. A.; Michael, J. P.; Hancock, R. D. *J. Chem. Soc., Dalton Trans.* **1983**, 1601-1606.

127. Gokel, G. W.; Garcia, B. J. *Tetrahedron Lett.* **1977**, *18*, 317-320.

128. Sakamoto, H.; Kimura, K.; Koseki, Y.; Matsuo, M.; Shono, T. *J. Org. Chem.* **1986**, *51*, 4974-4979.

129. Burgess, J. *Metal Ions in Solution*; Halsted Press: New York, 1978.

130. Freiser, H.; Charles, R. G.; Johnston, W. D. *J. Am. Chem. Soc.* **1952**, *74*, 1383-1385.

131. Jaffé, H. H.; Orchin, M. *Theory and Applications of Ultraviolet Spectroscopy*; John Wiley and Sons, Inc.: New York, 1962.

132. Berlman, I. B. *Handbook of Fluorescence Spectra of Aromatic Molecules*; 2nd ed.; Academic Press: New York, 1971.

133. Schulman, S. G. *Fluorescence and Phosphorescence Spectroscopy: Physicochemical Principles and Practice*; Pergamon Press: New York, 1977.

134. *Standards in Absorption Spectrometry*; Burgess, C.; Knowles, A., Eds.; Chapman and Hall: London, 1981.

135. Cherkasov, A. S. *Opt. Spec.* **1959**, *4*, 315-317.

136. Shizuka, H.; Nakamura, M.; Morita, T. *J. Phys. Chem.* **1979**, *83*, 2019-2024.

137. Good, N. E.; Winget, G. D.; Winter, W.; Connolly, T. N.; Izawa, S.; Singh, R. M. M. *Biochemistry* **1966**, *5*, 467-475.

138. Soares, H. M. V. M.; Conde, P. C. F. L. *Anal. Chim. Acta* **2000**, *421*, 103-111.

139. Arimori, S.; Ward, C. J.; James, T. D. *Chem. Commun.* **2001**, 2018-2019.

140. Wang, W.; Springsteen, G.; Gao, S.; Wang, B. *Chem. Commun.* **2000**, 1283-1284.

141. Ji, H.-F.; Dabestani, R.; Brown, G. M.; Hettich, R. L. *Photochem. Photobiol.* **1999**, *69*, 513-516.

142. de Silva, A. P.; Rupasinghe, R. A. D. D. *J. Chem. Soc., Chem. Commun.* **1985**, 1669-1670.

143. Bissell, R. A.; Calle, E.; de Silva, A. P.; de Silva, S. A.; Gunaratne, H. Q. N.; Habib-Jiwan, J.-L.; Peiris, S. L. A.; Rupasinghe, R. A. D. D.; Samarasinghe, T. K. S. D.; Sandanayake, K. R. A. S.; Soumillion, J.-P. *J. Chem. Soc., Perkin Trans. 2* **1992**, 1559-1564.

144. Burinsky, D. J.; Campana, J. E. *Org. Mass Spectrom.* **1984**, *19*, 539-544.

145. Greiner, G.; Maier, I. *J. Chem. Soc., Perkin Trans. 2* **2002**, 1005-1011.

146. Tian, H.; Xu, T.; Zhao, Y.; Chen, K. *J. Chem. Soc., Perkin Trans. 2* **1999**, 545-549.

147. Beecroft, R. A.; Davidson, R. S.; Whelan, T. D. *J. Chem. Soc., Chem. Comm.* **1978**, 911-913.

148. Tanaka, K.; Miura, T.; Umezawa, N.; Urano, Y.; Kikuchi, K.; Higuchi, T.; Nagano, T. *J. Am. Chem. Soc.* **2001**, *123*, 2530-2536.

149. Closs, G. L.; Miller, J. R. *Science* **1988**, *240*, 440-446.

150. Paddon-Row, M. N. *Acc. Chem. Res.* **1994**, *27*, 18-25.

151. de Silva, A. P.; Gunaratne, H. Q. N.; Gunnlaugsson, T.; Nieuwenhuizen, M. *Chem. Commun.* **1996**, 1967-1968.

152. de Silva, A. P.; Sandanayake, K. R. A. S. *J. Chem. Soc., Chem. Commun.* **1989**, 1183-1185.

153. Leray, I.; Habib-Jiwan, J.-L.; Branger, C.; Soumillion, J.-P.; Valeur, B. *J. Photochem. Photobiol. A: Chem* **2000**, *135*, 163-169.

154. Oguz, U.; Akkaya, E. U. *J. Org. Chem.* **1998**, *63*, 6059-6060.

155. Lincoln, S. F.; Stephens, A. K. W. *Inorg. Chem.* **1991**, *30*, 3529-3537.

156. Izatt, R. M.; Eatough, D. J.; Christensen, J. J. *Struct. Bonding* **1973**, *16*, 161-189.

157. Izatt, R. M.; Terry, R. E.; Nelson, D. P.; Chan, Y.; Eatough, D. J.; Bradshaw, J. S.; Hansen, L. D.; Christensen, J. J. *J. Am. Chem. Soc.* **1976**, *98*, 7626-7630.

158. Dishong, D. M.; Gokel, G. W. *J. Org. Chem.* **1982**, *47*, 147-8.

159. Frensdorff, H. K. *J. Am. Chem. Soc.* **1971**, *93*, 600-606.

160. Shannon, R. D. *Acta Crystallogr., Sect. A* **1976**, *A32*, 751-767.

161. Tsukube, H.; Furuta, H.; Odani, A.; Takeda, Y.; Kudo, Y.; Inoue, Y.; Liu, Y.; Sakamoto, H.; Kimura, K. In *Comprehensive Supramolecular Chemistry: Physical Methods in Supramolecular Chemistry*; Atwood, J. L., Davies, J. E. D., MacNicol, D. D., Vögtle, F., Lehn, J.-M., Eds.; Pergamon: New York, 1996; Vol. 8.

162. Martell, A. E.; Motekaitis, R. J. *The Determination and Use of Stability Constants*; VCH Publishers: Weinheim, 1988.

163. Beck, M. T.; Nagypal, I. *Chemistry of Complex Equilibria*; Ellis Horwood: Chichester, 1990.

164. Kuruscev, T., Private communication.

165. Catena, G. C.; Bright, F. V. *Anal. Chem.* **1989**, *61*, 605-609.

166. Haskard, C. A. Ph. D. Thesis, University of Adelaide, 1996.

167. Olmsted, J. O., III *J. Phys. Chem.* **1979**, *83*, 2581-2584.

168. Melhuish, W. H. *J. Phys. Chem.* **1961**, *65*, 229-235.

169. Demas, J. N.; Crosby, G. A. *J. Phys. Chem.* **1971**, *75*, 991-1024.

170. Leray, I.; Asfari, Z.; J, V.; Valeur, B. *J. Chem. Soc., Perkin Trans. 2* **2002**, 1429-1434.

171. *CRC Handbook of Chemistry and Physics*; 1st Student ed.; Weast, R. C., Ed.; CRC Press: Boca Raton, 1988.

172. Anderson, J. E.; Casarini, D.; Ijeh, A. I.; Lunazzi, L.; Tocher, D. A. *J. Am. Chem. Soc.* **1995**, *117*, 3054-3056.

173. Novak, I.; Potts, A. W. *J. Org. Chem.* **1996**, *61*, 786-787.

174. James, T. D.; Shinkai, S. *J. Chem. Soc., Chem. Commun.* **1995**, 1483-1485.

175. He, G. X.; Kikukawa, K.; Ikeda, T.; Wada, F.; Matsuda, T. *J. Chem. Soc., Perkin Trans. 2* **1988**, 719-724.

176. Otsuki, J.; Yamagata, T.; Ohmuro, K.; Araki, K.; Takido, T.; Seno, M. *Bull. Chem. Soc. Jpn.* **2001**, *74*, 333-337.

177. Li, Y.; Echegoyen, L. *J. Am. Chem. Soc.* **1994**, *116*, 6832-6840.

178. Nieboer, E.; Richardson, D. H. S. *Environ. Pollut., Ser. B* **1980**, *1*, 3-26.

179. Rurack, K.; Bricks, J. L.; Reck, G.; Radeglia, R.; Resch-Genger, U. *J. Phys. Chem. A* **2000**, *104*, 3087-3109.

180. Fery-Forgues, S.; Le Bris, M.-T.; Guetté, J.-P.; Valeur, B. *J. Phys. Chem.* **1998**, *92*, 6233-6237.

181. Pearson, A. J.; Hwang, J.-J.; Ignatov, M. E. *Tetrahedron Lett.* **2001**, *42*, 3537-3540.

182. Dalley, N. K. In *Synthetic Multidentate Macrocyclic Compounds*; Izatt, R. M., Christensen, J. J., Eds.; Academic Press: New York, 1978.

183. Dietrich, B.; Viout, P.; Lehn, J.-M. *Macrocyclic Chemistry: Aspects of Organic and Inorganic Supramolecular Chemistry*; VCH: New York, 1993.

184. More, M. B.; Ray, D.; Armentrout, P. B. *J. Am. Chem. Soc.* **1999**, *121*, 417-423.

185. Perrin, D. D.; Dempsey, B. *Buffers for pH and Metal Ion Control*; Chapman and Hall: London, 1974.

186. Duckworth, P., Private communication.

187. Gans, P.; Sabatini, A.; Vacca, A. *J. Chem. Soc., Dalton Trans.* **1985**, 1195-1200.

188. Hendrickson, K. M. Ph. D. Thesis, University of Adelaide, 1999.

189. Pitha, J.; Jones, R. N. *Can. J. Chem* **1966**, *44*, 3031-3050.

190. Eaton, D. F. *Pure & Appl. Chem.* **1988**, *60*, 1107-1114.

191. Perrin, D. D.; Armarego, W. L. *Purification of Laboratory Chemicals*; 3rd ed.; Permagon Press: Oxford, 1988.

192. Veheyden, J. P. H.; Moffatt, J. G. *J. Org. Chem.* **1970**, *35*, 2319.